INFORMATION TO USERS

This manuscript has been reproduced from the microfilm master. UMI films the text directly from the original or copy submitted. Thus, some thesis and dissertation copies are in typewriter face, while others may be from any type of computer printer.

The quality of this reproduction is dependent upon the quality of the copy submitted. Broken or indistinct print, colored or poor quality illustrations and photographs, print bleedthrough, substandard margins, and improper alignment can adversely affect reproduction.

In the unlikely event that the author did not send UMI a complete manuscript and there are missing pages, these will be noted. Also, if unauthorized copyright material had to be removed, a note will indicate the deletion.

Oversize materials (e.g., maps, drawings, charts) are reproduced by sectioning the original, beginning at the upper left-hand corner and continuing from left to right in equal sections with small overlaps. Each original is also photographed in one exposure and is included in reduced form at the back of the book.

Photographs included in the original manuscript have been reproduced xerographically in this copy. Higher quality 6" x 9" black and white photographic prints are available for any photographs or illustrations appearing in this copy for an additional charge. Contact UMI directly to order.

Investigation of the production performance of horizontal wells
in fractured bottom water drive reservoirs

Kandil, Ahmed Abdelmoti, Ph.D.

King Fahd University of Petroleum and Minerals (Saudi Arabia), 1993

Investigation of the Production Performance of Horizonal Wells in Fractured Bottom Water Drive Reservoirs

BY

AHMED A. KANDIL

A Thesis Presented to the

FACULTY OF THE COLLEGE OF GRADUATE STUDIES

KING FAHD UNIVERSITY OF PETROLEUM & MINERALS

DHAHRAN, SAUDI ARABIA

In Partial Fulfillment of the
Requirements for the Degree of

DOCTOR OF PHILOSOPHY

In

PETROLEUM ENGINEERING

June 1993

KING FAHD UNIVERSITY OF PETROLEUM & MINERALS
Dhahran, Saudi Arabia

COLLEGE OF GRADUATE STUDIES

This dissertation, written by Mr. Ahmed Abdelmoti Kandil under the direction of his Dissertation Advisor and approved by the Dissertation Committee, has been presented to and accepted by the Dean of the College of Graduate Studies, in partial fulfillment of the requirements for the degree of **DOCTOR OF PHILOSOPHY** in Petroleum Engineering.

Dissertation Committee:

Dr. Mohamed A. Aggour
Dissertation Advisor

Dr. Roger Butler
Member (External)
University of Calgary, Canada.

Dr. Khalid A. Al-Fossail
Member

Dr. Hasan S. Al-Hashim
Member

Dr. Hasan Y. Al-Yousef
Member

Dr. Khalid A. Al-Fossail
Department Chairman

Dr. Ala H. Al-Rabeh
Dean, College of Graduate Studies

Date: __14 - 6 - 9 3.__

ACKNOWLEDGMENT

The author takes this opportunity to express his sincere gratitude to Dr. Mohamed A. Aggour, the major advisor and Chairman of the Ph.D Committee, for his encouragement and guidance throughout this study. His constructive and critical review of the manuscript is greatly appreciated. The author is also grateful to the members of the dissertation committee Dr. Khalid A. AL-Fossail, Dr. Hasan S. AL-Hashim and Dr. Hasan Y. AL-Yousef for their many helpful suggestions and careful review of the manuscript. The author is indebted to professor Roger M. Butler of the University of Calgary, Alberta, Canada, who, as the external member of the committee, has provided valuable suggestions and critical review of the manuscript.

The author wishes to thank all the laboratory staff and technicians in the Petroleum Engineering Department and Central Research Workshop for their support and cooperations throughout the experimental work.

The author is much indebted to his parents, wife, children for their continued encouragement, understanding, patience and putting up with him all these years.

خلاصة الرسالة

اسم الطالب : أحمد عبدالمعطي قنديل

عنوان الدراسة : انتاجية الآبار الأفقية في مكامن الزيت ذات التصدعات
والدفع بالمياه السفلية .

التخصص : هندسة البترول .

تاريخ الشهادة : يونيو ١٩٩٣م .

تمت دراسة انتاجية الآبار الأفقية والرأسية في حالة وجود وعدم وجود
تصدعات في مكامن الزيت ذات الدفع بالمياه السفلية وذلك باستخدام نموذج ثلاثي
الأبعاد لمحاكاة المكمن الطبيعي وتمثيل الزيت بكيروسين ذو لزوجة منخفضة . وقد
اختير معدل إزاحة الزيت بالمياه ليحافظ على استقرار حركة سطح تلامس الزيت
والمياه حتى وصوله إلي البئر المنتجة .

وقد برهن هذا البحث على ان الآبار التي تتصل بالمكامن بمساحات أكبر تعطي
إنتاجية أعلى بكثير من مثيلتها ذات مساحات الاتصال الأصغر بالإضافة إلى إنخفاض
الضغوط بهذه الآبار . فمثلاً ، الآبار الأفقية ذات التصدعات يكون آداؤها أفضل من
مثيلتها بدون تصدعات وهذه بدورها أفضل من الآبار الرأسية . ومما يجذب الانتباه أن
الآبار المتصلة بالتصدعات العميقة والقريبة من طبقة المياه السفلية تعطي نتائج أفضل
من الآبار المتصلة بالتصدعات السطحية والبعيدة عن طبقة المياه السفلية .

وقد أجريت دراسة نظرية وتحليلية لشرح آلية انتاج الآبار الأفقية في المكامن
والأسباب التي تؤدي إلى تحسن الأداء في حالة وجود تصدعات بالمكامن . وقد أثبت هذا
البحث أن بئر واحدة أفقية يمكن أن تعطي نفس الأداء أو أفضل من الذي تعطيـ
مجموعة كبيرة من الآبار الرأسية التي قد لاتكون اقتصادية .

درجة الدكتوراة في الفلسفة
جامعة الملك فهد للبترول والمعادن
الظهران ، المملكة العربية السعودية
يونيو ١٩٩٣م

-iv -

ABSTRACT

STUDENT NAME : Ahmed Abdelmoti Kandil

TITLE OF STUDY : Investigation of the Production Performance
of Horizontal Wells in Fractured
Bottom Water Drive Reservoirs

MAJOR FIELD : Petroleum Engineering

DATE OF DEGREE : June 1993

The performance of unfractured and fractured horizontal and vertical wells in a three-dimensional rectangular reservoir model with bottom water drive has been studied. The oil employed was a low viscosity kerosene and the rate was chosen so that the oil-water interface would be stable until it approaches the well.

It was found that, in general, wells with greater contact area with the reservoir gave much more production before water breakthrough, and experienced lower pressure drop. Thus, for example, fractured horizontal wells were better than horizontal wells which, in turn were better than the vertical wells. Interestingly, very deep fractures extending towards the water zone improved the performance. The reasons for this are explained through an analysis of the production mechanisms.

Extrapolation of the results to reservoir scales indicates that long horizontal wells in quit reasonable and economic spacings can give performances equivalent to and even better than those expected of arrays of vertical wells so closely spaced that they could not be economic.

DOCTOR OF PHILOSOPHY DEGREE

KING FAHD UNIVERSITY OF PETROLEUM AND MINERALS
Dhahran, Saudi Arabia

June 1993

TABLE OF CONTENTS

LIST OF TABLES

LIST OF FIGURES

- xiv -

33

Chapter I
INTRODUCTION

Developments in horizontal-well technology and performance during the past few years have placed horizontal wells among the commercially viable well completion techniques [1].

Horizontal wells can improve production rates and recoveries by a variety of mechanisms. At their most basic, the long wellbores allow longer completed intervals and, therefore, increased production rates. In reservoirs overlying an aquifer or located under a gas cap, the increased standoff from the fluid contacts can improve the production rates without causing conning. Additionally, the longer wellbore length serves to reduce the drawdown for a given production rate and, thus, further reduces conning tendencies. Fractured reservoirs can also benefit from horizontal wells. Long wellbores are likely to intersect more fractures and hence improve both production rates and ultimate recovery [2].

Specific situations where horizontal wells can have advantages over vertical wells have been identified in the literature [3,4]; these are: 1. reservoirs where conventional wells have low productivity; 2. reservoirs with vertical fractures or fissures; 3. oil reservoirs where recovery is limited by gas or water conning; 4. thick continuous heavy oil and bitumen sands where steam

assisted gravity drainage is practical; and 5. hydraulically fractured reservoirs where the well can be drilled to accept either longitudinal (parallel) or a number of transverse (orthogonal) fractures.

The major disadvantage of horizontal wells is that only one pay zone can be drained per horizontal well. However, horizontal wells have been used to to drain multiple layers. This can be accomplished by either drilling a "staircase" type well where long horizontal portions are drilled in more than one layer, or creating vertical fractures perpendicular to the wells which could intersect more than one pay zone and thereby drain multiple zones. A second disadvantage of horizontal wells is their cost. Typically, it costs about 1.4 to 3 times more than a vertical well, depending upon drilling method and the completion technique employed [5]. A single horizontal well, however, can replace a number of vertical wells to produce the same segment of a reservoir. In this regard, the horizontal well will be more economical than vertical wells. A third disadvantage is that the horizontal well length may not be all effective. In other words, the fluid flow into the wellbore could be restricted in some portions of the completed interval(s) by either induced damage or reservoir heterogeneities. The effectiveness of the productivity of the completed interval may be checked with production logging.

The performance of horizontal wells for various reservoir and production conditions has seen extensive investigations in recent years [1-5]. However, no experimental work has been done to study the performance of fractured horizontal wells in bottom water drive reservoirs.

The present work, therefore, investigates experimentally and theoretically the production performance of unfractured and fractured horizontal wells in bottom water drive reservoirs. The performance of unfractured and fractured vertical wells is also investigated and compared to that of the horizontal wells.

Chapter II
LITERATURE REVIEW

In the 1950s and 1960s, horizontal wells were attempted in the Soviet Union and China, with disappointing results [3,6,7]. However early in the 1980s, major production successes using horizontal wells were reported at the Rospo Mare Field, offshore Italy [8] and at Prudhoe Bay [9].

Improvements in horizontal well technology have reduced the cost of drilling and completion. For example, the cost of drilling per foot of well decreased from US 462 to US 282 for horizontal wells as compared to US 233 for a conventional vertical well in the Prudhoe Bay project [9]. And with experience, the cost of long horizontal wells is becoming less than double the cost of vertical wells and, in some cases, it can almost approach equality [4].

In North America, the drilling of horizontal wells increased significantly in formations such as the naturally fractured Austin Chalk [10].

Norris, et. al. [11], presented a comprehensive review of current petroleum literature on the reservoir engineering aspects of horizontal well technology with the objective of providing an overview, discussion, and, when appropriate, recommendations for the following areas: 1. analytical solutions for one phase flow; 2. water or gas cresting; 3. numerical simulation; 4. hydraulic fracturing; and 5. well test analysis.

In the following sections, the most significant work on horizontal wells for heavy oil recovery is first reviewed. Then, the literature on water and gas cresting in horizontal wells are examined. The previous work on fractured horizontal wells is then discussed followed by a review of the application of horizontal wells in enhanced oil recovery. Finally, the pattern size and shape of regular arrays of horizontal wells arepresented.

2.1 HORIZONTAL WELLS IN HEAVY OIL RESERVOIRS

With the recent realization that the world's supply of conventional oil is limited, attention has begun to focus on the heavier, more viscous oils. The resource base for heavy oils is tremendous. It has been conservatively estimated that the volume of heavy oil in the world amounts to four trillion barrels [12,13]. This resource is widely dispersed throughout the world, making it attractive to many countries for reasons of internal security of oil supply. Deposits in Alberta, Canada and Orinoco Belt of Venezuela exceed 1 trillion barrels of oil. Table 2.1 provides a breakdown of the world's heavy oil resources by country [12].

The challenge faced for exploitation of the heavy oil resources is to be economically cost competitive with conventional oil recovery operations. To date, a select few of the heavy oil deposits have been exploited commercially [14]. The low productivity derived from the highly viscous oil has been typically insufficient for economic profitability. Horizontal well heavy oil processes offer an opportunity for commercial exploitation of the large resource base.

TABLE 2.1: World Bitumen Resoures [12].

Country	Number of Deposits	OOIP 3 (10 BBL)
Albania	1	371
Canada	7	2,432,600
Cuba	1	undetermined
Italy	4	14,155
Madagascar	2	24,800
Mexico	3	undetermined
Nigeria	1	undetermined
Peru	1	66
Romania	1	25
Trinidad and Tobago	1	60
USSR	10	557,024
USA	53	34,390
Venezuela	4	1,000,012
West Germany	4	undetermined
Zaire	1	1,925
Total	94	4,065,428

Source: Meyer and Fulton, 1982.

Butler [15] espoused the following advantages associated with horizontal wells over conventional wells in heavy oil reservoirs:

Heavy oil from Steamed Reservoirs:

1. More production per well

2. Better recovery

3. Better oil steam ratio

4. Better economics

Primary Production:

1. More contact with the reservoir

2. One well can replace several conventional wells

Several authors [1,16-21], proposed and used horizontal wells to recover heavy oil such as Tar-sands and Bitumen.

Butler [1] proposed a method, steam assisted gravity drainage (SAGD), for predicting the bitumen drainage from around a spreading steam chamber above a horizontal well, Fig. 2.1 [1].

Sugianto and Butler [20] used horizontal wells to recover heavy oil with bottom water using steam assisted gravity drainage. The ultimate recovery varied from 87% of the original oil in place (OOIP) for experimental runs without the bottom water, to 48% of the OOIP for the experimental runs with a ratio of bottom water zone/total bottom water and oil of 0.41. They recommended higher steam injection pressure for the cases without bottom water
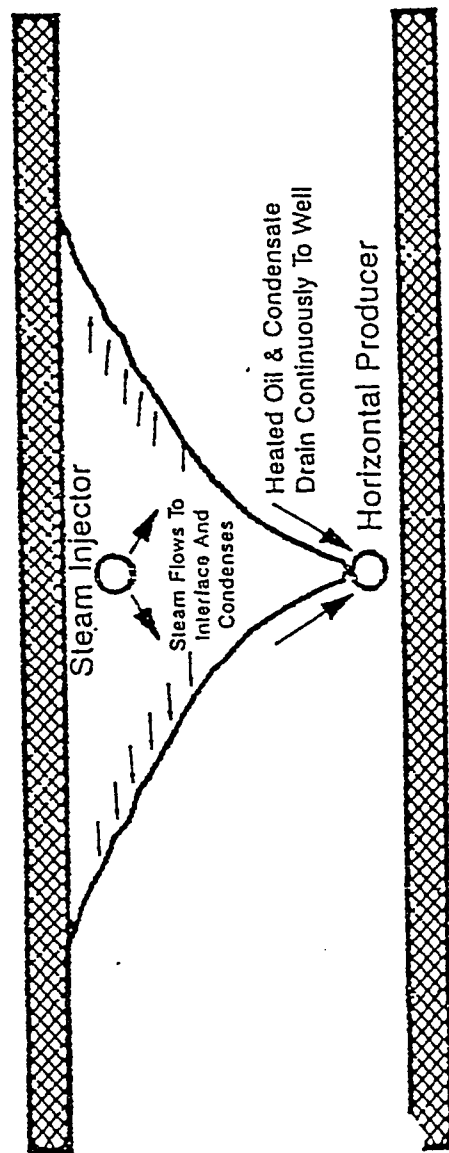
Figure 2.1: Steam-Assisted Gravity Drainage with Horizontal Producer, [1].

zone, and steam injection pressure should be comparable to the aquifer pressure in the cases with bottom water zone. They also pointed out that the cumulative oil recovery is lower as the thickness of the bottom water increases. They also concluded that although in most of the experiments, the production well was located above the water-oil contact, it was found that excellent recovery was obtained with the well located below the water-oil contact.

Doan and Farouq Ali [21] presented a scaled model which involves the flow of water, oil and steam in 3-dimensional 'cylindrical' model. They experimentally tested the effect of variable-diameter horizontal well, perforated casing, and steam injection rate on the pressure drop, fluid production rate, cumulative oil recovery, and steam oil ratio.

They concluded that:

1. A variable-diameter horizontal well offers superior performance when compared with constant diameter horizontal well. It can lower well pressure loss by reducing resistance to flow inside the wellbore, and thus leads to higher production rate, and better steam-oil ratio (SOR) and cumulative oil recovery. Also, a variable-diameter well can result in more uniform, even growth of steam zones and thus leads to better steam sweep efficiency and slower breakthrough of steam.

2. Perforated casings can seriously impede flow of heated oil and steam condensate into a horizontal well. Casing can also lead to

high SOR, low cumulative oil recoveries as well as delayed recovery. Further, it may act as heat sinks, diverting steam away from its intended target.

3. Higher steam injection rates can lead to slightly improved initial production rates. However, they can also result in high SOR, low and delayed oil recovery, as well as early steam breakthrough at the production well.

Horizontal wells have been used in several heavy oil fields. Asgarpour, et. al. [22] discussed the performance of one of twenty wells drilled in the Sparky Channel Sand in Saskatchewan. They showed that the well was producing ten times the rate of an average conventional vertical well in the same sand. They concluded that horizontal wells offer economically attractive option for field development and infill drilling.

2.2 WATER AND/OR GAS CRESTING (CONNING)

It is generally known that, a horizontal well with sufficient length would mean a larger contact area. Therefore, the same production rate can be achieved at a lower pressure drawdown when compared with the vertical well. In other words, the critical flow rate will be higher in case of horizontal well. Furthermore, the horizontal wells when strategically placed can reduce water/gas conning and result in improved cumulative recovery in view of the small drawdowns [23], Figs. 2.2 and 2.3.
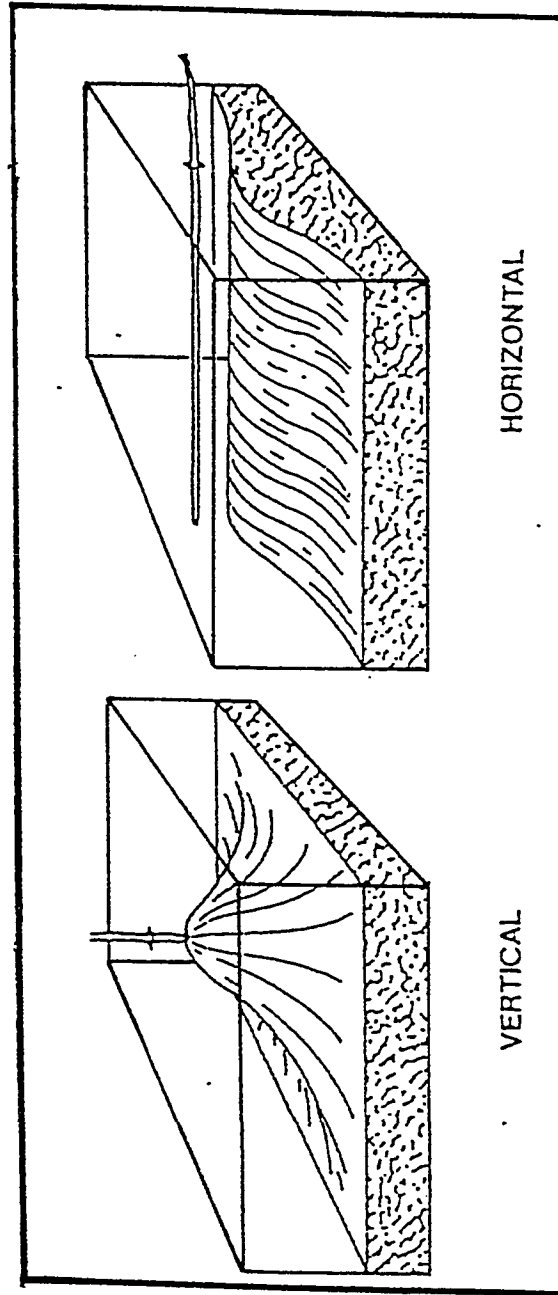
Figure 2.2: Water Coning Toward a Vertical Well and Cresting Toward a Horizontal Well, [23].
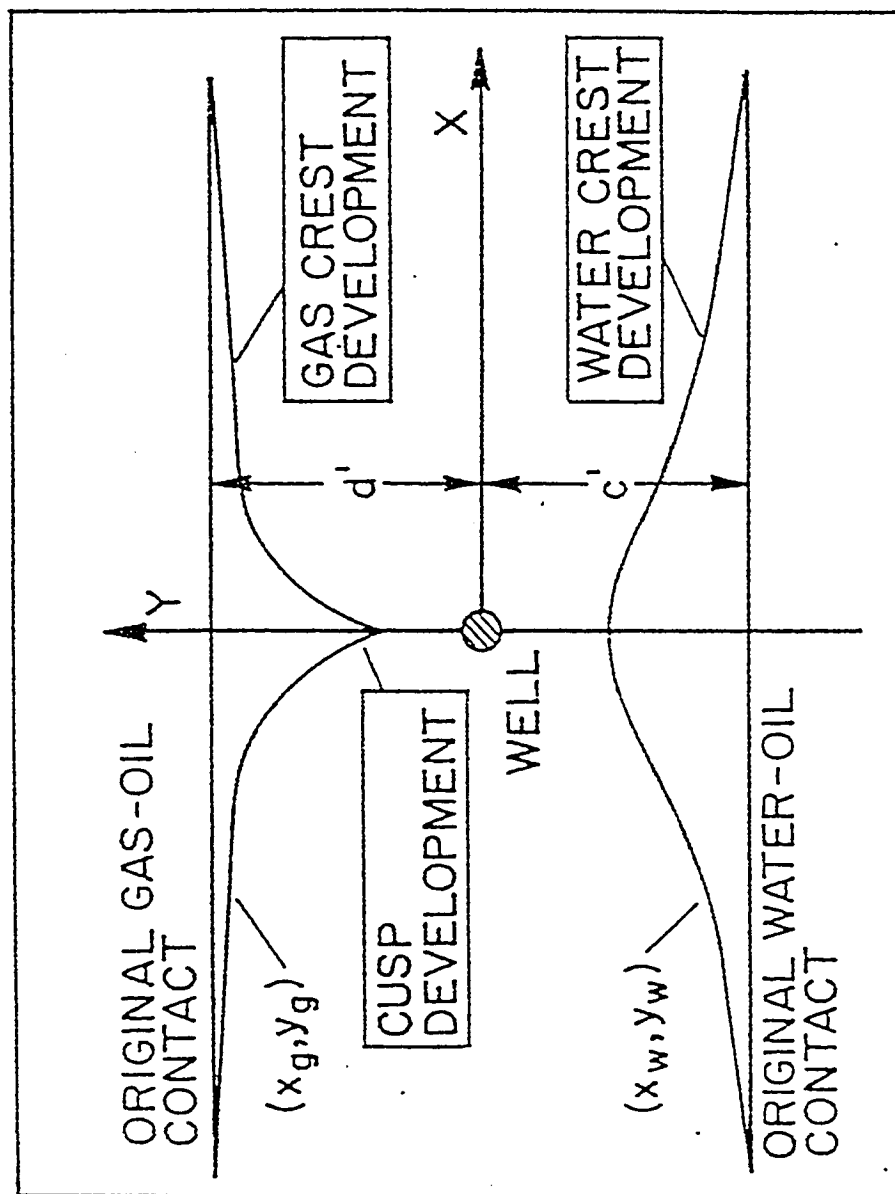
Figure 2.3: Schematic Vertical Cross-Section View of Gas and Water Cone Development in Horizontal Well, [23].

2.2.1   Horizontal Well Critical Rate

2.2.1.1   Water Cresting

Several authors [23-26] presented analytical and numerical solutions to predict the critical flow rate for a horizontal well.

Chaperon [23] presented an equation for a horizontal well fully drilled in a closed drainage area giving the critical rate as:

$$\frac{Q_c}{L} = 3.486 \times 10^{-5} \, \Delta \rho \, h \, \frac{k_h}{\mu} \, (\frac{k_v}{k_h})^{1/2} \, q_{lc} \left[\frac{X_A}{h} \, (\frac{k_v}{k_h})^{1/2} \right] \qquad (2.1)$$

Where:

Q_c = critical flow rate, m^3/hr

L = horizontal well length, ft

$\Delta \rho = \rho_w - \rho_o$, g/cc

h = oil thickness, ft

k_h = permeability in the horizontal direction, md

k_v = permeability in the vertical direction, md

μ = viscosity, cp

q_{lc} can be obtained from table (2.2), where;

$$a = \frac{X_A}{h} \, (\frac{k_v}{k_h})^{1/2}$$

TABLE 2.2: Horizontal Well: Critical Cone
Heights, Dimensionless Critical
Rates and Function F for Various
Values of a, [25].

a	q_{lc}	F
1	4.003	4.003
2	2.013	4.026
3	1.361	4.083
4	1.040	4.160
5	0.849	4.245
7	0.631	4.417
10	0.464	6.67
13	0.3695	4.80
20	0.254	5.08
30	0.177	5.31
40	0.137	5.48
70	0.082	5.74

For pseudosteady-state case $X_A = \dfrac{X_e}{2}$

where:

X_A = *Location of a constant pressure boundary, ft, and*;

X_e = *Location of an actual no flow boundary, ft.*

Chaperon presented an example which shows that as $\dfrac{k_v}{k_h}$ decreases, the critical flow rate decreases which keeps the cone away from the wellbore. He also concluded that the horizontal well may allow higher critical rates than the vertical well. The critical rate ,Q_{ch} , of horizontal well to that of vertical ,Q_{cv} , well is given by [23]:

$$\frac{Q_{ch}}{Q_{cv}} = \frac{L}{X_A} \frac{F}{q_{lc}} \; , \tag{2.2}$$

F and q_{lc} may be obtained from table (2.2).

Dikken [123] and Butler [124] have found that equation (2.1) predicts the critical rate four times higher than it should be.

Giger, et. al. [24,27] presented an analytical two-dimensional model to describe the shape of the water crest created by a horizontal well for producing an oil deposit bounded by a water-oil contact (WOC) surface. The horizontal well is situated near the roof of the reservoir for the Lateral-Edge-Water

and Bottom-Water-Drive cases. He presented the following equation for the critical flow rate in the case of Bottom-Water-Drive:

$$q_c = \frac{3}{2} \frac{k_h \Delta \rho\, g\, D}{\mu_o} \left[(1 + \frac{16\, Y_s^2}{3\, D^2})^{1/2} - 1 \right]$$

(2.3)

Where:

q_c = critical flow rate, STB/d.

$\Delta \rho = \rho_w - \rho_o$, g/cc

D = distance between two lines of horizontal wells, ft.

k_h = permeability in horizontal direction, md

μ = viscosity, cp

g = acceleration by gravity, 9.80 m/s²

Y_s = distance of the summit of the water crest to the top of the reservoir, ft.

2.2.1.2 Gas Conning:

For gas conning in horizontal wells, The critical flow rate may be calculated from [28]:

$$\frac{q_{o,h}}{q_{o,v}} = \frac{[h^2 - (h - l_h)^2]\, \ln(r_e/r_w)}{[h^2 - (h - l_v)^2]\, \ln(r_e/r_w')}$$

(2.4)

$$q_{o,v} = \frac{1.535 \times 10^{-3}\, (\rho_o - \rho_g)\, k_h\, [h^2 - (h - l_v)^2]}{B_o \ln(r_e/r_w)}$$

(2.5)

Where:

$q_{o,v}$ = vertical well critical rate, STB/day

ρ_o = oil density, gm/cc

ρ_g = gas density, gm/cc

h = oil column thickness, ft

l_v = distance between the gas/oil interface and perforated top of vertical well, ft

k_h = Permeability, md

l_h = distance between the horizontal well and the gas/oil interface

r_w' = effective wellbore radius, ft

The effective wellbore radius (r_w') appears in eqn. (2.5) can be obtained from;

$$r_w' = \frac{r_{eh}\,(L/2)}{a\left[1+\sqrt{1-[L/2a]^2}\,\right]\,[\beta h/(2r_w)]^{(\beta h/L)}} \qquad (2.6)$$

$$a = (L/2)\left[\,0.5+\sqrt{0.25+(2r_{eh}/L)^4}\,\right]^{0.5} \qquad (2.7)$$

Where:

β, anisotropic parameter, $= \sqrt{k_h/k_v}$

r_{eh} = drainage radius of horizontal well, ft

The effective wellbore radius (r_w') is related to the skin (S) via the relation;

$$r_w' = r_w \exp(-S)$$

(2.8)

2.2.1.3 Prediction of Breakthrough Time and Recovery Efficiency

!. Water and/or Gas Cresting:

Producing below the critical rates may not be economical. In these cases, breakthrough time and water/oil ratio (WOR) become important. Papatzocos, et. al. [25,29] presented correlations to predict breakthrough time for water and/or gas cresting:

$$t_{DBT} = \frac{q\,(\rho_o - \rho_g)\,k_v\,t_{BT}}{h_o\,\varphi\,\mu_o}$$

(2.9)

$$q_D = \frac{\mu_o\,q_o\,B_o}{2\,\pi\,L\,(k_v\,k_h)^{1/2}\,h\,g\,(\rho_o - \rho_g)}$$

(2.10)

Where:

q = flow rate.

h = oil thickness.

$\Delta\rho$ = $\rho_w - \rho_o$.

φ = porosity.

k_h = permeability in horizontal direction.

k_v = permeability in vertical direction.

μ = viscosity.

t_{BT} = breakthrough time.

t_{DBT} = dimensioless breakthrough time.

q_D = dimensioless rate.

g = acceleration by gravity, and;

L = horizontal well length.

Equations (2.9) and (2.10) are written in cgs units. For calculation of water breakthrough time, one should use the density difference between oil and water instead of the density difference of oil and gas.

The correlations may be found in Fig. 2.4. For single cone case, the distance between the well and the oil/water or oil/gas contact is substituted for h. Fig. 2.5 represents the situations where gas cap and aquifer are present, in these cases the optimum well location can be estimated. In these figures, h_o is the oil thickness, B_{opt} is the optimum well location and $\psi = (\rho_w - \rho_o) / (\rho_o - \rho_g)$.

II. Bottom Water Drive Reservoirs:

Ozcan and Raghavan [26] presented a mathematical model to study the performance of horizontal wells in bottom water-drive reservoirs. They discussed the productivity of horizontal wells before water breakthrough in terms of the efficiency of the displacement. They assumed that the bottom water drive reservoir can be represented as a constant pressure boundary;
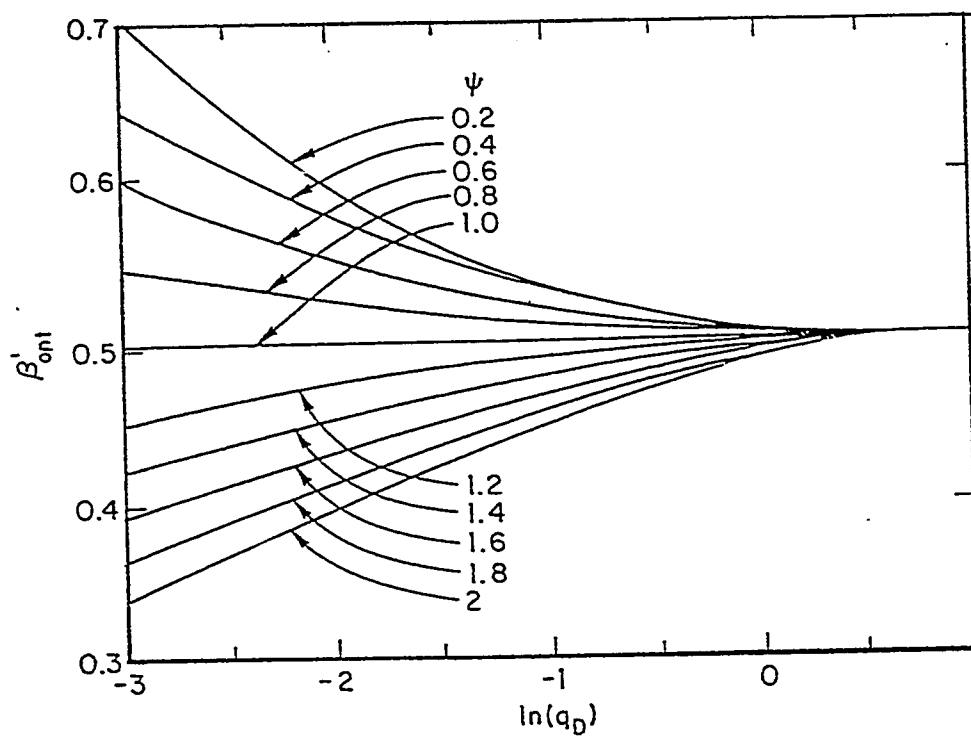
Figure 2.4: Optimum Well Placement as a Function of Dimensionless Rate (Two-Cone Case), [25].
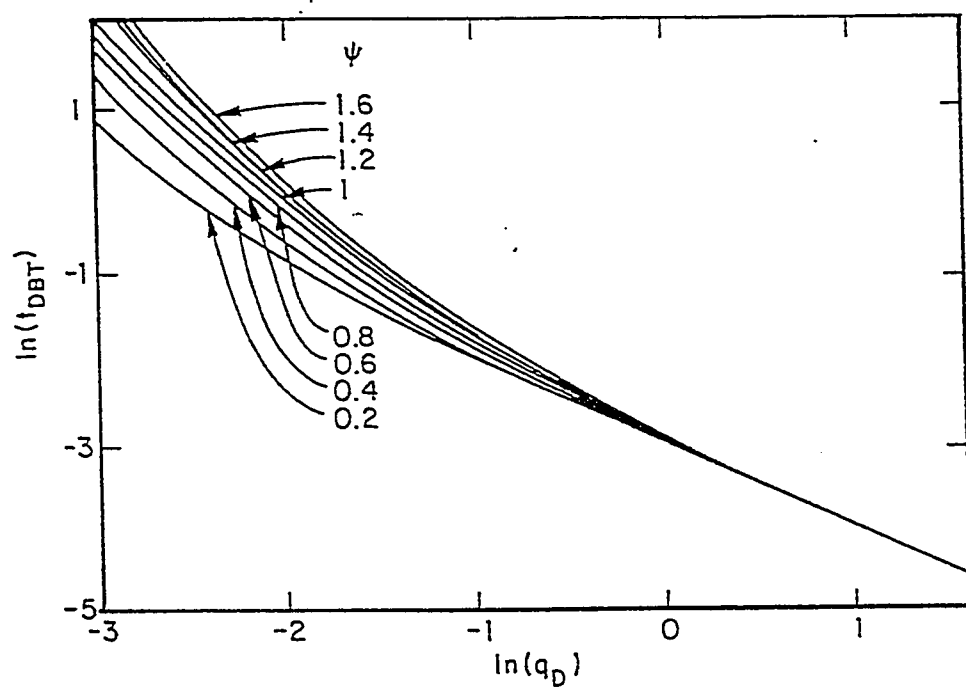
Figure 2.5: Dimensionless Time for Simultaneous Breakthrough for Water and Gas Coning (Two-Cone Case), [25].

i.e., pressure at the oil and water interface is constant. They presented the following equation for the water breakthrough time:

$$t_{BT} = (\frac{f_d h^3 E_s}{5.615 q_o B_o}) (\frac{k_h}{k_v})$$

(2.11)

Where:

$f_d = \varphi(1 - S_{wc} - S_{oir})$

f_d = microscopic displacement efficiency, dimensionless

q_o = flow rate, STB/day

k_h = horizontal permeability, md

k_v = vertical permeability, md

E_s = sweep efficiency, dimensionless

h = oil column thickness, ft

B_o = formation volume factor, RB/STB

S_{wc} = connate water saturation, fraction

S_{oir} = residual oil saturation, fraction

φ = porosity, dimensionless

Figs. 2.6, 2.7 and 2.8 [26] show the plots of sweep efficiency (E_s) for vertical and horizontal wells. In these figures, the effective well spacing (a_D), dimensionless well length (L_D), penetration ratio (b'), dimensionless vertical distance (Z_{WD}), and dimensionless wellbore radius (r_{WD}) are defined as:
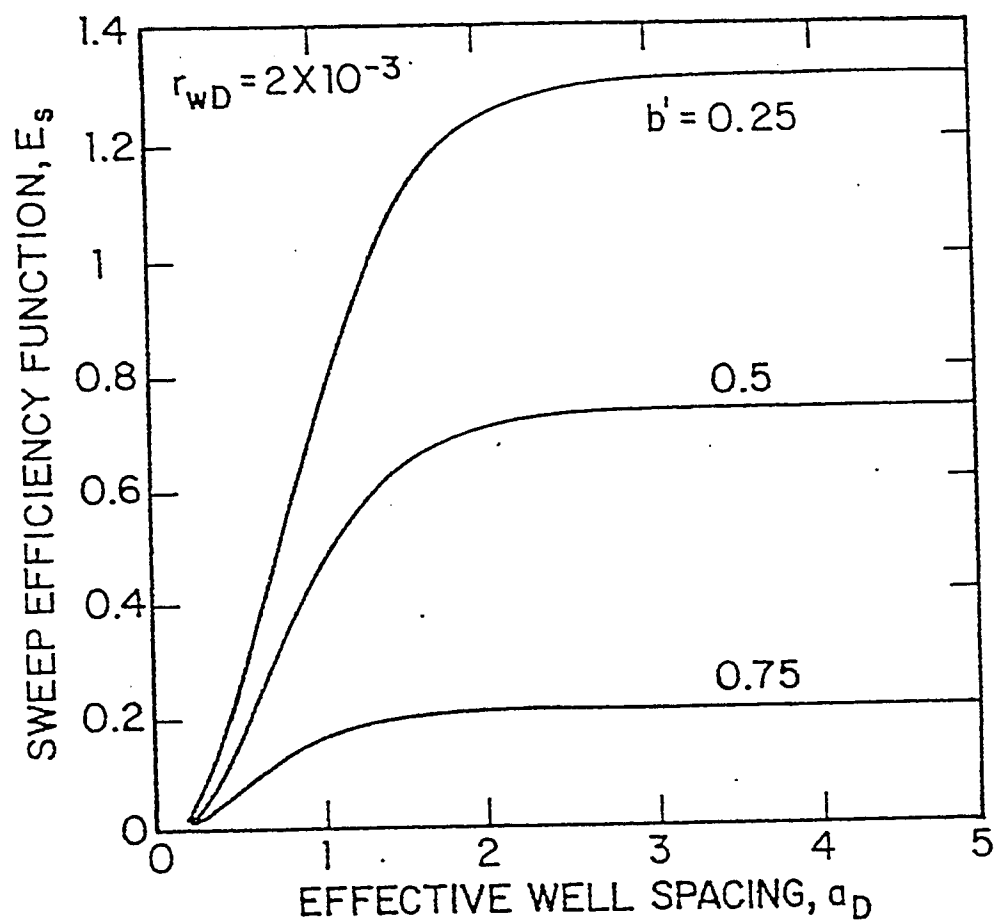
Figure 2.6: Sweep Efficiency for Vertical Wells, [26].
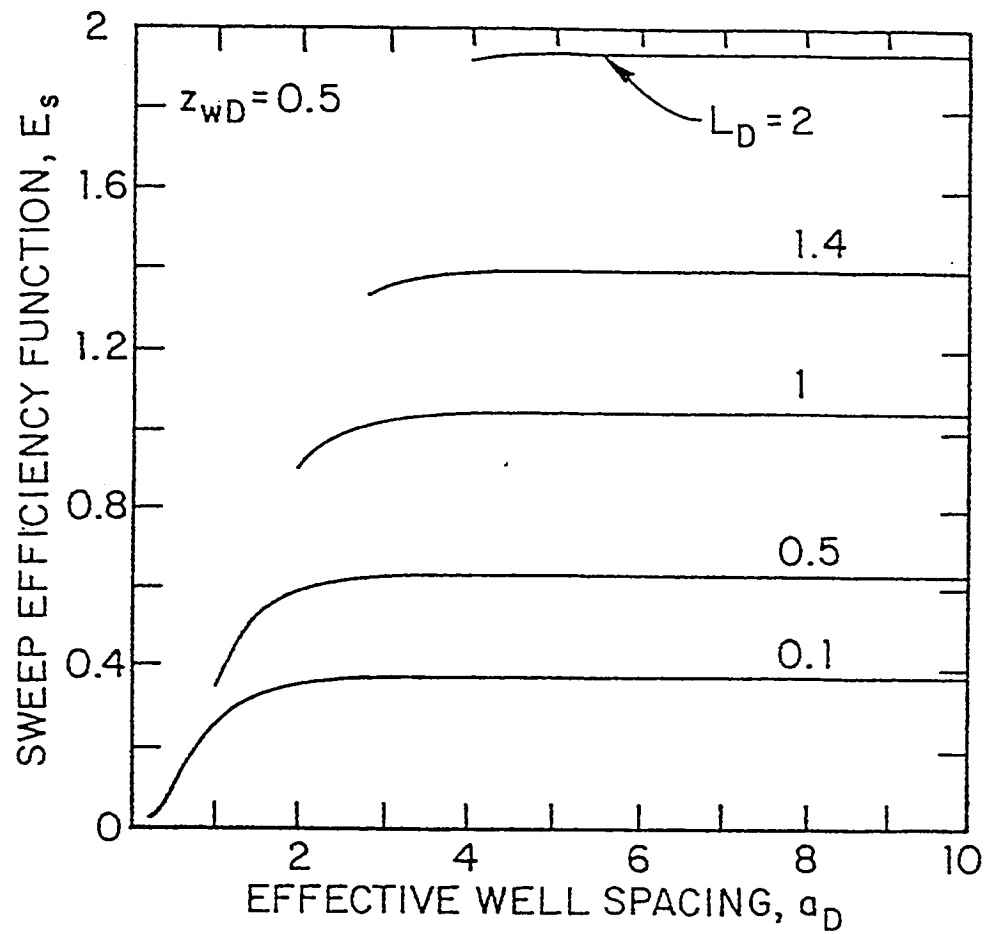
Figure 2.7: Sweep Efficiency for Horizontal Wells, [26].
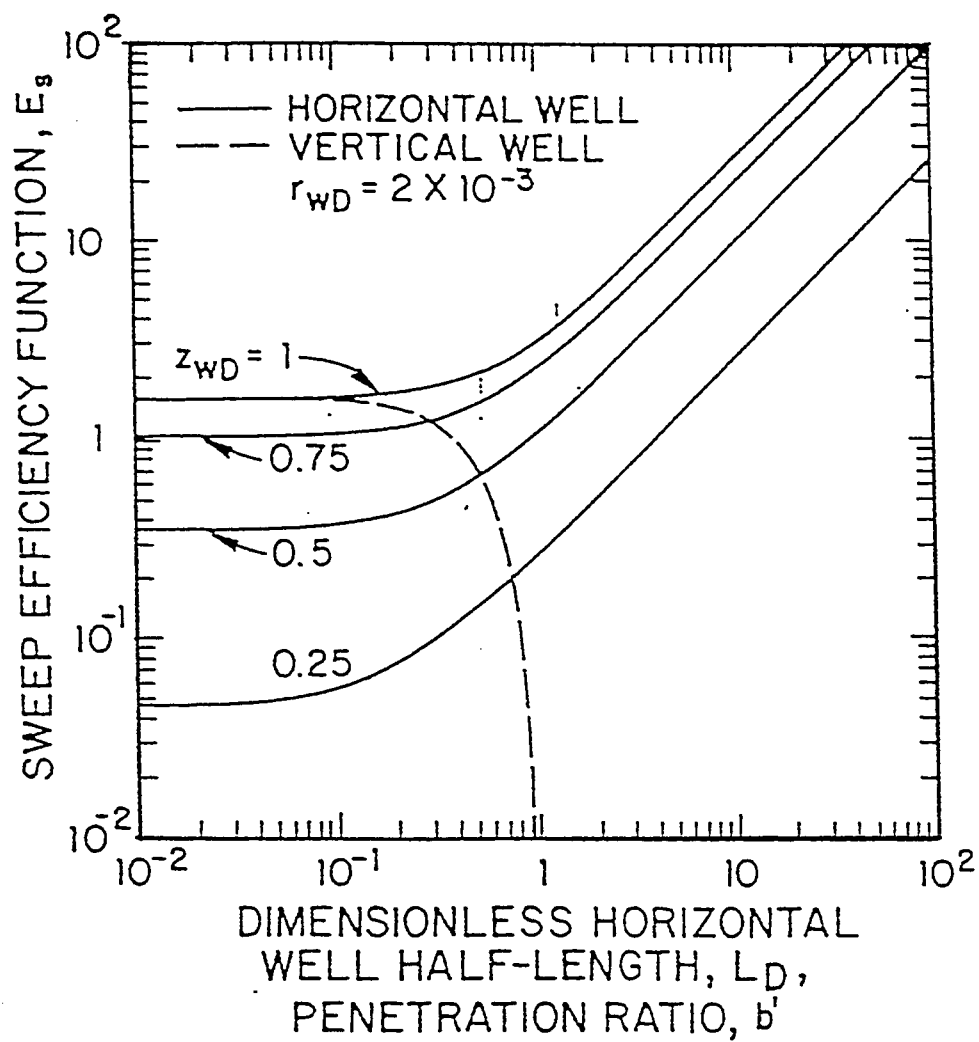
Figure 2.8: Sweep Efficiency for Horizontal and Vertical Wells, [26].

$$a_D = \frac{2X_e}{h}\sqrt{k_v/k_h}$$ (2.12)

$$L_D = \frac{L}{2h}\sqrt{k_v/k_h}$$ (2.13)

$$b' = \frac{h_p}{h}$$ (2.14)

$$Z_{WD} = \frac{Z_w}{h}$$ (2.15)

$$r_{WD} = \frac{r_w}{h}$$ (2.16)

Where;

X_e = half well spacing, ft

L = well length, ft

h_p = perforated interval, ft

Z_w = vertical distance of horizontal well oil water contact at time $t = 0$, ft

r_w = wellbore radius, ft.

For horizontal wells, Fig. 2.7 indicates that the sweep efficiency function (E_s) increases with increasing well length (increasing L_D) for a fixed well spacing. Increasing the well length for a fixed well spacing would, therefore, result in delaying water breakthrough. Fig. 2.7 also shows that if the well length is fixed, increasing well spacing, would delay water breakthrough. However,

beyond a certain value, an increase in well spacing would not increase the water breakthrough time as long as well length is fixed. Fig. 2.8 depicts sweep efficiency (E_s) for horizontal wells of different lengths located at different elevations from the oil-water contact. It is clear from Fig. 2.8 that as the dimensionless horizontal well elevation (Z_{wD}) increases, the sweep efficiency function (E_s) increases at fixed dimensionless horizontal half-length (L_D) and penetration ratio (b').

Supronowicz and Butler [30] used the potential distribution and streamline theory to analyze the production of crude oil from reservoirs which are underlain by an active aquifer. They considered the displacement of oil to a horizontal well, or a series of horizontal wells by a rising aquifer of unlimited water supply. The main objective of their study was to describe the progress of the interface between oil and water phases. The horizontal wells are introduced at the top of the reservoir, Fig. 2.9. It is assumed that both water and oil are immiscible but have the same properties: density and viscosity in particular. They used formulae given by Maxwell [31], and later by Muskat [32]. These formulae describe the velocity potential distribution and streamlines in a steady-state, two-dimensional potential field with the line of equally-spaced sinks, [30].

Supronowicz and Butler studied and analyzed the effect of recovery ratio, time to breakthrough and geometry of the potential field and the relation between them on the process of oil recovery in order to make it possible to optimize the process. Figs. 2.10, 2.11 and 2.12 [30] show the progress of of
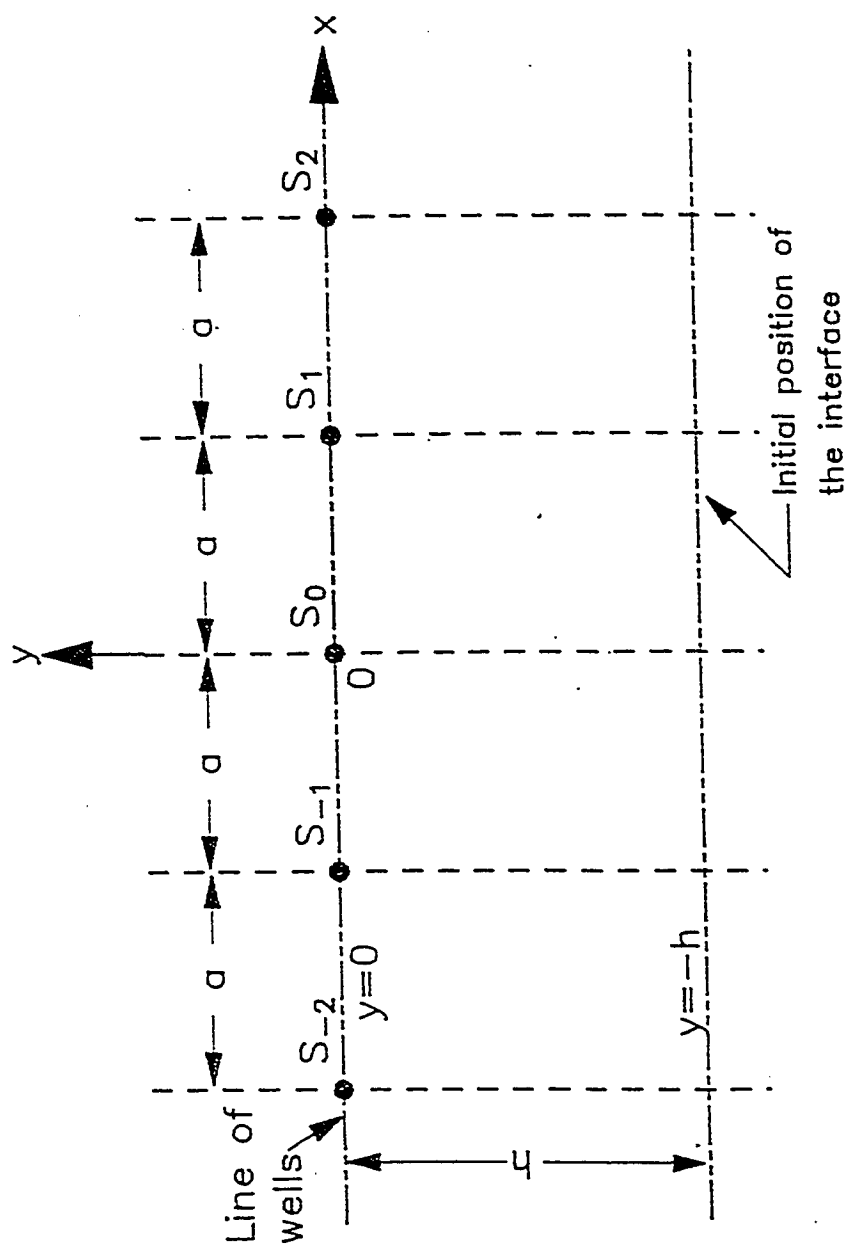
Figure 2.9: Cross Section of a Reservoir by the Plane Perpendicular to the Wells, [30].
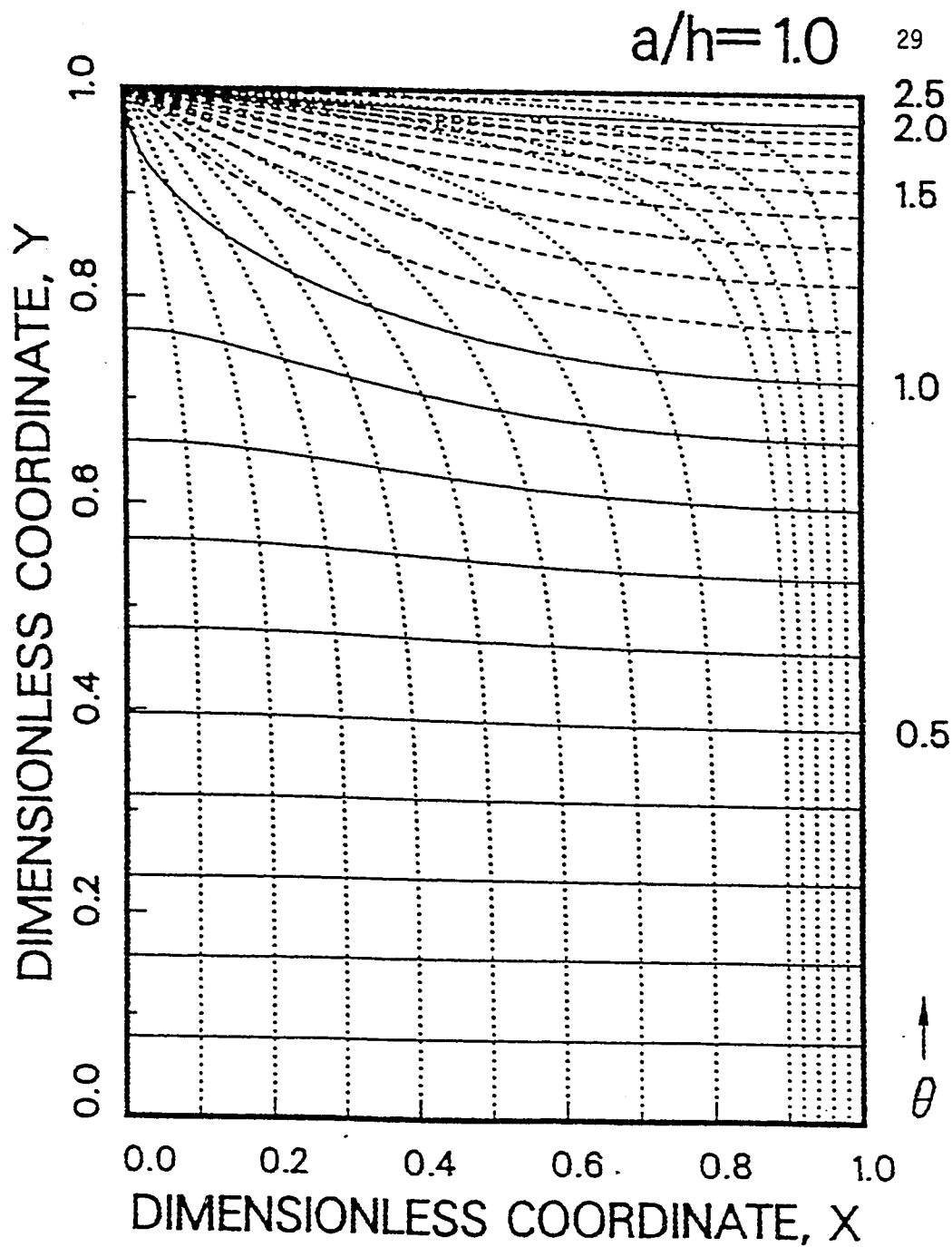
Figure 2.10: Interface Advancement and Streamlines in an Isotropic Res. with a/h = 1.0 or in an Anisotropic One with B = 1.0, [30].
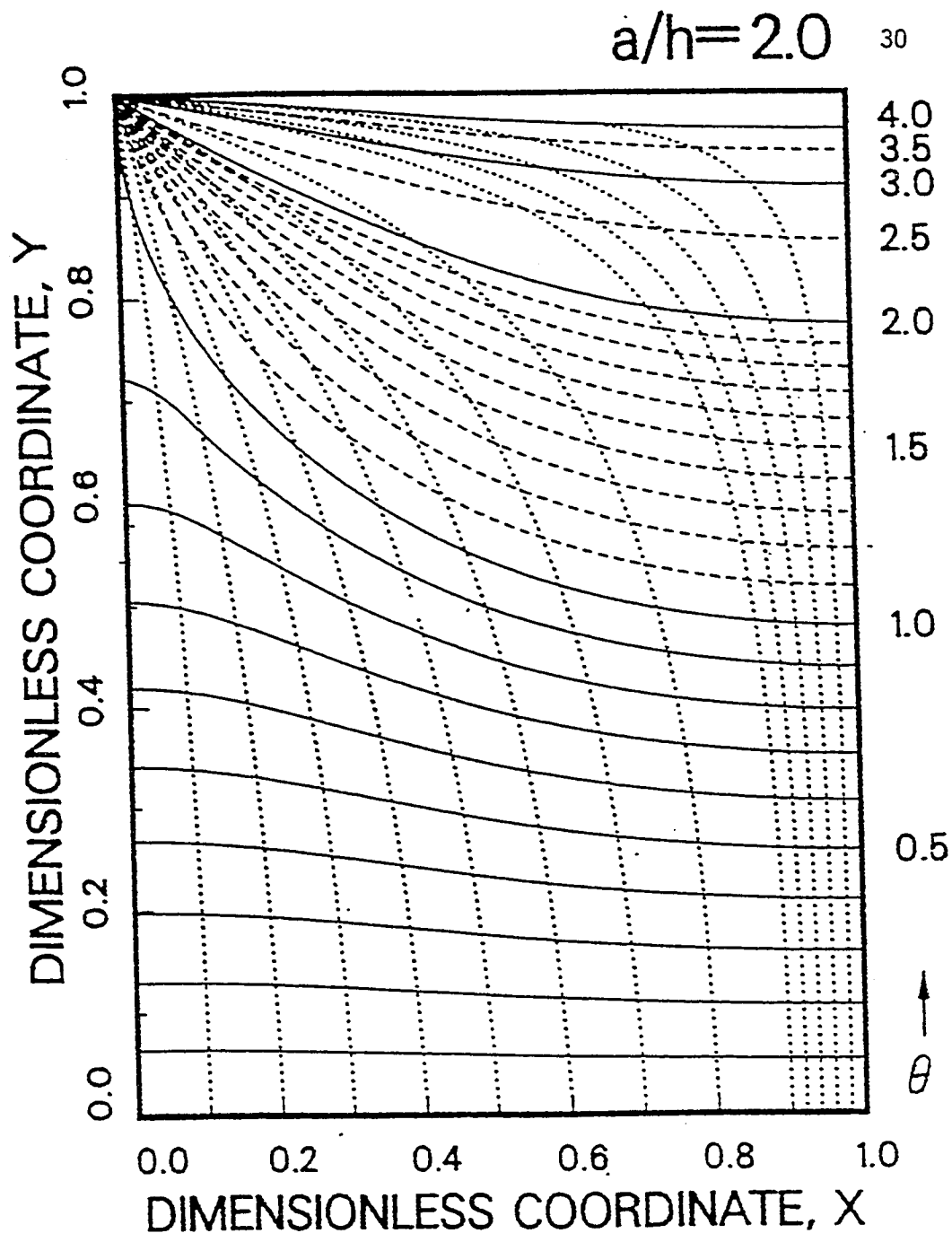
Figure 2.11: Interface Advancement and Streamlines in an Isotropic Res. with a/h=2.0 or in an Anisotropic One with B=0.5, [30].
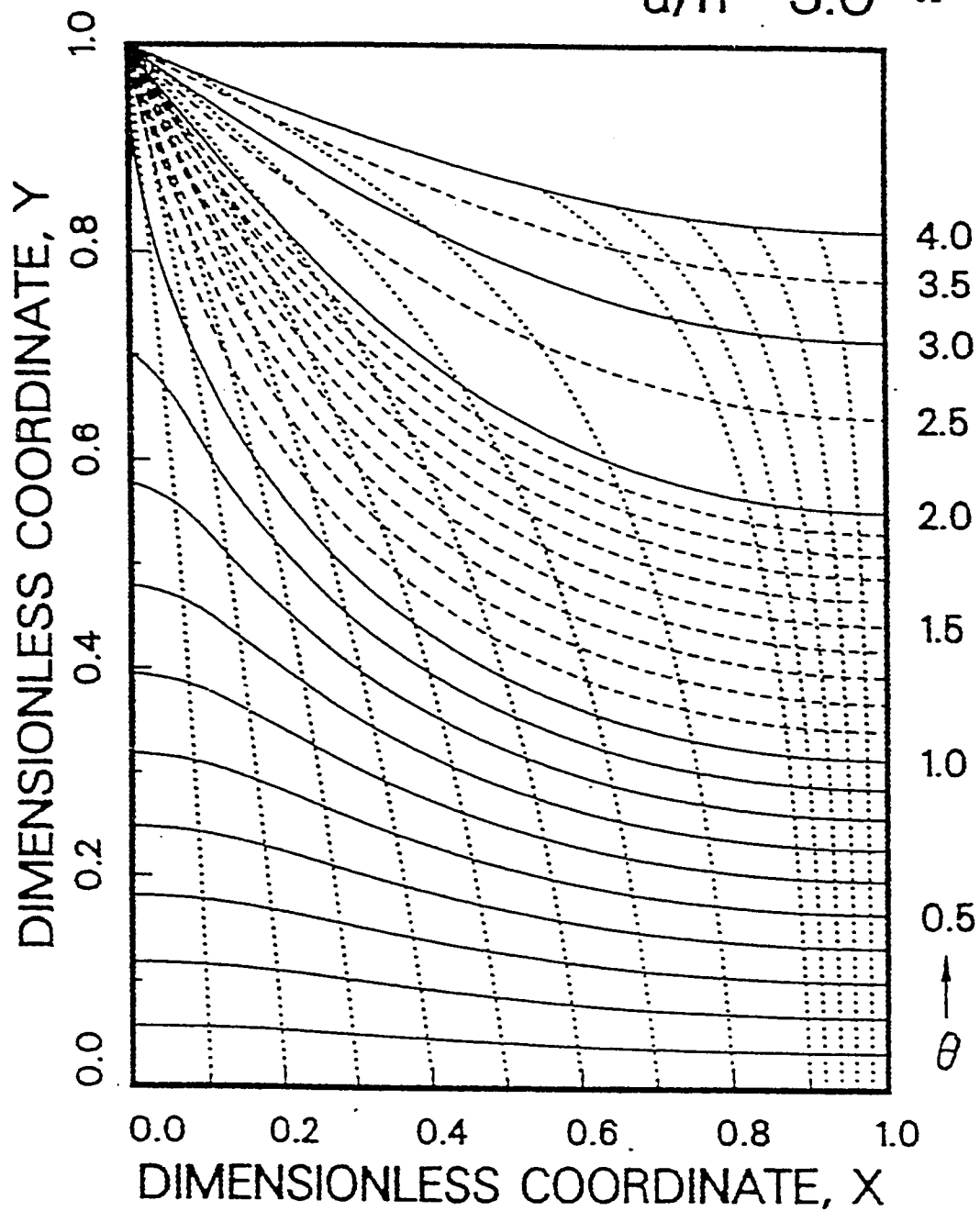
Figure 2.12: Interface Advancement and Streamlines in an Isotropic Res. with a/h = 3.0 or in an Anisotropic One with B = 0.333, [30].

the interface and some streamlines in the dimensionless coordinate system, X, Y. Dimensionless time (θ) has been introduced, so the subsequent positions of the interface have been plotted in dimensionless time intervals $\Delta\theta = 0.1$ for $\theta \leq 2.0$. Afterwards, the interfaces have been shown in $\Delta\theta = 0.5$ intervals. All the interfaces before breakthrough, and afterwards, the ones for $\theta = 2.0$, $\theta = 3.0$ and $\theta = 4.0$ are shown as solid lines, the other ones are dashed lines.

Streamlines are shown as dotted lines and they have been plotted starting at the bottom of the plot every $\Delta X = 0.1$ until $\Delta X = 0.9$, and afterwards, between $0.9 < X < 1.0$ at every $\Delta X = 0.02$.

They introduced a parameter β to account for anisotropic reservoirs.

Where:

$$X = \frac{x}{a/2},$$

$$Y = \frac{h+y}{h},$$

$$\theta = \frac{t}{T_b}, \text{ and }$$

$$\beta = \frac{h}{a}\sqrt{k_x/k_y}.$$

a = well spacing, and,

h = reservoir thickness

Fig. 2.13 shows the recovery ratio, cumulative water/oil ratio and cumulative oil/(water + oil) ratio during the progress of the recovery process as a function of dimensionless time up to $\theta = 4$ (i.e. for real time exceeding four times the time to breakthrough) and for five different values of a/h ratio.

Fig. 2.14 shows how the recovery ratio at time to breakthrough changes with the increase of well spacing/ reservoir thickness ratio. The relative time to breakthrough appears on Fig. 2.14 is the actual time to breakthrough T_b for a given a/h ratio divided by T_b for a/h = 1.0.

They concluded that when the density difference between oil and water is small, application of horizontal wells seems to be feasible for a light type of oil only, because of water fingering effect. They also concluded that if the production rate is kept below the critical rate, a higher density difference improves the recovery at water breakthrough because the water rise is retained by gravity. Further, they concluded that the only factor on which the progress of the interface depends is the well spacing to reservoir thickness ratio. Closer spacing of the horizontal wells allow more complete and more rapid recovery of the oil.

They pointed out that their model can be applied to both isotropic and anisotropic reservoir matrices.

34
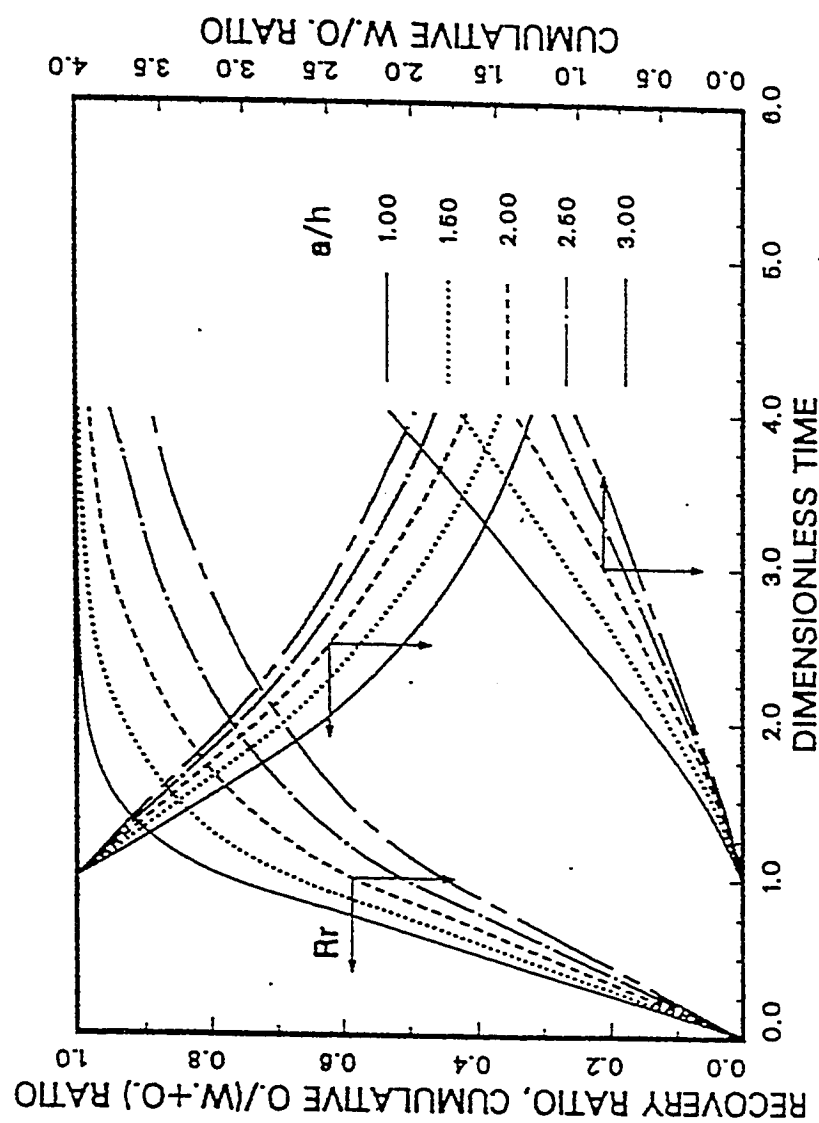
Figure 2.13: Recovery Ratio, Cum. WOR and Cum. Water Cut vs. Dimensionless Time for Five Different Values of a/h, [30].
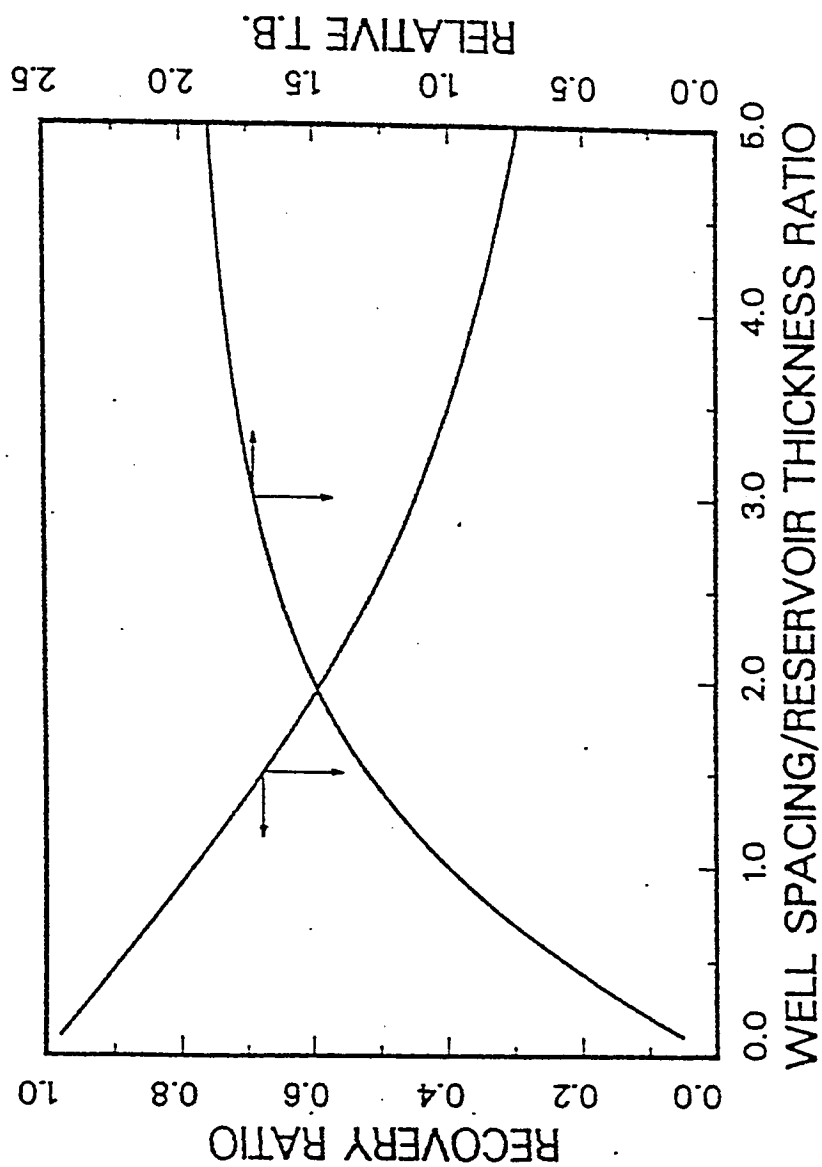
Figure 2.14: Recovery Ratio and Relative Time to Breakthrough vs. Well Spacing/Reservoir Thickness Ratio (a/h). [30].

2.3 FRACTURED HORIZONTAL WELLS

There are two types of fractures; natural fractures and induced (hydraulic) fractures. These two types are presented below:

2.3.1 Naturally Fractured Reservoirs

There are over 100 naturally fractured reservoirs in the United States and many more around the world containing an estimated 25-30% of the world oil reserves [33-36].

In such reservoirs, horizontal wells can be drilled to intersect a number of discrete discontinuities, and thus take advantage of favorable permeability anisotropy [3]. Butler [4] stated that a horizontal well can provide an unusually high advantage when it is drilled through a reservoir containing natural fractures. In this case, the construction of a horizontal well which intersects the fractures in a direction perpendicular to their surfaces, can result in improved productivity or, in cases where conning problem prevail, improved critical production rates. Dramatic improvements can also be obtained in Karstic reservoirs which typically contain irregular fractures and cavern-like cavities. In these reservoirs horizontal wells have better chances for intersecting voids and other highly productive regions than do vertical wells with their much shorter penetration. As an example, The Rospo Mare Field, offshore Italy, is a Karst carbonate reservoir characterized by caverns, voids and vertical fractures. The oil is very heavy ($11°API$) and viscous (300 cp) [7]. It is found that horizontal wells produce much more than conventional verti-

cal ones. It is worth mentioning that the Rospo Mare Field is characterized by the existence of an aquifer and it is possible to operate with relatively little water production. In North America, the drilling of horizontal wells increased significantly in formations such as the naturally fractured Austin Chalk and the Spraberry in West Texas [10].

2.3.2   Hydraulically (Induced) Fractured Reservoirs

In hydraulic fracturing, the desired fracturing pattern is determined from reservoir characteristics and fractured well performance considerations.

Soliman, et. al. [37,38] pointed out that a fracture treatment is desirable in the following circumstances: 1. restricted vertical flow caused by low vertical permeability or the presence of shale streaks; 2. the presence of natural fractures in a direction different from that of induced fractures; 3. low formation productivity; and 4. low stress contrast between the pay zone and the surrounding layers.

The horizontal wells can be drilled either parallel to the direction of minimum principal stress, thus creating transverse (orthogonal) fractures, or perpendicular to the direction of minimum principal stress, thus creating axial or longitudinal fractures [3,39-42], Figs. 2.15, 2.16, 2.17 and 2.18. Deciding on fracture orientation with respect to the wellbore is extremely important. One should decide whether designs similar to those of Figs. 2.17 and 2.18 should be considered.
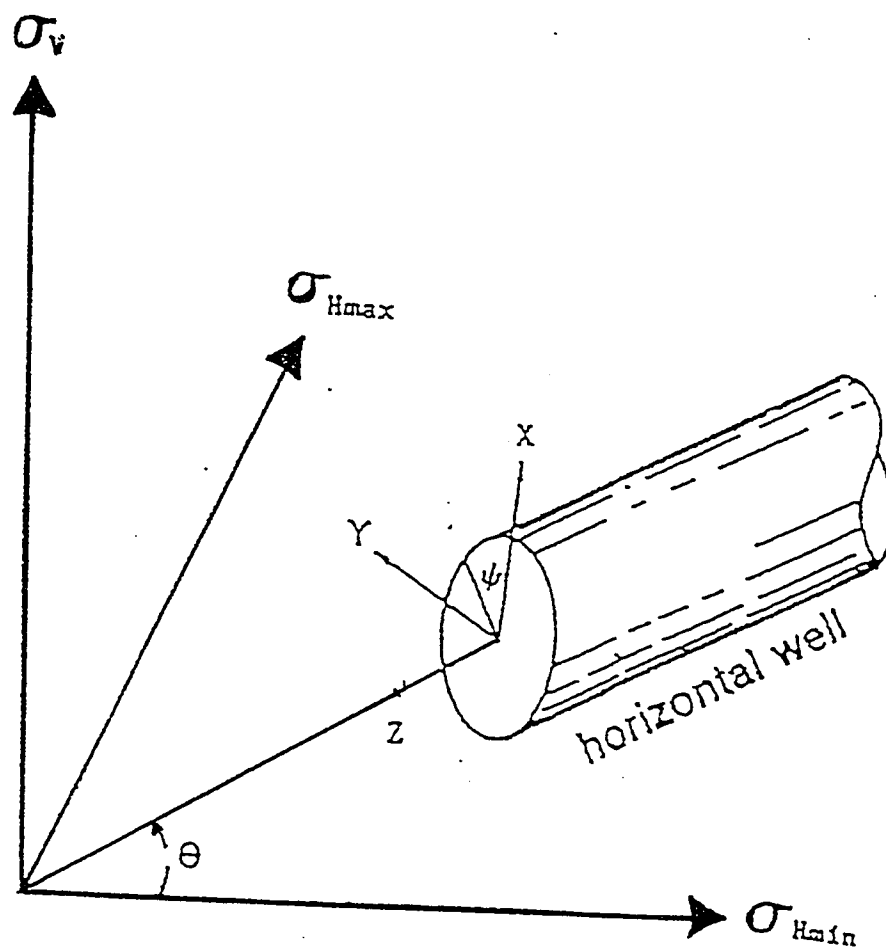
Figure 2.15: Horizontal Well configuration system in the In-Situ Stress Field, [42]. .
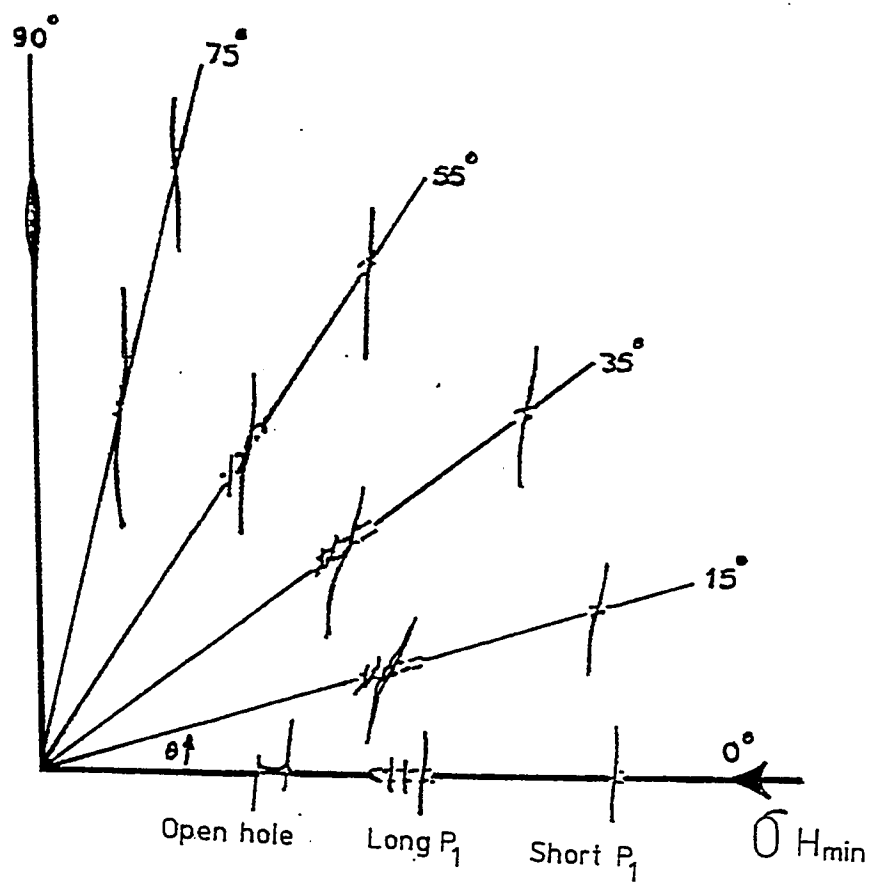
Figure 2.16: Top View of Fracture Induced at Various Wellbore Deviation angles, [42].
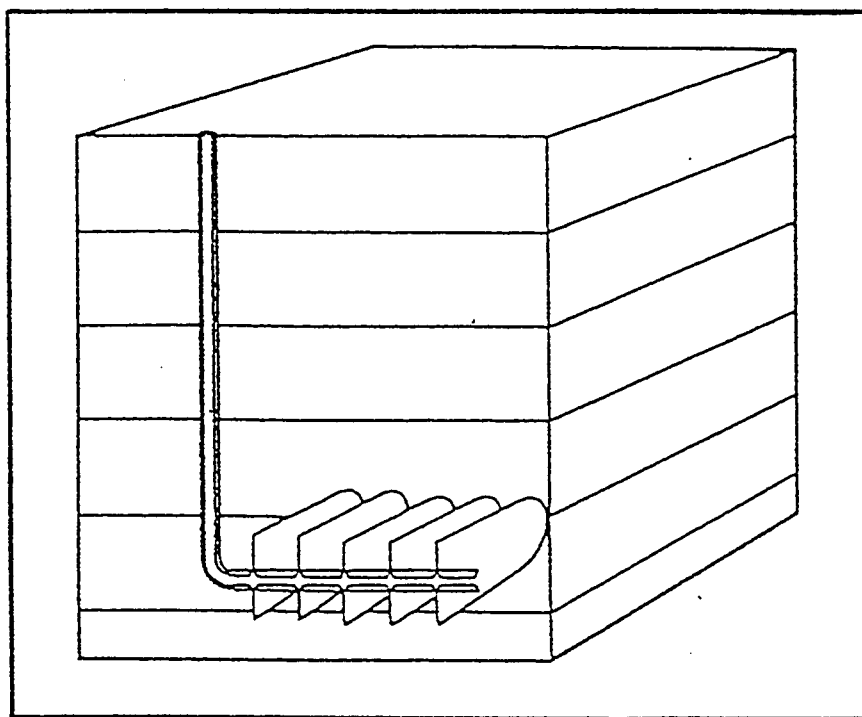
Figure 2.17: Multiple Transverse Hydraulic Fractures, [3].
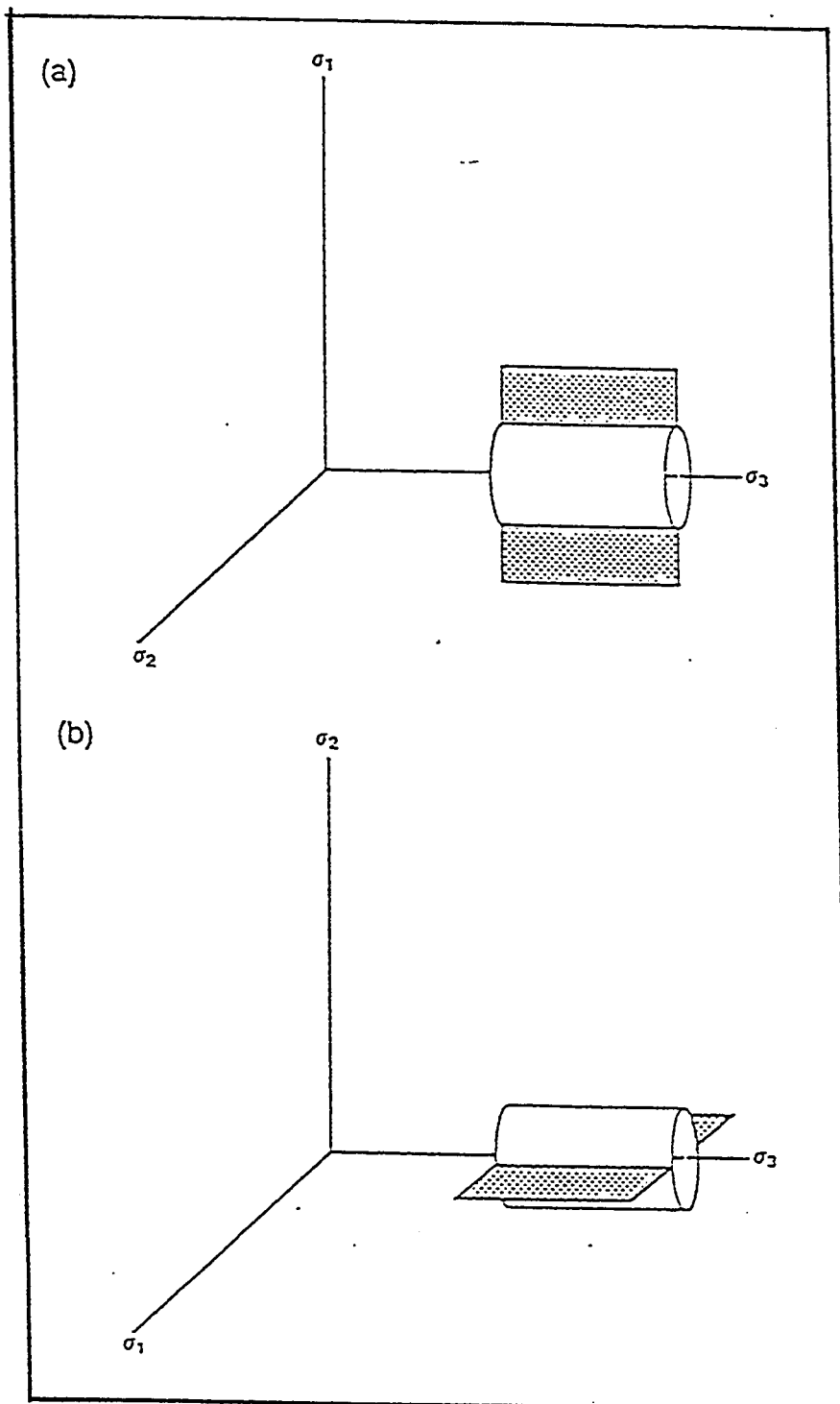
Figure 2.18: Longitudinal Hydraulic Fractures, [3]

2.3.2.1 Transverse or Orthogonal Fractures

The increased productivity caused by the presence of transverse fractures, Fig. 2.17, has been studied analytically and numerically by several authors [38,43,44,45,46,47].

Mukherjee and Economides [44] developed a simplified linear flow steady-state approach to calculate the number of infinite conductivity fractures equivalent to a drainhole. They presented the following equations to predict production rates:

$$(P_D)_{total} = P_D + (S_{ch})_c = \frac{k\,h\,\Delta P}{141.2\,q\,B\,\mu} \quad \text{for } oil \tag{2.17}$$

$$(P_D)_{total} = P_D + (S_{ch})_c = \frac{k\,h\,\Delta m(P)}{141.2\,q\,B\,\mu} \quad \text{for } gas \tag{2.18}$$

$$(S_{ch})_c = \frac{k\,h}{k_f\,w} \left(\ln(h/2r_w) - \pi/2 \right) \tag{2.19}$$

Where;

P_D = dimensionless pressure

k = permeability, md

h = reservoir thickness, ft

ΔP = pressure drop, psi

q = flow rate, bbl/d

B = formation volume factor, resbbl/STB

μ = viscosity, cp

k_f = fracture permeability, md

w = fracture width, ft.

r_w = wellbore radius, ft.

$m(P)$ = real gas pseudopressure, p s i^2/cp

$(S_{ch})_c$ = the choke skin effect.

The dimensionless pressure drop (P_D) can be obtained from Cinco-Ley and Samaniego [48]. The skin effect is additive to the dimensionless pressure (P_D) for each individual fracture. The skin effect is zero when the well is colinear with the fracture(s).

Economides, et. al. [3] presented an example to show the performance comparison between vertical well with vertical fracture and horizontal well with orthogonal vertical fracture.

Soliman, et. al. [38] and Schulte [43] considered a radial-linear flow model to study the early time (unsteady state) transient behavior of transverse fractures. In their model [38], it is assumed that the fluid flows linearly from the formation into the fracture, and then flows radially inside the fracture into the wellbore. The fracture is assumed to have two distinct conductivities that are radially discontinuous.

The equations governing fluid flow in the formation and fracture are solved with a single-phase finite-difference simulator. The simulator [47,49,50] which solves the governing equations implicitly, was applied to an actual field case. Table 2.3 gives the reservoir properties for Figs. 2.19

TABLE 2.3: Well and Reservoir Parameters
For Figures 2.19 - 2.22, [26] .

k ,md	0.10
Porosity, %	13.00
h, ft	272.00
Pi, psia	4000.00
T_{bh} , °F	150.00
P_{wf} , psia	50.00
A, acres	170.00
S_w , %	50.00
X_f , ft	136.00
C_t , md-ft	1,381.00
W, in.	0.19

through 2.22.

In Fig. 2.19, the total flow rate is plotted vs. the number of fractures at various times, while Figs. 2.20 and 2.21 show cumulative production vs. time and number of fractures, respectively.

Reservoir heterogeneity and directional permeability also affect the optimum number of fractures. The effect of directional permeability on the optimum number of fractures is investigated with the simulator by varying the ratio of horizontal permeabilities. Fig. 2.22 shows the cumulative production vs. the number of fractures at 6 and 24 months. The two permeabilities considered are k_x being the permeability parallel to the fracture plane (perpendicular to the horizontal wellbore axis) and k_y being perpendicular to k_x. It can be seen from Fig. 2.22 that as k_x/k_y increases, the optimum number of fractures increases. However economics should be considered for definite optimization.

Soliman, et. al. [38] studied the effect of fracture conductivity on the pressure drop through the system and pointed out that high fracture conductivity is extremely important for horizontal wells. Their discussion agrees with the conclusions reached by Soliman [45,46] who stated that the fracture performance depends on the magnitude and the distribution of conductivity and does not depend solely on the average conductivities, as concluded by Bennett, et. al. [47]. They also concluded that if high or essentially infinite conductivity is feasible, an optimum number of fractures may be obtained. This optimum number depends on formation and fluid properties and on the presence of
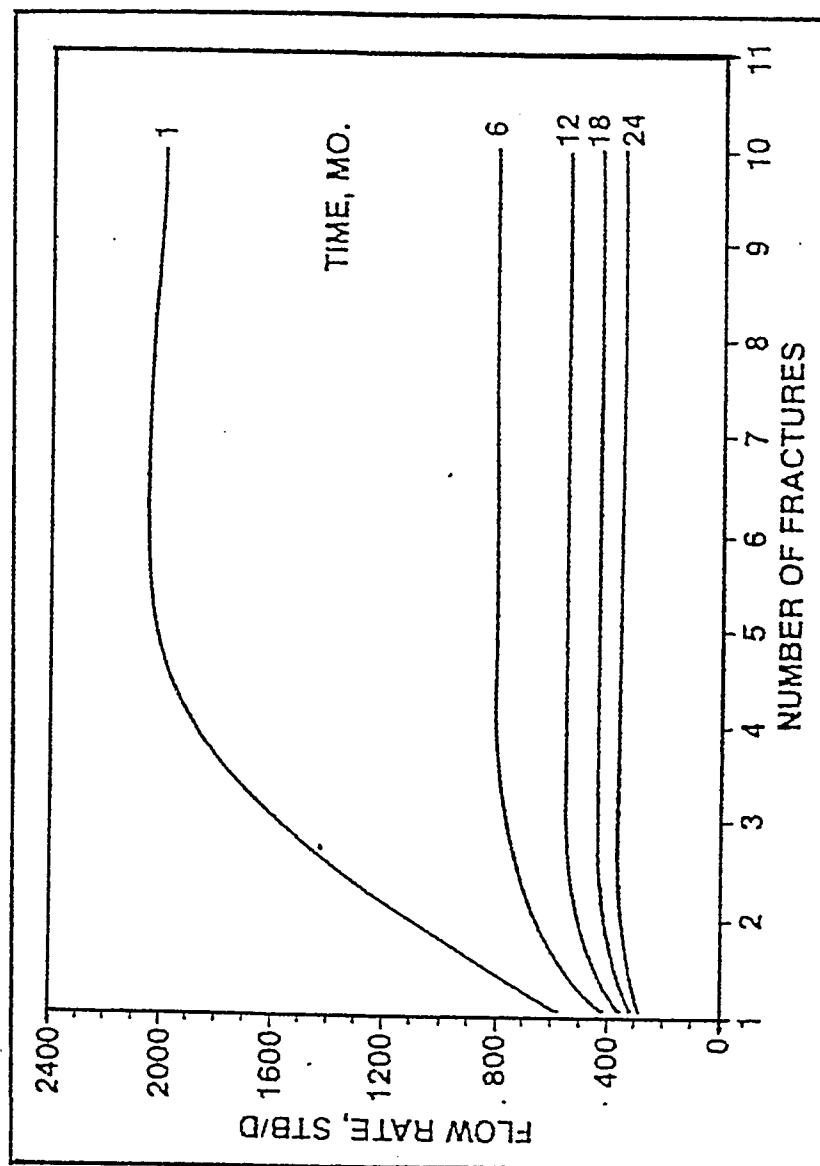
Figure 2.19: System Flow Rate vs. Number of Fractures, [38].
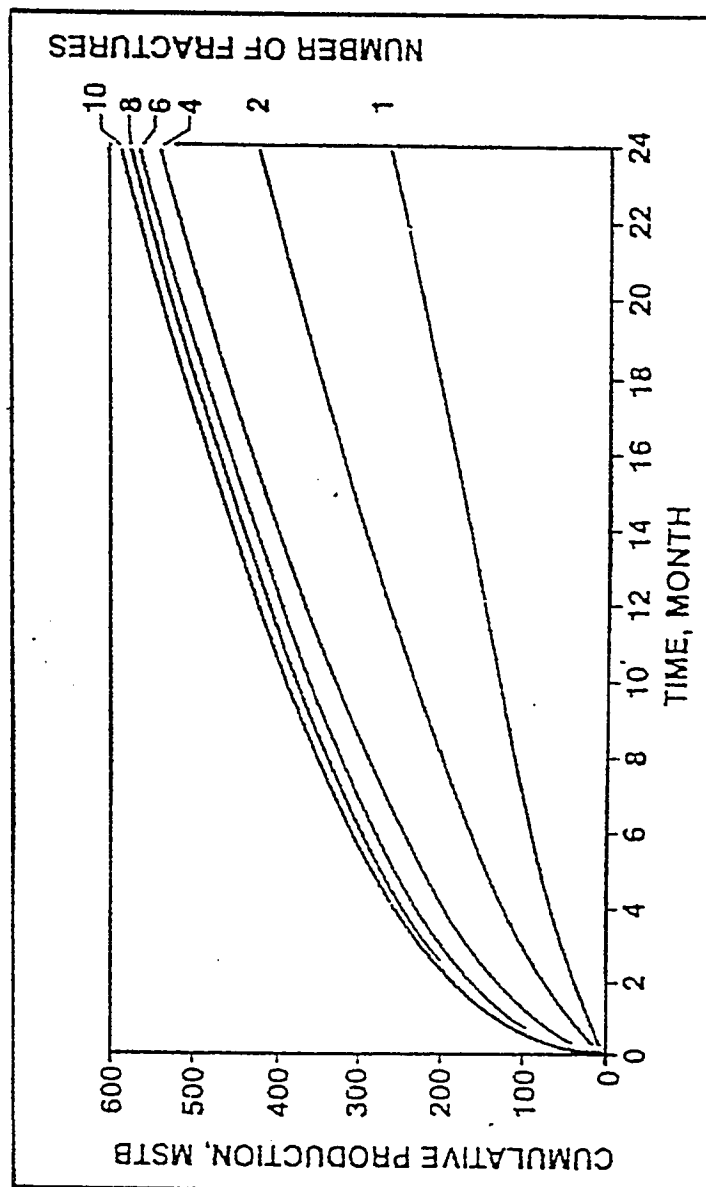
Figure 2.20: Cumulative Production vs. Time, [38].
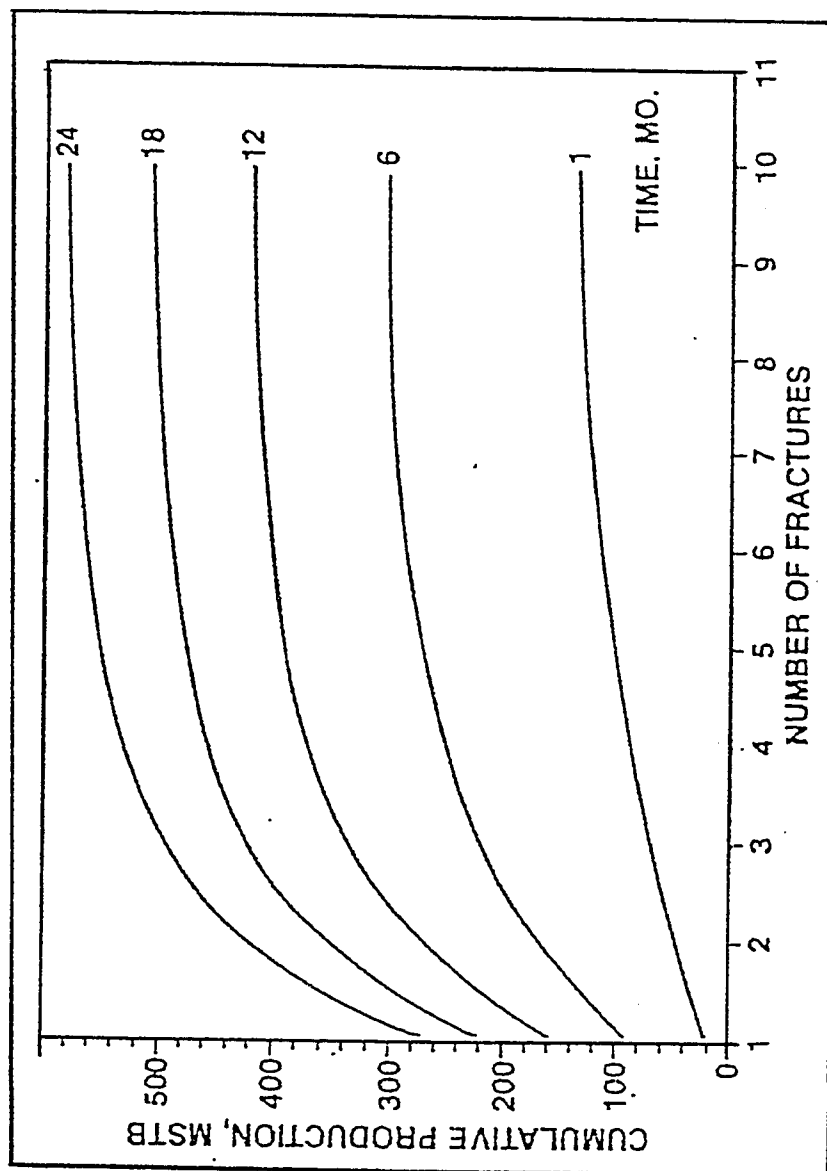
Figure 2.21: Cumulative Production vs. Number of Fractures, [38].
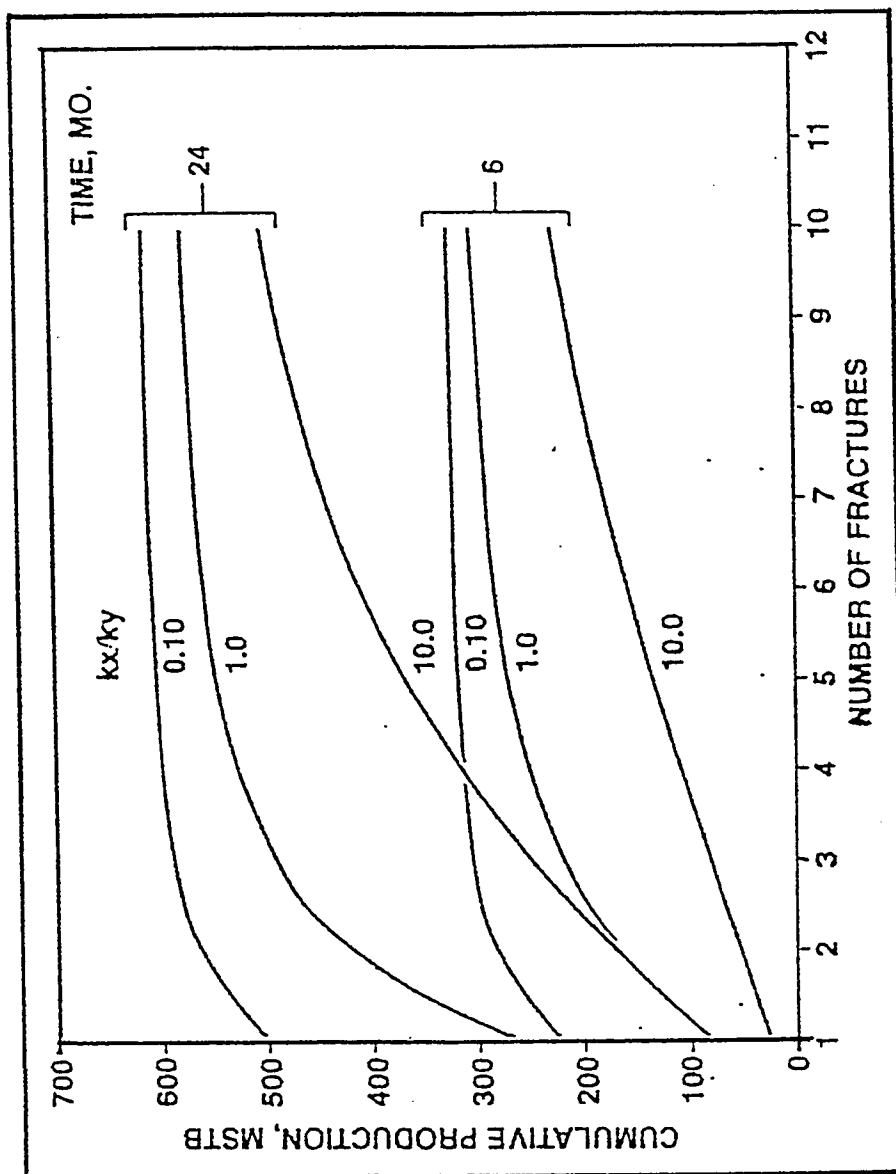
Figure 2.22: Cumulative Production vs. Number of Fractures for the Effect of Directional Horizontal Permeabilities, [38].

natural fractures.

The projected productivity improvement of creating a number of 100-ft radius fractures in a North Sea Chalk zone penetrated by a horizontal well is shown in Fig. 2.23 [35]. Note that the incremental gains for fracture densities greater than 6/1000 ft become progressively less due to the increased interference between the fractures.

2.3.2.2 Longitudinal (Axial) Fractures

In this case the well is drilled perpendicular to the direction of the minimum principal stress, or parallel to the maximum horizontal stress, Fig. 2.18.

Economides, et. al. [3] presented a performance comparison in Fig. 2.24, in which:

$(P\,I)_H$ = productivity index of a horizontal well with a longitudinal fracture.

$(P\,I)_V$ = productivity index of a fractured vertical well at steady state.

L = the horizontal well length and fracture length.

X_f = fracture length in a vertical well.

h = reservoir thickness.

F_{CD} = dimensionless fracture conductivity, or:

$$F_{CD} = \frac{k_f\,w}{k\,x_f}$$

(2.20)
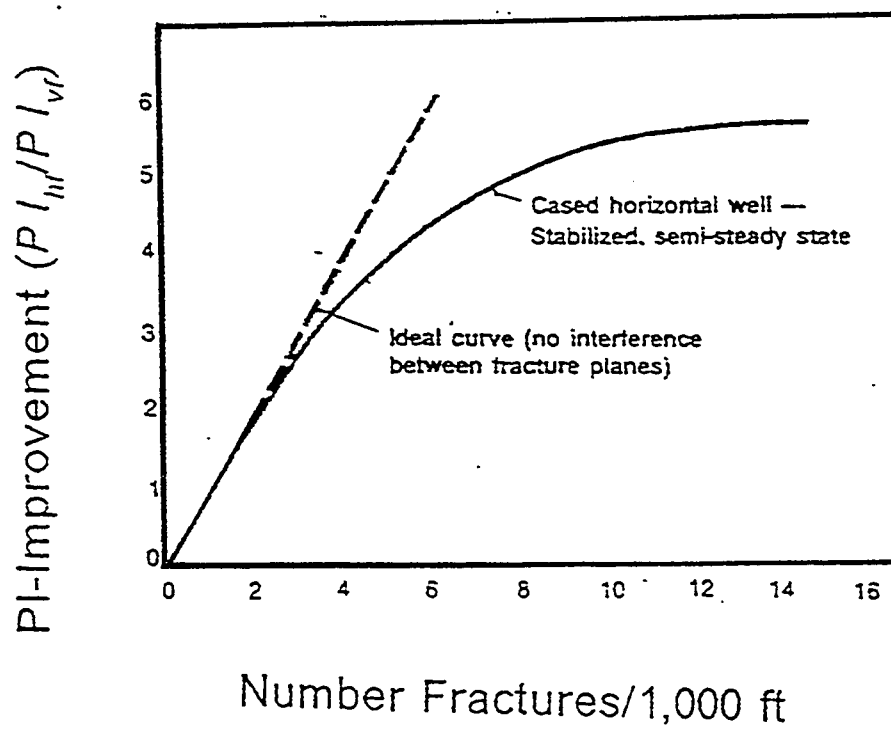
Figure 2.23: Multiple Fractures Performance, [35].
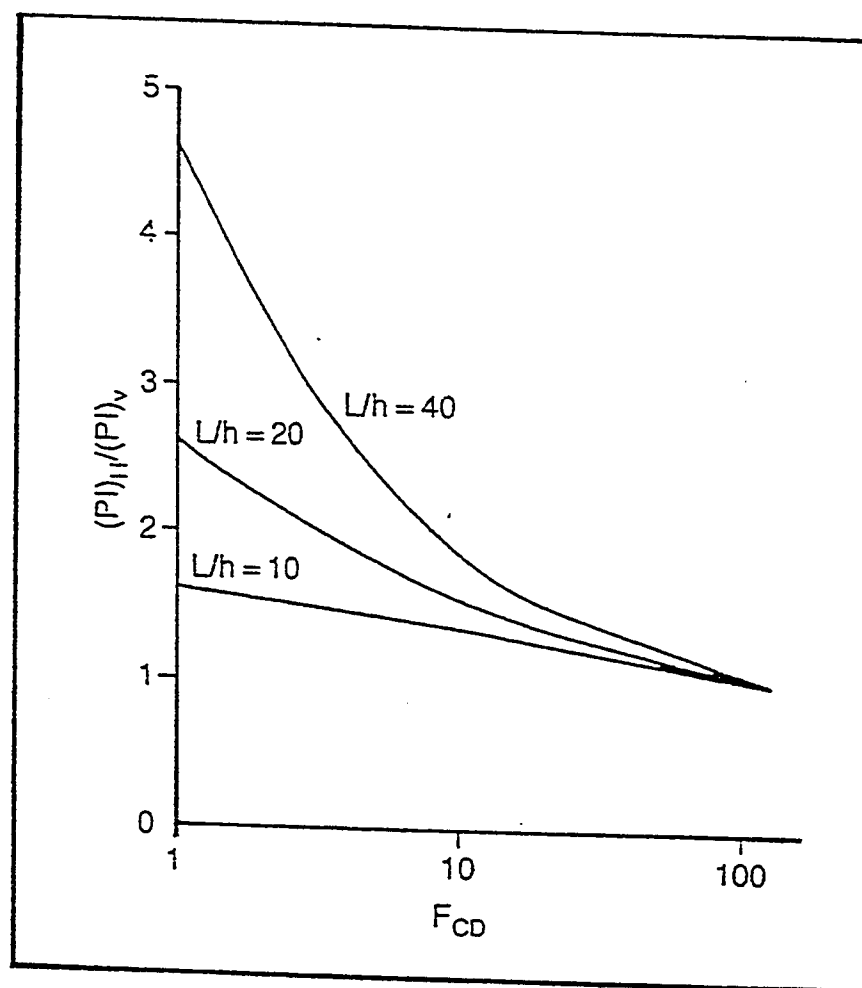
Figure 2.24: Productivity Index Ratios of Vert. Well/Vert. Fracture and Horiz. Well with a Longitudinal Fracture, [3].

Where;

k_f = fracture permeability.

w = width of the fracture.

Review of the performance of both transverse and longitudinal fractures indicates that below F_{CD} of 5 a transverse fracture would not be effective; consequently, it is not recommended to create transverse fractures in high permeability formations [11]

2.3.3 Fracture Treatment in Horizontal Well

Although few horizontal wells have been fractured to date, there are some guidelines that should prove helpful in designing fracture treatments for such wells [36]. Fracture treatments are commonly utilized in vertical wells to extend the effective well bore radius. The horizontal well bore has been compared to an infinite conductivity vertical fracture [28,34]. This has fostered an "either-or" approach when considering the use of horizontal well completions and fracture treatments. Yet there may be situations when these applications should be used in conjunction with optimizing reservoir drainage. Carmer [36] studied the practicalities of conducting a fracture treatment in a horizontal well and favorable conditions for fracture treatment applications.

Horizontal well performance is affected by the magnitude of reservoir height and degree of permeability anisotropy. Computer simulations indicate that production from a massive, low permeability reservoir will not be signifi-

cantly improved by the exclusive use of horizontal wellbore [28].

Reservoir permeability anisotropy, characterized by low vertical to horizontal permeability ratios ($\frac{k_v}{k_h} < 1$), also reduces the productivity of a horizontal well. Carmer [36] and Joshi [28] pointed out that creating vertical fracture in a horizontal well is necessary with layered rock such as an interbedded sand/shale sequence. In such cases where vertical to horizontal permeability ($\frac{k_v}{k_h}$) ratios can be extremely low, the vertical fracture will vertically connect the individual porosity layers.

Another phenomena that can impair the productivity of a horizontal well is the formation damage induced by drilling and completion operations. This problem is often rectified by perforating, surging, or small scale acid/solvent treatments. However, in naturally fractured formations or open hole type completions, the damage radius may be very sensitive or difficult to access. Fracture stimulation may be necessary to clean-up or by-pass this damage.

Careful considerations should be given to proximal gas caps or water aquifers when considering a fracture treatment. Fracturing treatments are obviously not appropriate for horizontal wells drilled for the purpose of eliminating gas/water conning. However, in low permeability reservoirs, conning may be inevitable at realistic production rates, even for an unfractured well [51].

Carmer [36] outlined the primary objectives of fracture treatments in horizontal wells as:

1- Extend the wellbore radius in the vertical plane

2- By-pass wellbore damage.

This will be most efficiently accomplished by creating a limited number of short, highly conductive fractures along the wellbore axis. Carmer [36] discussed a variety of completion and stimulation techniques that are available to expedite this process.

A horizontal wellbore, unlike a vertical well, may be fractured at several locations along its axis. This provides the potential to significantly increase contact area without the level of risk associated with excessive fracture height growth for those reservoirs requiring extensive fracture penetration [37,52-56].

Fracturing treatments in horizontal wells can be grouped into three general classifications. These include: the creation of single to multiple longitudinal fracture(s), the creation of multiple transverse fractures, and high rate, open-hole treatments sometimes referred to as "water fracs" or often described conceptually as dendritic fracturing [52].

Hudson and Matson [52] studied and presented three examples of the engineering methodology for each of these types of treatments in order to demonstrate their application. They used three-dimensional reservoir and fracturing simulators.

They concluded that:

1. Hydraulic fracturing of horizontal wells in low permeability reservoirs is technically feasible and, for favorable conditions, can provide a cost competitive, alternative reservoir drainage method.

2. Optimum fracture orientation and length can be ascertained by careful consideration of a reservoir's geometry, permeability, stress contrast, and fluid saturations.

3. Significant flow restrictions, resulting in production loss, can be created when fracturing a borehole substantially misaligned with the orientation of the in-situ principal stresses.

4. Slot-type perforating or notching may reduce the potential for undesirable reorientation effects due to wellbore/principal stresses.

5. Multiple, longitudinal fractures for certain stress scenarios and reservoir fluid distributions can be created to reduce the potential for undesirable fracture height growth.

6. Predicting the net present value, with reasonable accuracy, is the key to determining the applicability of the methods used in horizontal well stimulation.

2.4 HORIZONTAL WELLS FOR EOR AND WATERFLOODING

The use of horizontal wells has been increasing rapidly throughout the oil industry as advances in drilling and completion techniques continue [57-70].

The interest in horizontal-well waterflooding and enhanced oil recovery (EOR) is recent [71-82]. Horizontal injection wells have been proposed to increase flow rate and improve areal sweep efficiency.

Taber and Seright [83] described the improvements in sweep efficiency and flooding rates that are possible if horizontal wells are used for any EOR method which requires the use of both injection and production wells. In addition, the potential for increased microscopic displacement efficiency at the faster rates (with no increase in well-head pressure) is examined for some of the EOR methods. They considered opposed parallel production and injection horizontal wells and presented the following equations for five-spot pattern:

$$q_{HW} = q_L \left[\frac{\pi L}{\pi L + 4.60\, h \, \log(\frac{1/2\, h}{r_w})} \right] \qquad (2.21)$$

$$q_L = \frac{4.52 kh \Delta p}{\mu} \qquad (2.22)$$

Where:

q_{HW} = flow rate between opposed parallel horizontal wells, bbls/day

q_L = linear flow rate between parallel faces of a reservoir block, bbls/day

h = formation thickness, ft

k = permeability, darcies

r_w = well face radius, ft

Δp = pressure difference between injection and producing well, psi

μ = viscosity, cp

Equation 2.21 shows how closely the flow between the horizontal holes approaches a linear flood for very thin formations. However, for thick pay zones and/or close spacing, the horizontal-well rate departs appreciably from the linear flow maximum as more of the injected fluid flows in a radial-flow regime.

They also adapted Muskat's direct-line-drive equation [84] to estimate sweep efficiency (E_h) in a unit-mobility displacement for opposed horizontal wells as a function of formation thickness (h) and pattern size (L):

$$E_h = 1 - \frac{0.441h}{2L} \qquad (2.23)$$

Fig. 2.25 is generated using eqn. (2.22). This figure compares anticipated sweep efficiencies (at breakthrough for unit-mobility displacements in homo-
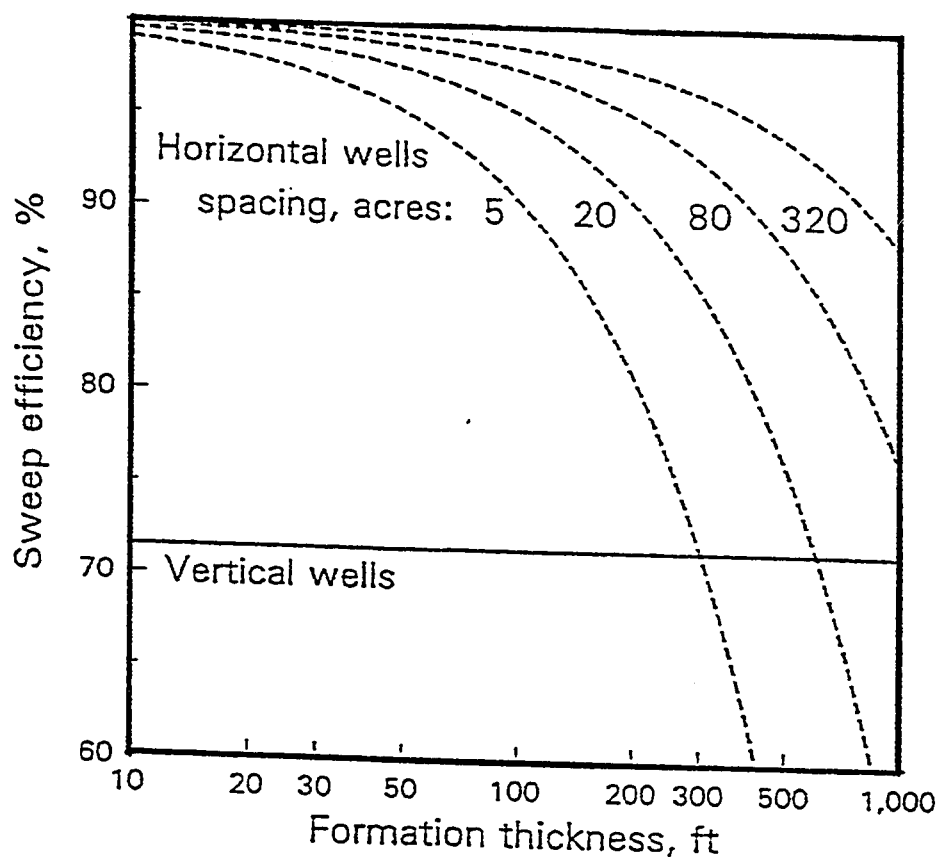
Figure 2.25: Comparison of Sweep Effcs for Vert. vs. Horiz. Wells (Parallel and Opposed in 5-Spot Pat., Unit mobility), [83].

3C

geneous formations) for opposed horizontal wells with those for vertical wells in a five-spot pattern. In this comparison, sweep efficiencies for the vertical wells are independent of well spacing and formation thickness. However, for horizontal wells, sweep efficiencies decrease with increased formation thickness and/or with decreased well spacing.

They concluded that:

1. The faster flooding rates and improved sweep efficiencies that are possible with combinations of horizontal injection and production wells should be very beneficial for waterflooding and the following EOR processes: thermal recovery, CO_2 flooding, hydrocarbon-miscible flooding, micellar/polymer (low IFT) flooding, and polymer flooding.

2. Injection/production rates can be increased (with no increase in pressure) by using combinations of horizontal injection and production wells in thin formation and at wide spacing. The advantage of faster rates with horizontal wells (compared to vertical-well pattern) decreases for thicker formations and/or closer spacing.

3. Significant increase in areal sweep efficiency are possible with horizontal injection and production wells. The sweep efficiency is greatest for thin formations and wide spacing. For thick formations and closer spacing, it appears that there will be no advantage over vertical well pattern.

4. The faster rates possible with horizontal wells should increase the microscopic displacement efficiencies for EOR methods such as micellar/polymer (surfactant) flooding, that show increased recoveries at higher capillary numbers.

5. Advantage of horizontal wells for CO_2 flooding include: (a) delayed CO_2 breakthrough because of the better sweep efficiency, (b) The potential for maintaining the minimum miscibility pressure (MMP) in the reservoir with no increase in the injection pressure, (c) better injectivity at the same pressures, and (d) the opportunity to convert more pumped producers to flowing well.

6. Polymer floods should be improved by the higher injectivity and lower rates of shear at the injection sandface (Fig. 2.26) that are possible with horizontal wells

7. Further research, development, and economic studies are needed to determine the most beneficial ways for the application of horizontal-well technology to all injection methods and EOR.

2.5 PATTERN SIZE AND SHAPE FOR REGULAR ARRAYS OF HORIZONTAL WELLS

Supronowicz and Butler [85] presented a two-dimensional model to calculate pressure distribution in the drainage area around a horizontal well. Knowing the pressure distribution, a method for pattern size optimization is
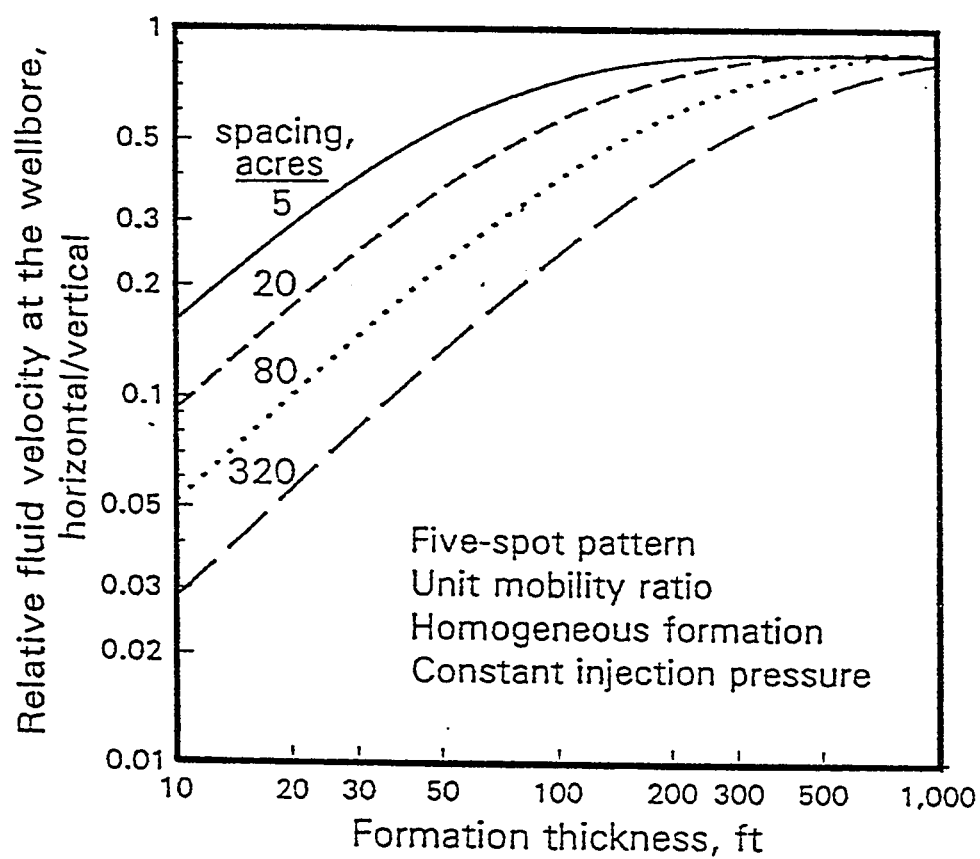
Figure 2.26: Comparison of Fluid Velocities at the Wellbore for Horizontal versus Vertical Well, [83].

developed. It is assumed that the well is placed in the center of a rectangular area of the reservoir, Fig. 2.27, and the pseudo-steady state flow period is only considered.

They used a finite difference scheme to replace the second order partial differential equation. The finite difference equations are written in a matrix notation as:

$$AP = d \qquad (2.24)$$

Where A is the matrix coefficients, d is vector coefficients and P is the expected solution matrix. More details can be found in [85,86].

For the construction of the grid system, the point-distributed grid method [87] is used. Results of some calculations are shown in Figs. 2.28 to 2.31 [85]. Figs. 2.28, 2.29 and 2.30 show the distribution of equipressure lines for different well lengths and different aspect ratio, $\alpha = b/a$ where a is the length of the drainage pattern and b is the width. Fig. 2.31 shows a three-dimensional projection of a pressure distribution in the pattern area. Dimensionless coordinates used for these figures are defined by:

$$X' = \frac{x}{a/2} \text{ , and;}$$

$$Y' = \frac{y}{b/2}$$
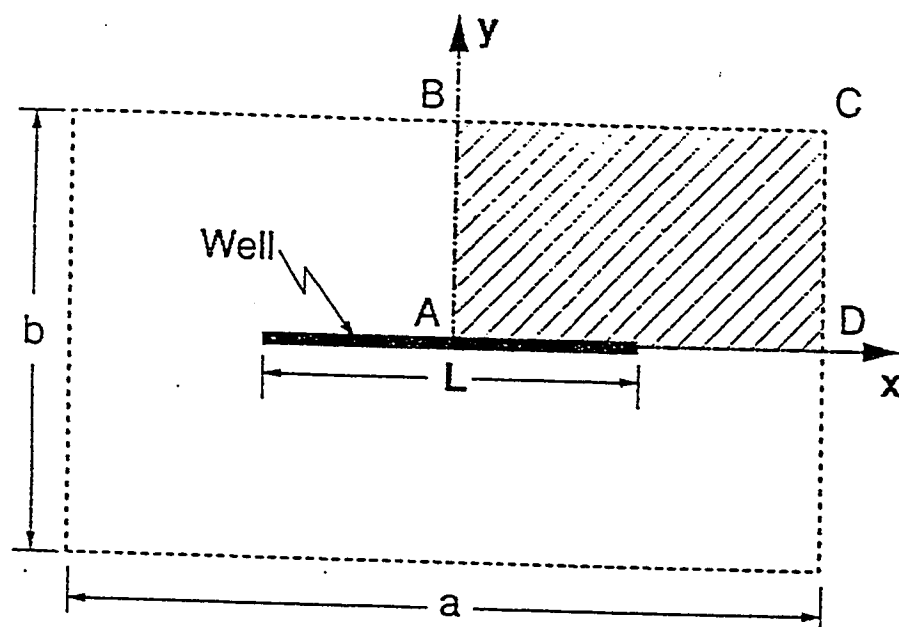
Figure 2.27: Schematic Diagram of a Rectangular Drainage Area with Centrally Located Horizontal Well, [85].
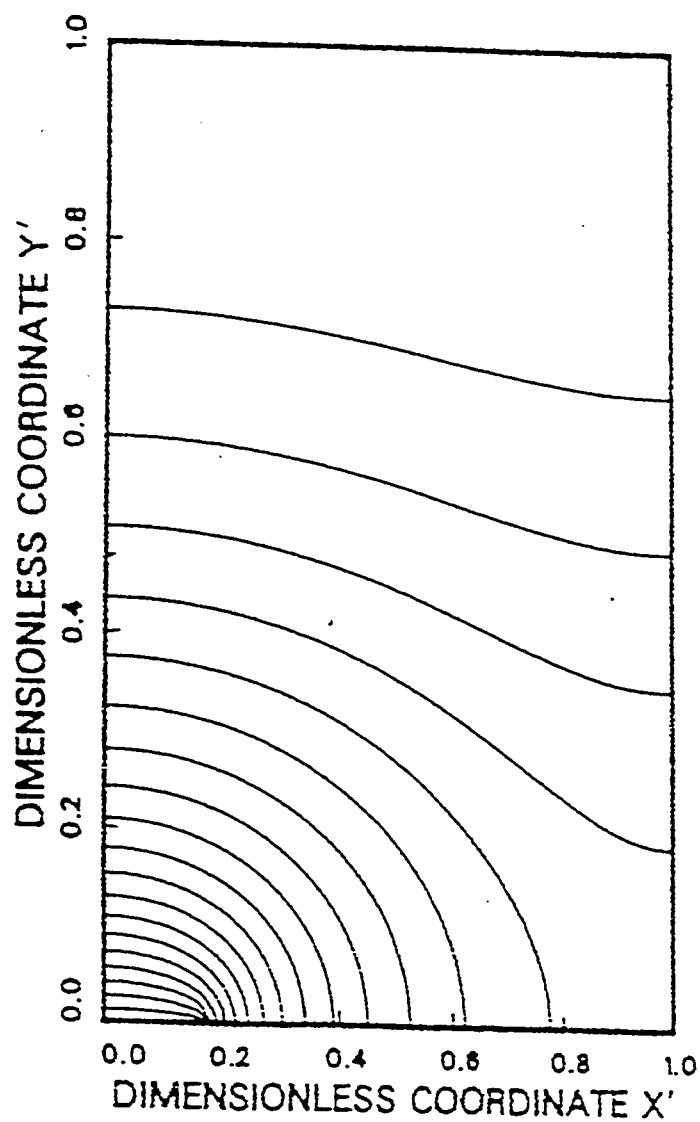
Figure 2.28: Pressure Distribution in the Drainage Area within m = 58, n = 58 w = 10, b/a = 1.5955, [85].
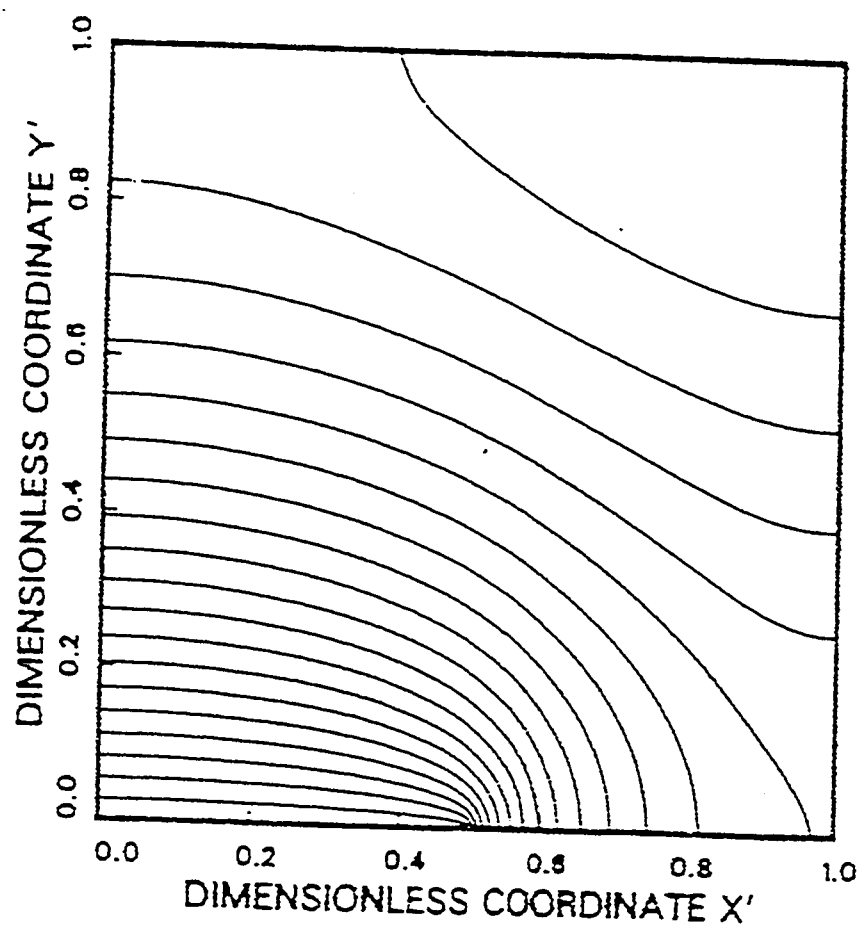
Figure 2.29: Pressure Distribution in the Drainage Area within
m = 100, n = 100 w = 50, b/a = 1.0, [85].
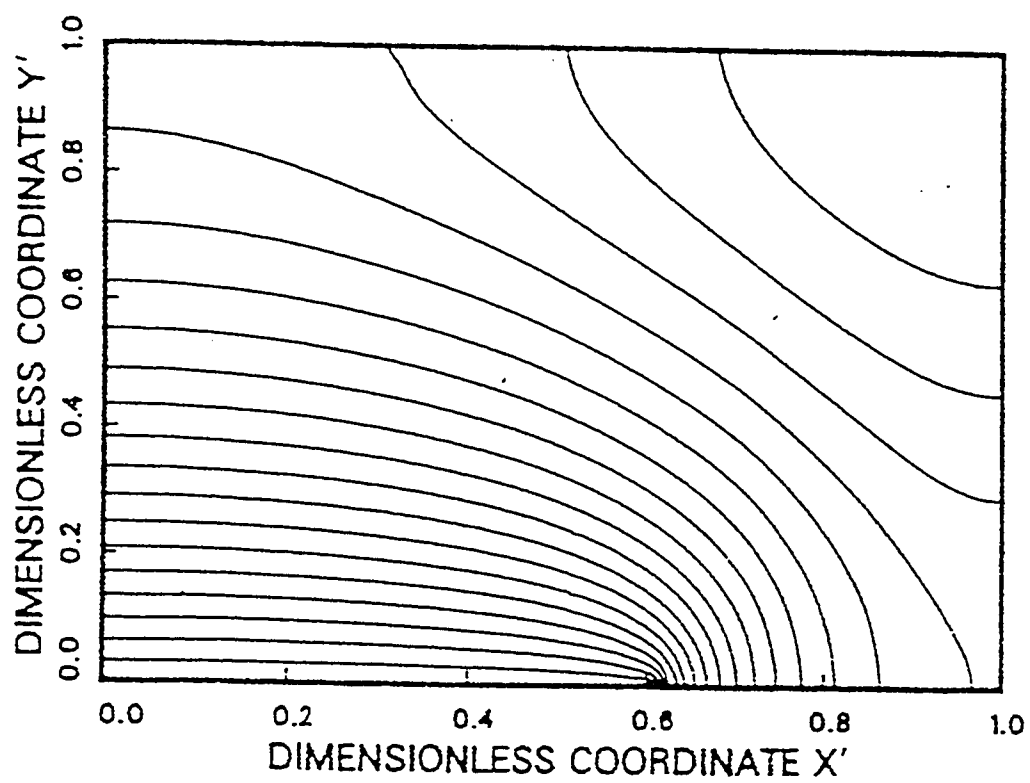
Figure 2.30: Pressure Distribution in the Drainage Area within m = 60, n = 60 w = 37, b/a = 0.6849, [85].
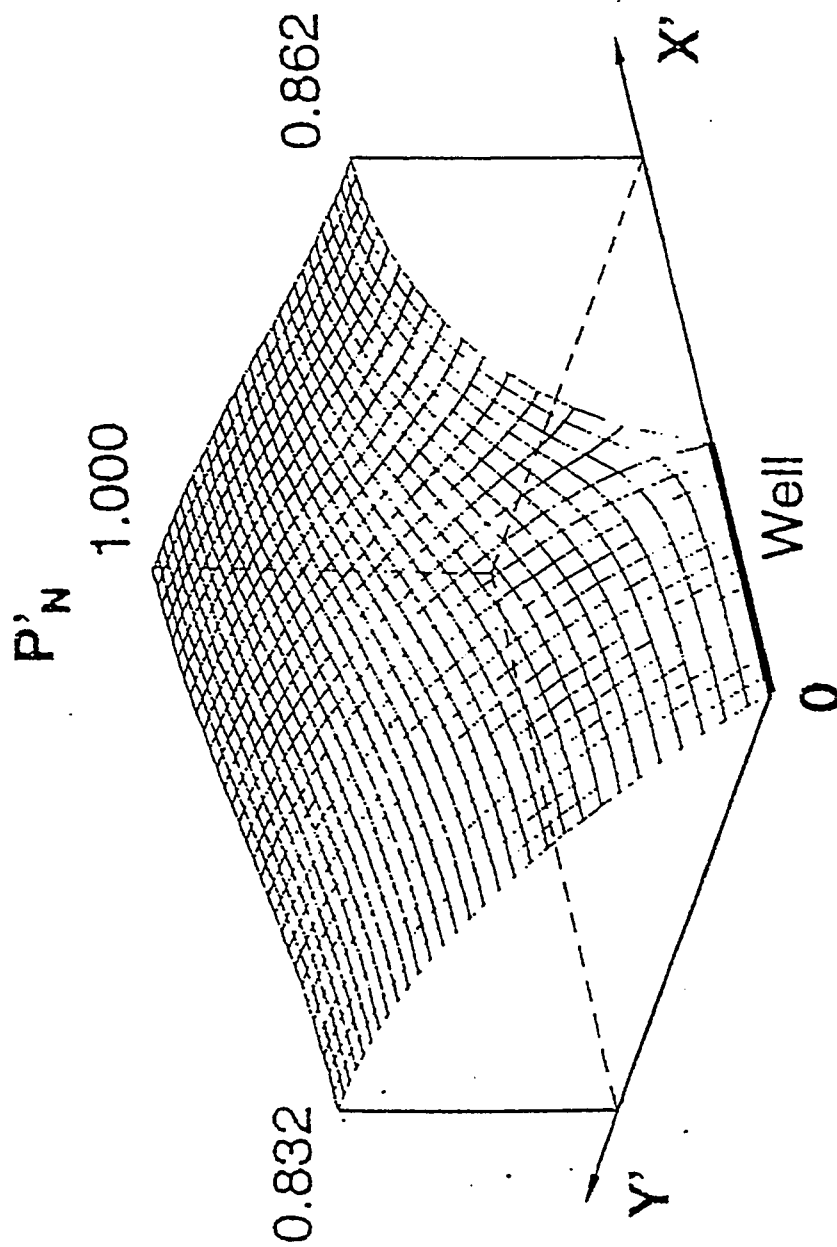
Figure 2.31: Three Dimensional Projection of the Normalized Dimless *s*: Pres. Dist. in the Drainage Area $m=31$, $n=31$, $w=15$, $b/a=1$, [8.5].

Supronowicz and Butler concluded that the simple empirical formula: $\alpha = \beta/(1 + \beta)$ may be used to define the relation between the optimal aspect ratios α and β where:

$\beta = A/L^2$,

$A = ab$, and;

$L =$ the length of the horizontal well.

Chapter III
STATEMENT OF THE PROBLEM AND
STUDY OBJECTIVE

Horizontal well technology is still developing. The literature is somewhat rich with recent research work dealing with this technology. Most of the work done, however, has been dealing with theoretical and numerical simulation of horizontal well performance. With the exception of the recent published experimental investigation of horizontal well performance for heavy oil recovery [1,13,14,18-22], very little experimental work has been done. In particular, no experimental work has been conducted to investigate the performance of horizontal wells in conventional oil reservoirs with bottom-water drive.

The main objective of the present study is, therefore, to investigate experimentally and theoretically the production performance of horizontal wells without and with fractures in bottom Water-drive reservoirs. the performance of horizontal wells is also compared with that of fractured and unfractured vertical wells.

To achieve this objective, a scaled model is built to simulate a typical section of a bottom water-drive reservoir. The reservoir model will be produced at a constant rate lower than the critical rate to stabilize the movement of the oil-water interface and eliminate the effects of viscous fingering on the

process. Various wellbore/fracture(s) configurations are studied: a series of vertical well, vertical well with vertical fractures, horizontal well, horizontal well with longitudinal fractures of various dimensions and horizontal well with single and multiple orthogonal fractures of various dimensions.

Comparison of the oil recoveries, water cuts and pressure drops of the various producing conditions is made to provide some basis for the determination of the best production strategy for such type of reservoirs.

Chapter IV
EXPERIMENTAL APPARATUS AND
PROCEDURES

4.1 APPARATUS

A schematic diagram of the experimental apparatus is shown in Figure 4.1; it consists of the following:

1. Three-Dimensional Physical Model:

A visual physical 3-dimensional scaled model is constructed using one inch (2.54 cm) thick plexiglass. The inner dimensions of the model are: 18 inches (45.72 cm) long, 12 inches (30.48 cm) wide, and 6 (15.24 cm) inches oil reservoir thickness. The bottom-water aquifer is represented by 2 inch (5.08 cm) water thickness underlying the oil reservoir. Using a dimensional ratio of 75 between the reservoir (prototype) and the model, this model would represent a section of a real reservoir of 112.5 ft long, 75 ft wide and 37.5 ft oil thickness. Details of the model scaling procedures are given in Appendix A. A 0.5 in. (1.27 cm) thick plexiglass plate uniformly perforated (805 perforations) separates the upper porous medium containing the oil from bottom water reservoir but provides excellent communication between the zones. A 150 mesh screen is
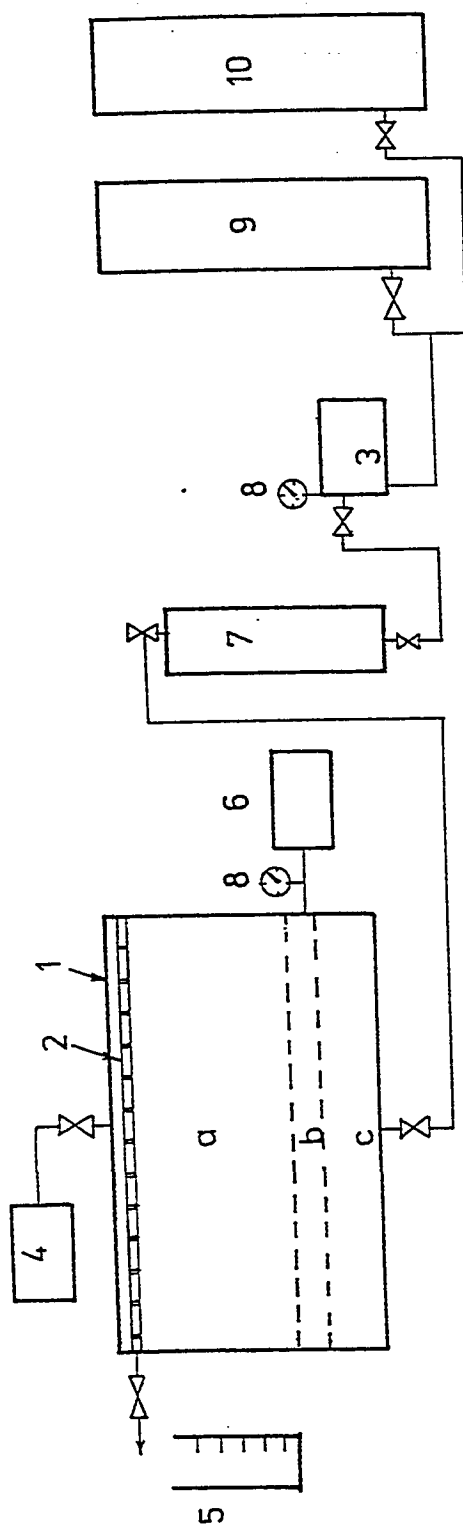
(1) Model
    (a) Oil Reservoir
    (b) Perforated Plate
    (c) Bottom water Reservoir
(2) Producer, horizontal well
(3) Injection Pump

(4) To Vaccum Pump
(5) Graduated Cylinder
(6) Pressure recorder
(7) Pulsation dampener
(8) Pressure Gauge
(9) Water Container
(10) Kerosene Container

Figure 4.1:   Schematic Diagram of the Model and Apparatus.

placed on the top of the perforated plate to retain the grains of the porous medium. A schematic of the three-dimensional physical model is shown in Fig. 4.2.

The wellbore is simulated by a tube of 0.25 inches (0.635 cm) OD and 0.181 inches (0.46 cm) ID. The tube is perforated using a perforator diameter of 0.0236 inches (0.06 cm); the number of perforations per inch is 28. For the horizontal well, the tube is inserted horizontally in the y-direction through the model at 5.125 inches (13.02 cm) above the bottom of the oil zone. For the vertical well, however, it is placed vertically in the z-direction at the center of the model.

The model sides and the perforated plate are fixed together, then the top, bottom, and sides of the model are tied to each other by bolts. Rubber seals are used to prevent leakage when the model is pressurized with fluids.

2. Fluid Injection Pump:

An Eldex double piston positive displacement pump model BBB-4 is used to inject water or oil during saturation of the pack with fluids. This pump is used also to inject water into the model during the recovery process. The pump is designed to inject fluids under a maximum back pressure of 5,000 psi at adjustable constant rates ranges between 0.2 and 100 cc/min. The pump rate is viscosity dependant.

75
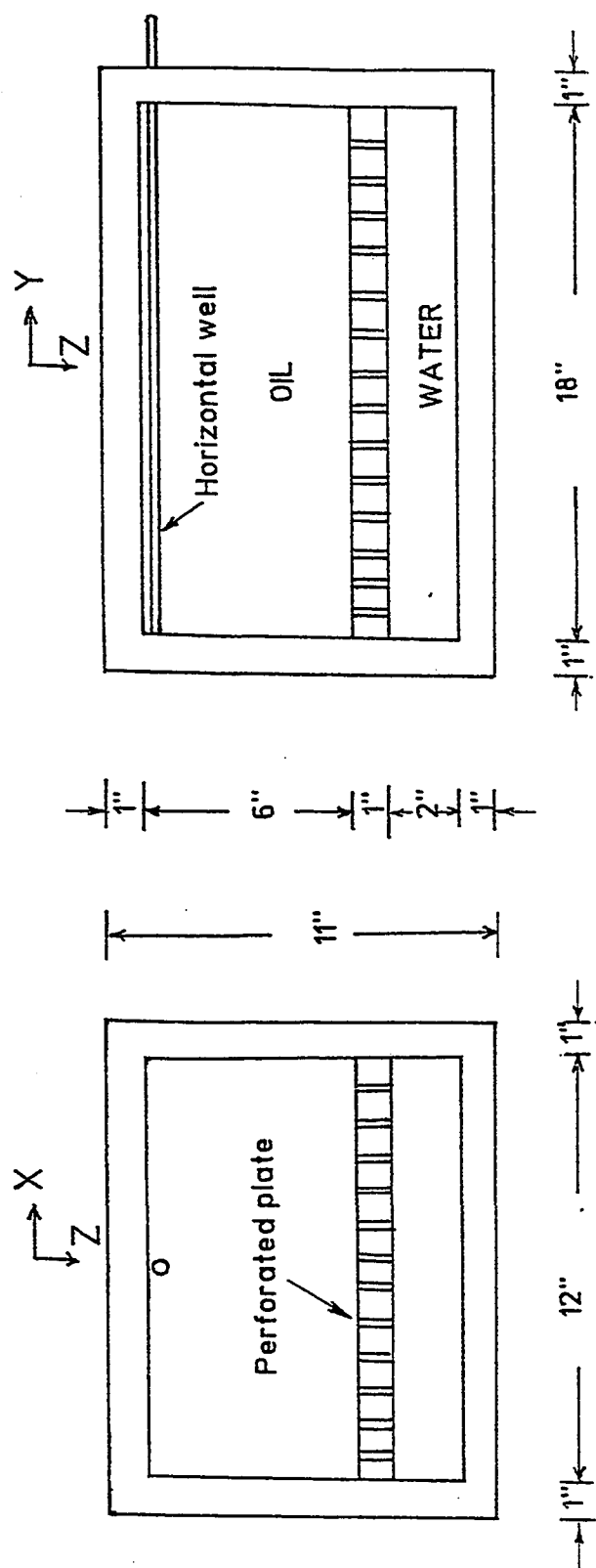
Figure 4.2: Schematic of the Three-Dimensional Physical Model.

3. Vacuum Pump:

A Pfeiffer Balzer Vacuum pump model DUO 008 is used to evacuate the air from the model. A vacuum pressure gauge is connected to the pump. This gauge ranges from maximum pressure of 100 mmHg to a minimum of absolute zero reading.

4. Hand Pump:.

Hand pump is used to calibrate the pressure digital display which is connected to a pressure transducer with a specific diaphragms ranges 0-1.25 psi.

5. Pressure Transducer, Digital Display, and Chart Recorder:

A Validyne pressure transducer model DP 303 with a digital display model CD23 is used to measure either the injection pressure or the pressure drop of the pack. The working range of the transducer is flexible by employing different diaphragms. A diaphragm ranges 0-1.25 psig is used in this study. The pressure due to fluids is acting on the transducer, which sends electric signals to the digital display. These signals can be recorded continuously on chart using a Soltec strip-chart recorder model 1243. During the displacement experiments, the the pressure transducer is connected and leveled at the bottom of the perforated plate below the oil reservoir. At this point, the static pressure is 0.25 psig for all runs since the water is injected upward at the bottom of the model. This pressure is due to the gravity-capillary equilibrium of fluids at static conditions.

6. Pulsation Dampener:

A cylindrical cell is used at the down stream of the injection pump to reduce or dampen the pressure pulses in order to obtain smooth pressure recording.

7. Graduated Cylinders:

Graduated cylinders of various volumes are used to collect and determine volume of fluids produced.

9. Auxiliary Equipment:

Fittings and valves, weighing balance, pressure gauges, and stop watch.

4.2 FRACTURE REPRESENTATION

Fracture design is based on the scaling criteria which are discussed in Appendix A. The fracture conductivity is kept infinite throughout the whole study while the fracture length, depth and width are varied from one experiment to another. For details, refer to Appendix A (section A.3).

The Fracture is represented by two connected sheets of wire-wrapped screen of 40 mesh size. This size of mesh is smaller than the grain size of the porous material to prevent it entering inside the fracture, and thus keeping the fracture open.

The following well/fracture geometries were employed in the present study, Fig. 4.3:

1. Vertical fracture with vertical well

2. Longitudinal fracture with horizontal well

3. Single orthogonal fracture with horizontal well

4. Multiple orthogonal fractures with horizontal well

In case of the vertical well with vertical fracture, the well is perforated throughout the fracture depth. In case of the horizontal well with longitudinal fracture, the well is perforated throughout the whole length of the fracture. However, for the horizontal well with orthogonal fracture, the well perforated interval is limited to the fracture width.

4.3 MATERIALS

4.3.1 Porous Media

Thirty mesh glass beads is used to pack the model. The porosity and absolute permeability are 36.2% and 400,000 md respectively. The procedure for the determination of the physical properties of the porous medium are described in Appendix B.

X
Z

Y
Z

9"

12"

(a) Horizontal well with longitudinal fracture

6"

1"

2"

18"
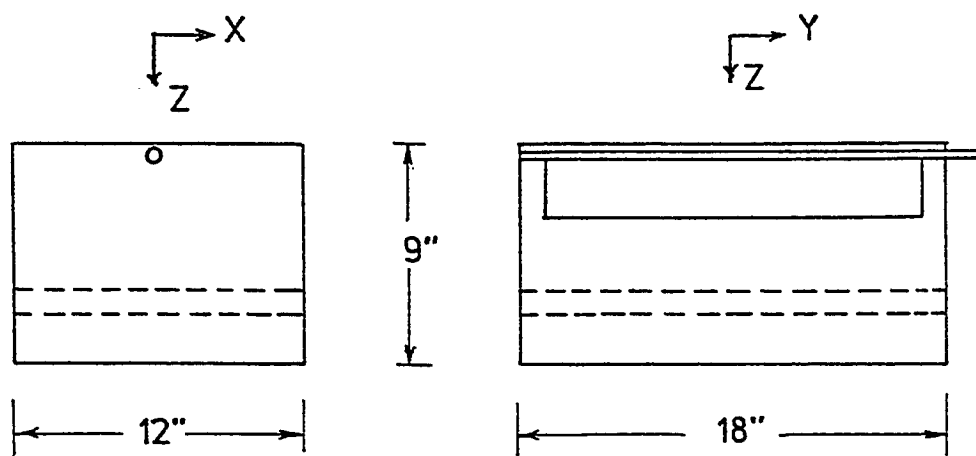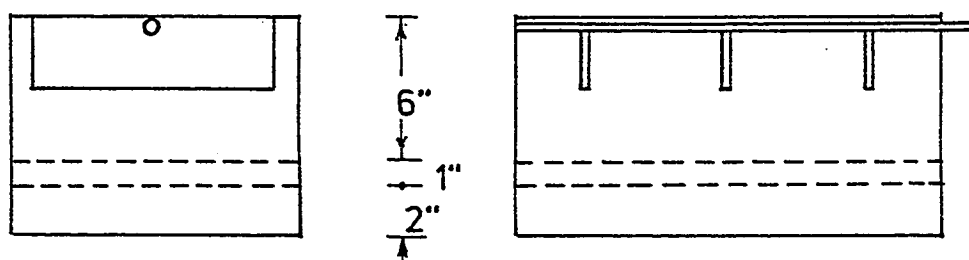
(b) Horizontal well with orthogonal fractures
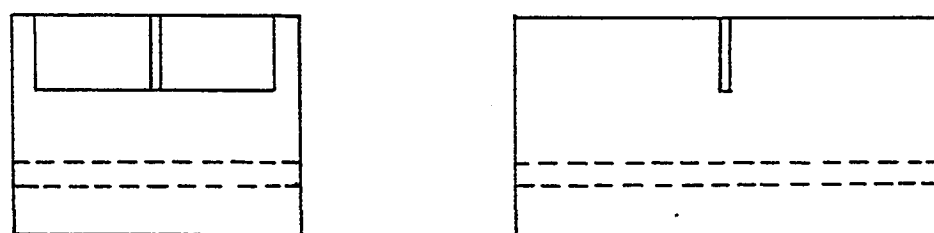
(c) Vertical well with vertical fracture

Figure 4.3: Schematic of the Wellbore and Fracture Geometries Employed in This Study

4.3.2 Fluids

The oil phase is represented by kerosene. Distilled water is used to displace oil toward the horizontal well. The density and viscosity of water are 1.016 g/cc and 1.08 cp respectively, and those of kerosene are 0.815 g/cc and 2.03 cp respectively.

4.4 EXPERIMENTAL PROCEDURES

The experimental procedures are divided into the following:

4.4.1. Cleaning and Packing Procedures

4.4.2. Saturation Procedures

    1. Evacuation of air

    2. Saturation with water

    3. Saturation with kerosene

4.4.3. Displacement Procedures

The experimental procedures are discussed in details as follows:

4.4.1 Cleaning and Packing Procedures

1. The model is first cleaned and tested under 5-10 psi for leaks.

2. The glass-beads are washed first with fresh water, then with water containing 1-2% HCl, and finally with distilled water. Then glass-beads are dried in an electric oven at 105°C

3. The glass-beads are then weighed to assure that the same amount is packed each run.

4. A vertical well or a horizontal well with or without fractures is placed at a specific position.

5. The model is packed with glass-beads using shaker to pack the glass-beads as uniformly as possible.

6. The model is sealed and evacuated. The valves, connections, pressure transducer with the digital display and chart recorder, pump, and graduated cylinders are set ready for saturating with fluids.

4.4.2 Saturation Procedures

1. Evacuation of air: A vacuum pump is used to evacuate the air from the packed model to avoid having significant gas saturations. The process continues until a pressure indicator connected to the vacuum pump reads 2-3 mm Hg (0.04-0.06 psig).

2. Saturating the system with water: While the the packed model is still under vacuum, water is injected at the bottom of the model and produced at the top till it reaches steady state. The injected pore volume (PV), porosity (φ) and absolute permeability (k_{ab}) of the pack are calculated. Details are presented in Appendix B.

3. Saturating the system with kerosene: Kerosene is then injected at the top and fluids are produced at the bottom until no more water is

produced and the steady state condition is achieved. This process is carried out under pressure of 1.0 psig to avoid having unstable process due to the effect of gravity. Then, initial volumes of water and oil are calculated. Utilizing volume of water estimated in the previous step, initial water (S_{wi}) and oil saturations (S_{oi}) are calculated and documented in Appendix C. Higher initial water saturations (26%-36%) are obtained with the three dimensional model (runs HW-04 through HW-20) compared to 16.5% with the linear model (run # HW-03). This is believed to be due to the nature of the two-phase flow in 3-dimensions and the convergence of the streamlines at the points of injection and production. Therefore, the corners of the model may not be swept well with kerosene. However, in the linear model, the streamlines are parallel in the direction of the fluid flow, hence the lowest initial water saturation. Twenty four hours is allowed for equilibrium of oil and water before starting the displacement run. During this time and due to the higher initial water saturation in the 3-dimensional model, mobile water, if any, may move under gravity-capillary forces downward and as a result oil moves in the opposite direction (upward).

4.4.3 Displacement Procedures

Water is injected into the bottom water reservoir at a fixed rate (~40 cc/min). At the same time the well is opened for production. The injection ceases at 96-100% water cut. The injection pressure is recorded while the pres-

sure at the production end is kept at atmospheric in all runs. The produced fluids (oil+water) are collected in graduated cylinders and volumes are measured. The residual oil saturation is calculated from the difference in volume of the initial charge and the produced oil.

The following experiments were performed:

1. Two base runs using horizontal and vertical wells without fractures.

2. Three runs with vertical wells having vertical fractures of various dimensions.

3. Three runs with horizontal wells having longitudinal fractures of various dimensions.

4. Four runs with horizontal wells having single orthogonal fractures.

5. Four runs with horizontal wells having multiple orthogonal fractures; two, three and four fractures.

6. Three runs to examine the reproducibility of the results.

7. One run with linear vertical model to estimate rock properties.

4.5 INJECTION RATES AND PRESSURES

The injection rate is based on some screening criteria which considers the critical flow rate at which water cresting may occur. The critical rates are calculated from eqns. (2.1) [23] and (2.3) [24]. The calculations are presented

in Appendix D for rates lower than the critical rate (about 241 cc/min.). This rate is calculated from equation (2.1) (1333 cc/min.) and multiplied by 0.181 which is the dimensionless microscopic displacement efficiency $(\varphi(1.0 - S_{wi} - S_{or}))$. A rate of injection of 40 cc/min. is used throughout the study to allow enough time for fluid collection and results analysis (about 220 minutes).

To have an idea about the range of injection pressures, the pressure drops across the model at different rates are calculated from Darcy's law for linear vertical upward flow [88]:

$$q = -1.127^*10^{-3} \frac{kA}{\mu} (\frac{\partial P}{\partial s} + 0.433 \, \gamma_f) \tag{4.1}$$

Where:

q = rate, BBl/d,

k = permeability, md,

A = area of the model, horizontal cross section, ft^2,

μ = viscosity, cp,

P = pressure, psi,

s = distance, ft

γ_f = specific gravity of fluid.

Knowing k, A, q, and γ_r, $\frac{\partial P}{\partial S}$ is calculated in psi/ft; then, the pressure drop across the model is calculated by multiplying $\frac{\partial P}{\partial S}$ by the height of the model, see Appendix D. Then, the injection pressure is calculated from:

$$P_{inj} = \Delta P + P_{prod} \tag{4.2}$$

Where:

P_{prod} = production pressure, psi

ΔP = pressure drop across the model, psi

Chapter V
RESULTS AND DISCUSSION

In the present study, the experiments were conducted on the simulated bottom water drive reservoir described in chapter 4. Production parameters (oil recovery, water cut and pressure drop) were obtained with the following geometries:

Vertical well, vertical wells with vertical fractures of various dimensions, horizontal well, horizontal wells with longitudinal fractures of various vertical depths, z_f, and horizontal wells with single or multiple orthogonal fractures of various depth, z_f, and extensions, x_f.

In this chapter, the experimental results are presented, analyzed, and discussed. Comparisons of the various cases studied are presented to investigate the effects of wellbore geometries and fracture orientations and dimensions on the production parameters.

5.1 CASES STUDIED

Table 5.1 lists the various cases investigated in the present study. In the table, the following abbreviations are used:

UVW : unfractured vertical well,

UHW : unfractured horizontal well,

FVW : fractured vertical well,

FHW : fractured horizontal well,

FHW/LF : horizontal well with longitudinal fracture(s),

FHW/SOF : horizontal well with single-orthogonal fracture, and

FHW/MOF : horizontal well with multiple-orthogonal fractures.

5.2 DISCUSSION OF RESULTS

The details of the experimental and calculated results are presented in Appendix C for each of the cases studied.

In the following subsections, the present results are discussed by comparing different cases in order to determine the effects of the wellbore and fracture geometries on the production parameters. The following order is followed:

5.2.1.   Unfractured vertical well vs. unfractured horizontal well

5.2.2.   Unfractured vertical well vs. fractured vertical wells

5.2.3.   Unfractured horizontal well vs. fractured vertical wells

TABLE 5.1: Summary of the Various Cases Investigated in This Work.

Run Number	Description
3	Vertical Linear Model
4	UHW
5	UHW
6	UVW
7	FHW/LF - 2 in. x 10 in.
8	FHW/LF - 1 in. x 10 in.
9	FHW/LF - 3 in. x 10 in.
10	FHW/SOF - 2 in. x 10 in.
11	FHW/SOF - 2 in. x 4 in.
12	FHW/SOF - 3 in. x 10 in.
13	FHW/SOF - 1 in. x 10 in.
14	FHW/SOF - 3 in. x 10 in.
15	FHW/MOF - 2 in. x 10 in., 2 F
16	FHW/MOF - 2 in. x 10 in., 3 F
17	FHW/MOF - 2 in. x 10 in., 4 F
18	FVW/VF - 2 in. x 10 in.
19	FVW/VF - 3 in. x 10 in.
20	FVW/VF - 1 in. x 10 in.

UHW : unfractured horizontal well
UVW : unfractured vertical well
FHW : fractured horizontal well
FVW : fractured vertical well
LF : longitudinal fracture
SOF : single orthogonal fracture
MOF : multiple orthogonal fracture
VF : vertical fracture

5.2.4. Unfractured horizontal well vs. fractured horizontal wells with longi-
tudinal fractures

5.2.5. Unfractured horizontal well vs. horizontal well with single-orthogonal
fracture

5.2.6. Unfractured horizontal well vs. horizontal wells with multiple-
orthogonal fractures

5.2.7. Fractured vertical wells vs. fractured horizontal wells

5.2.1 Unfractured Vertical Well vs. Unfractured Horizontal Well

In this study, the vertical well perforated interval is 2.4 inches (6.10 cm) at
the top of the reservoir model. The horizontal well is placed at 0.25 inches
(0.635 cm) below the top of the reservoir model along its length of 18 inches
(45.72 cm), and is perforated over a length of 16 inches (40.64 cm). Fig. 5.1
shows a schematic of the model and wells orientations.

Figure 5.2 shows a comparison of the oil recovery as a function of the
water injected in pore volumes for the unfractured vertical and horizontal
wells. A linear relation is observed until water breakthrough for the two
wells. The oil recovery and the water injected at water breakthrough are 58
%OOIP and 0.40 pv, respectively for the UHW compared to 23% and 0.15 pv
for the UVW. At water breakthrough, the oil recovery of the UHW is about 2.5
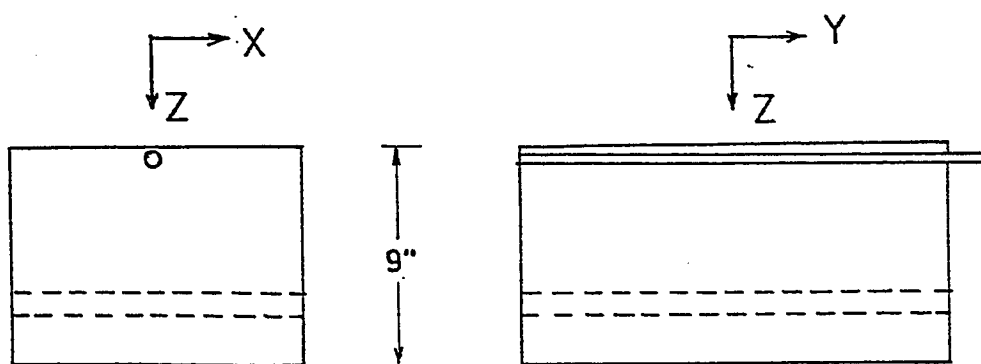
(a) Horizontal well
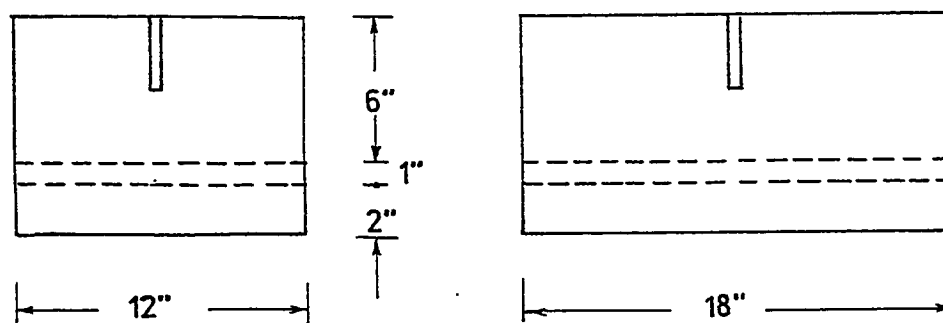
(b) Vertical well

Figure 5.1: Schematic of the Model and Wells Orientations.
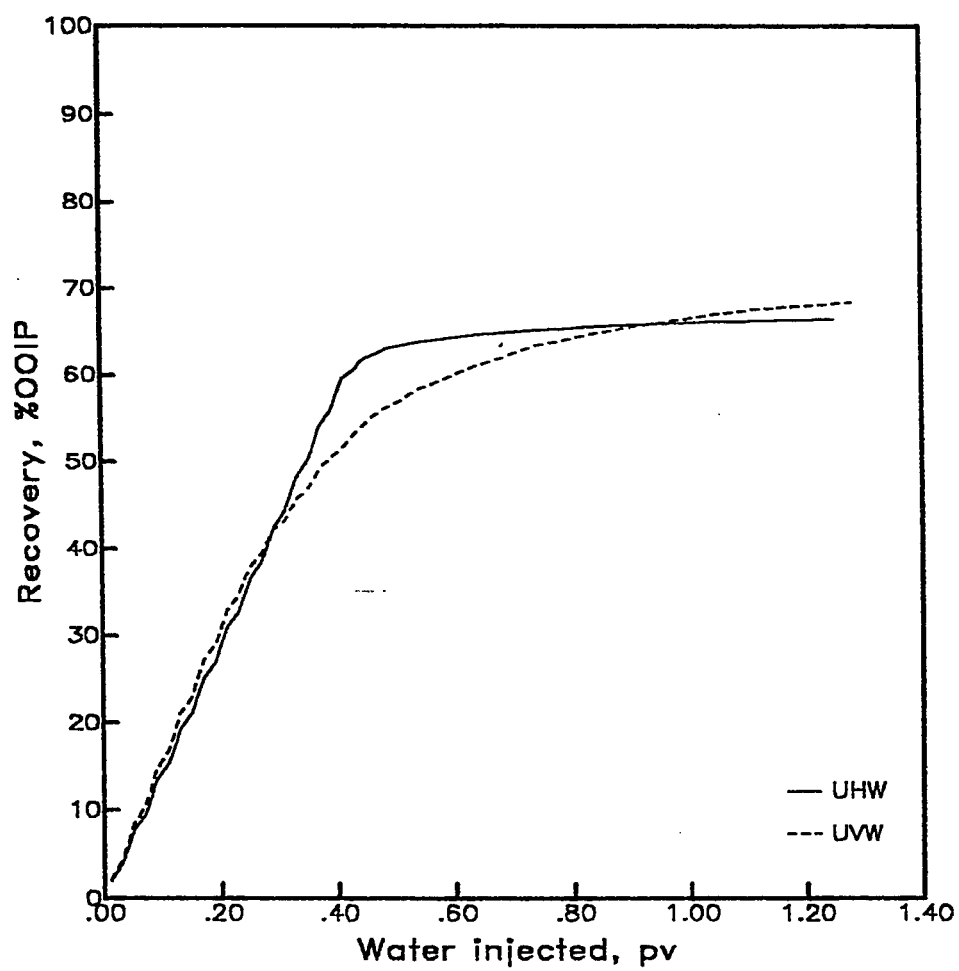
Figure 5.2: Oil recovery vs. pore volume injected for unfractured horizontal and vertical wells.

times that of the UVW. After water breakthrough, only 8 %OOIP of additional oil is produced in the case of the UHW compared to 43.5% in the case of the UVW. It may be concluded that most of the oil recovered with the UHW (~88 per cent of recovered oil) is produced before water breakthrough. However, most of the oil recovered for the UVW (~65 per cent of recovered oil) is produced after water breakthrough.

Figures 5.3 and 5.4 compare the water cut as a function of the water injected and the oil recovery respectively. It is observed from the figures that water production starts after flooding 0.40 pv of water and recovering 58% OOIP for the UHW compared to 0.15 and 23% for the UVW. The results indicate earlier water breakthrough and lower recovery at breakthrough for the vertical well as compared to the horizontal well. It is believed that the main reason is that less area is in contact with the reservoir in case of the vertical well compared to that of the horizontal well and as a result, higher pressure drop develops around the vertical wellbore due to the convergence of flow lines around the wellbore. This pressure drop affects the stability of the water/oil interface and enhances the development of water conning. Hence the earlier water breakthrough. After water breakthrough, a steep increase in water cut is noted for the UHW. At water cut of 95%, the water injected is 0.64 pv with corresponding oil recovery of 64.4% OOIP for the UHW compared to 1.08 pv and recovery of 67% for the UVW. It is noted that for the UVW, more volume of water is injected (1.08 pv) to reach the same water cut compared to the UHW (0.64 pv) which means that the flooding process is more efficient with the UHW.

Figure 5.3: Producing water cut vs. pore volume Injected
for unfractured horizontal and vertical wells.
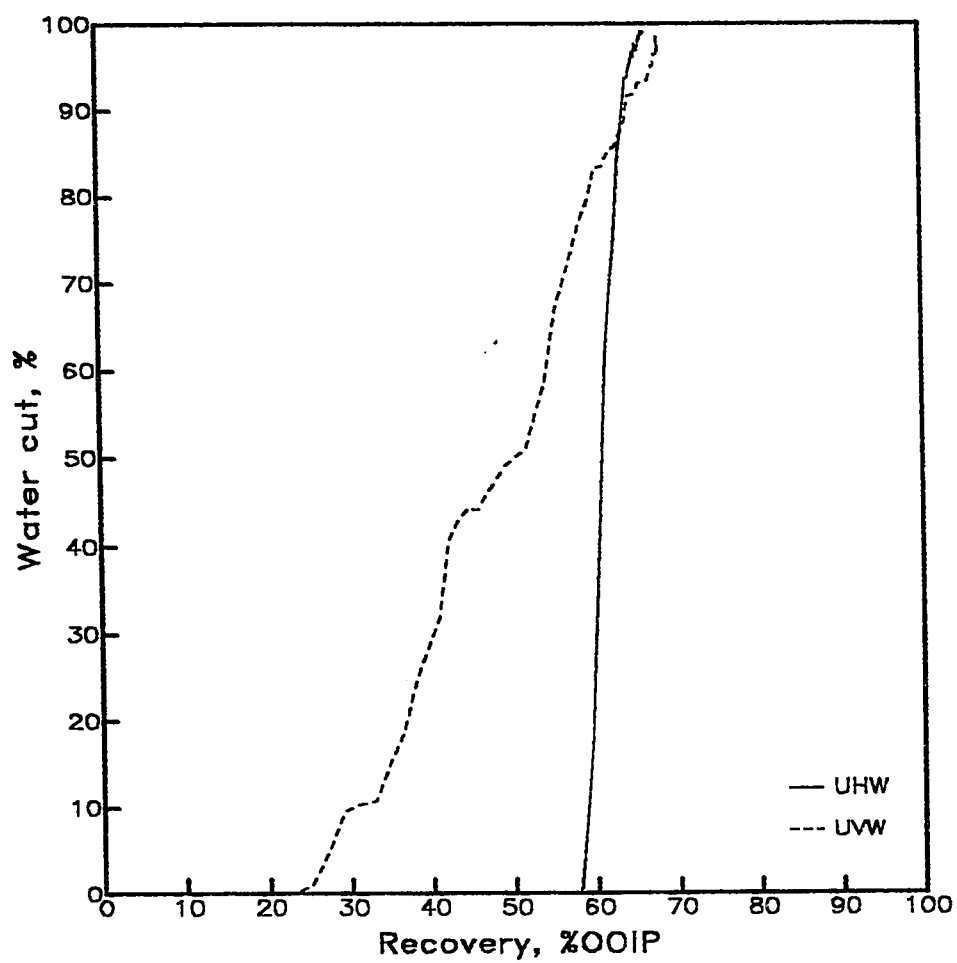
Figure 5.4: Producing water cut vs. oil recovery for
unfractured horizontal and vertical wells.

It is concluded then that the oil recovery at water breakthrough and the pore volume injected are largely affected by the orientation of the producing well. However, the ultimate oil recoveries are found to be very close for the vertical and horizontal wells. It may be pointed out that the ultimate oil recovery is independent of the orientation of the wellbore, rather it is a function of the rock and fluid properties.

It is worthwhile to mention that the same area is drained using both the horizontal and vertical wells. However, the model is designed to represent a small section of an oil reservoir with 112.5 ft long, 75 ft wide and 37.5 ft oil thickness. The horizontal well, however, can be extended to drain much larger area compared to the vertical one. Therefore, if a reservoir having a drainage area of two acres is assumed (for example a case of a narrow reservoir extends between two faults), then the the horizontal well could replace ten vertical wells.

Another comparison arises when a horizontal or vertical well drains the same area but with different shapes. The ideal shape of the drainage area for the vertical well is square, however, the rectangular shape is more suitable for the horizontal well. Assume vertical and horizontal wells drilled to drain five acres under gravity stabilization (stable water oil interface) with negligible capillary pressure. Using the following data from Table A.1, the critical rate is calculated for the vertical well, equation (2.5), and for the horizontal well, equation (2.3):

$$k = \text{reservoir permeability, 19.644 md.}$$

k_{ro} = relative permeability to oil, assumed 1.0 at S_{wi}

μ_o = viscosity of oil, 2.03 cp

$\Delta\gamma_i = \gamma_w - \gamma_o = 0.20$

Using eq. (2.5) in squared shape area, a vertical well with wellbore radius of 3.5 in. and 50% penetration can produce 0.934 B/D. To keep stable water/oil interface, this critical rate must be decreased as the water/oil interface progresses. However, with a rectangular area of 2904 ft long and 75 wide (5.0 acres), the horizontal well (2904 ft length) can produce up to 50.1 B/D, equation (2.3), with a stable water/oil interface which is about 54 times higher than the production of the vertical well.

With a porosity of 0.10, initial water saturation of 30% and residual oil saturation of 20%, the oil that can be recovered from five acres is 72,729 bbls. The time needed to produce this oil using the horizontal well is about 3.98 years compared to about 213.34 years for the vertical well. It is clear that, the vertical well in an optimum reservoir shape is not practical in low permeability reservoirs under gravity stability.

Figure 5.5 shows the pressure drop as a function of the water injected. Major differences are noted between the UVW and the UHW. Initially, the system is at static equilibrium under gravity-capillary forces with oil water contact at the bottom of the oil reservoir and pressure drop of 0.25 psig. This pressure drop is measured at the bottom of the perforated plate and is due to the capillary-gravity equilibrium. It is approximately equal to the pressure due to a static head of kerosene (0.235 psig) or $\rho_o g h_k$. Where h_k is the initial
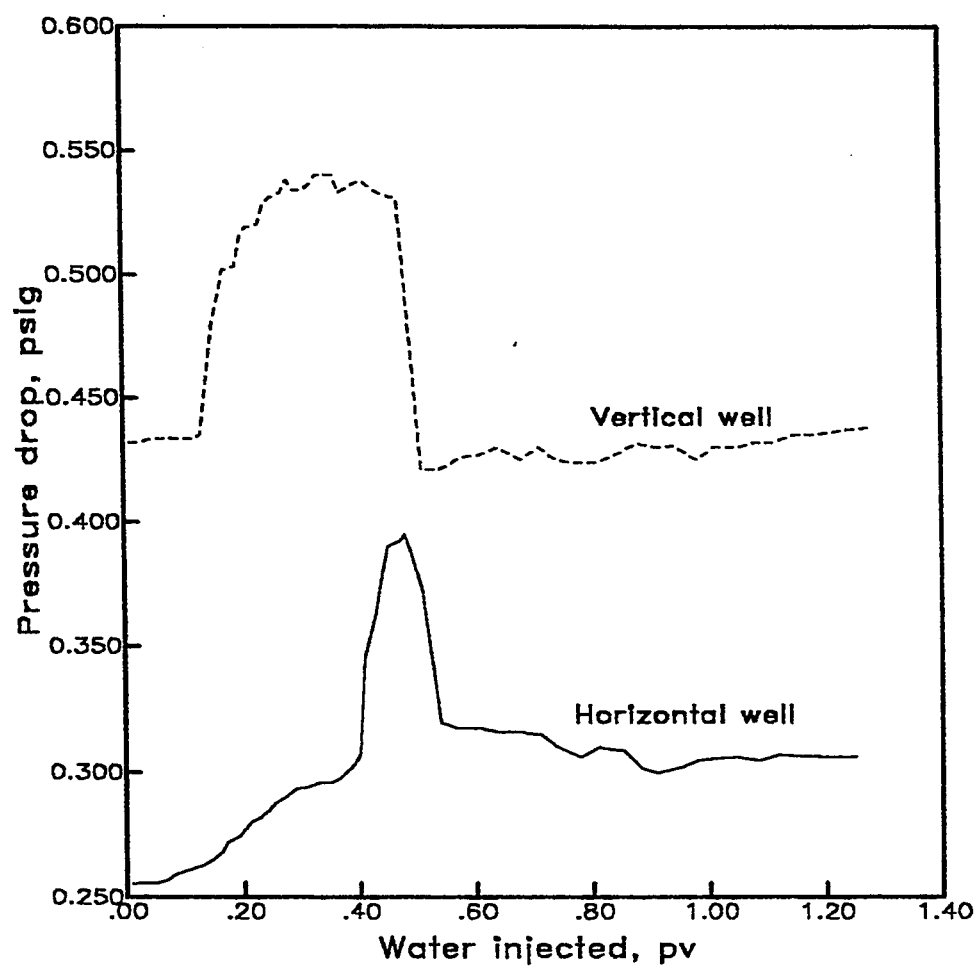
Figure 5.5: Pressure drop vs. pore volume injected for unfractured hotizontal and vertical wells.

height of kerosene above the point of measurement at the bottom of the per-forated plate, ρ_o is the kerosine density, and g is the gravity acceleration constant. The little difference between the observed value (0.25 psig) and the calculated value (0.235 psig) is probably due to the effect of capillary pressure which may cause imbibition of some water into the oil zone.

Water is injected at constant rate of 40 cc/min. (0.362 B/D) into the bottom water reservoir. Once the injection starts, a steep increase in the pressure drop from 0.25 psig to 0.43 psig is noted for the UVW compared to 0.26 psig for the UHW. This sudden increase in the pressure drop is due to the initiation of the fluid flow through the system (porous media, perforations and wellbores). The pressure increase is much higher in case of the vertical well due to the limited perforated interval (2.4 inches) compared to the horizontal well (16 inch perforated interval). If, however, the whole model area is allowed to produce, the pressure needed to initiate the flow through the porous media, would be much less and would be the pressure drop due to viscous forces in the porous media.

After this point, almost a constant pressure drop is recorded for the UVW compared with a gradual increase for the UHW. AT water breakthrough, the pressure drop reaches 0.435 psig for the UVW compared to 0.305 psig for the UHW. A sharp increase in the pressure drop is noted during the two-phase flow through the perforations and wellbore, the pressure reaches a maximum of 0.55 psig and 0.40 psig for the UVW and UHW respectively. As the water cut increases (about 85%), water becomes the continuous phase and oil

becomes the intermittent phase in the wellbore and, therefore, the pressure drop decreases and stays almost constant till the end of the run.

It may be concluded that the UHW exhibits lower pressure drop as a result of the longer completed interval and consequently, a larger contact area with the reservoir. It may be noted that the horizontal well with larger contact area (6.7 times that of the vertical well) stabilizes the water/oil interface until water breakthrough. This is noted from the difference in the pressure drop at the start of production (0.26 psig) and at water breakthrough (0.305 psig). This difference is 0.045 psig which is almost the pressure drop due to the gravity difference between water and oil. However, the process is not stable under gravity with the vertical well since the effect of $\Delta \rho g h$ is not shown on the pressure behavior of the vertical well after the start of production until water breakthrough (Figure 5.5). This means that viscous forces dominate the flooding process in the case of the vertical well and as a result, viscous fingers are developed and hence the earlier water breakthrough. For the horizontal well under the same production conditions, however, the progress of water/oil interface is more stable.

During the two-phase flow in the perforations and wellbores, viscous forces dominate in both the vertical and horizontal wells. However, as the water cut increases, the pressure drop reduces to the pressure needed to left and drive the water through the system. For the horizontal well, the pressure is: $\rho_o g h + \Delta \rho g h +$ pressure needed to drive the flow through the system. This pressure can be also calculated from $\rho_w g h +$ pressure needed to drive the flow through the system.

5.2.2 Unfractured Vertical Well vs. Fractured Vertical Wells

In this study, a fracture extends in the x-direction and penetrates the oil zone vertically in the z-direction is created, Fig. 5.6. The extension of the fracture (x_f) is 5 inches (12.70 cm) while the depth (z_f) and width (w_f) are varied. See eq. (A.64) and table A.2. The ratio of fracture depth (z_f) to the oil zone thickness (h) is defined as the fracture penetration ratio (FPR). Details of the fracture design and scaling are found in Appendix A (section A.2). The production performances of three different FPR, namely 0.167, 0.333 and 0.500 are investigated. The UVW is assigned a FPR of zero.

Figure 5.7 compares the oil recovery as a function of the water injected for the UVW and the FVWs with the three different fracture penetration ratios. Differences in recovery performances are noted among the cases shown. The UVW (FPR=0) is showing the lowest oil recovery. About 23% OOIP is produced just before water breakthrough at the producing well. After water breakthrough, the oil recovery increases gradually reaching 66.50% OOIP at 1.0 pv of water injected. For the FPR of 0.167, the oil recovery at water breakthrough increases to 62.50 %OOIP which represents 270% increase compared to that of the UVW. After injecting 1.0 pv of water, the recovery increases to 73.63% OOIP. For the FPR of 0.333, i.e. doubling the fracture depth, water breaks through later with oil recovery of 68.18% OOIP or about 290% of that of the UVW. The recovery then increases by about 9% to reach 77.26% at 1.0 pv of water injected. For the FPR of 0.500, or three times the first FPR, oil recovery at water breakthrough is about 72.46% OOIP which is
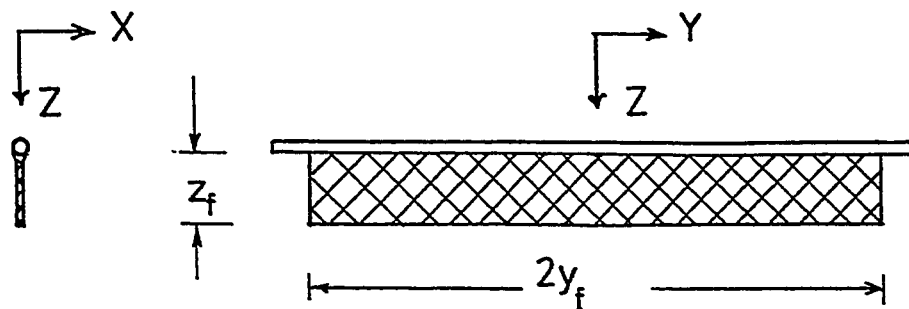
(a) Longitudinal fracture
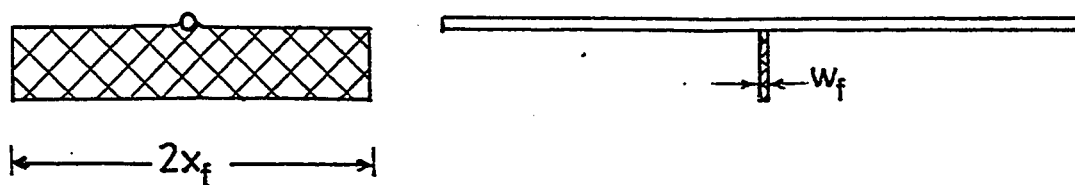
(b) Single orthogonal fracture

(c) Vertical fracture

Figure 5.6: Schematic of the Longitudinal, Orthogonal and Vertical Fractures.
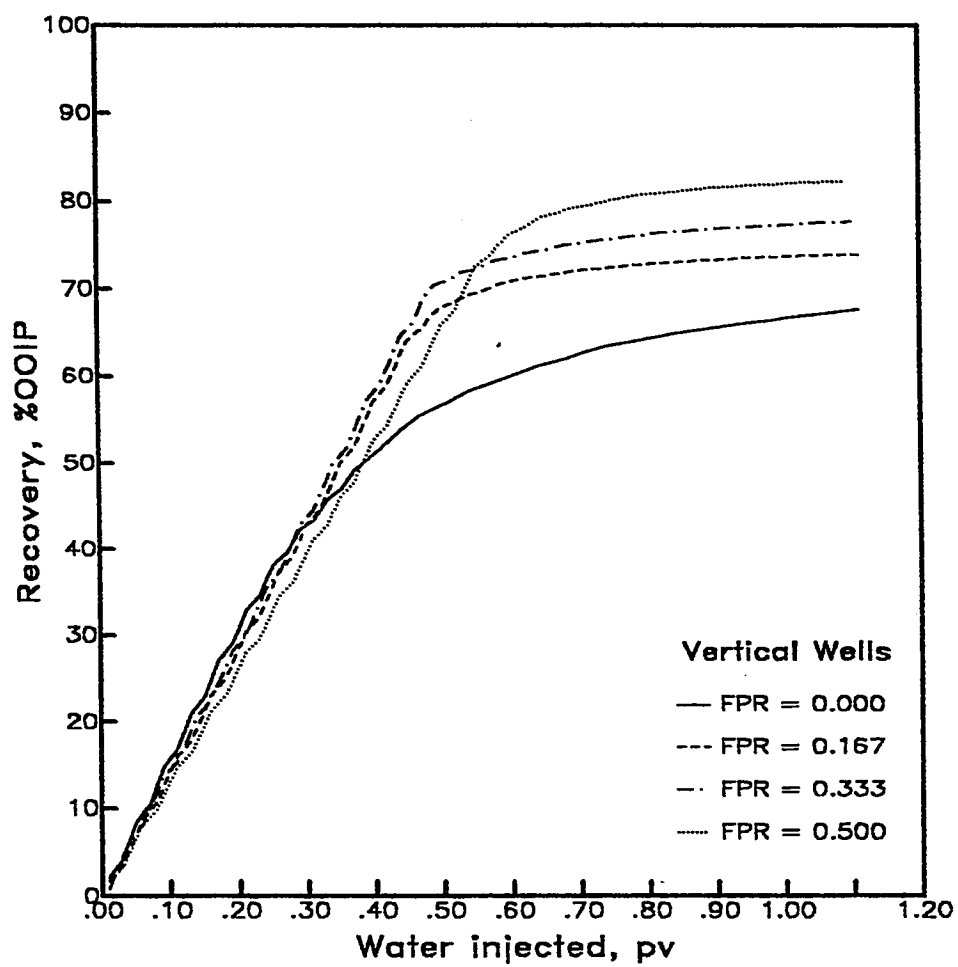
Figure 5.7: Oil recovery vs. pore volume injected for the vertical wells.

315% of that of the UVW. After injecting 1.0 pv, the recovery increases to 82% OOIP compared to 66.50% for the UVW.

Figure 5.8 shows the oil recovery as a function of the FPR (z_f/h). The results indicate that increasing the FPR increases the oil recovery. However, the increase in recovery due to increasing the FPR is not as significant when compared to the recovery from the fractured well versus the unfractured well.

Figures 5.9 and 5.10 show the water cut as a function of the water inject-ed and the oil recovery, respectively, for the UVW and the FVWs. It is observed that water breaks through after injecting 0.15 pv for the UVW (FPR=0.0) compared to 0.44, 0.47 and 0.55 for the FVWs with FPR of 0.167, 0.333 and 0.500, respectively. After water breakthrough, water cut increases very rapidly for the FVWs compared to a gradual increase for the UVW. At water cut of 95%, the water injected reaches 1.08 pv for the UVW compared to 0.75, 0.84 and 0.90 pv for the FVWs with FPR of 0.167, 0.333 and 0.500, respectively.

These results show that the presence of vertical fractures with vertical wells in bottom water drive reservoirs improves the production performance. Oil recovery is increased and water breakthrough is delayed. In addition, less amount of water injected is required to produce the same amount of oil com-pared to the UVW. It is also observed that the deeper the fracture, the higher the oil recovery. It is believed that different production (recovery) mecha-nisms prevail when the fracture is present, therefore, the production perform-ance is completely different from that of the UVW. The production mecha-
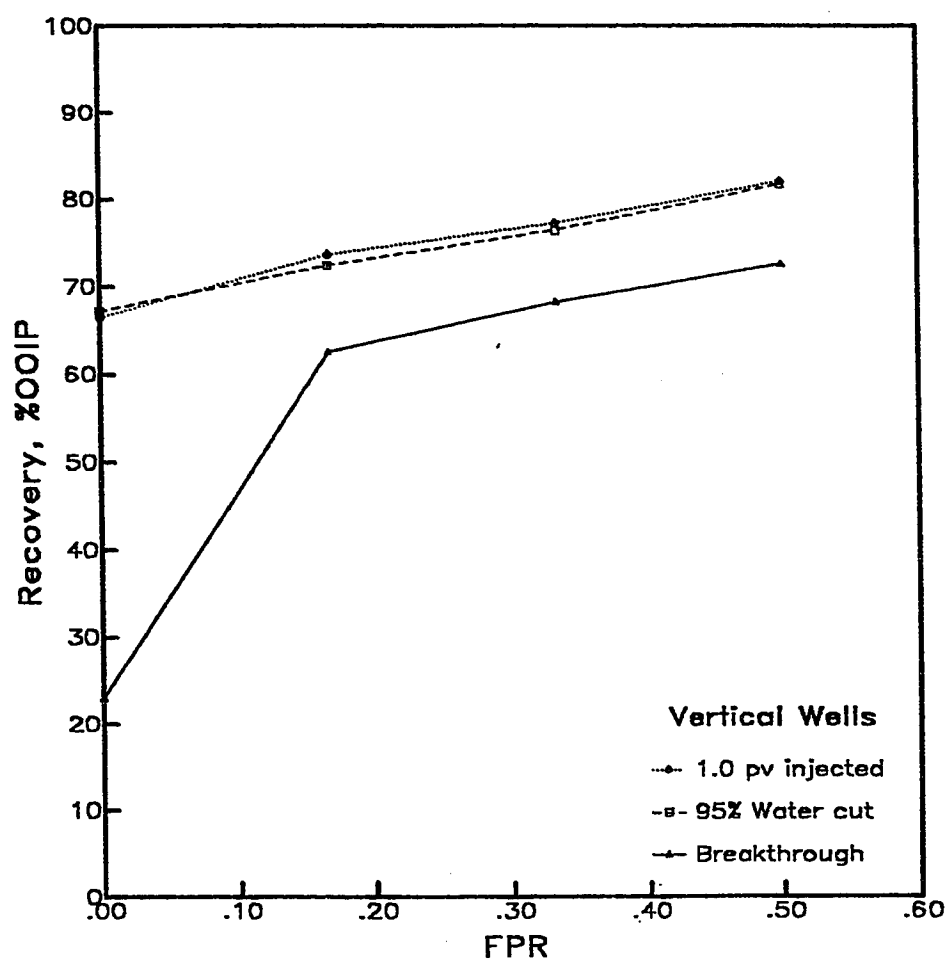
Figure 5.8: Oil recovery vs. fracture penetration ratio for the vertical wells.
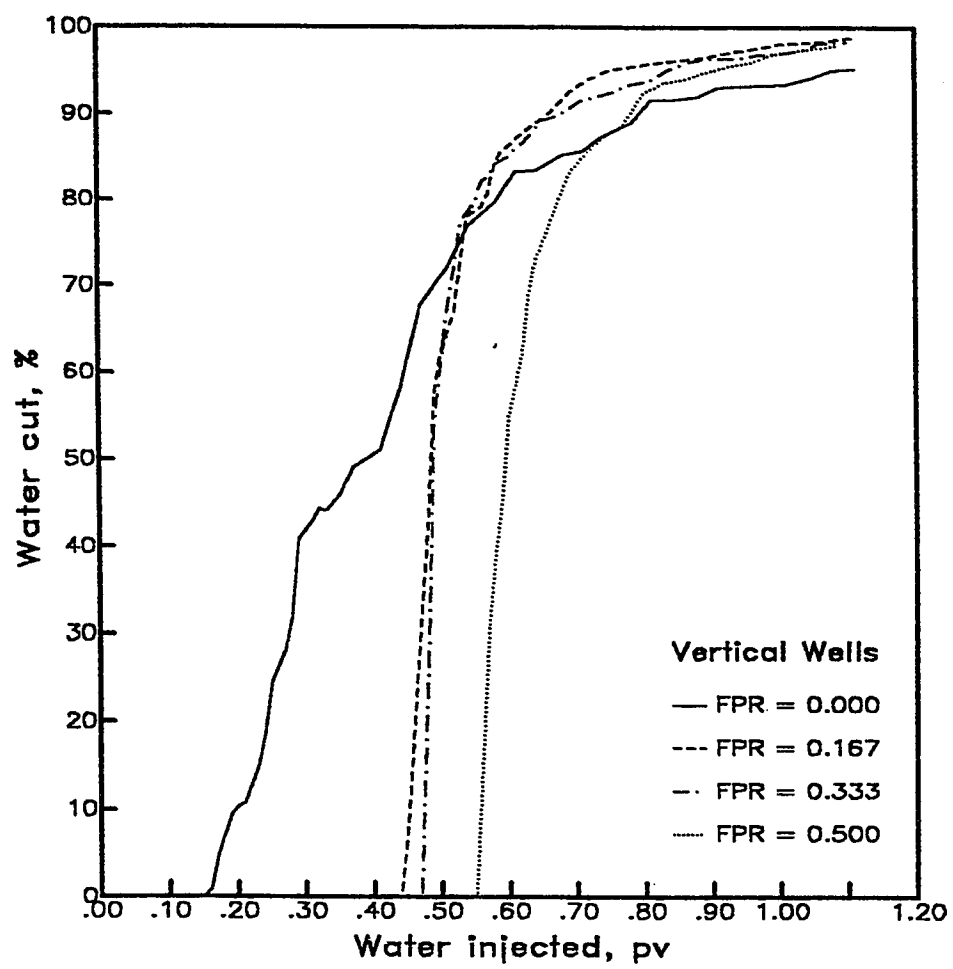
Figure 5.9: Producing water cut vs. pore volume injected
for the vertical wells.
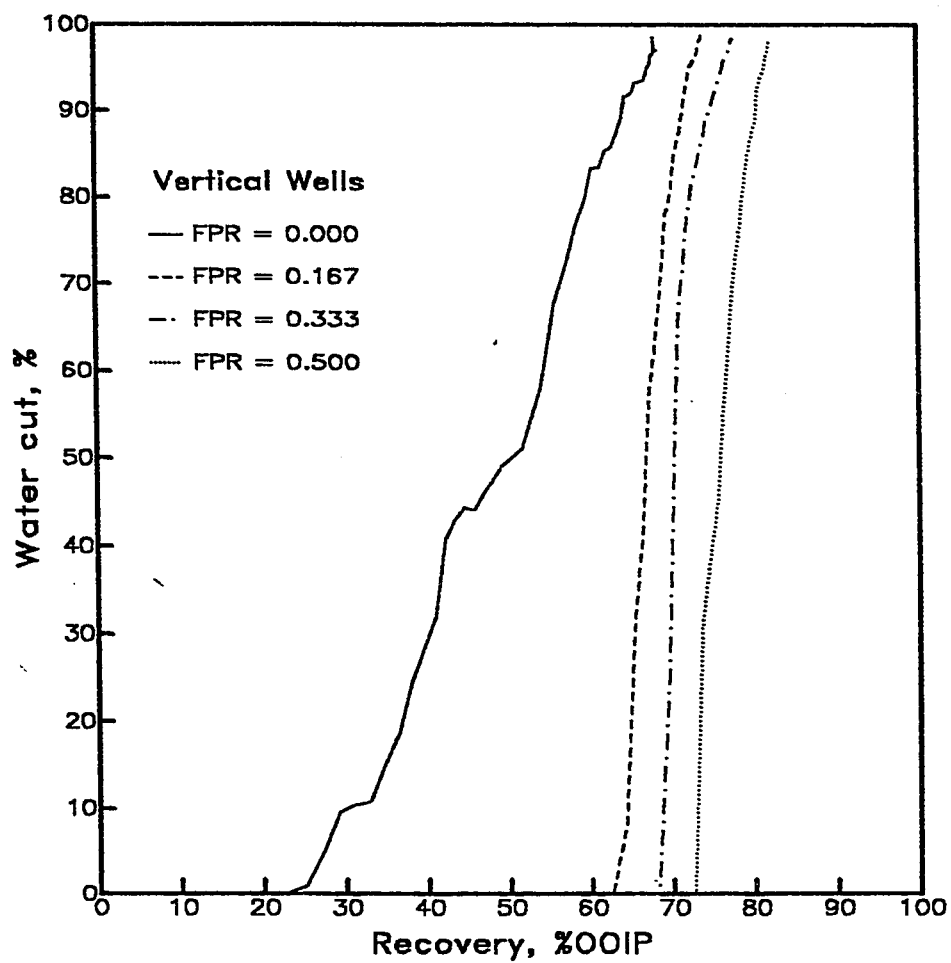
Figure 5.10: Producing water cut vs. oil recovery
for the vertical wells.

nisms of such systems are discussed in chapter 6.

Figure 5.11 compares the pressure drop as a function of the pore volume of water injected for the UVW and the FVWs. As soon as water injection starts, the pressure drop increases sharply from the initial static equilibrium pressure of 0.250 psig to 0.430 psig for the UVW compared to 0.310, 0.305 and 0.3045 psig for the FVWs with FPR of 0.167, 0.333, and 0.500, respectively. This increase in pressure is due to the initiation of the fluid flow through the system (porous media, perforations and wellbores). This point was explained in detail in section 5.2.1. The pressure drop then stays almost constant for the UVW till water breakthrough. A small gradual increase in the pressure drop is, however, observed for the FVWs during this period. At this point, the pressure drop reaches 0.435 psig for the UVW compared to 0.353, 0.348 and 0.347 psig for the FVWs with FPRs of 0.167, 0.333 and 0.500, respectively. This gradual increase in the pressure drop for the FVWs is due to the advance of water in the fracture and the matrix. This creates a change in the pressure drop due to the difference in gravity of water and oil. In the fracture, for example, this change in the pressure drop is $\Delta \rho g h_{wf}$ which is proportional to the height of the water in the fracture (h_{wf}) at different stages of the flooding process. At water breakthrough, this pressure increase is about 0.043 psig which is exactly $\Delta \rho g h$. Where h is the initial oil zone thickness (6.0 inches), $\Delta \rho$ is the density difference between water and oil, and g is the gravitational constant. It is noted that since the fracture has infinite conductivity, the pressure drop due to viscous forces is negligible in the fractures; rather, the gravity forces have the major effect. This is further
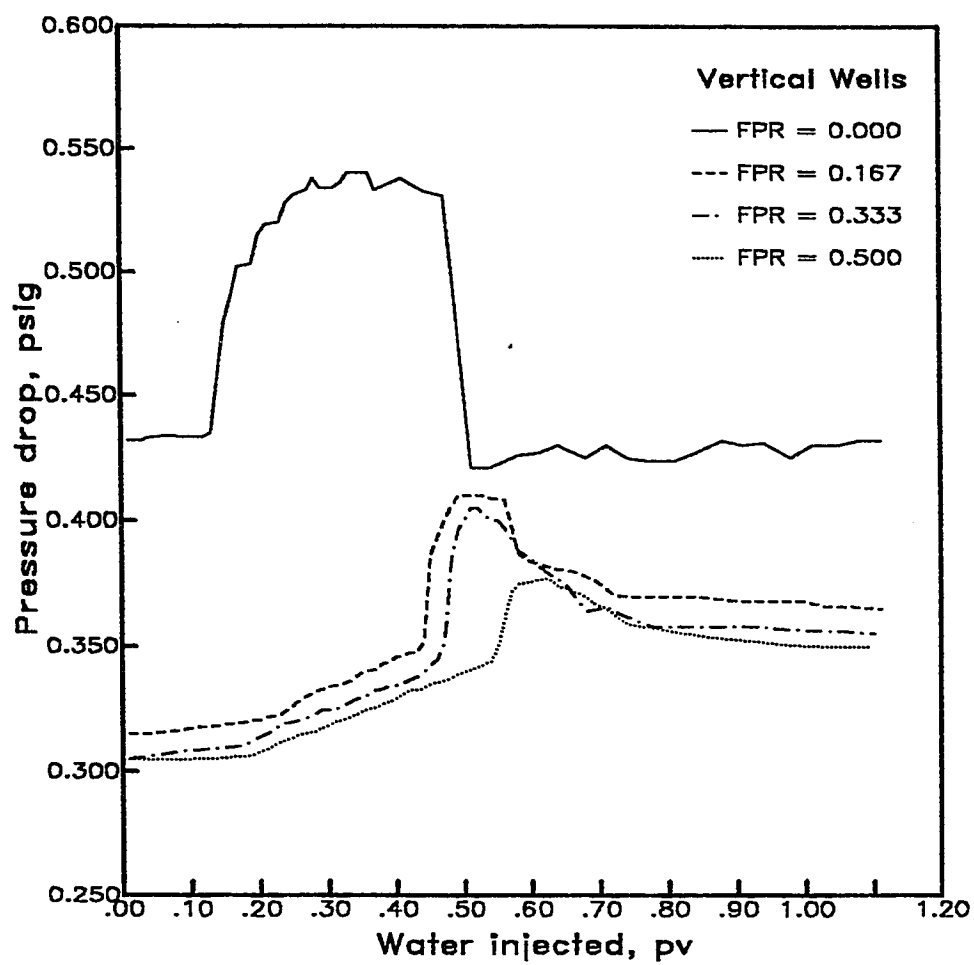
Figure 5.11: Pressure drop vs pore volume injected for the vertical wells.

explained in chapter 6.

Once the first water droplet enters the the wellbore, the pressure drop increases rapidly showing high pressure drop during the two-phase flow in the perforations and wellbores. During this period, the flooding process is controlled by viscous forces and the pressure drop reaches a maximum of 0.550 psig for the UVW compared to 0.410, 0.405 and 0.377 psig for the FVWs with FPR of 0.167, 0.333 and 0.500, respectively. It is noted from Fig. 5.11 that as the fracture becomes deeper, the effect of viscous forces becomes less and as a result the difference in the pressure drops at water breakthrough and the peak point on each curve is reduced. These differences are 0.06, .05 and .027 psig for the FVWs with FPR of 0.167, 0.333 and 0.500, respectively compared to 0.12 psig for the UVW. It can be seen that the pressure drop of the FVWs is always lower than that of the UVW. This is mainly due to the larger contact area of the fractures (43.62 sq. inches for two-inch deep fracture) with the reservoir compared to that of the unfractured vertical well (3.77 sq. inches for 2.4 inch-perforated interval out of 6.0 inches thickness of the oil zone). It is also due to the geometry of the flow through fractured reservoirs which is different from that through unfractured reservoirs. See chapter 6 for more details.

It may be stated that the minimum pressure drop (ΔP_{min}) required for the flooding process is the pressure needed to left the fluid against the gravity (ΔP_g) from the initial static pressure drop (ΔP_s) plus the pressure needed to drive the fluids through the system (ΔP_d). This last pressure is necessary to

drive the fluids against the viscous forces due to darcy flow through the porous media, fracture(s), perforations and wellbore (ΔP_{vs}) and also to control the pressure created by the capillary forces (ΔP_c). This could be written in an equation form as:

$$\Delta P_{min} = \Delta P_g + \Delta P_d \qquad (5.1)$$

Where:

$$\Delta P_d = \Delta P_{vs} + \Delta P_c \qquad (5.2)$$

Or:

$$\Delta P_{min} = \Delta P_{vs} + \Delta P_c + \Delta P_g \qquad (5.3)$$

More details are presented in chapter 6.

From the present results, it may be concluded that the pressure drop decreases as the FPR increases. The reason is that the deeper the fracture, the less the distance the fluid particles move to reach the fracture where viscous forces become negligible. In addition, the deeper the fracture, the more the contact area of the reservoir with the fracture which results in lowering the pressure drop.

5.2.3 Unfractured Horizontal Well vs. Fractured Vertical Wells

In this section, the production performance of the UHW is discussed and compared to that of the FVWs. As mentioned earlier, the UHW is horizontally placed at 0.25 inches below the top of the reservoir (the total thickness of the oil zone is 6.0 inches) in the y-direction with a perforated interval of 16 inches (40.64 cm) out of the 18-inch length of the model (Fig. 5.1). The FVWs are vertically-fractured with three different fracture penetration ratios (FPRs) of 0.167, 0.333 and 0.500. The vertical well is perforated over an interval equal to the fracture depth (z_f).

Figure 5.12 compares the oil recovery as a function of the water injected for the unfractured horizontal well and fractured vertical wells. Investigation of the figure shows that the FVWs provide better performance compared to the UHW (FPR=0.0). The performance of the deepest fracture (FPR = 0.500) is being the best followed by the intermediate fracture (FPR = 0.333), then the shallowest fracture (FPR = 0.167). At water breakthrough, the UHW produces the lowest oil recovery of 58% OOIP compared to 62.50%, 68.16% and 72.46% for the FVWs with FPRs of 0.167, 0.333 and 0.500, respectively.

Figure 5.13 compares the oil recovery at water breakthrough of the present cases as a function of the FPR. In the figure, a FPR of zero is assigned for the UHW. It is observed that the oil recovery increases with increasing FPR. It is also observed that at water breakthrough, the recoveries at different FPRs almost fit a straight line which may suggest that the UHW is
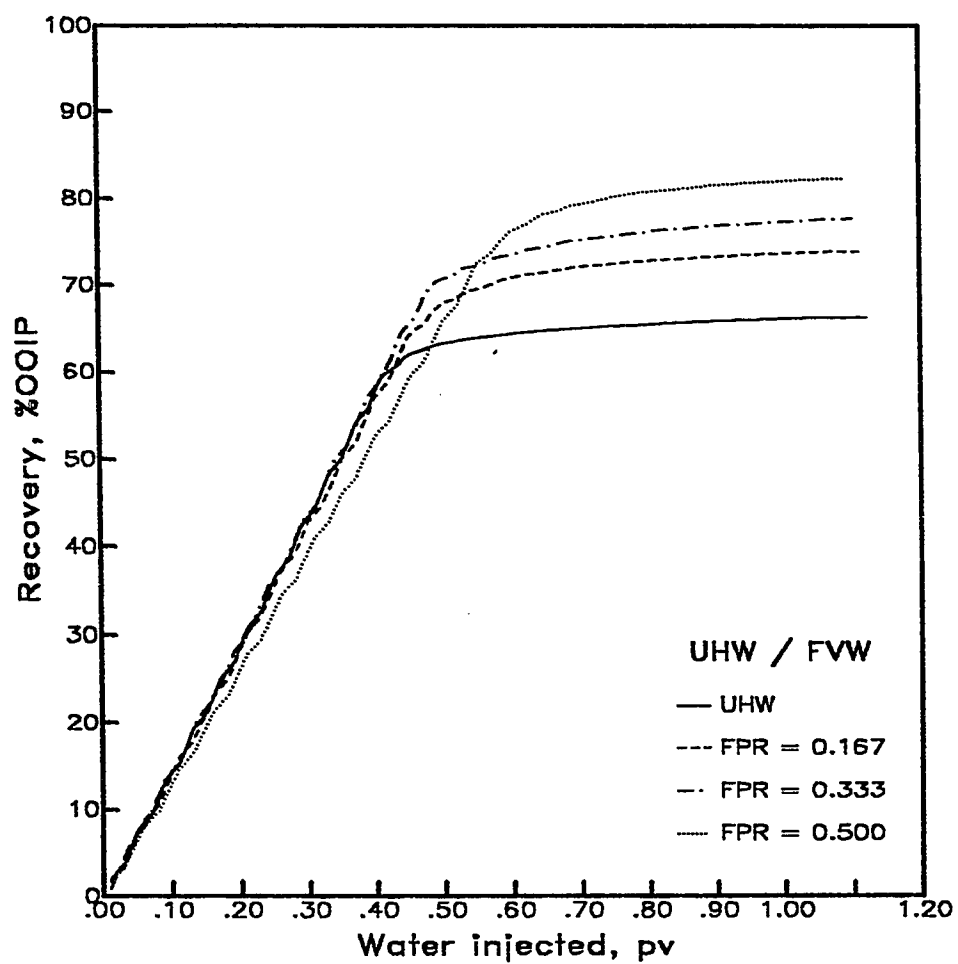
Figure 5.12: Oil recovery vs. pore volume injected for unfrac. horz. well and frac. vert. wells.
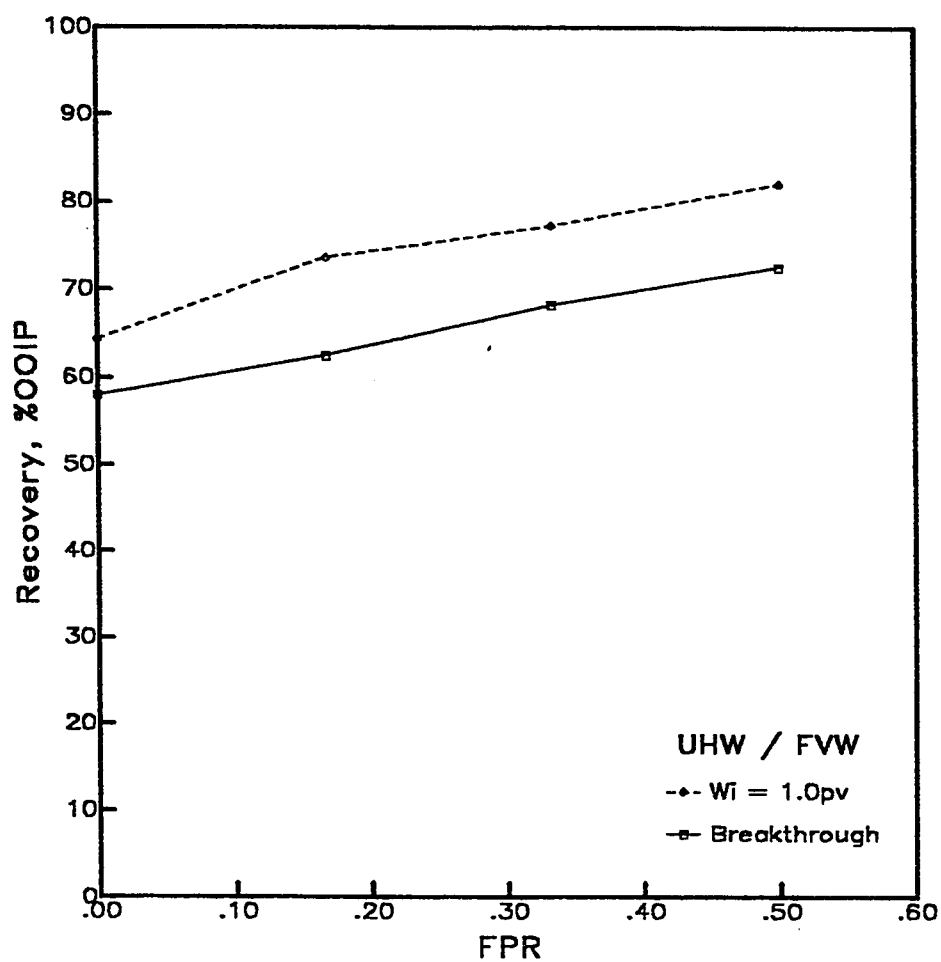
Figure 5.13: Oil recovery vs. fracture penetration ratio
for unfrac. horz. well and frac. vert. wells

behaving similar to a vertically-fractured well with fracture depth (z_f) equals

$2r_{wH}$ where r_{wH} is the radius of the horizontal wellbore. This has been previously noted by several authors [2, 28,44,120,121,125,126].

Figures 5.14 and 5.15 show the water cut as a function of the water injected and the oil recovery, respectively, for the UHW and the FVWs. It is shown from figure 5.14 that, at water breakthrough, the pore volumes of water injected are 0.44, 0.47 and 0.55 pv for FPRs of 0.167, 0.333 and 0.500 respectively compared to 0.40 pv for the UHW. After water breakthrough, a steep increase in water cut is noted for the cases studied. At 95% water cut, the pore volumes of water injected are 0.64, 0.75, 0.84 and 0.90 pv with corresponding oil recoveries of 64.40% OOIP, 72.44%, 76.42% and 81.64% for the UHW and the FVWs with FPR of 0.167, 0.333 and 0.500, respectively.

Figure 5.15 shows that the water cuts are increasing rapidly in a similar manner for all cases studied which may support the idea of considering the UHW as fractured vertical well with limited FPR.

Figure 5.16 presents the pressure drop as a function of the water injected for the UHW and the FVWs. At the start of the flooding process, the pressure drop increases sharply from the initial static value of 0.25 psig to the point where the production starts (dynamic conditions) at 0.26 psig for the UHW compared to 0.310, 0.305 and 0.3045 psig for the FVWs with FPRs of 0.167, 0.333 and 0.500, respectively. The pressure drop then increases gradually and reaches 0.305, 0.353, 0.348 and 0.347 psig at water breakthrough for the UHW and the FVWs with FPR of 0.167, 0.333 and 0.500, respectively. Under
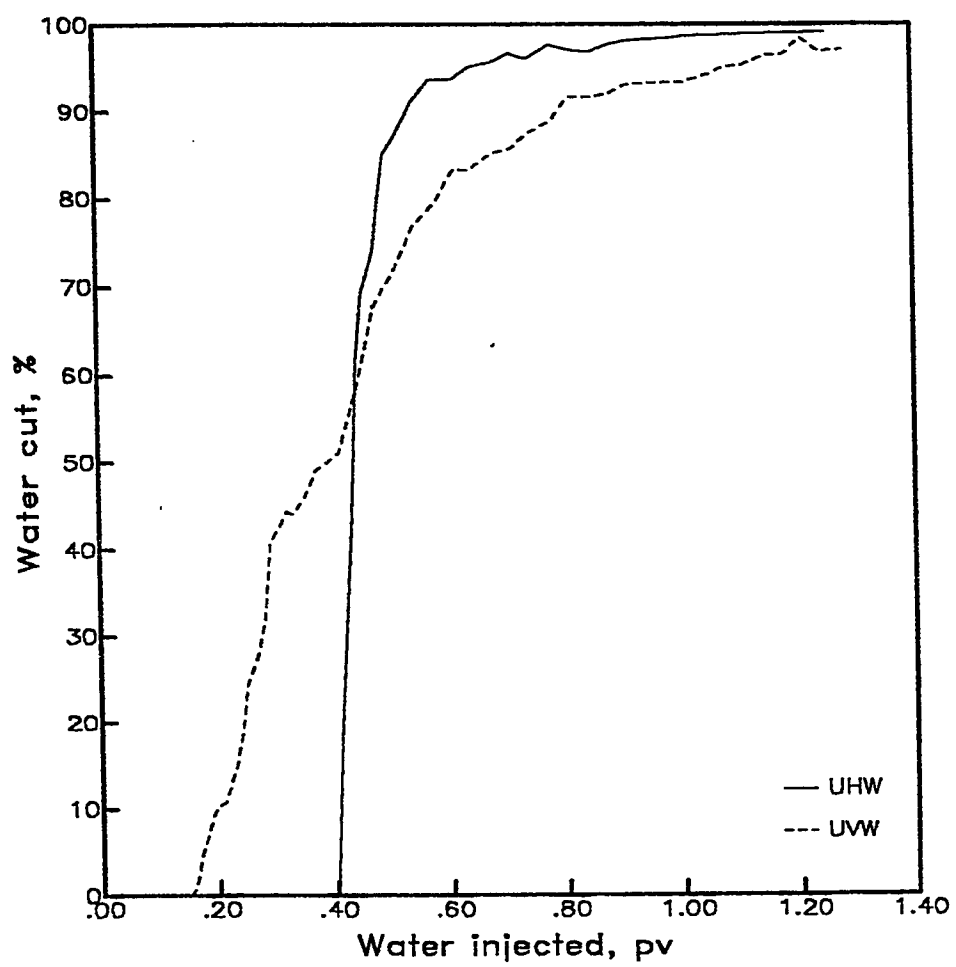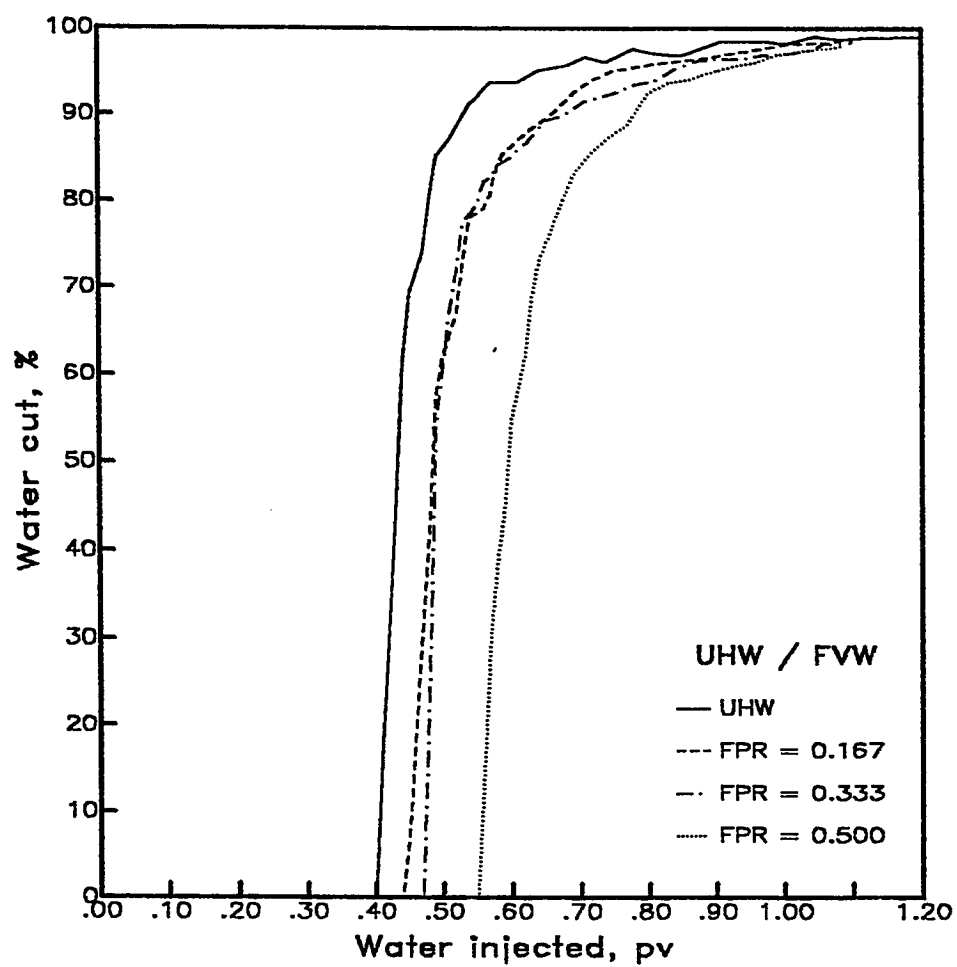
Figure 5.14: Producing water cut vs. pore volume injected
for unfrac. horz. well and frac. vert. wells
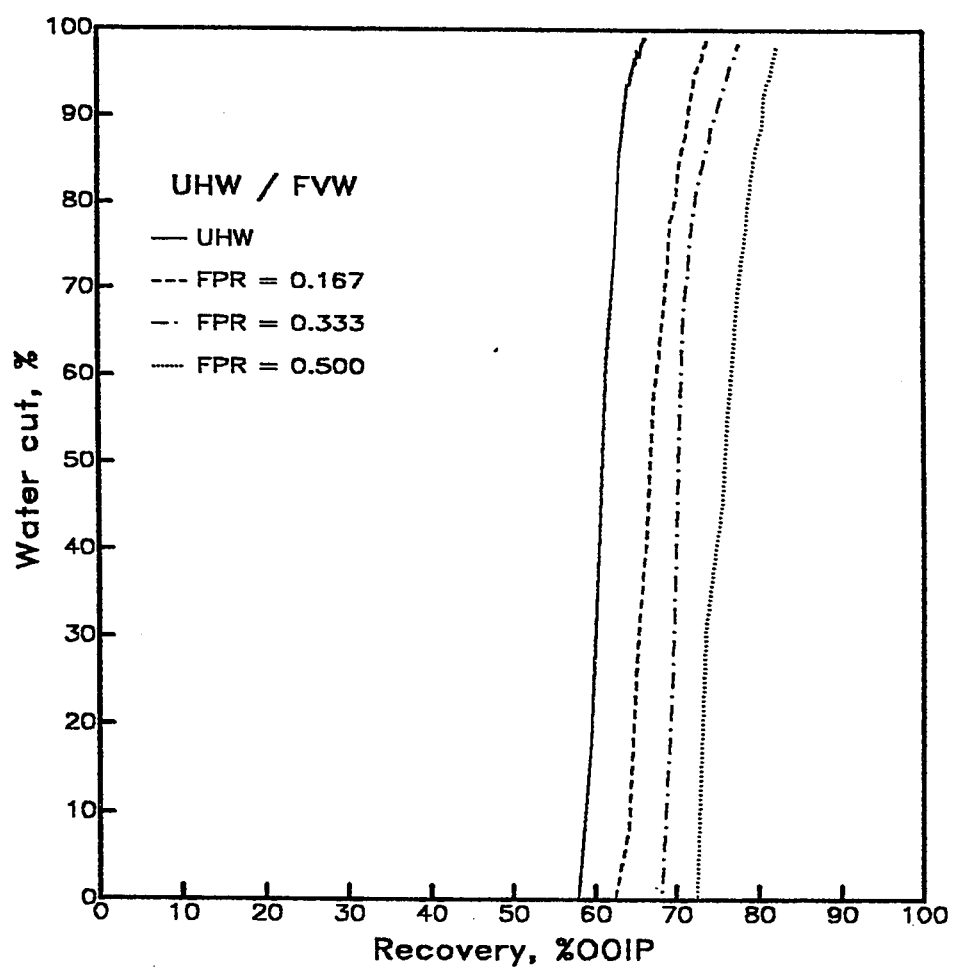
Figure 5.15: Producing water cut vs. recovery for unfrac. horz. well and frac. vert. wells
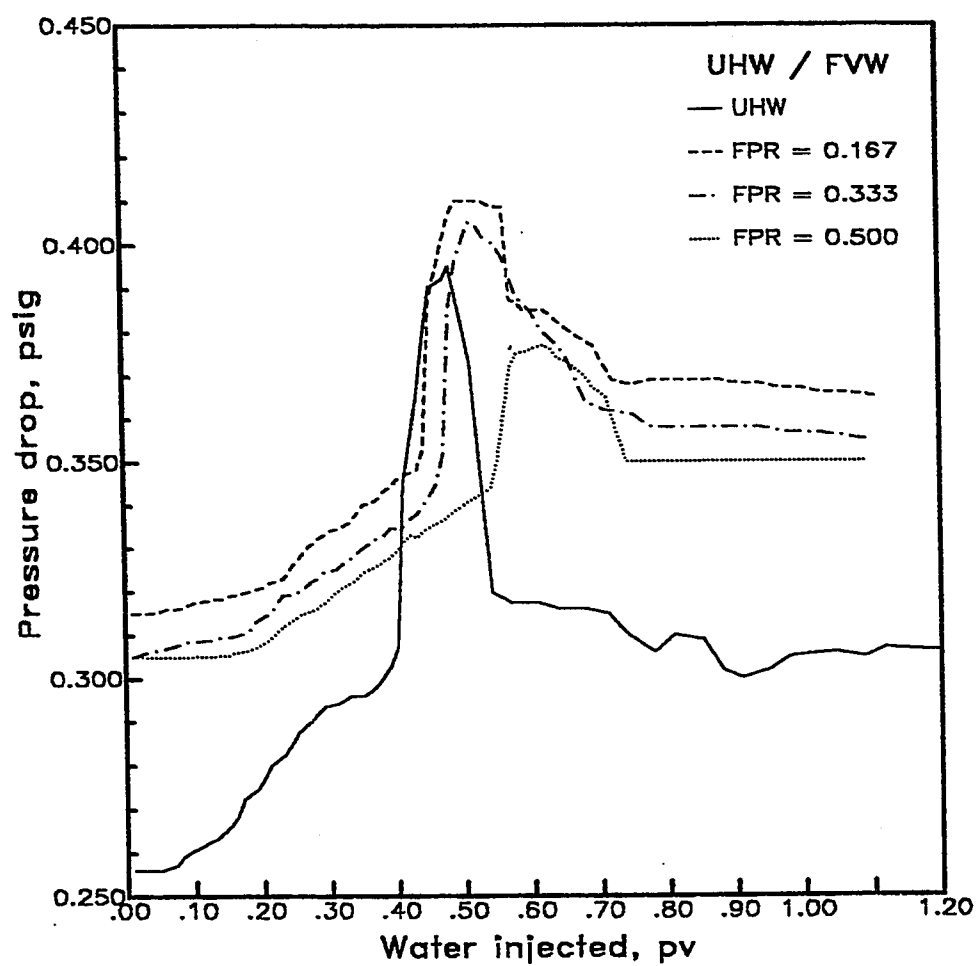
Figure 5.16: Pressure drop vs pore volume injected for unfrac. horz. well and frac. vert. wells.

dynamic conditions, it is observed that the increase in the pressure drop is proportional to the height of the water oil contact in the system for all cases. At water breakthrough, this increase is almost 0.043 which is equivalent to $\Delta \rho g h$.

Although the contact area for the UHW is less than that of the fractured vertical wells, it is observed that the pressure drop for the UHW is less than that of the FVWs. This may be attributed to the longer perforated interval of the UHW which will create flow nets different from those of the FVWs. Therefore, the flow lines converge at a much larger area (25.14 sq. inches) around the wellbore for the UHW compared to the FVWs (3.14 sq. inches for 2.0 inch-deep fracture). It is also observed that the deeper the fracture, the lower the pressure drop. The reason is that as the fracture gets deeper, more area of the reservoir is exposed to the fracture which further reduces the pressure drop, (for example, the area of contact is 22.92 sq. inches for the vertical well with 1-inch-deep fracture compared to 64.10 inches for the vertical well with 3-inch-deep fracture).

Comparing the production performance curves of the UHW to those of the FVWs with different FPRs, it may be concluded that better breakthrough and ultimate recoveries are obtained with the FVWs. However, the UHW is showing lower pressure drop due to the longer perforated interval and, therefore, the convergence of the flow lines into a larger area around the wellbore.

5.2.4 Unfractured Horizontal Well vs. Horizontal Wells with Longitudinal Fractures

In this study, the horizontal well is placed at 0.25 inches from the top of the oil reservoir in the y-direction, as mentioned earlier, and the fracture is created along the axis of the wellbore. The extension of the fracture $(2y_f)$ is equal to the perforated interval of the wellbore, 16 inches (40.64 cm). The fracture extension ratio (FER = $2y_f/L$) is 0.889. Three different fracture penetration ratios (z_f/h) of 0.167, 0.333 and 0.500 are investigated; where L is the length of the model, 18 inches (45.72 cm) and h is the oil zone thickness, 6.0 inches (15.24 cm).

Figure 5.17 shows the oil recovery as a function of the water injected for the UHW and the FHW/LF. A FPR of zero is assigned to the UHW. At water breakthrough, a substantial increase in the oil recovery is observed for the FHWs. About 77.77%, 80.71% and 83.33% of the original oil in place are recovered for the FPRs of 0.167, 0.333 and 0.500, respectively, compared to 58.00% OOIP for the UHW. Small additional recoveries are obtained after water breakthrough for all cases.

Figure 5.18 compares the oil recoveries at water breakthrough and at 95% water cut for the various cases. It is observed from the figure that fracturing a horizontal well increases the recovery. Beyond a FPR of 0.333, however, the depth of the fracture does not have a very significant effect on the ultimate oil recovery. It is further observed that a deeper fracture, FPR=0.500, would produce an amount of water-free oil equivalent to the ulti-
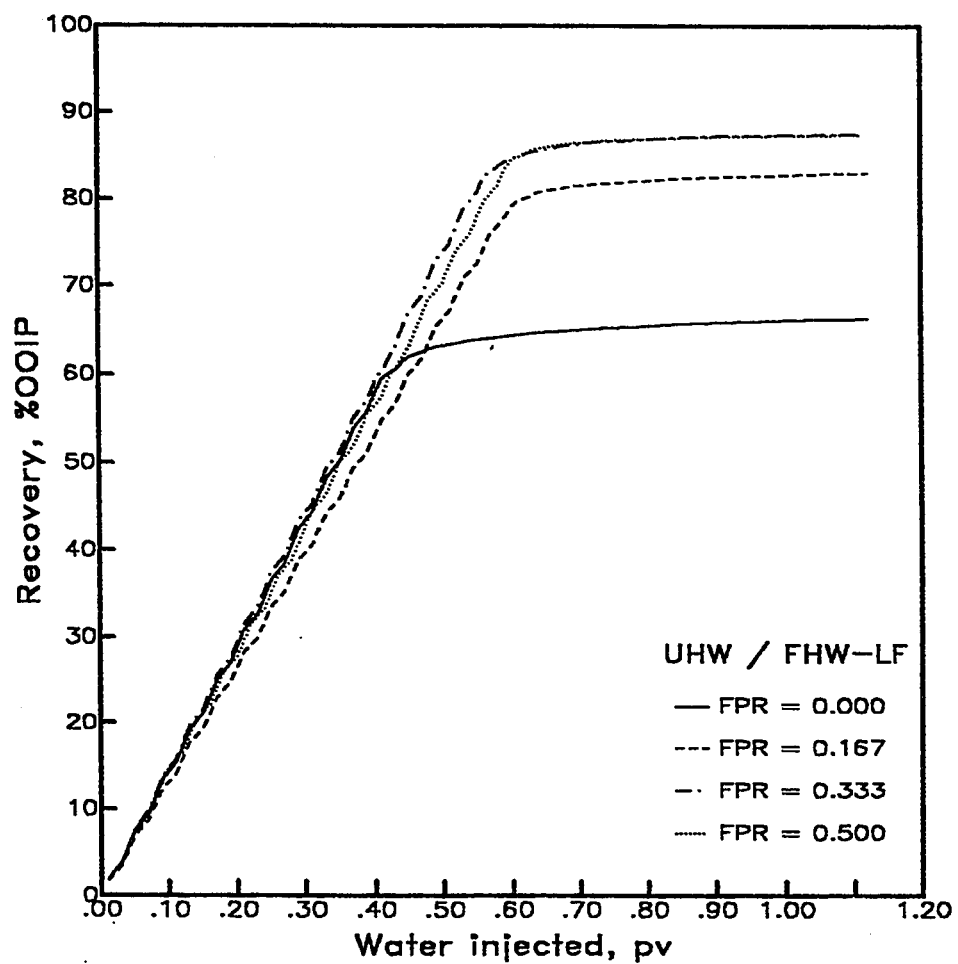
Figure 5.17: Oil recovery vs. pore volume injected for
horz. wells with longitudinal fractures
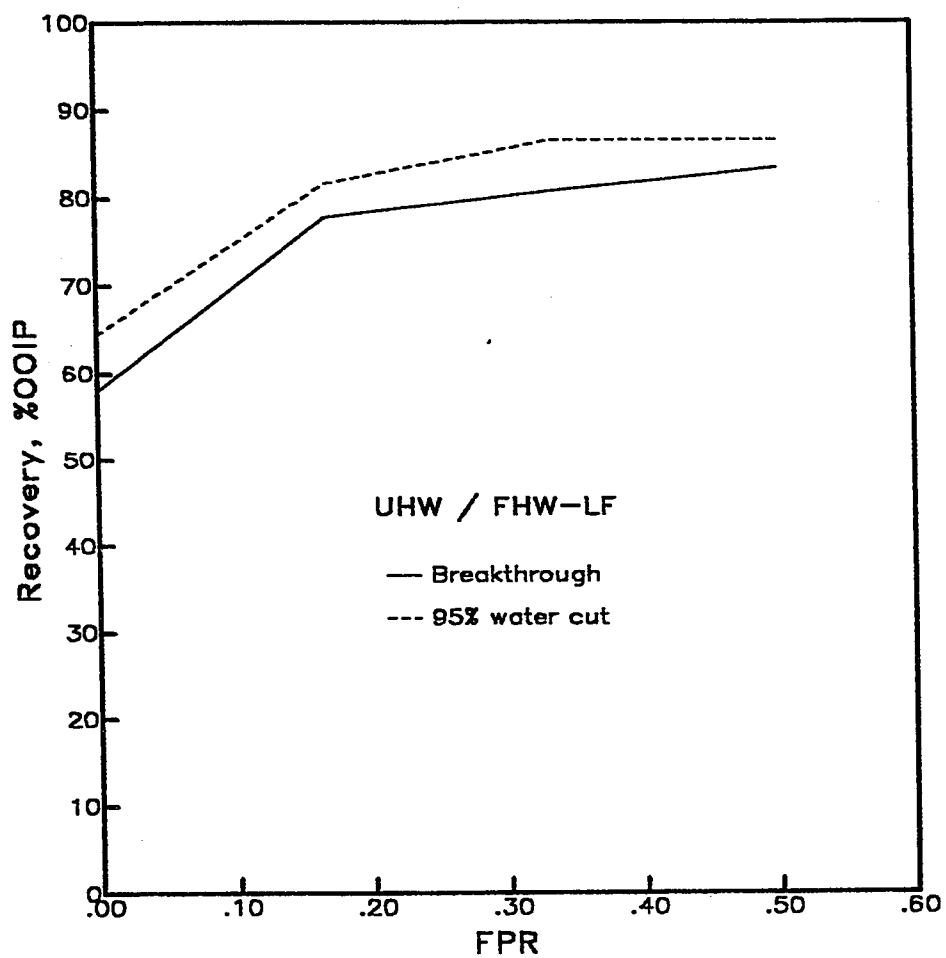
Figure 5.18: Recovery vs. fracture penetration ratio for horizontal wells with longitudinal fractures

mate recovery with a shallower fracture. The additional oil recovered after water breakthrough is relatively small compared to the recovery at water breakthrough. This would mean that a production strategy in which a horizontal well with a relatively deep fracture is used and the production is terminated after water breakthrough may be economically feasible.

Figures 5.19 and 5.20 are plots of the water cut as a function of the water injected and the oil recovery, respectively, for the UHW and the FHW/LF. Figure 5.19 shows that the pore volume of water injected at water breakthrough for the longitudinal fractured horizontal well (about 0.57) is higher than that for the UHW (0.40 pv). Further, it is not affected significantly by the FPR. After water breakthrough, steep increase in the water cut is obtained. At water cut of 95%, the water injected reaches about 0.73 pv for the FHW/LF and 0.64 pv for the UHW, with the corresponding oil recovery being (Fig. 5.20) about 82%, 86.5% and 86.5% OOIP for the FHW/LF with FPRs of 0.167, 0.333 and 0.500, respectively, and 64.4% for the UHW.

Figure 5.21 shows the pressure drop as a function of the water injected for the UHW and the FHW/LF. Gradual increase in the pressure drop is observed as soon as the flooding process starts. After this point the pressure drop increase is proportional to the height of water/oil interface in the system. At water breakthrough, the pressure drop reaches 0.303 psig for the FHW/LF compared to 0.305 psig for the UHW. This increase in the pressure drop from the start of production is almost equal to $\Delta\rho gh$ or 0.043 psig, where h is the initial height of the oil zone.
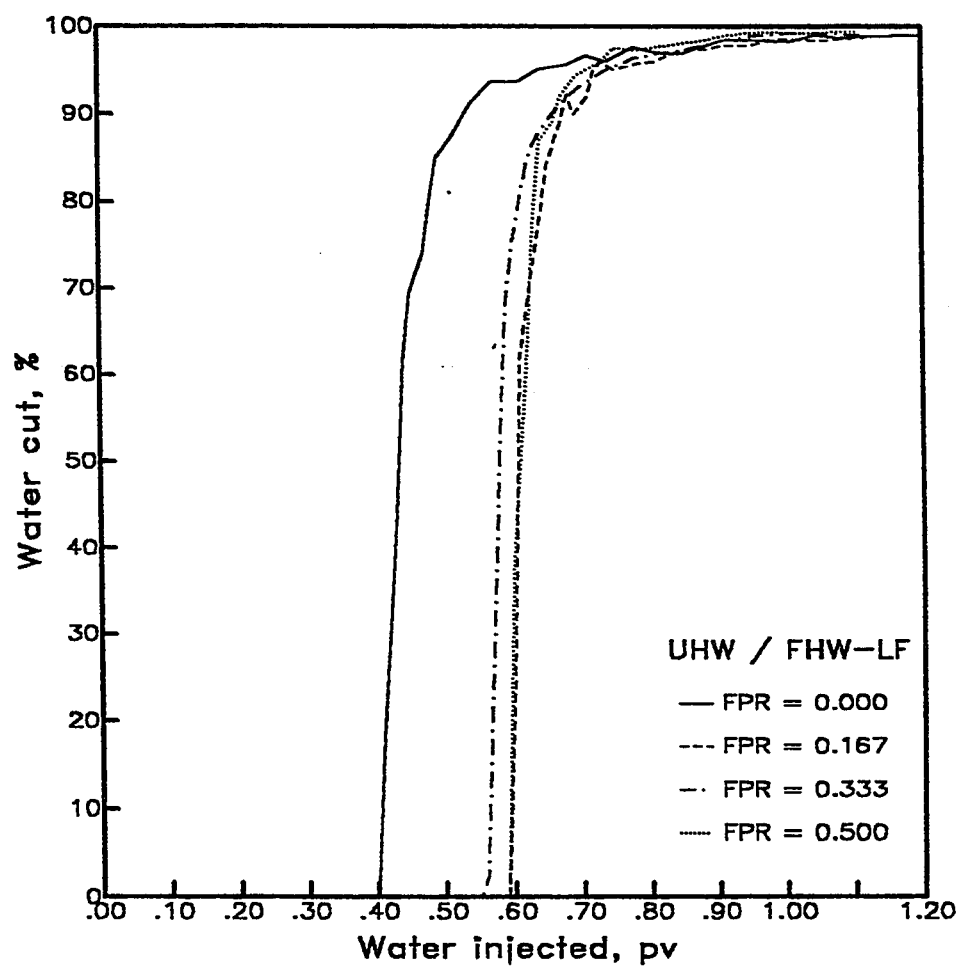
Figure 5.19: Producing water cut vs. pore volume injected
for horizontal wells with longitudinal fractures
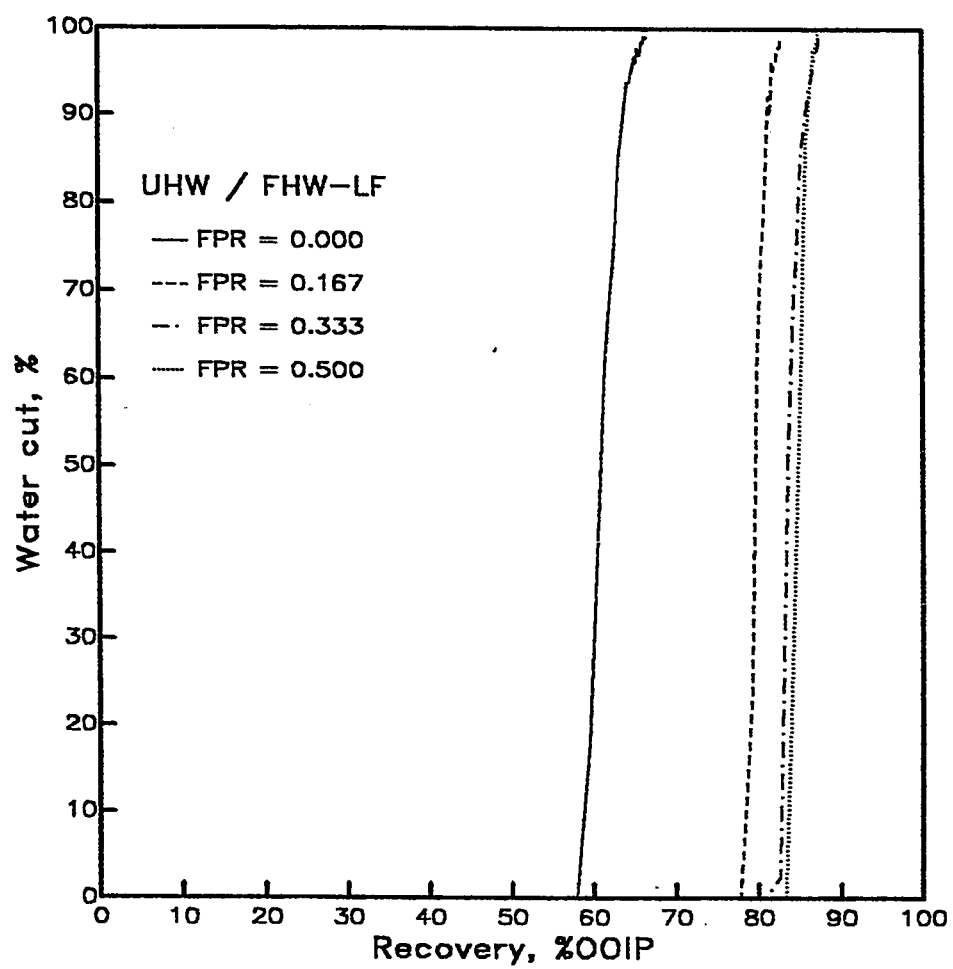
Figure 5.20: Producing water cut vs. recovery for horz. wells with longitudinal fractures
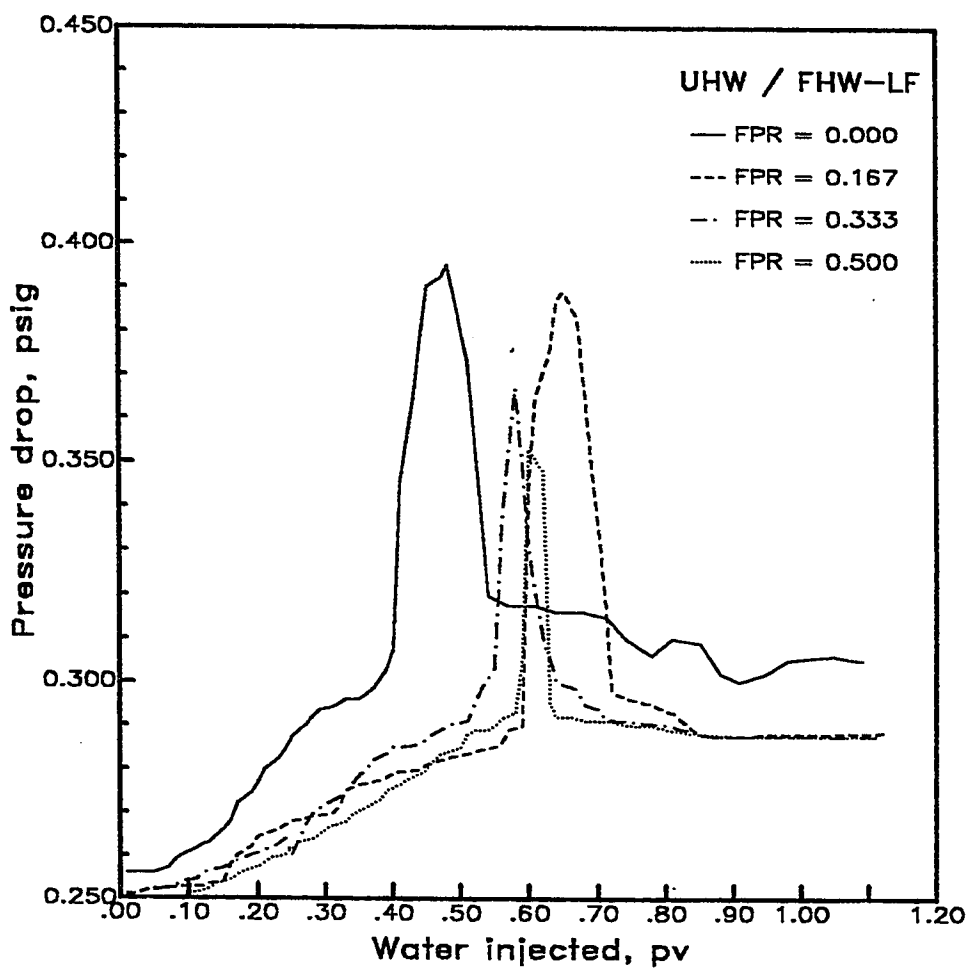
Figure 5.21: Pressure drop vs pore volume injected for horizontal wells with longitudinal fractures

After water breakthrough, the pressure drop reaches a maximum of 0.389, 0.387 and 0.353 psig for the FHWs/LF with FPRs of 0.167, 0.333 and 0.500, respectively, compared to 0.395 psig for the UHW during the two-phase flow period.

5.2.5 Unfractured Horizontal Well vs Horizontal Well with Single Orthogonal Fracture

In this case, a single fracture is created orthogonal to the wellbore. The fracture is extended in the x-direction with a fracture extension ratio (FER) defined as $\frac{2x_f}{W}$, where x_f is the fracture half length and W is the width of the oil reservoir. The perforated interval of the fractured well is limited to the width of the fracture.

In this study, the following two cases are considered:

CASE I : The fracture extension ratio (FER) is fixed at 0.833 and the effects of three different FPRs (z_f/h) on the production performance are investigated.

CASE II: The fracture penetration ratio (FPR) is fixed at 0.333 and the effects of two different FERs ($2x_f/W$) on the recovery performance are investigated.

The results of each case are discussed and compared to the UHW. The UHW is considered to have FPR and FER of zeros.

5.2.5.1 CASE I: Different Fracture Penetration Ratios

In this case, fracture penetration ratios (FPR) of 0.000 0.167, 0.333 and 0.500 are considered for the horizontal well.

Figure 5.22 shows the oil recovery as a function of the water injected for this case. Differences in the oil recovery are observed at and after water breakthrough. Water breaks through first in the UHW with recovery of 58% OOIP compared with 73.64%, 76.25% and 77.53% OOIP for the FHW with FPR of 0.167, 0.333 and 0.500, respectively. About 10% to 14% of the oil recovered is added to the recovery after water breakthrough (at 1.0 pv of water injected).

Figure 5.23 plots the oil recovery versus the FPRs for Case I. Significant improvements in breakthrough and ultimate recoveries result with the presence of fractures. Increasing the fracture penetration, however, has little effect on the oil recoveries.

It may be concluded that creating a highly-conductive fracture with a depth of 0.20 to 0.30 of the initial oil thickness in a bottom water drive reservoir is sufficient to produce most of the oil (~83.0% OOIP for FPR of 0.300 compared to ~86% OOIP for FPR of 0.500). In hydraulic fracturing, increasing the depth of the fracture beyond these values will not add much to the oil recovery. However, in naturally fractured reservoirs there is no control on the fracture dimensions, and, therefore, the fractures may further extend down into the bottom water aquifer or up into the gas cap.
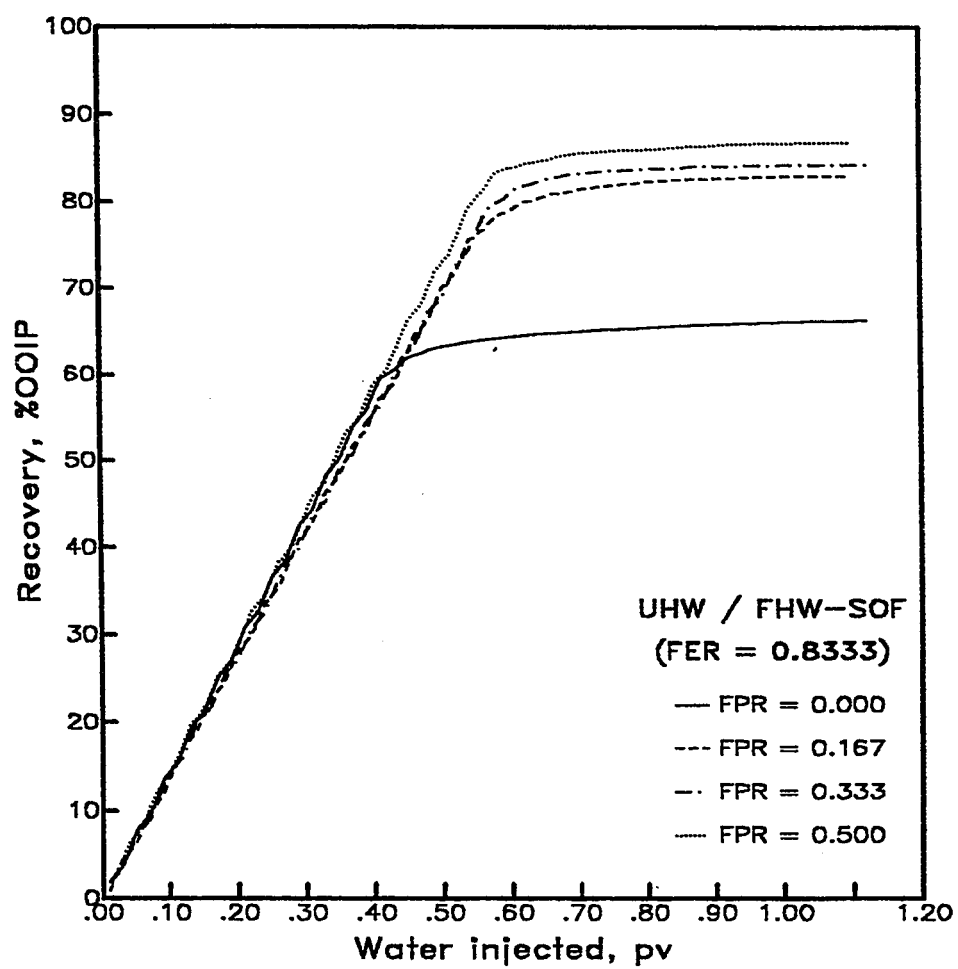
Figure 5.22: Recovery vs. pore volume injected for horizontal wells with SOF, case I
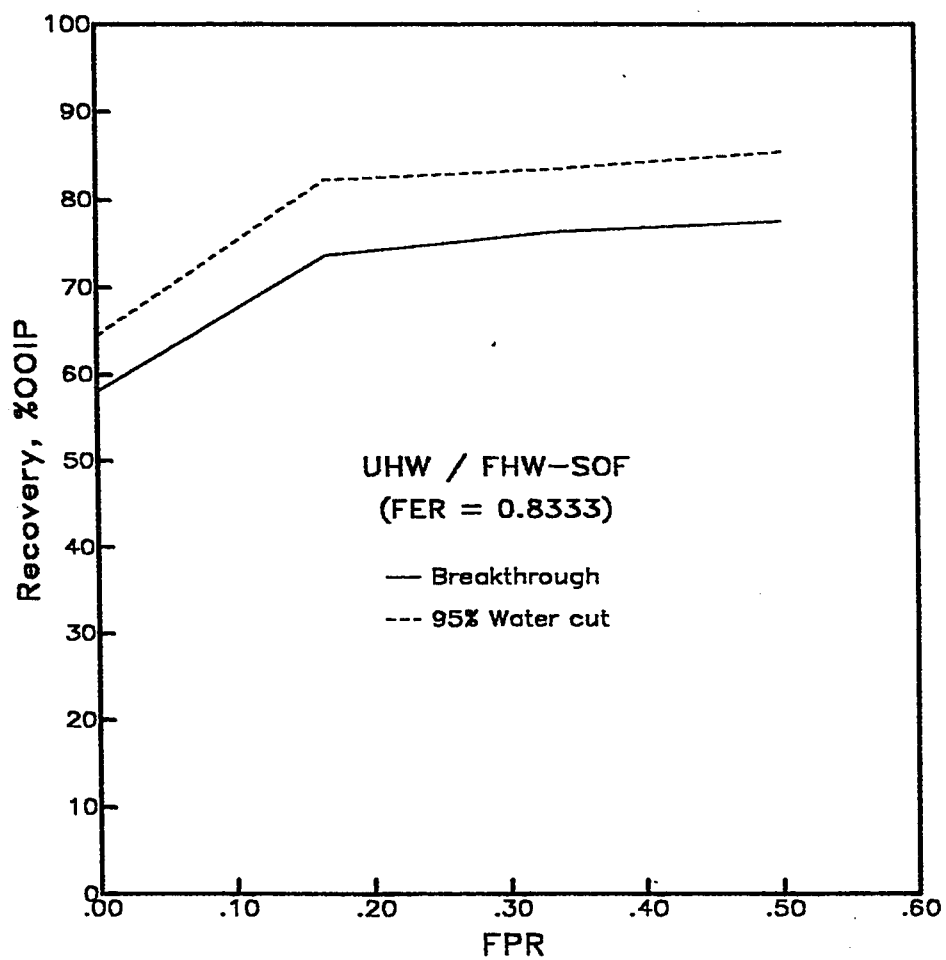
Figure 5.23: Recovery vs. fracture penetration ratio for horizontal wells with SOF, case I

Figures 5.24 and 5.25 show the water cut as a function of the water inject-
ed and the oil recovery, respectively. At water breakthrough, it is observed
that the pore volumes of water injected for the three fractured wells are
almost similar (about 0.54 pv) but higher than that for the UHW (0.40 PV).
Figure 5.25 shows that water cut steeply increases after water breakthrough.

It may be worthwhile to compare the oil recovery of the deepest fracture
at water breakthrough (77.53% OOIP) to the recovery of the shallowest one at
a water cut of 95% (82.25% OOIP). This comparison indicates that it might
be more appropriate to create a deep fracture and produce water-free oil
than creating a shallow fracture and produce up to a water cut of 95% to add
only about 5% OOIP to the production. This would eliminate the costly sur-
face production facilities needed for handling the produced water. Economics,
however, would be the deciding factor for the choice. An alternative operat-
ing strategy would be to reduce the rate as water tends to breakthrough. This
would mean a lower rate for the smaller penetration.

Figure 5.26 shows the pressure drop as a function of the water injected
for the FPRs of 0.000 (UHW)), 0.167, and 0.333 with FER of 0.833. Differences
in the pressure drop among the FPRs are noted. As soon as injection starts,
the pressure drop rises from the initial equilibrium static pressure drop of
0.25 psig to 0.26, 0.31 and 0.28 psig for the UHW, FPR of 0.167 and 0.333,
respectively. After this point a gradual increase in the pressure drop until
water breakthrough is observed for all cases. It is observed that the increase
in the pressure drop for these cases after the initiation of flow through the
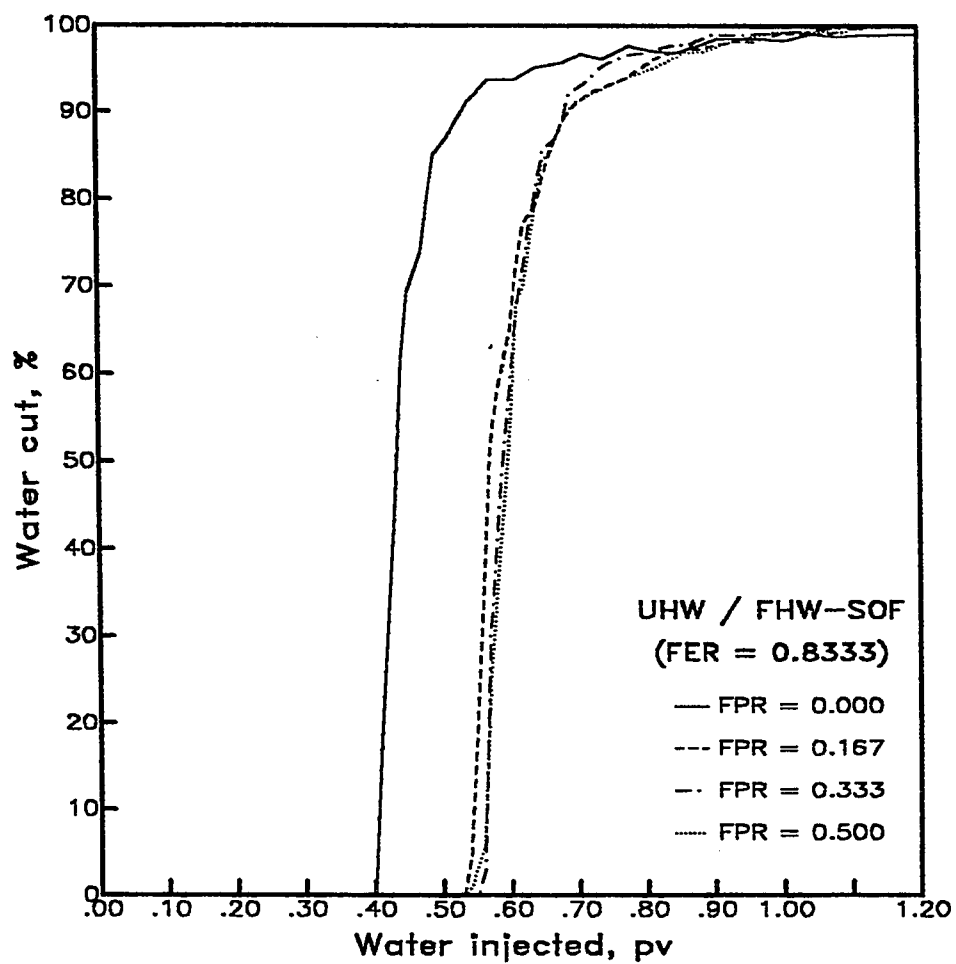
Figure 5.24: Producing water cut vs. pore volume injected for horizontal wells with SOF, case I
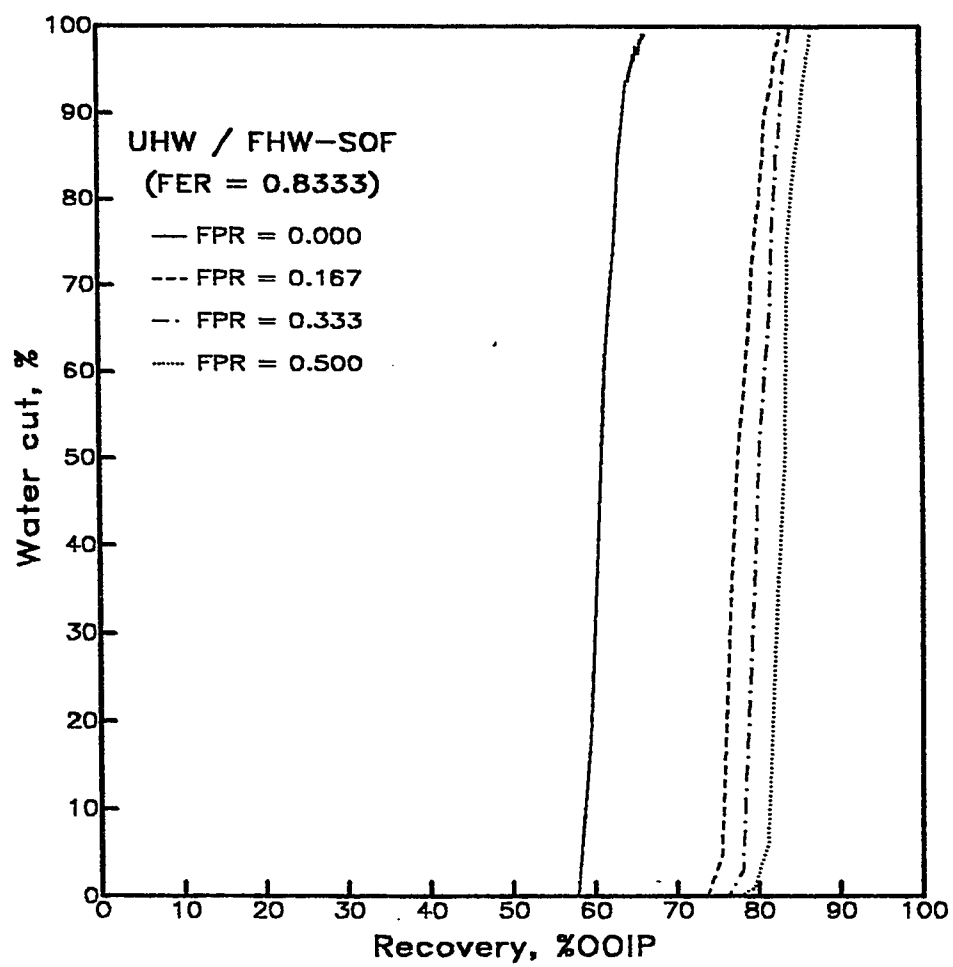
Figure 5.25: Producing water cut vs. recovery for horizontal wells with SOF, case I
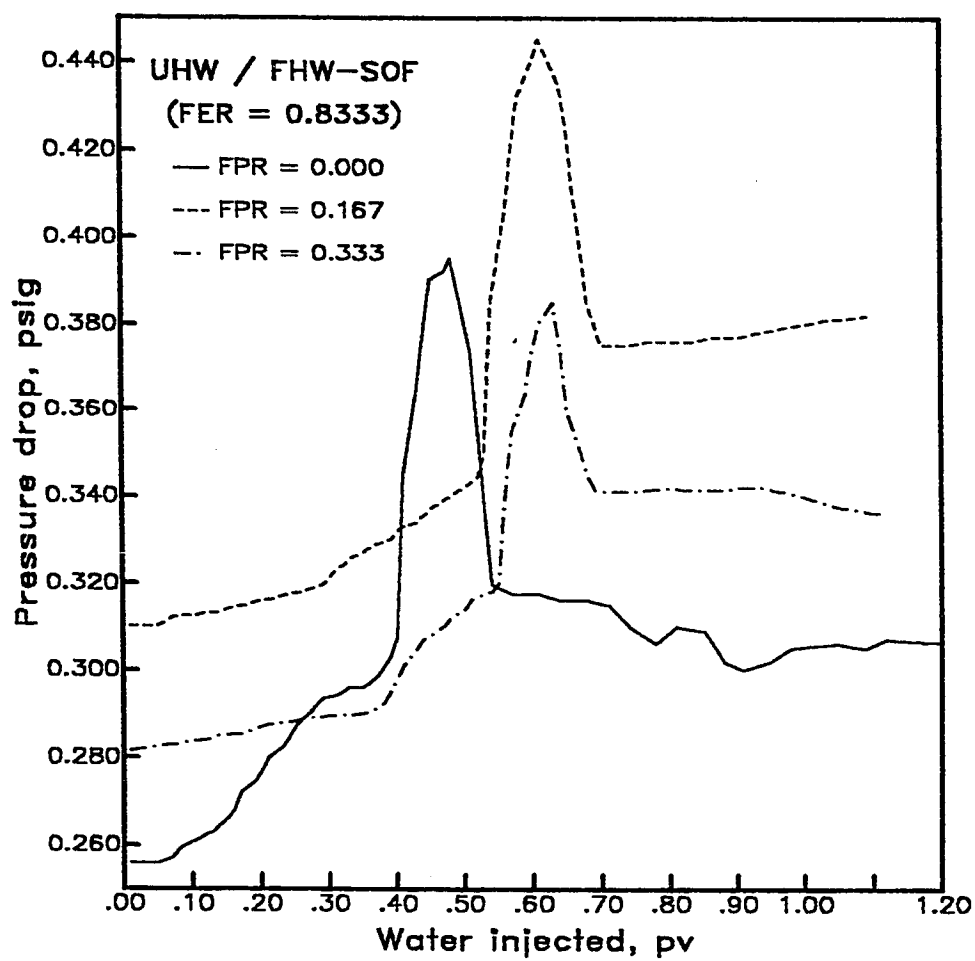
Figure 5.26: Pressure drop vs pore volume flooded for horizontal wells with SOF, case I

system is proportional to the height of the water/oil interface. At water break-through, the pressure drops are 0.305, 0.353, 0.324 psig for FPRs of zero (UHW), 0.167 and 0.333, respectively. After water breakthrough, the pressure drop continues to increase reaching maxima of 0.395, 0.445 and 0.385 psig for the FPRs of zero, 0.167 0.333, respectively. After injecting 1.00 pv of water, the pressure drop recorded is 0.306, 0.388 and 0.340 psig for zero, 0.167 and 0.333 FPRs, respectively.

It is noted that the pressure drop is higher for the FHW/SOF during the flooding process, however, the oil recovery is improved when the fracture is present. The reason for the higher pressure drop is mainly due to the limited perforated interval and the geometry of the flow in the fractures and around the wellbores for the FHW/SOF. It is also observed that the pressure drop increases with decreasing the FPR. For the FHW/SOF, the flow is radial in the fracture around the perforations. In shallower fractures, less area is in con-tact with the reservoir and therefore the pressure drop is higher in the shal-lower fracture compared to the deeper fracture. The higher recovery is due to the presence of the fracture which hinders the water cresting.

5.2.5.2 CASE II: Different Fracture Extension Ratios

In this case, the fracture extension ratio (FER) is varied. Two FERs of 0.333 and 0.833 are investigated and compared to the UHW (FER = 0.0).

Figure 5.27 shows the oil recovery as a function of the water injected for case II. At water breakthrough, about 72.51% OOIP is recovered for the FER
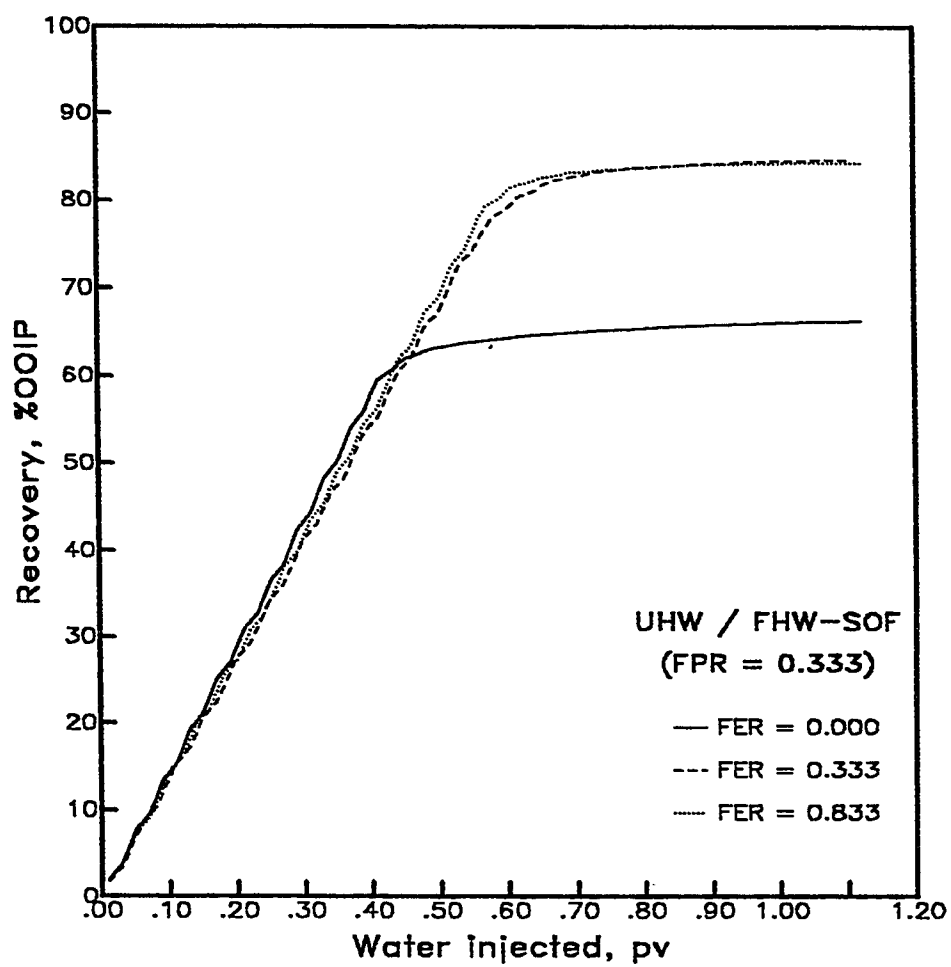
Figure 5.27: Recovery vs. pore volume injected for horizontal wells with SOF, case II

of 0.333 compared to 76.25% OOIP for the EPR of 0.833. The oil recovery is 58% OOIP for the UHW (FER=0.0). After water breakthrough and at about 0.70 pv of water injected, the oil recoveries are identical for the fractured wells (about 82% OOIP). After injecting 1.00 pv of water, the recovery reaches 84.20% OOIP for both the fractured wells compared to 66% OOIP for the UHW.

For the FHW/SOF, it may be concluded that the longer the fracture extension the better the oil recovery at water breakthrough, however, Beyond a FPR of 0.333, the ultimate oil recovery does not improve as shown in Fig. 5.28.

Figures 5.29 and 5.30 show the water cut as a function of the water injected and the oil recovery for case II. Water breakthrough occurs at almost the same pore volume injected (0.53 pv) for both the FHWs. For the UHW, water breaks through at a lower value (0.40 pv) of the pore volume injected. It is shown in Fig. 5.30 that, at a water cut of 70%, the oil recoveries of the FHW's become identical and follow the same performance until the end of the process. However, more water injection is needed to reach the ultimate recovery for the shorter fracture. At water cut of 95%, the pore volume injected to reach 83.5% OOIP is 0.79 and 0.75 for the FERs of 0.333 and 0.833, respectively.

Figure 5.31 shows the pressure drop as a function of the water injected for case II. As soon as the flooding process starts, the pressure drop increases from the initial static value of 0.25 psig to 0.2815 psig for the FHWs
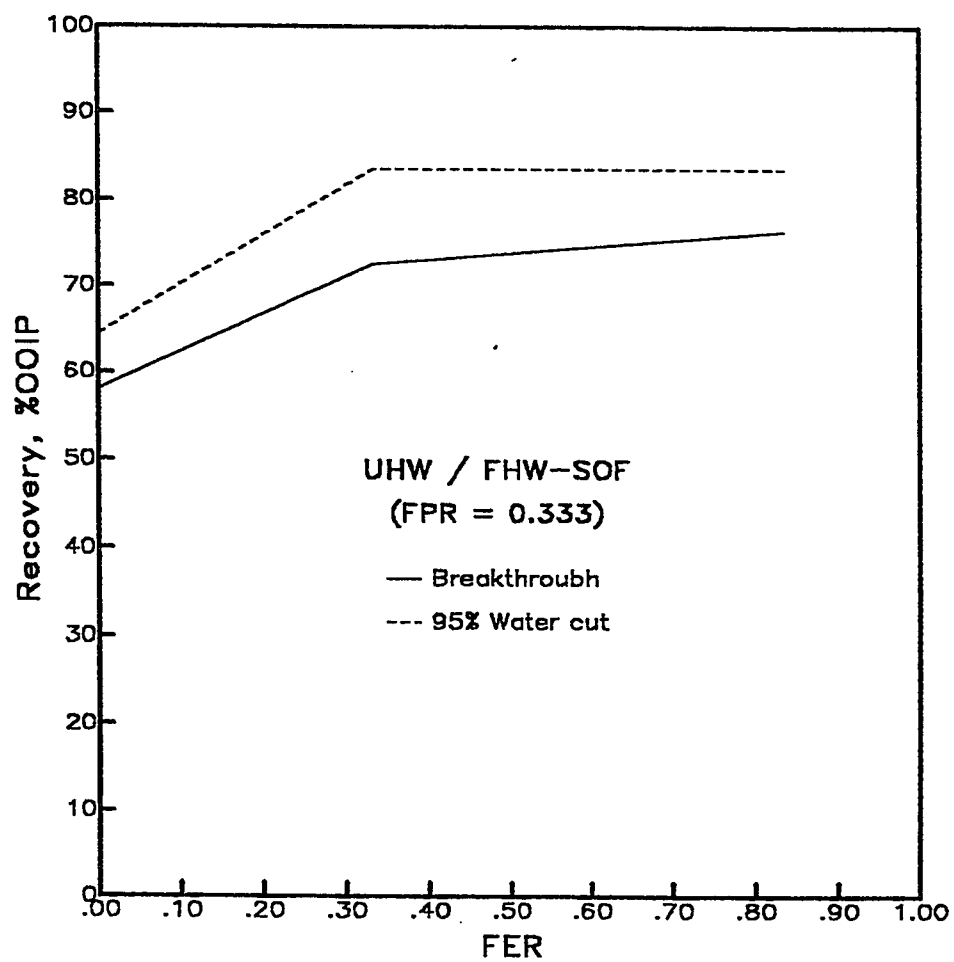
Figure 5.28: Recovery vs. fracture extension ratio
for horizontal wells with SOF, case II
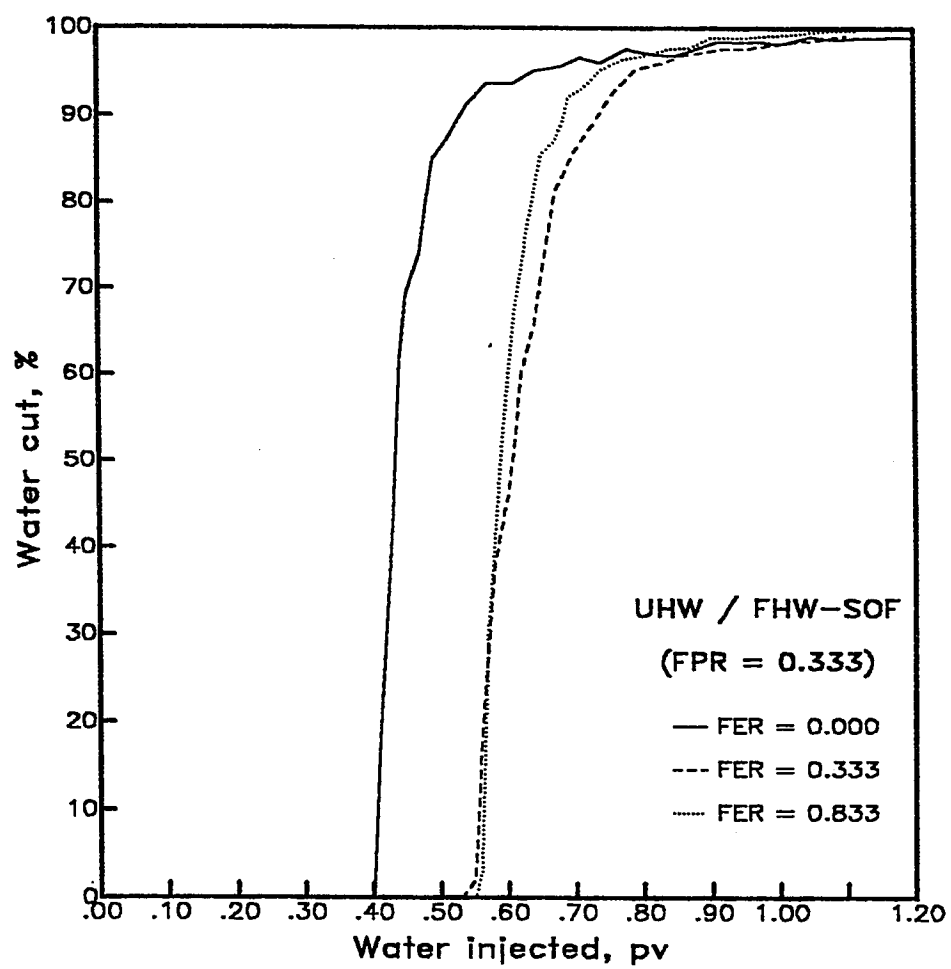
Figure 5.29: Water cut vs. pore volume injected
for horizontal wells with SOF, case II
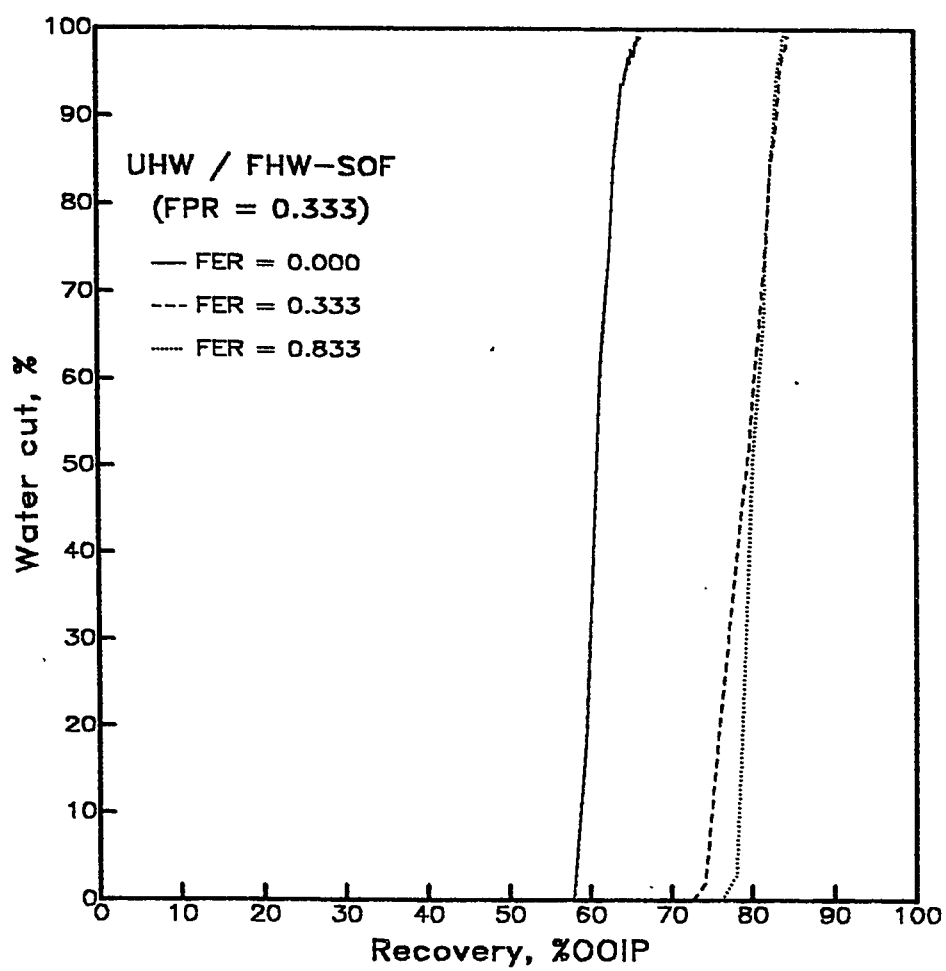
Figure 5.30: Producing water cut vs. recovery for
horizontal wells with SOF, case II
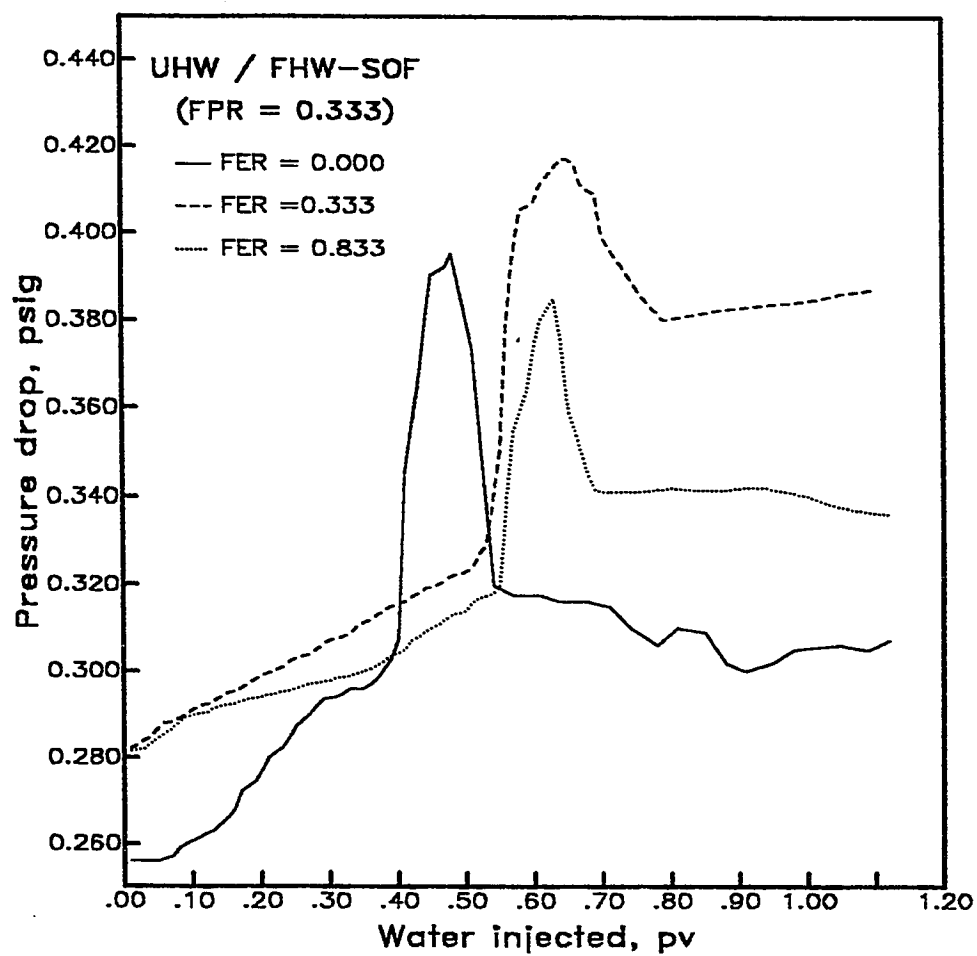
Figure 5.31: Pressure drop vs pore volume Injected
for horizontal wells with SOF, case II

compared to 0.260 psig for the UHW. As the process continues, the effect of fracture extension on the pressure behavior becomes more pronounced. At water breakthrough, the pressure drop increases gradually to 0.325 psig for the FER of 0.333 compared to 0.324 psig for the FER of 0.833 and 0.305 psig for the UHW. The maximum pressure drop reaches 0.417 and 0.385 psig for the FERs of 0.333 and 0.833, respectively, compared to 0.395 psig for the UHW during the two-phase flow period in the wellbore. After injecting 1.0 pv of water, the pressure drop recorded is 0.385, 0.340 and 0.305 psig for FER of 0.333, 0.833 and the UHW, respectively.

It may be concluded that using single orthogonal fracture with longer extension improves the breakthrough oil recovery, requires less volume of water injected to reach the ultimate oil recovery, decreases the pressure drop and delays water breakthrough. However, the ultimate oil recovery does not change with increasing the FER. It may also be concluded that the shorter the fracture extension, the higher the pressure drop. Relatively more viscous forces are created which leads to higher pressure drop and hence the relative earlier water breakthrough. The lower pressure drop associated with the UHW is due to the long perforated interval of the UHW compared to the perforated intervals of the FHWs which are limited to the fracture widths.

5.2.6 Unfractured Horizontal Well vs. Horizontal Wells with Multiple Orthogonal Fractures

In this study, the effects of a number of orthogonal fractures on the production performance of horizontal wells are investigated. Four experiments were performed for this purpose using one, two, three and four equally-spaced orthogonal fractures. The horizontal well was placed at the top of the oil reservoir as described before. The dimensions of all fractures were fixed at a FPR of 0.333 and a FER of 0.833. The well was perforated only at the location(s) of the fracture(s). Therefore, fluids would flow radially through the fractures into the wellbore [38]. The results of the unfractured horizontal well were used as the basis for comparison. Throughout the discussion, n_f is defined as the number of orthogonal fractures (OF) and is assigned a value of zero for the unfractured well.

Figure 5.32 shows the oil recovery as a function of the water injected for the UHW and the FHW/MOF. Water breakthrough occurs first in the UHW followed by the FHW/MOF with one, two, three and four fractures, respectively. The oil recovery at water breakthrough is 58%, 76.25%, 78.86%, 81.70% and 82.19% OOIP for number of fractures (n_f) of zero, one, two, three and four, respectively. This represents an increase in the oil recovery by 131%, 136%, 141% and 142% for the FHW with n_f of one, two, three and four, respectively compared to the UHW. It can be observed that there is only 1% increase in the recovery when n_f is increased from three to four.
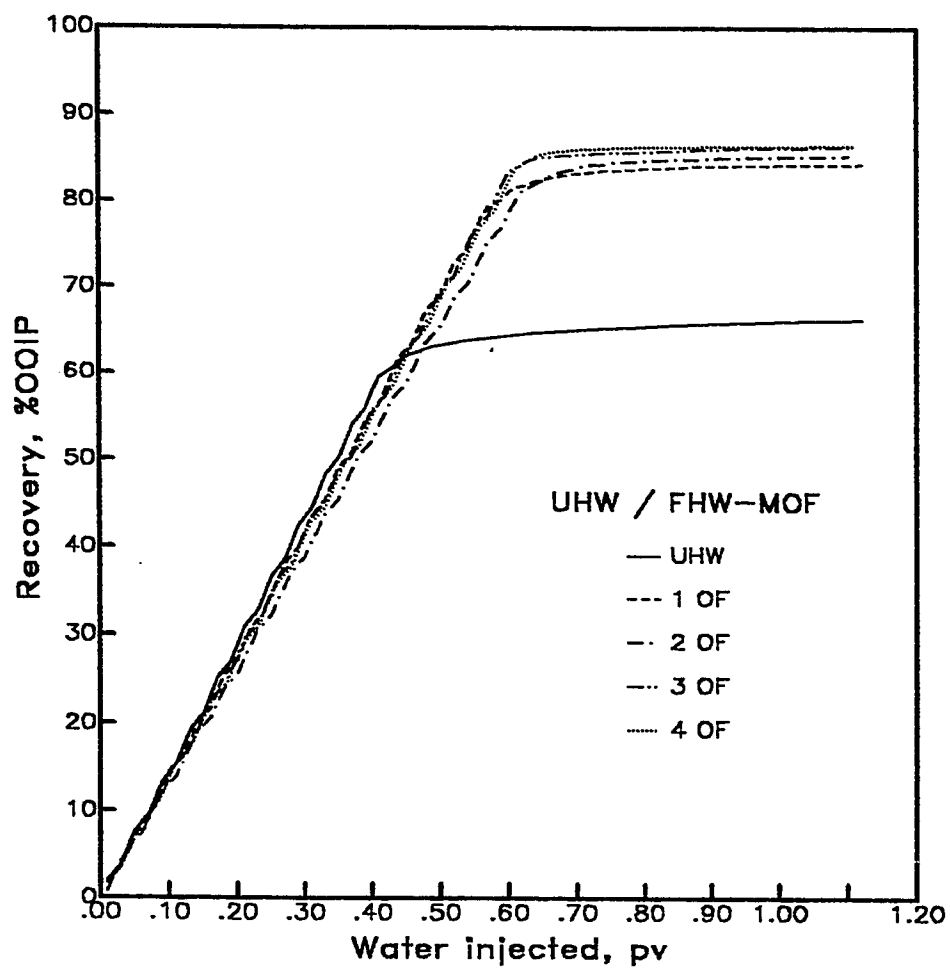
Figure 5.32: Recovery vs. pore volume injected
for horizontal wells with MOF.

After water breakthrough, small increases in the oil recovery are observed. At water cut of 95%, the recovery reaches 64.4%, 83.47%, 84.5%, 85.38% and 85.86% OOIP for number of fractures of zero (UHW), one, two, three and four, respectively. In comparison to the unfractured well, there is an increase in the oil recovery of 129.6%, 131.2%, 132.5% and 133.3% for the fractured horizontal well with n_f of one, two, three and four, respectively. The increases in oil recoveries after the first fracture are limited. It is observed from Fig. 5.33 that the oil recovery at water breakthrough increases with increasing the number of fractures up to three fractures. However, the ultimate oil recovery is not showing much increase after the first fracture. It may be noted that the recovery may reach about 82% OOIP of water-free oil with three fractures. Almost the same recovery, however, may be produced with one fracture only at a water cut of 95%.

Figures 5.34 and 5.35 show the water cut as a function of the water injected and the oil recovery, respectively for the UHW and the FHW/MOF. It is observed from the figures that the pore volume of water injected till water breakthrough increases by fracturing the well. For two or more fractures, however, the pore volume of water injected till breakthrough does not change that much.

Figure 5.35 shows that a significant increase in the oil recovery is obtained with the orthogonal fractures compared to the UHW. The number of fractures, however, has only a small effect on production (2% to 4% OOIP).
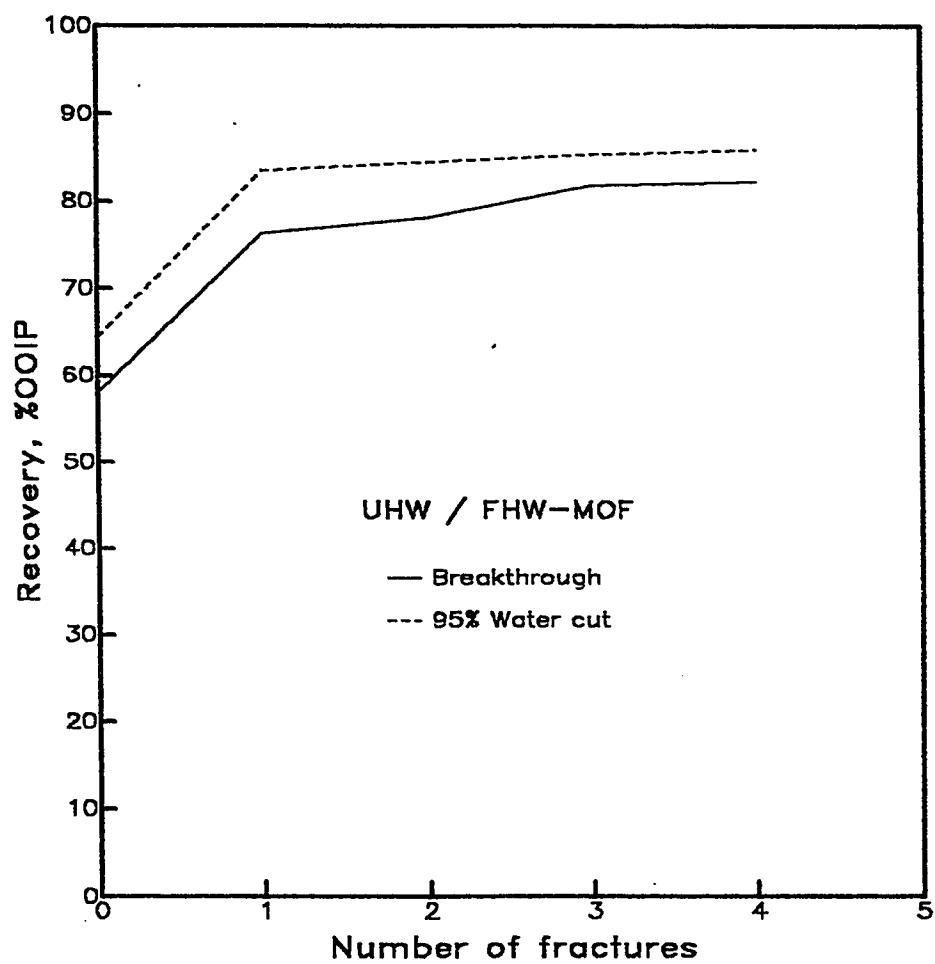
Figure 5.33: Recovery vs. number of fractures
for horizontal wells with MOF.
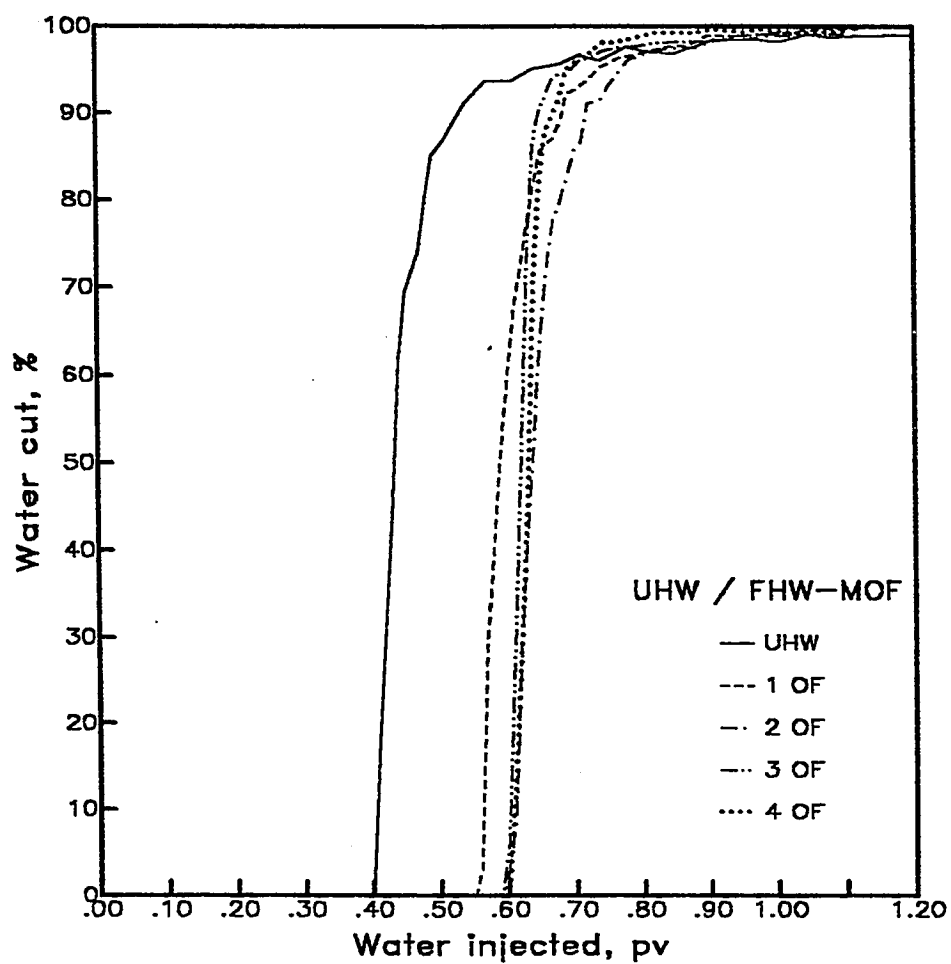
Figure 5.34: Water cut vs. pore volume injected
for horizontal wells with MOF.
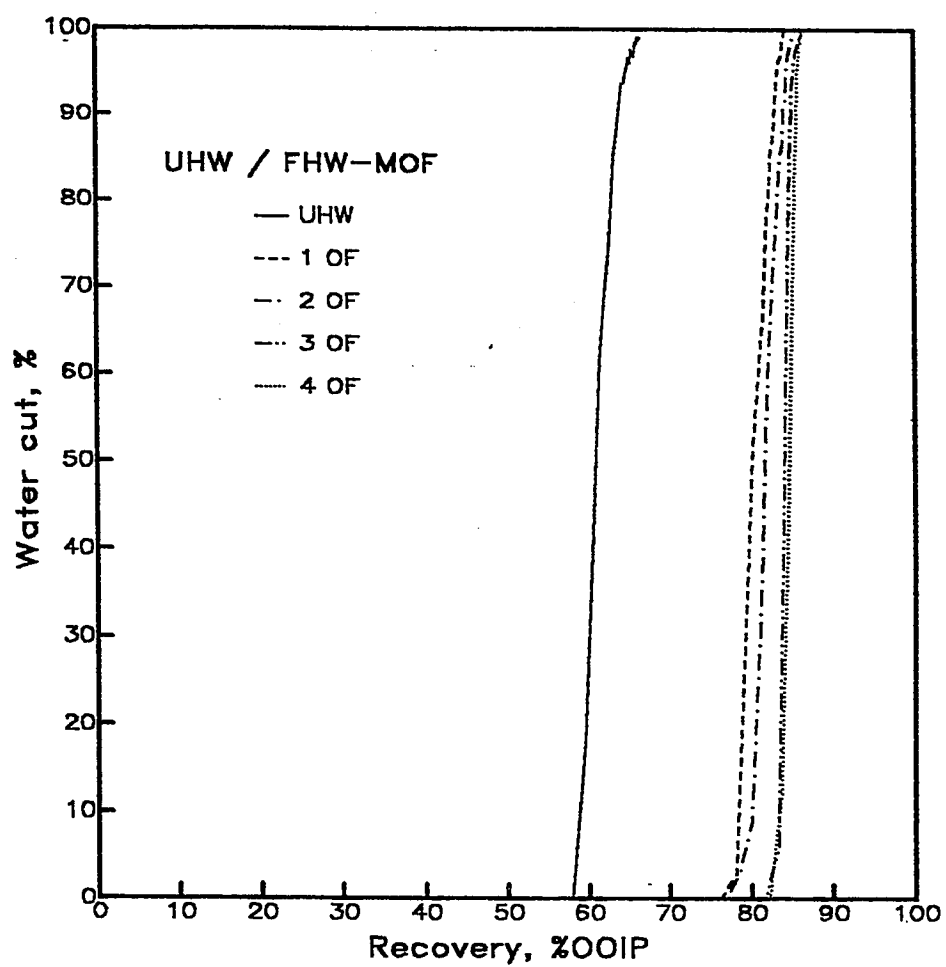
Figure 5.35: Producing water cut vs. recovery
for horizontal wells with MOF.

Figure 5.36 shows the pressure drop as a function of the water injected for the UHW and n_f of one and three orthogonal fractures. As soon as the production starts, the pressure drop increases from the initial static reading of 0.25 psig into 0.2815 psig and 0.2765 psig for n_f of one and three, respectively compared to 0.26 psig for the UHW ($n_f = 0$). After this point, a gradual increases in the pressure drop for all cases are noted until water breakthrough. At water breakthrough, the pressure drop reaches 0.325 and 0.320 psig for n_f of one and three, respectively, compared to 0.305 psig for the UHW. The gradual increase in the pressure drop for all cases under study from the start of production till water breakthrough are found to be proportional to the height of the water-oil interface in the system. At water breakthrough, the increase in the pressure drop from the start of production is about 0.0435 psig, or $\Delta \rho g h$ where; h is the initial height of the oil zone (0.5 ft.).

After water breakthrough, the pressure drop increases rapidly and reaches a maximum value of 0.385 and 0.370 psig for n_f of one and three, respectively, compared to 0.395 psig for the UHW. This rapid increase is mainly due to the dominance of viscous forces during the two-phase flow period through the perforations and the wellbore. As the water cut increases, the pressure drop decreases to 0.341 and 0.335 for the n_f of one and three, respectively compared to 0.316 psig for the UHW.

It is observed that the UHW is experiencing the lowest pressure drop throughout the process except during the two phase peak; it is showing the
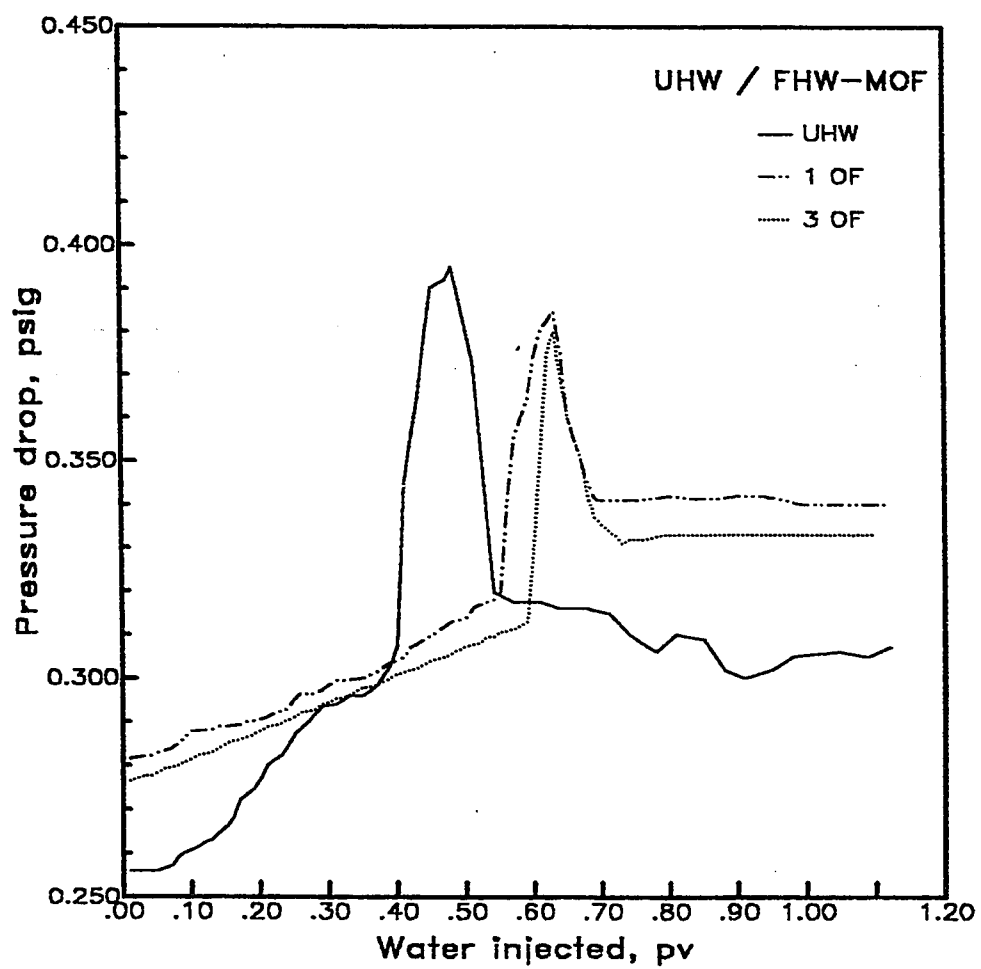
Figure 5.36: Pressure drop vs pore volume injected for horizontal wells with MOF.

maximum pressure drop of 0.395 psig compared to 0.385 and 0.370 psig for one and three fractures, respectively. This is mainly due to the flow converges into a larger area $(2\pi r_w L_w)$ of 25.14 sq. inches for the UHW compared to a small area in case of the orthogonal fracture $(2\pi r_w w_f)$ of 0.284 sq. inches; where r_w is the wellbore radius, L_w is the wellbore length and w_f is the fracture width. Therefore, the pressure drop becomes higher in case of horizontal well with multiple orthogonal fractures.

It may be generally concluded that creating multiple orthogonal fractures in horizontal wells delays the water breakthrough, increases the oil recovery and increases the pressure drop through the system. The pressure drop, however, decreases with increasing the number of orthogonal fractures. The oil recovery increases with the number of fractures up to a limit (three fractures at water breakthrough and one at 95% water cut), beyond which the oil recovery does not change much with increasing the number of fractures.

In field applications, careful design of the wellbore and fracture geometries and dimensions as well as careful study of the reservoir engineering aspects are extremely important in order to optimize the number of orthogonal fractures and to achieve successful technical and economical projects.

5.2.7 Fractured Vertical Wells vs. Fractured Horizontal Wells

In this section, the production performances of vertical wells with vertical fractures (FVW), horizontal wells with single-orthogonal fractures (FHW/SOF) and horizontal wells with longitudinal fractures (FHW/LF) are compared and discussed. Three fracture penetration ratios (FPR) are studied for each case; these are 0.167, 0.333 and 0.500. The fracture extension ratios (FER) are taken as 0.833 for the FVW and FHW/SOF and 0.889 for the FHW/LF. The fractures extend in the x-direction for the vertical wells and horizontal wells with orthogonal fractures, while they extend in the y-direction for the horizontal wells with longitudinal fractures, see Figure 4.3.

It is worthwhile to mention that although the wellbore/fracture configurations are different among the cases under study, each case is designed to drain the same reservoir volume. Hence, the comparison of the production performance may result in the best production configuration that can be used. It should be noted that the horizontal well can be extended to drain much more area compared to the vertical well. In field applications, economics as well as well/fracture configurations are the most important parameters to consider.

Detailed discussion and comparison of the production performance of fractured wells with FPR of 0.333 are presented as an example of the various fracture penetration ratios studied. This is followed by general discussion and comparison of the production parameters at various FPRs.

It is worthwhile to mention that the dimensions of the fractures considered in this example are 0.181 inch width x 2 inch depth x 16 inch extension for the FHW/LF, 0.181 inch width x 2 inch depth x 10 inch extension for the FHW/SOF, and 0.181 inch width x 2 inch depth x 10 inch extension for the FVW/VF. The corresponding contact areas with the matrix are 69.76, 43.6 and 43.6 sq.in. for the FHW/LF, FHW/SOF and FVW/VF, respectively.

Figure 5.37 shows the oil recovery as a function of the water injected for fractured vertical and horizontal wells with a FPR of 0.333. Differences in the recovery performance are noted among the cases studied. At water breakthrough, the oil recovery for the FVW is the lowest with 68.18% OOIP, the FHW/SOF comes in the middle with 76.25% and the FHW/LF shows the highest oil recovery of 80.71% OOIP. Further increase in the oil recovery after water breakthrough is observed. At water cut of 95%, the oil recovery increases to 76.42%, 83.47% and 86.5% OOIP for the FVW, FHW/SOF and FHW/LF, respectively.

It is observed that the ultimate oil recovery (at 95% WC) depends on both the FPR and the wellbore/fracture configuration used. It is also observed that the oil recovery at water breakthrough for the FHW/LF is better than the ultimate oil recovery for the FVW by about 106% and close to the ultimate oil recovery for the FHW/SOF (97%). Therefor, it may be more economic to create longitudinal fractures and produce until water breakthrough than creating single orthogonal fractures in horizontal wells or vertical fractures in vertical wells and producing up to 95% water cut. This may eliminate the need for the
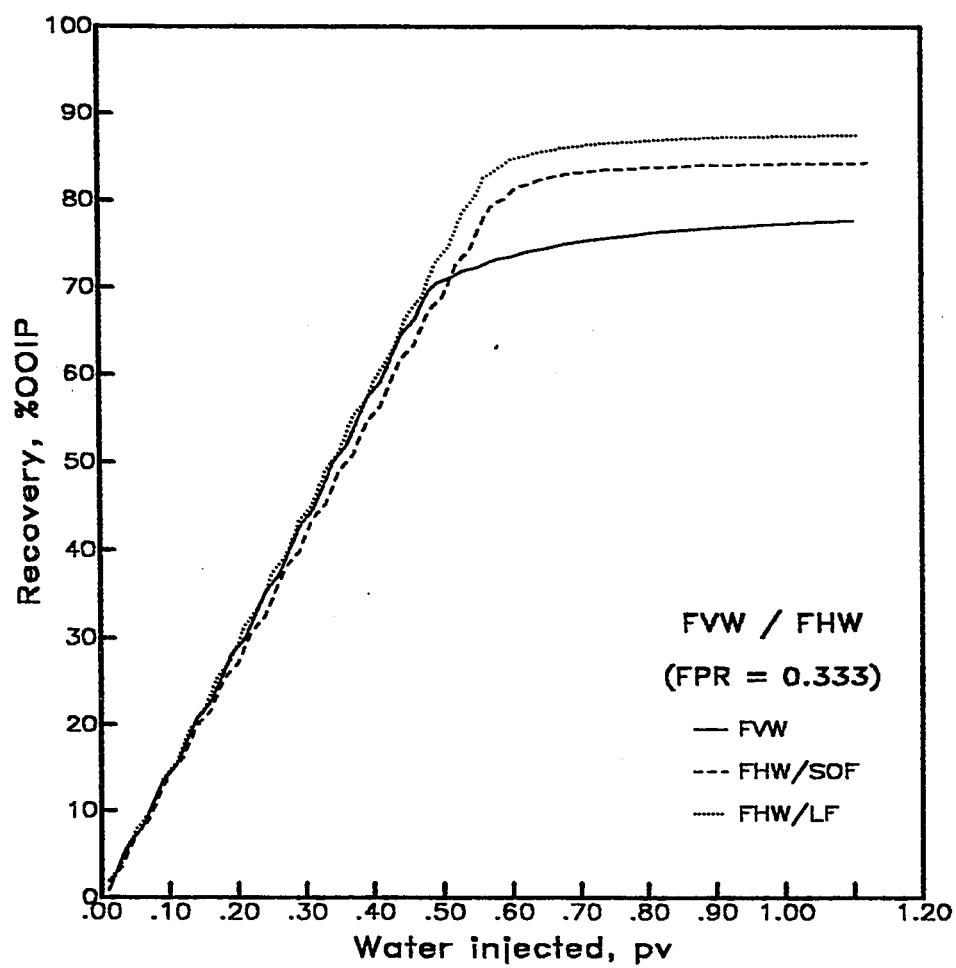
Figure 5.37: Recovery vs. pore volume Injected for
fractured horizontal and vertical wells

costly production facilities to handle the produced water. It may be conclud-
ed that the recovery performance of the FHW/LF is the best compared to
either that of the FHW/SOF or that of the FVW.

Figures 5.38 and 5.39 show the water cut as a function of the water inject-
ed and the oil recovery, respectively. At water breakthrough, the FVW shows
the lowest water injected with 0.47 pv compared to 0.55 for the FHW/SOF and
the FHW/LF. After water breakthrough, the FVW keeps to have the lowest
pore volume injected until water cut of 88% is reached. After this point, the
water injected exceeds that of the FHWs. At water cut of 95%, water injected
is 0.84 pv for the fractured vertical well compared to 0.75 pv for the fractured
horizontal wells.

After water breakthrough, it is observed from Fig. 5.39 that the water cut
increases very rapidly. At water cut of 95%, the oil recovery increases to
112%, 109% and 107% of the oil recovery at water breakthrough for the FVW,
FHW/SOF and FHW/LF, respectively. It is also observed that although the
water injected is similar for the FHW/SOF and the FHW/LF (Fig. 5.38), the cor-
responding oil recovery (Fig. 5.39) is always better for the FHW/LF through-
out the flooding process.

Figure 5.40 shows the pressure drop as a function of the water injected
for the FVW and the FHW. The lowest pressure drop shown is for the
FHW/LF, the FHW/SOF comes in the middle and the FVW records the highest.
For all cases, the initial equilibrium static pressure drop is 0.25 psig.
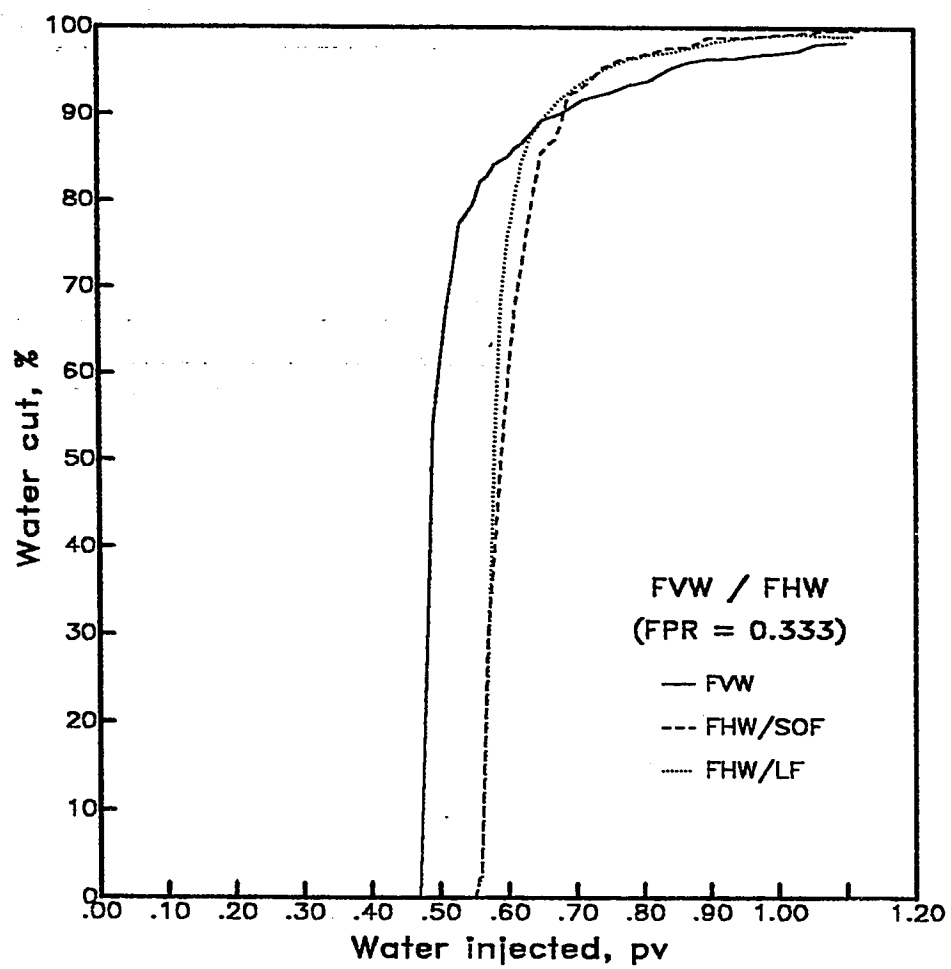
Figure 5.38: Water cut vs. pore volume injected for
fractured horizontal and vertical wells
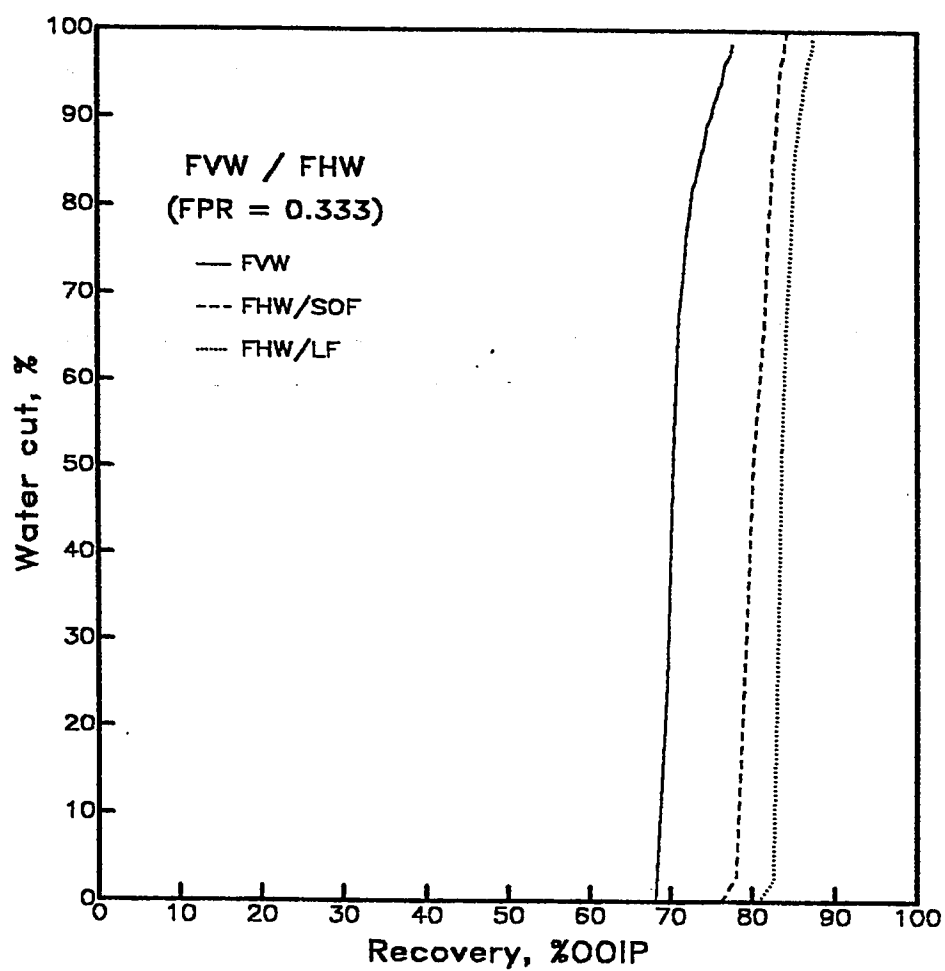
Figure 5.39: Producing water cut vs. recovery for
fractured horizontal and vertical wells
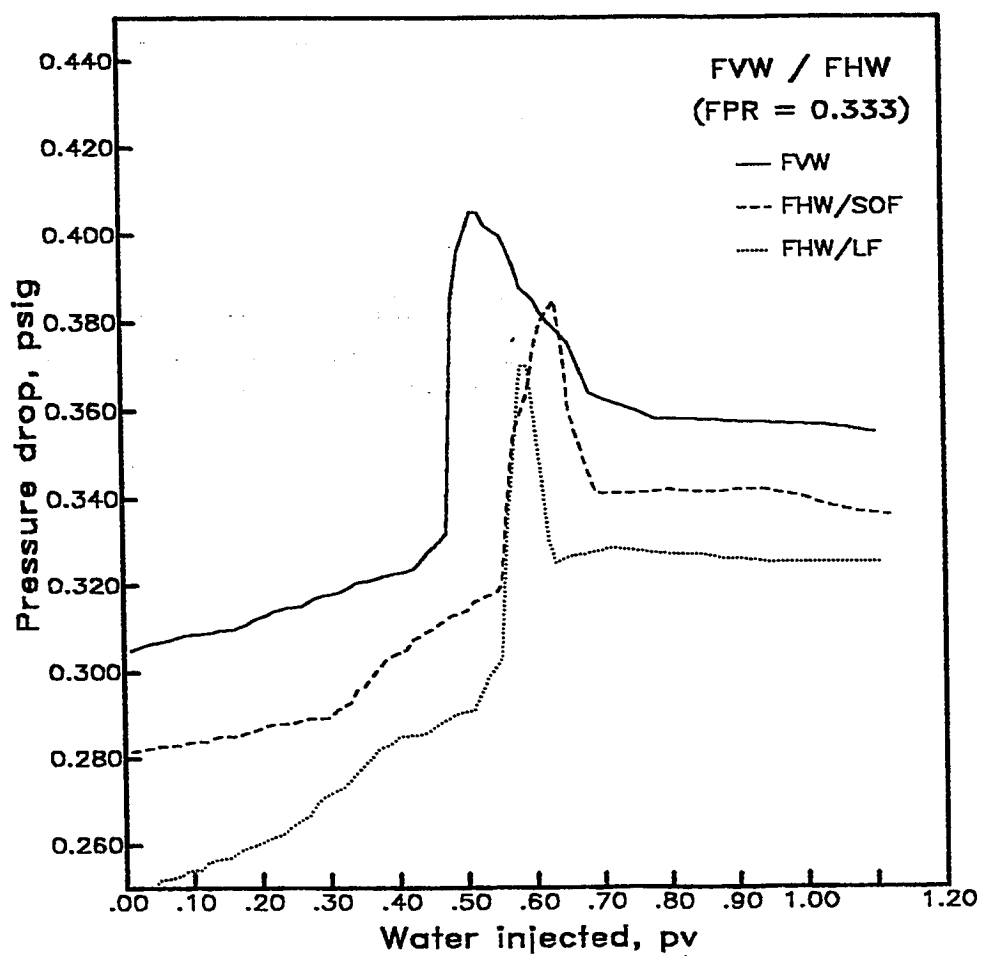
Figure 5.40: Pressure drop vs pore volume injected for
fractured horizontal and vertical wells

For the FHW/LF, because of the longer perforated interval (16.0 inches out of 18.0 inches length of the model, equal to the fracture extension), the flow is linear upward inside the fracture with stable water/oil interface and therefore, the pressure drop needed to initiate the flow through the fractured system is almost negligible and as a result once the flooding process starts the pressure drop increases gradually from 0.25 psig (static pressure due to $\rho_o gh$) to 0.293 psig at water breakthrough. This increase is exactly equal to $\Delta \rho gh$ where h is the initial oil zone thickness (6.0 inches), ρ_o is the oil density (0.815 gm/cc) and $\Delta \rho$ is the density difference between water and oil, or $\rho_w - \rho_o$ (0.20 gm/cc). This analysis shows clearly how the water/oil interface is stable in this type of fractures. However, after water breakthrough, the pressure drop exceeds $\Delta \rho gh$ and reaches a maximum of 0.383 psig at 0.56 pv injected. This increase is due to the viscous forces created from the competition between oil and water as they rush simultaneously into the perforations and then the wellbore. It is, therefore, suggested to increase the diameter and the number of perforations as well as the wellbore diameter in the field to lower this pressure increase after water breakthrough. Another strategy for the production is to reduce the rate to keep the water/oil interface stable and therefore delay the water breakthrough. As the water cut increases, the pressure drop decreases to 0.325 psig and keeps almost constant until terminating the operation at 99% water cut (1.0 pv injected).

For the FHW/SOF, the perforated interval is limited to the width of the fracture which causes the flow inside the fracture to converge radially around the wellbore. Therefore the pressure drop increases to 0.280 psig at the start

of production and then increases gradually with stable water/oil interface to reach 0.323 psig at water breakthrough. During the two-phase period, the pressure drop reaches a maximum of 0.385 psig and then declines to 0.340 psig as water phase dominates in the flow after injecting 1.0 pv of water.

For the FVW, the perforated interval is limited to the depth of the fracture. This type of configuration would cause the geometry of the flow (flow nets) through the formation, fracture and wellbore to be different from that of the horizontal wells. This would help increase the pressure drop through the system, and as a result once the production starts the pressure drop increases steeply from 0.25 psig (initial static pressure) into 0.31 psig. This increase is necessary to initiate the flow of fluids through the system. After this point the the water/oil interface moves under gravity stability and the increase in the pressure drop is proportional to the height of the water in the fracture (h_{wf}), see Figure 6.3. At water breakthrough, the height of the water in the fracture becomes equal to the initial oil zone thickness (h). Therefore, the pressure drop increase is $\Delta \rho g h$ or 0.043 psig which when added to the observed pressure drop at the start of production (0.31 psig), the total pressure drop would be 0.353 psig which is exactly the same observed value at water breakthrough. After water breakthrough, the flooding process is dominated by viscous forces and the pressure drop reaches a maximum of 0.405 psig. As water cut increases, water becomes the continuous phase and the gravity equilibrate the viscous forces and therefore the pressure drop decreases to 0.357 psig at 1.0 pv of water injected.

It may be pointed out that the recovery performance is related to the contact area for each case. Therefore, the FHW/LF is showing the best recovery and the lowest pressure drop. However, although the contact areas for the FHW/SOF and the FVW/VF are the same, the FHW/SOF is showing better recovery and lower pressure drop. This may be attributed to the effect of gravity which is more pronounced in case of FHW/SOF since the perforations are higher in position compared to the FVW/VF. This means that the water moves a greater distance (h) to reach the point of production in case of the horizontal well compared to a less distance $(h - h_p)$ for the vertical well; where h is the initial oil zone height and h_p is the height of perforated interval in the vertical well. Hence, the later water breakthrough in case of the FHW/SOF.

The pressure drop is higher for the FVW/VF because of the nature of the fluid flow in the fracture and around the wellbore which is different from that of the FHW. The convergence of stream lines at the perforations of the FHW/SOF compared to almost vertical parallel streamlines in the fracture toward a long perforated interval in case of FHW/LF makes the pressure drop higher for the FHW/SOF compared to the FHW/LF.

For all cases, It is noted that the increase in the pressure drop after the initiation of the fluid flow through the system is exactly equal to $\Delta \rho g h$ (0.043 psig) which means that upon creating fractures, the process becomes gravity stable and the progress of the water/oil interface becomes stable without viscous fingering. However, as water breaks through, there is a competition

between the two phases in the perforations and the wellbore and, as a result, the pressure drop is increased to keep the flow of fluids through the system. As the water-cut increases water becomes the continuous phase and pressure decreases to a value that is able to left the water against the gravity and drive the fluids through the system.

Figure 5.41 shows the oil recovery at water breakthrough as a function of fracture penetration ratio for the FVW and the FHW. For all cases, the recovery increases with increasing the FPR showing the best recovery for the FHW/LF and lowest for the FVW. The effect of the fracture depth on the recovery of each case studied is also shown. For the FVW, the recovery increases by about 2.72, 2.96 and 3.15 times that of the UVW for the FPR's of 0.167, 0.333 and 0.500, respectively. It may be observed that deeper fractures with the vertical well are needed to recover the same amount of oil that could be recovered by the FHW.

Figure 5.42 shows the ultimate oil recovery (at 95% WC) as a function of the FPR for the cases studied. It is shown that the ultimate oil recovery increases with increasing the FPR. However, for the FHW/LF, no increase in the recovery is observed beyond a FPR of 0.333. It is believed that the maximum displaceable oil is achieved (86.5% OOIP). For the FHW/SOF, the recovery increases only by about 2% OOIP from 83.47% for the FPR of 0.333 to 85.45% OOIP for the FPR of 0.500. The increase in the recovery is about 7% OOIP for the FVW (from 76.42% to 81.64% OOIP). It may be concluded that the deeper the fracture (up to a limit) the better the oil recovery. for fractured vertical and horizontal wells. .
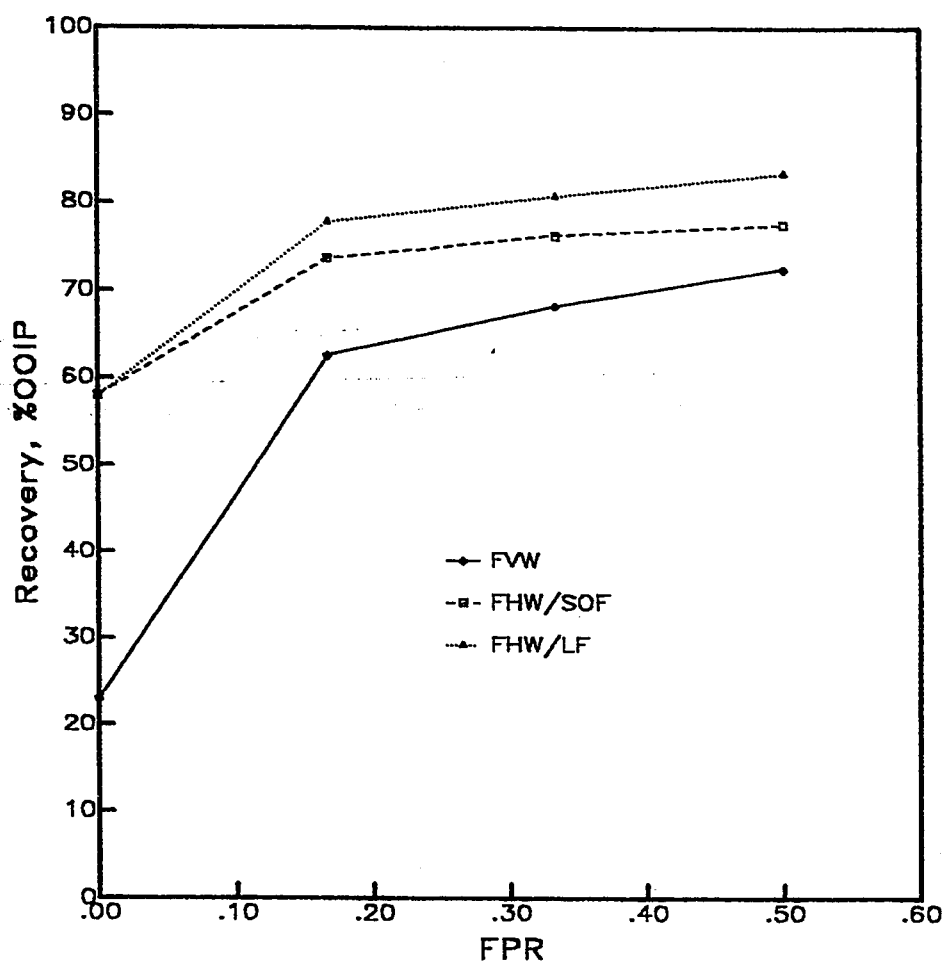
Figure 5.41: Breakthrough recovery vs. fracture penetration
ratio for fractured horizontal and vertical wells
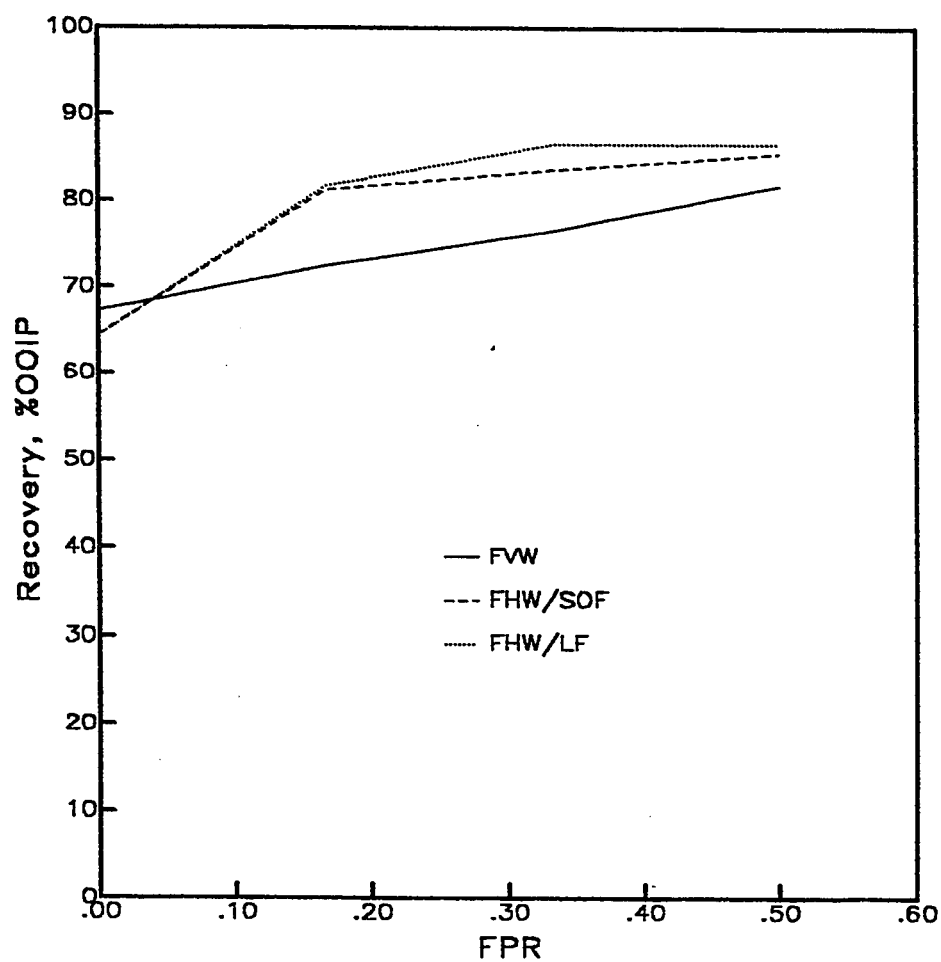
Figure 5.42: Ultimate recovery vs. fracture penetration ratio for fractured horizontal and vertical wells.

It may be generally suggested that creating fractures with a FPR of 0.15-0.25 for a horizontal well with longitudinal fracture, 0.20-0.30 for horizontal well with single orthogonal fracture and 0.40-0.50 for vertical well with vertical fracture are appropriate in a homogeneous isotropic reservoir with bottom water drive. With these FPRs, most of the oil in place can be recovered with one of the three wellbore/fracture configurations studied. The FHW/LF is the best configuration followed by the FHW/SOF and then the FVW. However, these suggested FPRs are approximate and are concluded from this study. Careful study of the reservoir aspects, technical feasibility of fracturing and economics of each project is necessary in order to achieve the best wellbore/fracture configuration.

Figures 5.43 and 5.44 show the pressure drop as a function of the FPR at water breakthrough and at 1.0 pv injected, respectively. It is observed that the pressure drop is the lowest for the FHW/LF both at water breakthrough and at 1.0 pv injected. At water breakthrough, the pressure drop is almost independent of the FPR for the FHW/LF. However, it is decreasing as the FPR increases for the FHW/SOF and the FVW.

After injecting 1.0 pv, the pressure drop slightly decreases with increasing the FPR for the FVW and the FHW/LF. However, for the FHW/SOF, the pressure drop increases compared to the UHW, but it then decreases with increasing the FPR. The reason for the increase is the limited perforated interval for the FHW/SOF compared to the FHW/LF.
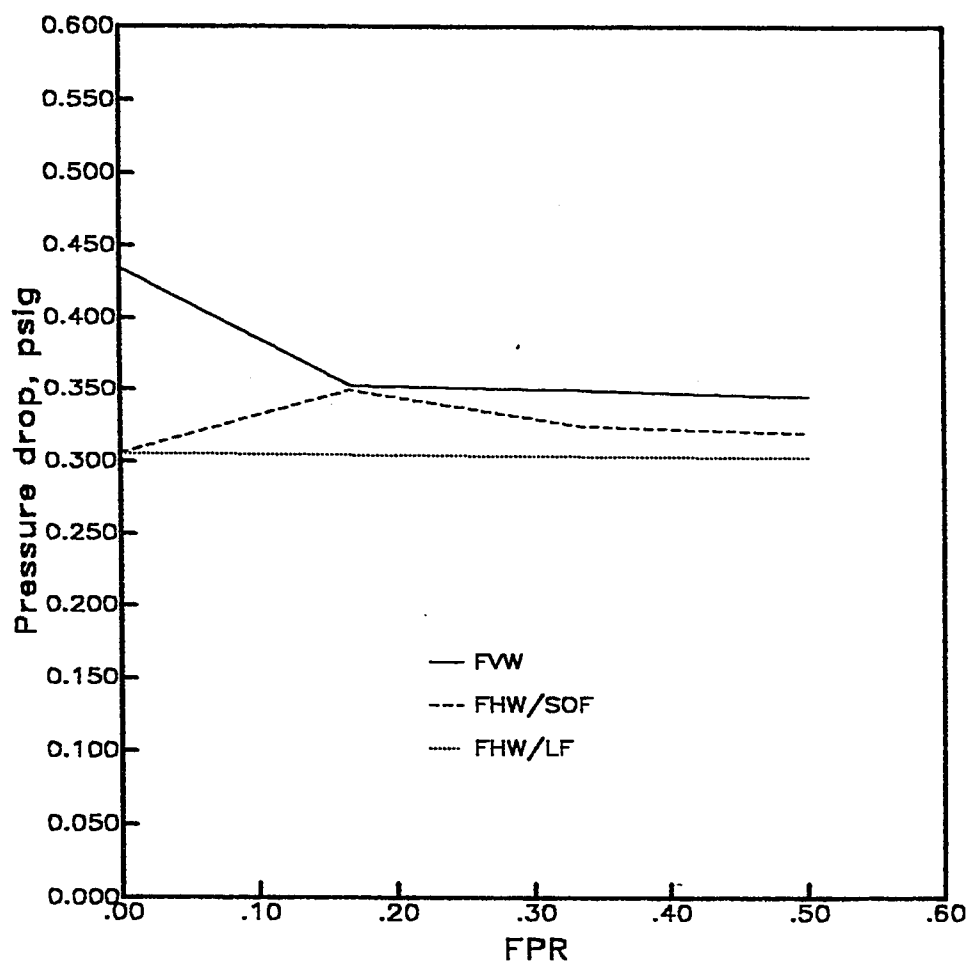
Figur 5.43: Pressure drop vs fracture penetration ratio at water
B.T. for fractured horizontal and vertical wells
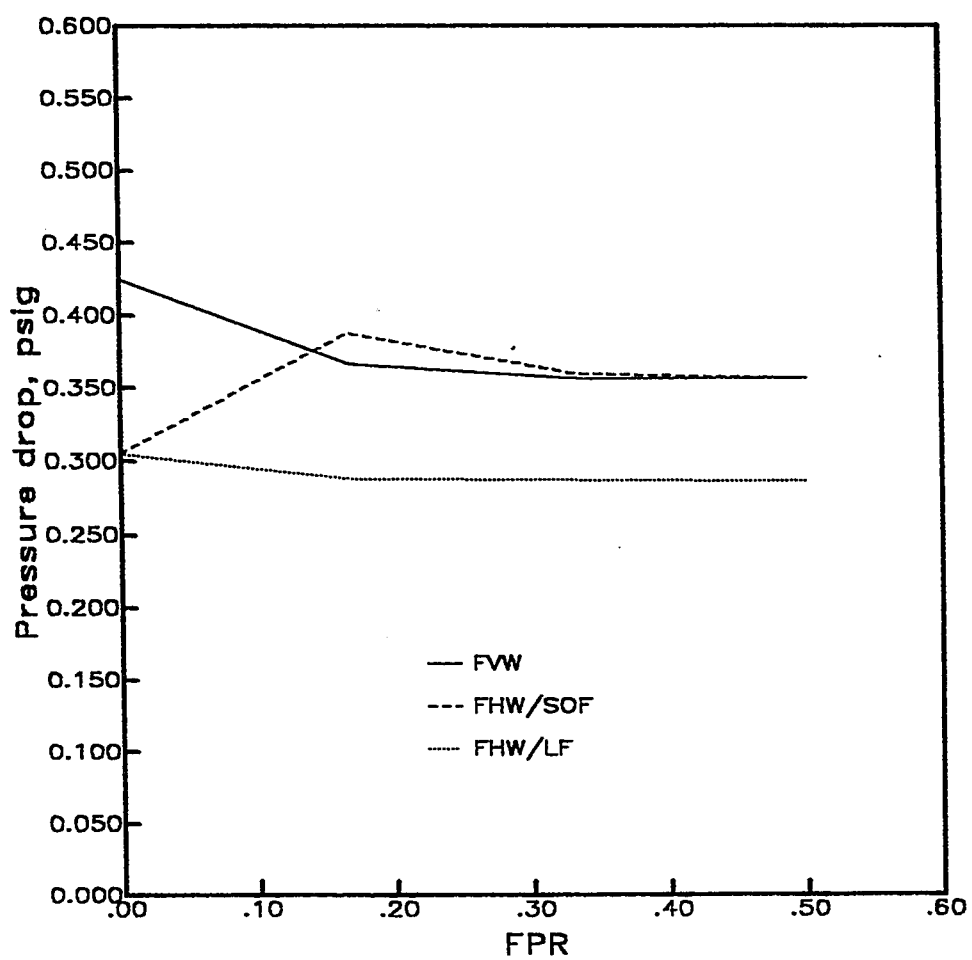
Figure 5.44: Pressure drop vs fracture penetration ratio at
1.0 pv of water injected for FHWs and FVWs.

It is, therefore, concluded that the FHW/LF provides the best production performance (highest oil recovery, lowest pressure drop and water injected). The FHW/SOF comes next with the FVW being the last of the three configurations studied.

Chapter VI
PRODUCTION MECHANISMS OF
HORIZONTAL WELLS

6.1 INTRODUCTION

The behavior of naturally and hydraulically fractured reservoirs when a single fluid is flowing has been studied extensively [50,89-99]. Most of this work considers vertical fractures only. When more than one fluid is flowing, the flow paths become much more complex and the flow behavior of such system is not fully understood. The discontinuities in permeability and capillary pressure between the matrix blocks and fractures introduce new recovery mechanisms. The production of oil from reservoirs with extensive interconnected fractures has been recognized to be controlled by capillary imbibition [100-102]. However, when a fracture is induced through a horizontal well in a bottom water drive reservoir, the gravitational forces play a role that is as important as capillary forces. Further, the oil is also forced from the matrix into the fracture by flow created from the drive.

The purpose of this chapter is to present an understanding of the recovery mechanisms of horizontal wells in fractured bottom water-drive reservoirs. Section 6.2 includes some of the literature on both theoretical and experimental aspects of fluid flow in reservoirs containing interconnected

fractures. Sections 6.3 presents theoretical and simplified approaches to analyze the effects of the forces applied (viscous, capillary and gravity) on the fluid flow through fractured reservoirs. Finally, section 6.4 discusses the mechanisms which may affect the production performance of fractured horizontal wells in bottom water-drive reservoirs.

6.2 PREVIOUS WORK

Bear [111] defines the imbibition process as the spontaneous displacement of the non-wetting fluid by the wetting fluid due to interfacial tension. The main concept is that water is being drawn into a matrix block by capillary pressure while oil is expelled in the opposite direction.

Aronofsky, Masse and Natanson [112] suggested an abstract model based on the variation of recovery with time during the imbibition process. They assumed that the oil production is a continuous monotonic function of time and that it converges to a finite limit. The second basic assumption is that none of the properties which determine the rate of convergence changes sufficiently during the process to affect this rate or the limit. They presented a function of the form:

$$R = R_L (1 - e^{-\lambda t}) \qquad (6.1)$$

Where :

R = the recovery of oil, %OOIP,

R_L = the limit towards which R converges,

λ = a constant giving rate of convergence, and

t = time.

They used eq. (6.1) to extrapolate field recoveries.

Graham and Richardson [113] presented a theoretical and experimental study of the effect of the imbibition phenomena on the displacement of oil from a fractured reservoir. They used Darcy's law and the definition of capillary pressure to describe the flow of oil and water through the system. The laboratory investigation was performed on a dimensionally scaled model of a single element of a fractured-matrix reservoir. They studied the effect of water injection rate and fracture width on the recovery of oil. They concluded that for a given fracture width, the lower the injection rate, the greater the oil recovery for a given amount of water injected. They also concluded that there would be no water produced from the oil sand until much of the recoverable oil has been produced.

Bokserman, Zheltov and Kocheshlcov [114] generalized their continuum approach for one-phase, incompressible flow to flow of oil and water. The motion of oil and water in the fractures is described by a set of of differential equations for the filtration of immiscible liquids by allowing capillary imbibition. The conservation of mass and Darcy's law are:

$$\varphi_2 \frac{\partial S_{w2}}{\partial t} + \nabla u_{w2} + u_w^\cdot = 0 \tag{6.2}$$

$$-\varphi_2\frac{\partial S_{o2}}{\partial t}+\nabla u_{o2}+u_o^\cdot=0 \tag{6.3}$$

$$u_{w2}=-\frac{k_2 k_{rw2}(S_{w2})}{\mu_w}\nabla\Phi_w \tag{6.4}$$

$$u_{o2}=-\frac{k_2 k_{ro2}(S_{o2})}{\mu_o}\nabla\Phi_o \tag{6.5}$$

Where,

φ_2 = porosity of the fracture

S_{w2} = water phase saturation in the fracture

S_{o2} = oil phase saturation in the fracture

t = time

u_{w2} = Darcy's flux of water phase in the fracture

u_{o2} = Darcy's flux of oil phase in the fracture

$u_w^\cdot$ = source function for water, see eqns. (6.6) and (6.7)

$u_o^\cdot$ = source function for oil, see eqns. (6.6) and (6.7)

k_2 = permeability of the fracture

k_{rw2} = relative permeability to water in the fracture

k_{ro2} = relative permeability to oil in the fracture

Φ_w = fluid flow potential for water phase

Φ_o = fluid flow potential for oil phase

μ_w = viscosity of water phase

μ_o = viscosity of oil phase, and;

$$\nabla = i \frac{\partial}{\partial x} + j \frac{\partial}{\partial y} + k \frac{\partial}{\partial z}.$$

In their model, it is assumed that the volume of fractures is ignored in comparison with the capacity of the matrix blocks and assumed that the total amount of water entering the system is sucked (imbibed) by the blocks. Hence, the main flow is through the fractures; since the fluids are exchanged due to imbibition on the interconnection surfaces between the matrix blocks and fractures.

In incompressible flow, the volume of water entering the blocks equals the volume of oil produced in the fractures; thus,

$$u_o^* = -u_w^* = |u^*| \tag{6.6}$$

From the results of laboratory imbibition experiments performed by Mattax and Kyte [118], Bokserman, et.al [114] obtained the following source function:

$$u^* = C\varphi_1 S_{w1} s_v^2 \sigma \cos\theta \frac{\sqrt{(k_1/\varphi_1)}}{\mu_o} \left[s_v^2 \sigma \cos\theta \frac{\sqrt{(k_1/\varphi_1)}}{\mu_o} .t \right]^{1/2} \tag{6.7}$$

Where,

C = constant

φ_1 = porosity of the matrix

S_{w1} = water phase saturation in the matrix

s_v = volumetric specific area

σ = interfacial tension,

θ = contact angle

k_1 = permeability of the matrix

μ_o = oil viscosity, and;

t = time

The expression inside the square brackets is dimensionless time. Bokserman used this model to describe the flow behavior in the case of a moving imbibition zone, as shown in Figure 6.1.

Kleppe and Morse [115] studied the flow behavior in a matrix-fracture system both experimentally and numerically. They found that for k_f (fracture permeability) higher than k_m (matrix permeability), the recovery was rate sensitive. This was in agreement with what has been found previously [113,116117]; but for fracture capacity approximately one tenth the matrix flow capacity, the effect of the rate was negligible. The major shortcoming for the numerical models for simulation of the imbibition production mechanism is the relative permeability and capillary pressure concepts.

174
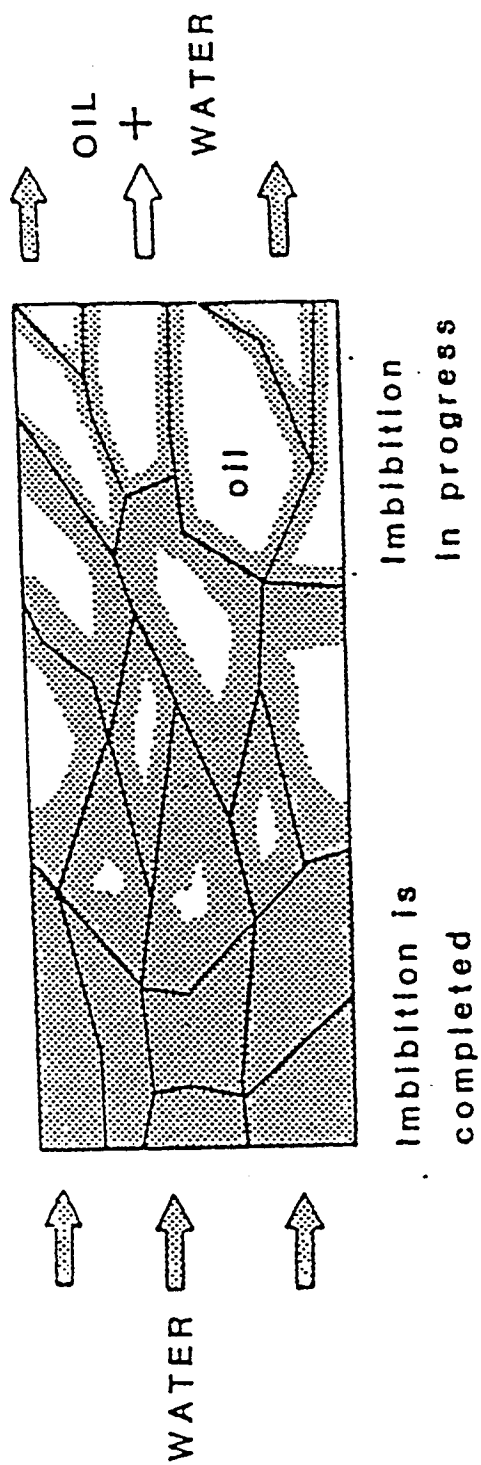
Figure 6.1: Water Imbibition in Fractured Rock, [114].

Kazemi and Merill [116] performed experimental work on artificially fractured sandstone cores. They injected water into the fracture only, and observed oil production and breakthrough time in relation to injection velocity and capillary pressure. Their results indicated that at low water velocities, imbibition caused the water to advance through the matrix faster than it did through the fracture. However, at high water velocities, or at low capillary pressures, water breakthrough in the fractured rock occurred much sooner than in unfractured rock. Kazemi also observed that the final oil recoveries by pure imbibition and forced displacement are nearly the same.

Mannon and Chilinger [117] studied the effect of water injection rate on imbibition rate using a laboratory model. They found that the higher the rate of water injection, the greater the imbibition rate and ultimate oil recovery. The laboratory model used by Mannon and Chilinger is very similar to Graham and Richardson's model [113], but the results are not quite in agreement. Graham and Richardson found that the higher the injection rate, a greater amount of water was required to be injected to produce a given amount of oil. Mannon and Chilinger also indicate that viscous forces may be operative in Graham and Richardson's model under certain conditions and, therefore, less suited for pure imbibition studies.

In summary, all previous work indicate that imbibition is the most important mechanism in the displacement of oil by water in reservoirs having extended interconnecting fractures. The gravity forces and viscous forces can be very important depending on the characteristics of the matrix blocks and the fluids.

6.3 FLUID FLOW THROUGH FRACTURED RESERVOIRS

6.3.1 Theoretical Approach

Fluid flow Through porous media is controlled by four different forces. These are applied pressure, viscous, capillary and gravitational forces. The objectives of this section is to study and analyze the effects of these forces on the fluid flow in fractured reservoirs. Following is a theoretical derivation of the pressure drop associated with each of these forces and its relative magnitude for fractured and unfractured reservoirs. The derivation of these pressure drops is based on the scaling equations presented in Appendix A.

6.3.1.1 Derivation of Capillary and Gravity Rate Equations

Scaling criterion is based on geometric, kinematic and dynamic similarities between the laboratory model and the field prototype.

The geometric similarities are preserved when the dimensions (length, width and height) of the model and prototype are kept similar in dimensionless forms.

When the flow nets (stream and equipotential lines) are similar in the model and prototype, the two systems are then kinematically similar.

The dynamic similarity is based on the similarity of the viscous, capillary and gravity forces in both the model and prototype.

In order to satisfy the scaling process, the equations of flow of fluids through porous media, the capillary pressure equations, the saturation equation and the initial & boundary conditions are transformed into dimensionless forms. The dimensionless parameters in each equation should be the same for the model and prototype to keep similarities in the the two systems. Detailed conversions of the equations into dimensionless forms can be found in Appendix A.

Equations (A.33), (A.38) and (A.41) are written here, for convenience, as:

$$\left[\frac{h^2}{WL} \right]_m = \left[\frac{h^2}{WL} \right]_p \tag{6.8}$$

Equation (6.8) arises from the conditions for geometric similarity in the model and the prototype.

$$\left[\frac{\sigma h \cos\theta \sqrt{k_z \varphi}}{q \mu_o} \right]_m = \left[\frac{\sigma h \cos\theta \sqrt{k_z \varphi}}{q \mu_o} \right]_p \tag{6.9}$$

$$\left[\frac{\Delta \rho g k_z h^2}{q \mu_o} \right]_m = \left[\frac{\Delta \rho g k_z h^2}{q \mu_o} \right]_p \tag{6.10}$$

The dimensionless group in equation (6.9) balances capillary forces with viscous forces. Similarly equation (6.10) balances gravity and viscous forces.

Dividing eq. (6.9) and (6.10) by eq. (6.8) gives:

$$\left[\frac{\sigma\cos\theta\sqrt{k_z\varphi}}{q\mu_o} \frac{WL}{h} \right]_m = \left[\frac{\sigma\cos\theta\sqrt{k_z\varphi}}{q\mu_o} \frac{WL}{h} \right]_p \tag{6.11}$$

$$\left[\frac{\Delta\rho g k_z WL}{q\mu_o} \right]_m = \left[\frac{\Delta\rho g k_z WL}{q\mu_o} \right]_p \tag{6.12}$$

Where

WL = area (A) of flow, and

h = thickness of the oil zone.

It is useful to separate the effects of gravity, viscous drag, capillary and pressure drive in the above equations as follows:

Using eqs. (6.11) and (6.12), dimensionless rates may be defined for capillary and gravity difference as:

$$q_{CD} = \left[\frac{A\sigma\cos\theta\sqrt{k_z\varphi}}{q\mu_o h} \right] \tag{6.13}$$

$$q_{GD} = \left[\frac{A k_z \Delta\rho g}{q\mu_o} \right] \tag{6.14}$$

Where:

$$q_{CD} = \frac{q_c}{q} = \text{dimensionless rate due to capillary forces, and}$$

$$q_{GD} = \frac{q_G}{q} = \text{dimensionless rate due to gravity forces.}$$

The relations defined by equations (6.13) and (6.14) can be related to hypothetical capillary and gravity "rates" defined as:

$$q_c = \left[\frac{\sigma\cos\theta\sqrt{k_z\varphi A}}{\mu_o h} \right] \qquad (6.15)$$

$$q_G = \left[\frac{Ak_z\Delta\rho g}{\mu_o} \right] \qquad (6.16)$$

There is a rate due to darcy (viscous) flow defined as:

$$q_{vs} = (\frac{k_z A}{\mu_o h})\Delta P_{vs} \qquad (6.17)$$

Where $\Delta P_{vs}=$ the pressure drops due to viscous force

6.3.1.2   Derivation of Capillary and Gravity Pressure Equations

Equations (6.15) and (6.16) may be written in the form of eq. (6.17) and thus used to define pressure terms for the individual "rates" as follows:

$$q_c = (\frac{k_z A}{\mu_o h})\Delta P_c \qquad (6.18)$$

and,

$$q_G = (\frac{k_z A}{\mu_o h})\Delta P_g \qquad (6.19)$$

Where;

$$\Delta P_c = \sigma cos\theta\sqrt{\varphi/k} \qquad (6.20)$$

is the pressure drop due to capillary and

$$\Delta P_g = \Delta\rho g h \qquad (6.21)$$

is the pressure drop due to gravity.

The total flow rate (q) may be written as the summation of the three rates, due to viscous, capillary and gravity forces as:

$$q = q_{vs} + q_c + q_G \qquad (6.22)$$

Using eqns. (6.17), (6.18) and (6.19), eq. (6.22) may be written as:

$$q = (\frac{k_z A}{\mu_o h})[\Delta P_{vs} + \Delta P_c + \Delta P_g] \qquad (6.23)$$

Or,

$$q = (\frac{k_z A}{\mu_o h})[\Delta P] \qquad (6.24)$$

Where:

$$\Delta P = \Delta P_{vs} + \Delta P_c + \Delta P_g \tag{6.25}$$

is the total applied pressure drop.

The meaning of this equation depends upon the situation. A very simple example is that of the initial, upwards, linear displacement of oil by water as shown in Figure 6.2. In this example the applied pressure must balance the pressure due to gravity, $\Delta P_g = \rho_o gh$, the capillary pressure, $\Delta P_c = \Delta \rho gh_c$, and the viscous drag, $\Delta P_{vs} = \dfrac{q\mu h}{kA}$.

In an equation form, the pressure drop through the system may be written as:

$$\Delta P = (\frac{q\mu h}{kA}) + \Delta \rho gh_c + \rho_o gh$$

Where h_c is the height of the transition zone due to capillary pressure. This height is assumed to be constant at static and dynamic conditions.

6.3.1.3 Pressure Analysis

The pressure analysis is based on comparing the pressure drop of unfractured and fractured reservoirs. The following analysis relates to the movement of fluids through a fractured reservoir in which oil is transferred by imbibition from the matrix blocks into fractures. or perhaps just higher permeability regions containing flowing water. Pressure drops for different forces are analyzed as follows:
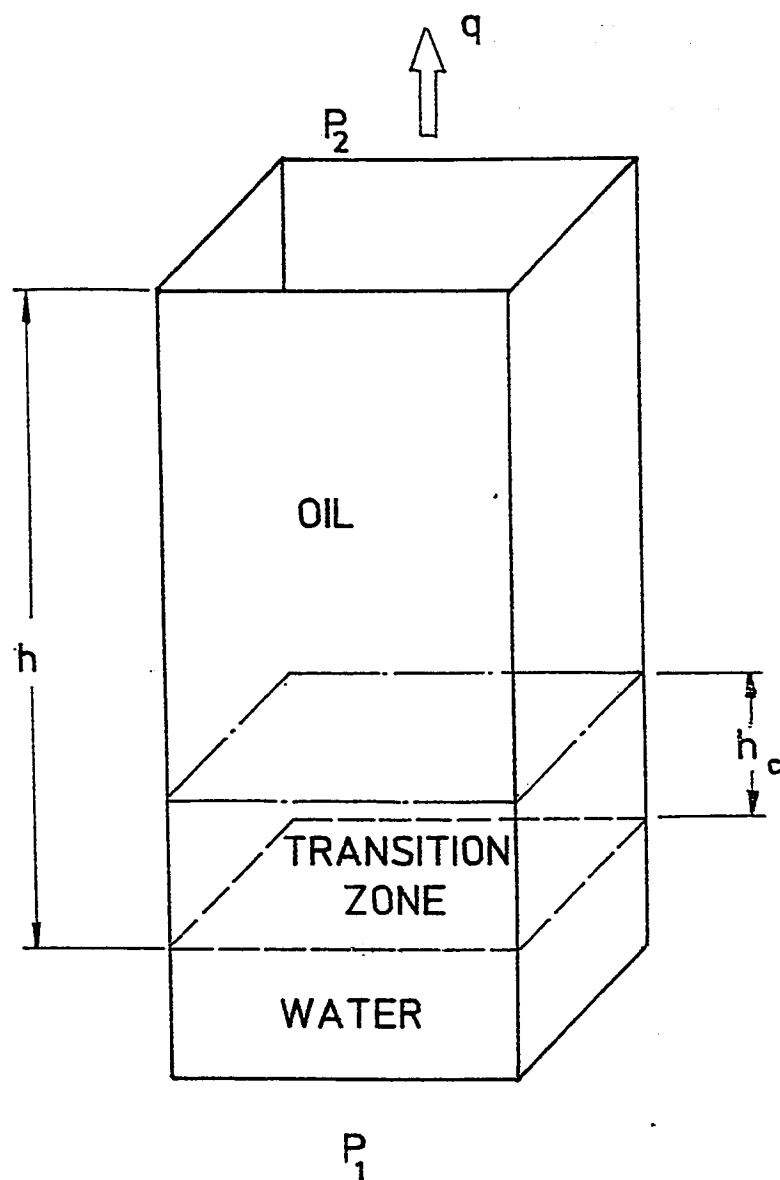
Figure 6.2:   Linear Vertical Displacement of Oil by Water

1. Capillary pressure:

The pressure drop due to capillary forces of an unfractured reservoir is compared to that of a fractured reservoir using eqn. (6.20) as follows:

$$\frac{\Delta P_{c_m}}{\Delta P_{c_f}} = \frac{(\sigma\cos\theta\sqrt{\varphi/k})_m}{(\sigma\cos\theta\sqrt{\varphi/k})_f} \tag{6.26}$$

Where the subscripts m and f are assigned for the matrix and fracture, respectively.

Assume the matrix and fracture are strongly water wet and σ_m equal σ_f, therefore, eq. (6.26) becomes:

$$\frac{\Delta P_{c_m}}{\Delta P_{c_f}} = \sqrt{\varphi_m k_f/\varphi_f k_m} \tag{6.27}$$

For the present physical model, we have:

$\varphi_m = 0.362$

$\varphi_f = 1.0$

$k_m = 400 \; darcies$, and

$k_f = 1.77*10^6$ darcies for 0.181 inch-width and 2.0 inch-deep fracture.

Therefore,

$$\frac{\Delta P_{c_m}}{\Delta P_{c_f}} \sim 40$$

Therefore, the pressure drop due to capillary $(\Delta P_c = \Delta P_o - \Delta P_w)$ is much higher in the matrix compared to the fracture. As a result oil may flow under capillary imbibition from the matrix into the fracture and, consequently, water flows in the opposite direction. It may be stated that the capillary forces are very important in fractured reservoirs; the water is sucked by the matrix and as a result oil is expelled into the fractures.

2. Gravity pressure:

The gravity affects the flow of fluids in a two-porosity, two-permeability (matrix and fracture) system, Fig. (6.3). The relative magnitude of the gravity pressure in the matrix to that in the fracture may be written using equation (6.21) as:

$$\frac{\Delta P_{g_m}}{\Delta P_{g_f}} = \frac{\Delta \rho g \Delta h_{wm}}{\Delta \rho g \Delta h_{wf}} = \frac{\Delta h_{wm}}{\Delta h_{wf}} \tag{6.28}$$

Where:

Δh_{wm} : change in the elevation of WOC in the matrix at time $t + \Delta t$, and

Δh_{wf} : change in the elevation of WOC in the fracture at time $t + \Delta t$.

Figure 6.3: Displacement of Oil by Water in Fractured Bottom Water Drive Reservoir

Equation (6.28) shows that the relative magnitude of the gravity pressure in the matrix to that in the fracture would be maximized in favor of the process if the fracture is filled with water ($\Delta h_{wf} \sim h$) and the matrix is filled with oil ($\Delta h_{wm} \sim 0$). On the other hand, this ratio would maximize against the recovery process if the former situation is reversed. In all cases, equilibrium has to take place. However, the pressure should be lower in the well in order to produce oil and therefore the fracture pressure must be always lower than that of the matrix.

The pressure drop at time t due to gravity between the fracture and matrix may be written as:

$$\Delta P_g = \Delta P_{g_f} - \Delta P_{g_m} = \Delta \rho g (h_{wf} - h_{wm}) \qquad (6.29)$$

Where:

h_{wm} : the elevation of WOC in the matrix at time t and

h_{wf} : the elevation of WOC in the fracture at time t.

It may be observed that if the water-oil contact (WOC) is at the same level in the matrix and fracture during the flooding process, the gravity would not affect the flow from the fracture into the matrix or vice versa. However, if the WOC is higher in the fracture (which is the case), water could flow under gravity from the fracture into the matrix and oil would flow in the opposite direction. In this case, the gravity is in favor of the process. If, however, the

WOC is higher in the matrix, the gravity would affect the process negatively; i.e., water would flow from the matrix into the fracture. Such a well would be a water injection well and would probably require an external source of water.

3. Viscous pressure drop:

Equation (6.17) may be written as:

$$\Delta P_{vs} = \frac{q_{vs}\mu_o h}{k_z A} \qquad (6.30)$$

The ratio of the viscous forces in the matrix to that in the fracture may be written as:

$$\frac{\Delta P_{vs_m}}{\Delta P_{vs_f}} = \frac{q_{vs_m} k_f A_f}{q_{vs_f} k_m A_m} \qquad (6.31)$$

A_f, k_f, A_m, and k_m are the area of flow and permeability of the fracture, and the area of flow and permeability of the matrix, respectively.

For the present physical model:

$k_f = 1.77*10^6$ darcies,

$k_m = 400$ darcies,

$A_f = 0.278\ ft^2$, and

$$A_m = 1.50 \, ft^2.$$

If the rate exchanged between the fracture and matrix due to viscous forces is assumed to be the same, then, the ratio in eq. (6.31) is:

$$\frac{\Delta P_{vs_m}}{\Delta P_{vs_f}} \sim 820$$

It may be stated, therefore, that the pressure drop due to viscous forces is much less in the fracture than in the matrix due to the higher conductivity of the fracture.

From the analysis presented above, it is concluded that the capillary imbibition is a very important mechanism in fractured reservoir. The gravity induced drive depends on the relative position of the WOC in the matrix and fracture. The less viscous forces in the fracture compared to the matrix results in higher WOC in the fracture. However, if the production/injection rate is high in a reservoir containing extended interconnected fractures, viscous forces would dominate and, as a result, water would break through earlier. Therefore, the production/injection rate should be controlled so that water does not bypass directly to the production well. With a system involving fractures extending downwards from a horizontal well, this means that the rate must be controlled so that the water-oil contact remains below the well. Attempts to increase the rate draw the interface upwards but there is a limiting, critical, rate at any one time at which the interface within the fracture reaches the well. As pointed out earlier, in this study, the flow through the

fracture is controlled by gravity forces; therefore, equation (6.16) may be used to predict the critical oil rate in the fracture. This equation is written here as:

$$q_G = \frac{A_f k_f \Delta \rho g}{\mu_o}$$

(6.32)

where A_f is the cross section area of the fracture normal to the direction of the flow $(w_f {}^* 2x_f\, or\, w_f {}^* 2y_f)$, w_f is the width of the fracture, x_f is half of the extension of the fracture in x-direction and x_f is half of the extension of the fracture in y-direction, and k_f is the permeability of the fracture in z-direction. The flow is assumed linear upward in the z-direction.

If, however, the capillary forces are active in the fracture, the production/injection rate may be in the range of

$$q = q_c + q_g$$

(6.33)

or;

$$q = (\frac{A_f k_f}{\mu_o h})[\Delta P_c + \Delta P_g]$$

(6.34)

It should be pointed out that if the rates in equations (6.32) and (6.34) are exceeded, the water/oil interface would become unstable, and as a result, water would break through earlier. It is assumed that the wellbore is able to produce the oil from the fracture with no restriction.

6.3.2   A Simplified Approach

This approach discusses and explains the production mechanisms of horizontal wells in bottom water drive reservoirs with multiple orthogonal fractures. The multiple orthogonal fractures present a huge contact area with the reservoir, therefore, the capillary imbibition is a very important mechanism for oil recovery. In addition, the location of the horizontal well at the top of the bottom water drive reservoir allows the gravity to act due to the difference in fluid densities and the height of the reservoir. In such cases viscous forces may be neglected.

In the following analysis, a fractured matrix block saturated with oil then displaced with water is considered, Figure 6.4. In this case, two sets of forces will play a role in the displacement process:

1. Gravity forces due to the difference in densities between oil and water, and;

2. Capillary forces due to the interaction of surface forces within the pores.

The flow rate per unit cross sectional area is: defined by Darcy's law as [101]:
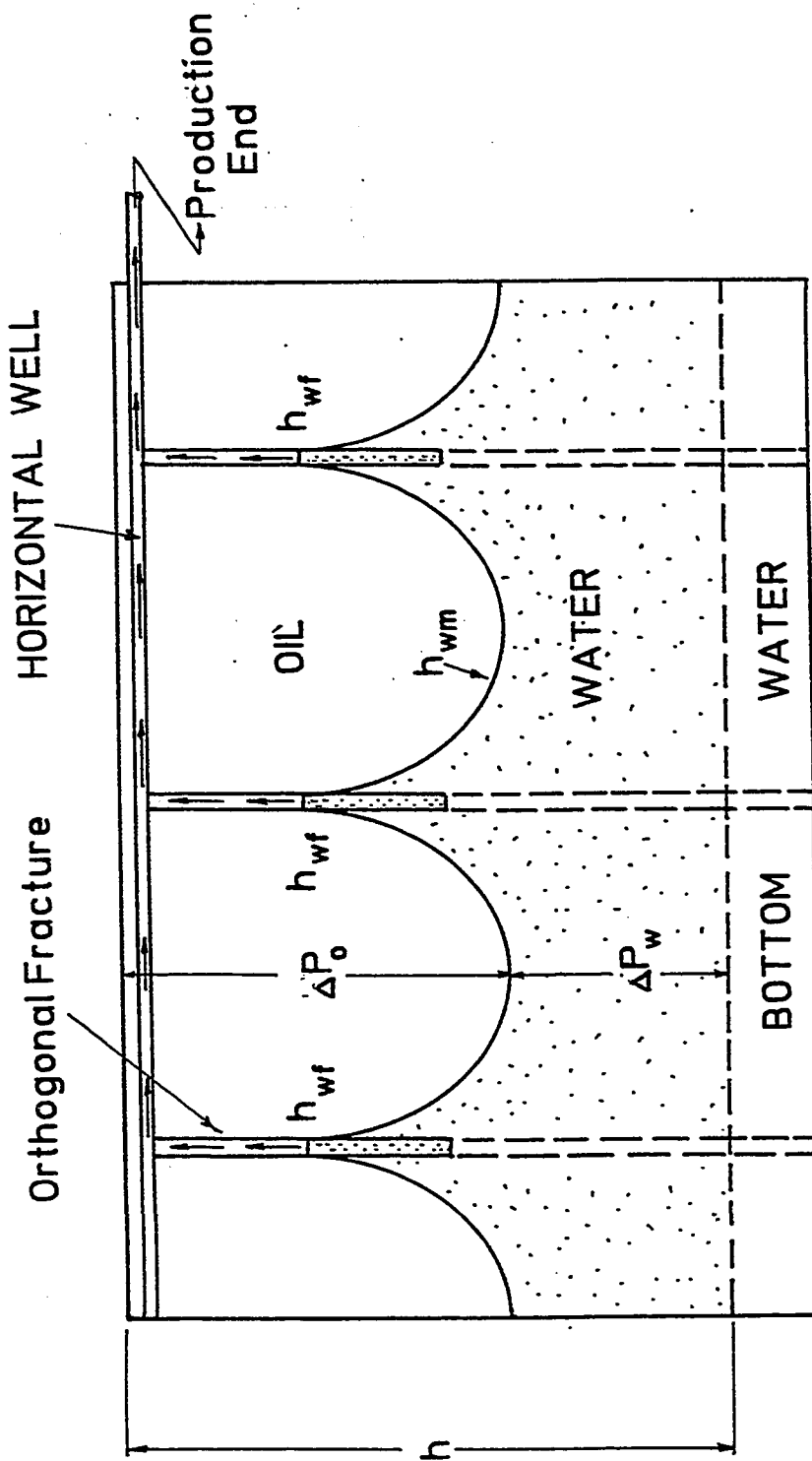
Figure 6.4: Displacement of Oil by Water in Multiple-Orthogonal Fractured Reservoir with Horizontal Well

$$u = \frac{k_w \Delta P_w}{\mu_w h_{wm}} = \frac{k_o \Delta P_o}{\mu_o (h - h_{wm})}$$ (6.35)

Where:

ΔP_w = pressure drop in the water phase,

ΔP_o = pressure drop in the oil phase,

k_w = water effective permeability,

k_o = oil effective permeability,

μ_w = water viscosity

μ_o = oil viscosity

h = thickness of the oil zone (matrix)

h_{wm} = water level in the matrix

and;

$$\Delta P = \Delta P_o + \Delta P_w$$ (6.36)

Where, the difference in pressure which leads to this displacement is:

$$\Delta P = (h_{wf} - h_{wm}) \Delta \rho g + P_c$$ (6.37)

Where:

h_{wf} = elevation of the WOC in the fracture

And;

$$P_c = P_o - P_w$$ (6.38)

is the capillary pressure

From eqs. (6.35) and (6.36), we have:

$$\frac{\Delta P_w}{\Delta P} = \frac{h_{wm}}{h_{wm} + (h - h_{wm})M}$$

(6.39)

Where M is the mobility ratio, defined as:

$$M = \frac{\mu_o}{\mu_w}\frac{k_w}{k_o}$$

(6.40)

Initially, the WOC is at the bottom of the oil zone, or; $z_w = h_w = 0.0$. In this case, eq. (6.36) shows that the gravity has no effect; however, capillary imbibition is taking place. In other words, water will rise in the formation under capillary imbibition. In this case, using eqns. (6.36), (6.39) and (6.35), the total pressure drop is:

$$\Delta P = P_c = P_o$$

(6.41)

Let's consider the extreme condition in which once the displacement starts, water rises and fill the whole fracture. In this case, $h_w = h$, while $z_w = 0.0$, and ΔP_w in equation (6.39) is zero. The the total pressure drop becomes:

$$\Delta P = \Delta \rho g h + P_o \qquad (6.42)$$

It can be seen that if ΔP is positive in eqs. (6.40) and (6.41), the capillary and gravity work together and as a result water flows unde ΔP from the fracture into the matrix and oil is expelled into the fracture.

The actual process is somewhere between these two cases. In other words, the capillary is always acting; however, the gravity magnitude depends on the relative position of the water-oil contact. Viscous force must be taken into consideration; however, the process should be controlled by gravity and capillary forces for better performance.

At and after water breakthrough, h_w = h and z_w approaches h, therefore the gravity effect becomes very small. The process, then, is capillary dependent until water rises in the matrix up to the total thickness. At this time water only is produced.

6.4 VERTICAL WATER/OIL DISPLACEMENT IN FRACTURED RESERVOIRS

6.4.1 Features of the Production Performance of Fractured Reservoirs

The production performance of fractured wells is different from that of unfractured wells in bottom-water-drive reservoirs. The presence of the fracture creates a very highly permeable medium within the matrix blocks. These fractures affect the flow behavior of the fluids and create specific production mechanisms through the reservoir. As á result, the recovery performance of fractured reservoirs exhibits major differences from that of unfractured reservoirs. These may be summarized in this study as:

1. Under the same injection rate, the oil recovery is much higher in a fractured reservoir than in an unfractured reservoir. Moreover the water breakthrough is delayed and the two phase production period is shortened. It is believed that the two phase transition zone is greatly minimized in the fractured reservoir compared to the unfractured reservoir. The high transmissibility of the induced fractures, due to high permeability, requilibrates any change in the level of fluids in the matrix and fracture(s). If a channel (fracture) is created in a sand block saturated with water, the water would flow from the sand body into the channel. As a result, the level of water requilibrates in both the sand block and channel.

2. The water cut is lower in a fractured reservoir than in unfractured reservoir. This behavior is due to the segregation of oil through the fracture(s) toward the top of the reservoir where the horizontal well should be normally located in a bottom water drive reservoir.

3. The pressure drop is normally lower in a fractured reservoir than in an unfractured reservoir. This is mainly due to increasing the area of contact with the reservoir where $P = \dfrac{F}{A}$. Where P is the pressure due to applied forces (F) on an area A. The forces are viscous, gravity and capillary forces.

6.4.2 Production Mechanisms of Fractured Reservoirs

This improved production performance of the horizontal and vertical wells with fractures is due to certain production mechanisms develop in fractured-matrix systems. These production mechanisms assure a great supply of fluids from the matrix as a result of gravity and capillary imbibition combined with segregation.

Consider the reservoir situation that is shown in Figure 6.5. A high conductivity fracture extends down from the horizontal production well right into the water below. If there is no production from the well, the water oil contact within the fracture will be equal to that of the bottom of the reservoir transition zone. In the reservoir matrix some water will be above this WOC because of capillary forces. If the pressure in the well is now reduced, water will rise in the fracture and oil will be driven by the resulting potential gradi-

197
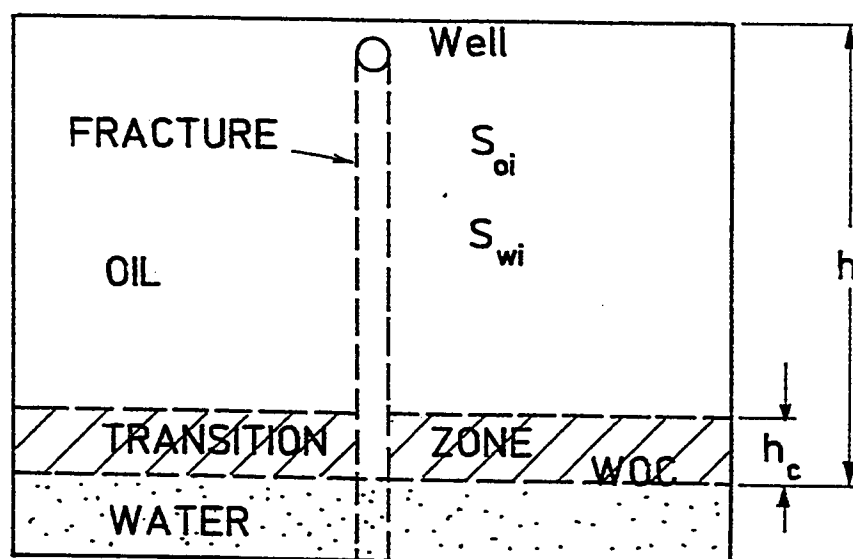
Figure 6.5: A Situation Where a Highly Conductive Fracture Extends Down to the Bottom Water Reservoir

ent from the reservoir into the fracture:

1. Oil will be produced and will have to be removed to control the well-bore pressure

2. The water oil contact and the transition zone will rise as oil is moved. The transition zone will rise more rapidly near the wellbore and will become curved.

3. Water will flow from the drive source to replace the water flowing into the matrix.

4. The thickness of the transition zone in the matrix will decline near the wellbore and the saturation gradient will decrease in that region. As a result imbibition will occur to some extent in that region.

The above will all occur at increased rates as the well pressure is lowered up to the point where the fracture WOC is drawn into the well. At this point, water is produced as well as oil and there is no further gain in rate. This limit occurs when the wellbore pressure is decreased by an amount $(\rho_w - \rho_o)gh$. Where h is the height of the well above the initial WOC. Obviously, it is desirable to have the well located close to the top of the reservoir.

The situation for maximum production is now as shown in Figure 6.6.

The thickness of the transition zone becomes somewhat less than the one which corresponded to static conditions because it is necessary for water to be drawn into it continuously by imbibition. The rate at which this can occur
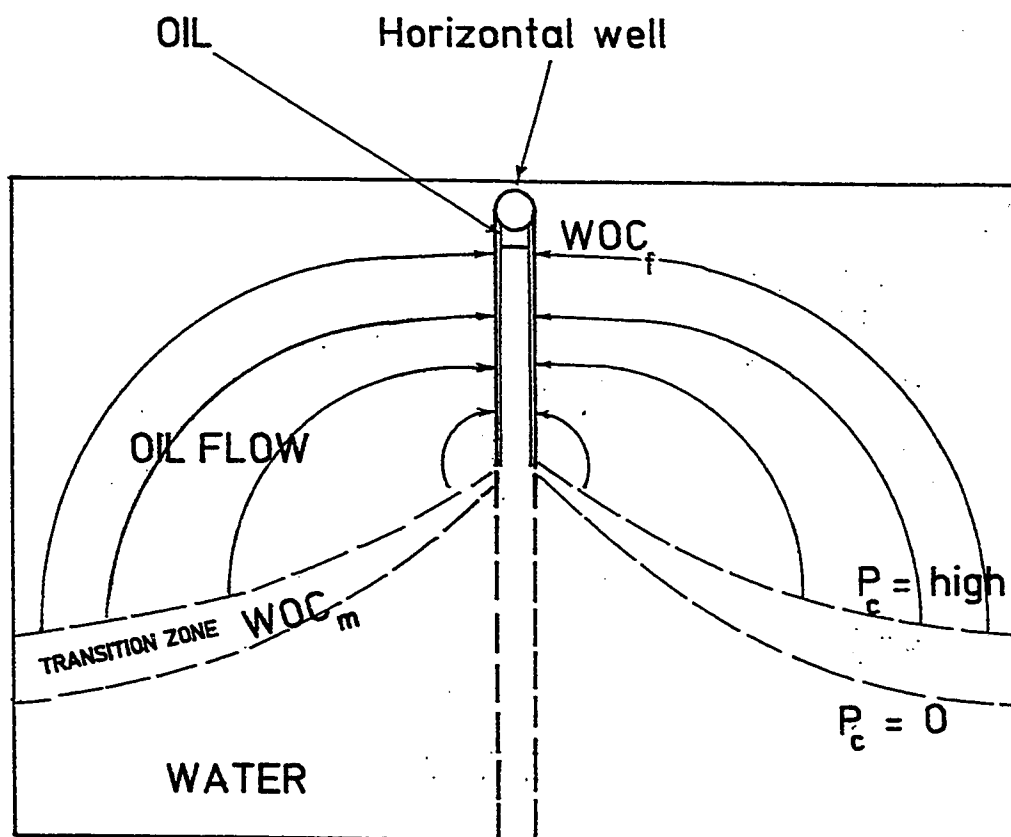
Figure 6.6: Production Mechanisms of Fractured Horizontal Well in Bottom Water Drive Reservoir

is limited by the driving force, capillary pressure and the resistance for the darcy flow.

If the rate is maintained constant and below the initial critical rate, the WOC in the fracture starts out below the top and climbs as oil is produced and as the matrix WOC also climbs. Eventually, when it reaches the well, water breakthrough occurs. The fractional recovery at which this occurs depends upon the extent of the fracture system, e.g. multiple orthogonal fractures allow the production of oil at a fixed rate with less Δh and hence there is a high recovery at breakthrough.

6.4.3 Production Mechanisms of Unfractured Reservoirs

Similar considerations apply to production from an unfractured horizontal well. In this case there is an additional resistance to flow created by the convergence to the wellbore. In some cases (wide and/or thin reservoirs) this has negligible effects. However with thicker or narrower patterns as shown in Figure 6.7, there can be a substantial loss in rate and/or less recovery at water breakthrough for a given rate

At any time less than the breakthrough time, a pressure balance , Figure 6.8, may be written as follows:

$$\Delta P = P_i - P_w = \rho_o g(h - h_w) + \rho_w g h_w + \Delta P_d$$

or:

$$\Delta P = P_i - P_w = \rho_o g h + \Delta \rho g h_w + \Delta P_d$$
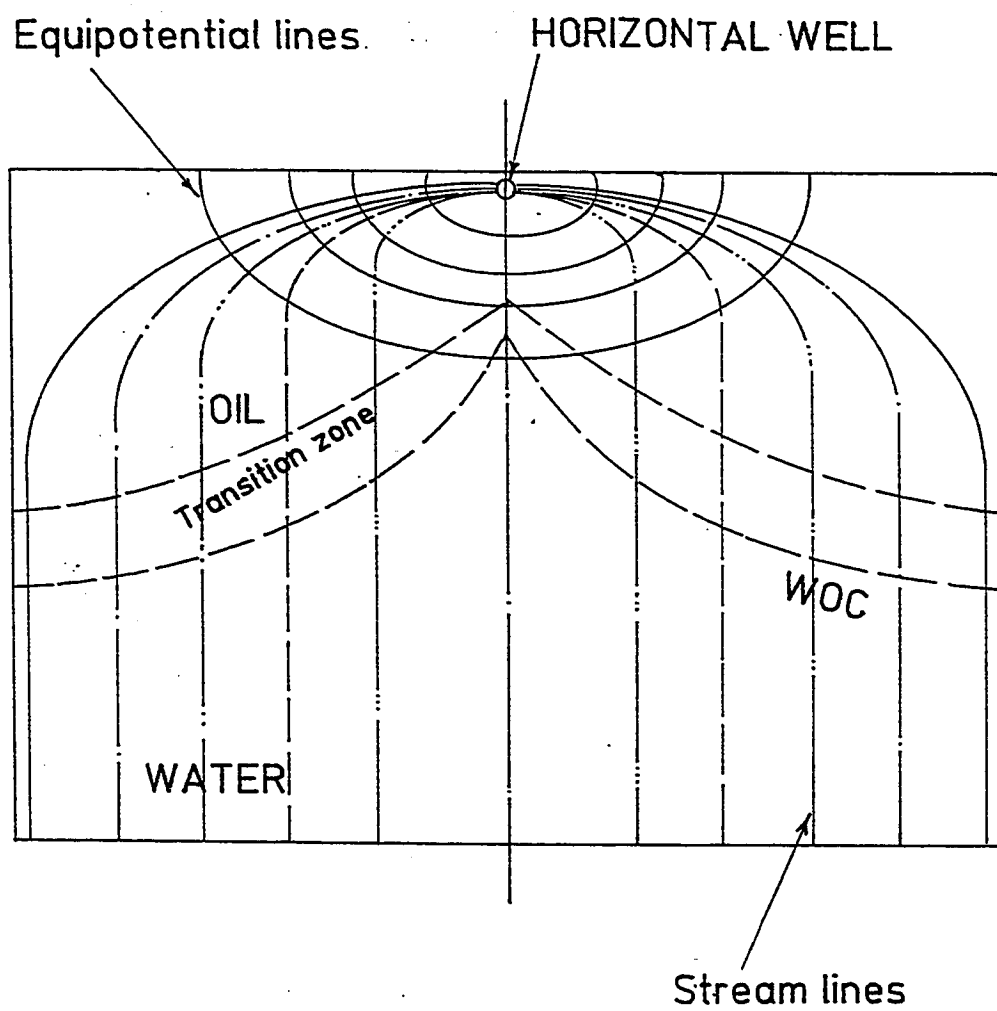
Figure 6.7: Production Mechanisms of Horizontal Well with no Fracture in Bottom Water Drive Reservoir
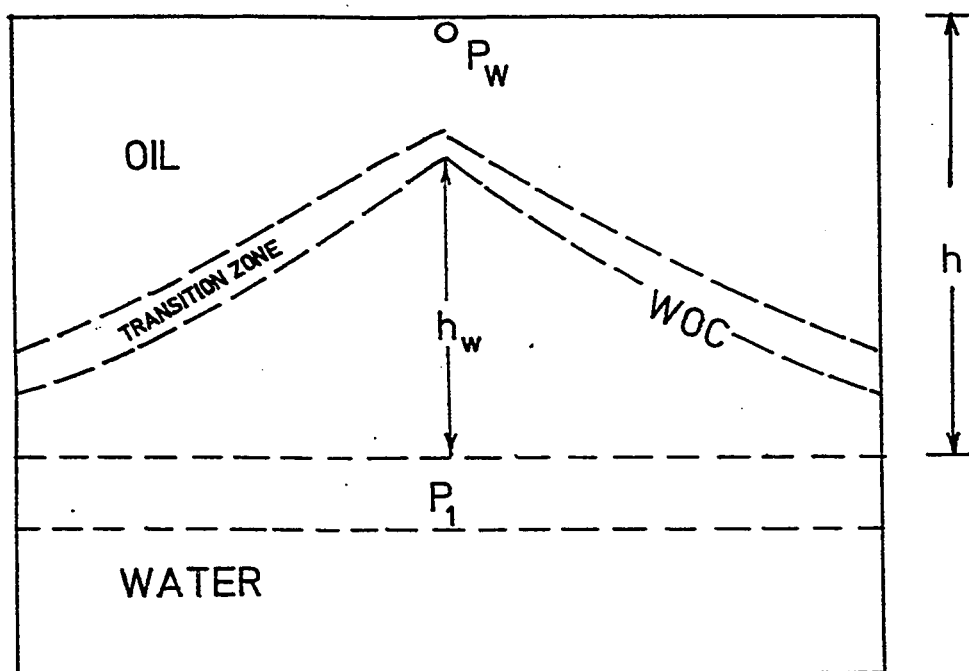
Figure 6.8: Pressure Balance for a Case of Horizontal Well with no Fracture

The pressure at the production well may be written as:

$$P_w = (P_1 - \rho_o gh) - \Delta\rho gh_w - \Delta P_d$$

Where ΔP is the total pressure drop across the system, $(P_1 - \rho_o gh)$ is the initial static pressure, and $\Delta\rho gh + \Delta P_d$ is the drawdown, where ΔP_d is the pressure drop due to capillary and viscous (darcy) forces. This last term may be neglected in the fracture and considered in the matrix. The original thickness of the reservoir is defined by h and the height of water, in a vertical plane below the well, is defined by h_w.

There is, however, another condition for a stable interface which is that the pressure gradient at the interface must not exceed $\Delta\rho gh$. If this is exceeded, interface instability occurs and viscous finger forms. Thus, since it is not possible to draw the interface as high, for a given rate, a lower recovery is obtained at breakthrough.

Because of the longer perforated intervals, horizontal wells require less drawdowns than the vertical wells for a given production rate or allow higher rates for a given drawdown. Also it is expected that longer horizontal wells would yield better results than the shorter ones because of the larger contact area and, therefore, smaller convergent radial pressure gradients; and also because of improved sweep efficiency resulting from using narrower patterns which are swept more efficiently.

6.4.4   Summary of the Production Mechanisms

From the previous discussion , the production mechanisms of fractured horizontal wells may be summarized as:

6.4.4.1   Driving Mechanisms before Water Breakthrough

I. Oil Zone:

During the flooding process, the difference between higher pressure in the matrix block and lower pressure in the fracture may drive the oil from the matrix pores towards the fracture.

II. Water-Invaded Zone:

Within the fracture, the pressure drop is less than that of the matrix block, therefore, as the flooding process continues, the oil water contact will be higher in the fracture than in the matrix block. At this stage, it is expected that water moves fast through the fracture and early water breakthrough occurs. However, new recovery driving forces prevail in the fractured reservoir. The oil is moved from the matrix through driving, gravitational, and capillary forces into the fracture where the gravitational forces dominates. Within the fracture the oil segregates upward, due to gravity difference between oil and water, toward the producing well.

The predominance of capillary or gravity forces is influenced by the current relative position of the oil water contact in the fracture and matrix block. If the oil water contact is advancing equally through the fracture and matrix block, the production of oil from the matrix block would be dominated by capillary forces. If, however, the oil water contact is higher in the fracture, which may be the case, than that in the matrix block, the capillary and gravitational forces would combine and drive the oil from the matrix block toward the fracture network. The magnitude of gravitational forces depends on the current relative position of the oil water contact through the fracture and the matrix block. Under these forces (capillary and gravity), water is imbibed (sucked) from the fracture into the matrix block; consequently, oil is expelled into the fracture from the matrix block, segregated and produced under gravity. This processes continue until water breakthrough.

6.4.4.2 Driving Mechanisms after Water Breakthrough

After water breakthrough, the fracture is filled with water and the matrix block is totally immersed in water. Oil is then trapped in the matrix pores. In this case, oil is produced as a result of continuous injection according to the displacement theories [111,119,122]. The displacement process in this case is controlled by viscous and capillary forces.

Chapter VII
SUMMARY AND CONCLUSIONS

7.1 SUMMARY

A scaled three-dimensional model was built to investigate the production performance of fractured and unfractured horizontal and vertical wells in bottom-water drive reservoirs. Different fracture geometries and dimensions were investigated and compared. The main findings of this study may be summarized as:

7.1.1 Vertical Well vs. Horizontal Well:

1. Ultimate recovery is almost the same

2. Recovery at water breakthrough is ~90% of ultimate recovery for the UHW, while it is only ~33% for the UVW.

3. Water breakthrough is delayed for the UHW but water production increases then very rapidly.

4. Pressure drop is less for the UHW than for the UVW.

7.1.2 Fractured Vertical Well vs. Unfractured Vertical Well:

1. Recovery at breakthrough is higher for the fractured well and increases with increasing fracture penetration.

2. Higher ultimate recovery is obtained with the fractured well.

3. Water breakthrough is delayed for the fractured well.

7.1.3 Fractured Vertical Well vs. Unfractured Horizontal Well:

1. Higher breakthrough and ultimate recoveries are obtained with the FVW.

2. Delayed water breakthrough for the FVW.

3. Pressure drop is less for the UHW than that for the FVW.

7.1.4 Horizontal Well vs. HW with Longitudinal Fracture:

1. Water breakthrough is delayed and ultimate Recovery is higher for the fractured well.

2. Ultimate recovery and recovery at BT increase with fracture penetration up to a limit, the penetration then has no effect on recovery

3. Residual oil saturation of ~9% is obtained with fractured well compared to ~23% for the unfractured well.

4. Pressure drop is less for the fractured well.

7.1.5 Horizontal Well vs. HW with Single Orthogonal Fracture:

1. Higher recovery at water breakthrough is obtained with the fractured well.

2. Recovery increases with increasing the fracture vertical penetration

3. Lower pressure drop is obtained with the fractured well.

4. Recovery at breakthrough increases with increasing fracture extension, however, the ultimate recovery is not affected.

5. Higher pressure drop is experienced with smaller fracture extension

7.1.6 Horizontal Well vs. HW with Multiple Orthogonal Fractures:

1. Recovery at water breakthrough increases with increasing the number of fractures up to a limit (three fractures in this study). Additional fractures have no effect.

2. Ultimate recovery also increases with the number of fractures, but no effect is observed beyond two fractures in this study.

3. Pressure drop decreases as the number of fractures is increased.

7.1.7 Fractured Vertical Wells vs. Fractured Horizontal Wells:

1. The highest oil recovery is obtained in the case of the FHW/LF followed by the FHW/OF and then the FVW/VF. Consequently residual oil saturation is highest for the FVW/VF.

2. Both the FHW/LF and FHW/MOF have the same ultimate recovery with the the FHW/LF having slightly higher recovery at water break-through

3. Pressure drop is highest for the FVW/VF and lowest for the FHW/LF

4. The cumulative water oil ratio decreases with increasing fracture penetration or fractures number.

7.2 CONCLUSIONS

From the previous findings, the following conclusions are made for bottom water drive reservoirs:

1. For the same drainage volume, both vertical and horizontal wells would yield the same ultimate recovery. The horizontal well, however, has the major advantage of recovering most of the oil before water breakthrough. In addition, the horizontal well can be extended to produce larger volume of the reservoir.

2. Using horizontal wells in artificially or naturally fractured reservoirs improves the production performance as they result in higher ultimate and breakthrough recoveries and delayed water breakthrough.

3. A fractured vertical well would provide better performance than unfractured horizontal well. However, the fractured horizontal well would perform much better than the fractured vertical well yielding higher recoveries and lower pressure drop.

4. The horizontal well with longitudinal fracture provides the best performance which can only be approached by multiple orthogonal fractures.

5. Increasing the number of orthogonal fractures increases the contact area with the reservoir; therefore, the performance of horizontal wells is improved. There is, however, a limit beyond which no further improvement would be possible. At this limit, the well performs similar to a horizontal well with longitudinal fracture.

6. Increasing the fracture vertical penetration, in general, improves both ultimate and breakthrough recoveries. However, there is a limit beyond which further increase in penetration will be insignificant.

7. For horizontal wells with orthogonal fractures, increasing the fracture extension results in increasing the recovery at water breakthrough; however, the ultimate oil recovery is not improved.

8. The recovery mechanisms of fractured reservoirs are shown to be influenced mostly by gravitational and capillary imbibition.

REFERENCES

1. Butler, R.M.: "A New Approach to the Modeling of Steam-Assisted Gravity Drainage," JCPT, (May-June 1985), pp. 42-51.

2. Sherrard, D.W., Brice, W.W., and MacDonald, D.G.: " Application of Horizontal Wells at Prudhoe Bay," JPT (November 1987) 1417-1425.

3. Economides, M.J., and Notle, K.G.: "Reservoir Stimulation," 2nd Edition, TX 77023 (1989) 19-.

4. Butler, R.M.: "The Potential for Horizontal Wells for Petroleum Production," JCPT (May-June 1989) vol. 28, No. 3, 39.

5. Joshi, S.D.: "Horizontal Well Technology," PennWell Publishing Company, Tulsa, Oklahoma, 1991.

6. Grigorian, A.M.: "Forage des Couches Productives par Units Puits Horizontaux et a Completion Multiple, Nedra, Moscow (1969), French Translation by Inst. Francais du Petrole, IFP 27746 (Feb. 1980).

7. Reiss, L.H.: "Production from Horizontal Wells after 5 Years," JPT (November 1987) 1411-1416.

8. Reiss, L.H. et al.: "Offshore European Horizontal Wells," Paper OCT 4791, 1984.

9. Wilkirson, J.P., Smith, J.H., Stagg, T.O. and Walters, D.A.: " Horizontal Drilling Techniques at Prudhoe Bay, Alaska," Paper SPE 15372, 1986.

10. Edlund, P.A.: "Application of Recently Developed Medium Curvature Horizontal Drilling Technology in the Sprabreey Trend Area," Paper SPE/IADC 17170, 1987.

11. Norris, J.L. Hunt, Soliman, M.Y., and Puthigai, S.K.: " Predicting Horizontal Well Performance: A Review of Current Technology" , Paper SPE 21793, Presented at the Western Reg. Meet., Long Beach, CA, March 20-22, 1991

12. Aguilera, R., et al. : "Horizontal Wells," Gulf Publishing Company, Houston, Texas, 1991.

13. Meyer, R.F. and Fulton, P.A.: "Toward an Estimate of World Heavy Crude Oil and Tar Sands Resources," Proc. 2nd Intl. Conference on Heavy Crude and Tar Sands. United Nations Inst. for Training and Research, Caracas, 1982.

14. Carrigy, M.A.: "Thermal Recovery from Tar Sands," JPT, vol. 35, No. 13, p 2149-2157, Dec. 1983.

15. Butler, R.M.: "The Potential of Horizontal Well," Advances in Petroleum Recovery & Upgrading Technology Conference, Calgary, Alberta, Canada (June 14-15, 1984).

16. Islam, M.R. and Chakma, A.: "Comprehensive Physical and Numerical Modeling of a Horizontal Well" , Paper SPE 20627, Presented at the 65th Ann. Tech. Conf. and Exh., New Orleans, LA, Sep. 23-26, 1990.

17. Meszaros,G. Chakma, A. and Islam, M.R.: "Scaled Model Studies and Numerical Simulation of Inert Gas Injection With Horizontal Wells" , Paper SPE 20529, Presented at the 65th Ann. Tech. Conf. and Exh., New Orleans, LA, Sep. 23-26, 1990.

18. Ahner, P.F. and Sufi, A.H.: "Physical Model Steamflood Studies Using Horizontal Wells" , Paper SPE/DOE 20247, Presented at the SPE/DOE 7th Symp., Tulsa, OK, April 22-25, 1990.

19. Islam, M.R. and Chakma, A.: "A New Recovery Technique for Heavy Oil Reservoirs with Bottom water." , Paper SPE/DOE 20258, Presented at the SPE/DOE 7th Symp., Tulsa, OK, April 22-25, 1990.

20. Sugianto, s. and Butler, R.M: "The Production of Conventional Heavy Oil Reservoirs with Bottom Water Using Steam-Assisted Gravity Drainage," JCPT,(March-April 1990), vol.27, No.5, pp. 78-86.

21. Doan, Q., and Farouq Ali, S.m.: "Scaling Criteria and Model Experiments for Horizontal Wells" Paper no. CIM/SPE 90-128, presented at the International Technical Meeting, Petroleum Society of CIM and SPE, Calgary, June 10 to 13, 1990.

22. Asgarpour, S., Springer, S., Pantell, P., and Singhal, A.: "Enhanced Heavy-Oil Production by Horizontal Drilling - Case Study," Paper no. CIM/SPE 90-126, presented at the International Technical Meeting, The Petroleum Society of CIM and SPE, Calgary, June 10 to 13, 1990.

23. Chaperon, Isabele: "Theoretical Study of Conning Towards Horizontal and vertical wells in Anisotropic Formations: Subcritical and Critical Rates," Paper SPE 15377 presented at the 1986 SPE Ann. Tech. Conf. and Exib., New Orleans, October.

24. Giger, F.M.: "Analytic Two-Dimensional Models of Water Cresting before Breakthrough for Horizontal Wells." Paper SPE Reservoir Eng., November 1989.

25. Papatzocos, P., Henery, T.R., Martensen, R. and Skjaeveland, S.M : "Cone Breakthrough Time for Horizontal Wells," Paper SPE 19822 presented at the 1989 SPE Ann. Tech. Conf. and Exib., Reservoir Eng. vol., San Antonio, Tx, October.

26. Ozcan, E. and Raghavan, R.: "Performance of Horizontal Wells Subject to Bottom Water Drive," SPE Res. Eng. (August 1990) 375.

27. Karcher, B.J., Giger, F.M., and Combe, J.: "Some Practical Fo mulas to Predict Horizontal Well Behavior," Paper SPE 1543,presented at SPE 61st Annual Technical Conference and Exhibition, New Orleans, Louisiana, Oct. 4-8, 1986.

28. Joshi, S.D.: "Augmentation of Well Productivity Using Slant and Horizontal Wells," JPT, pp.729-739, June 1988.

29. Papatzocos, P., Gustafson, S.A. and Skjaeveland, S.M : "Critical Time for Cone Breakthrough in Horizontal Wells," presented at Seminar on Recovery from Thin Oil Zones, Norwegian Petroleum Directorate, Stavanger, Norway, April 21-22, 1988.

30. Supronowicz, R., and Butler, R.M.: "Vertical Confined Water Drive to Horizontal Well, Part I: Water and Oil of Equal Densities," presented at the 3rd Technical Meeting of the South Saskatchewan Section,the Petroleum Society of CIM, Regina, September 25-27, 1989.

31. Maxwell, J.C.: "A Treatise on Electricity and Magnetism," 3rd Edition, vol.I, p.310 et seq, Oxford University Press, London, 1892. (1st Edition 1873).

32. Muskat, M.: "The Flow of Homogeneous Fluids Through Porous Media," 1937, reprinted by International Human Resources Development Corporation, Boston, 1982.

33. Reis, J.C.: " Oil Recovery Mechanisms in Fractured Reservoirs During Steam Injection," Paper SPE/DOE 20204 presented at the SPE/DOE 7th Symp., Tulsa, OK, April 22-25, 1990.

34. Nelson, R.A.: "Geologic Analysis of Naturally Fractured Reservoirs, Gulf Publishing, Houston, TX (1985).

35. Saidi, A.M.: "Reservoir Engineering of Fractured Reservoirs: Fundamental and Practical Aspects, Total Edition Press, Paris (1988).

36. Carmer, D.D.: "Guides Exist for Fracture Treatment in Horizontal Wells," OGJ SPECIAL March 27, 1989, Oil & Gas Journal, 41-52.

37. Soliman, M.Y., Rose, Bob, EL Rabaa,W., and Hunt, J.L.: " Planning Hydraulically Fractured Horizontal Completions," World Oil (Sept. 1989) 54-58.

38. Soliman, M.Y., Hunt, J.L., and EL Rabaa,W.: "Fracturing Aspects of HorizontaL WELLS," JPT (Aug. 1990) 966-973.

39. Hsiao, C.: "A Study of Horizontal Wellbore Failure," Paper SPE 16927 presented at the 1987 SPE Ann. Tech. Conf. and Exib., Dallas, sept. 27-30.

40. Yew, C.H., And Li, Y.: "On Fracturing Design of Deviated Wells," SPE Production Engineering (Nov. 1988) 428.

41. Soliman, M.Y.: "Interpretation of Pressure Behavior of Fractured, Deviated Horizontal Wells," Paper SPE 21062 presented at the 1990 SPE Latin American Eng. Conf., Riode Janeiro, October.

42. El Rabaa, W.: " Experimental Study of Hydraulic Fracture Geometry initiated From Horizontal Wells", Paper SPE 19720 presented at the 1989 SPE Ann. Tech. Conf. and Exib., San Antonio, Tx, Oct. 8-11, 1989.

43. Schulte, M.W.: "Production from a Fractured Well with Well Inflow Limited to Part of the Fracture Height," SPE Production Engineering (Sept. 1986).

44. Mukherjee, H. and Economides, M.J.: " A Parametric Comparison of Horizontal and vertical Well Performance," Paper SPE 18303 presented at the 1988 SPE Ann. Tech. Conf. and Exib., Reservoir Engineering delolume, Houston, Oct. 2-5.

45. Soliman, M.Y.: "Design and Analysis of a Fracture With Changing Conductivity," J.Cdn.Pet.Tec. (Sept.-Oct. 1986) 62-67.

46. Soliman, M.Y.: "Fracture Conductivity Distribution Studied," Oil & Gas J. (feb. 10,1986) 89-93.

47. Bennett, C.O. et al. : "Influence of Fracture Heterogeneity and Wing Length on the Response of Vertically Fractured Wells," SPEJ (April 1983) 219-30.

48. Cinco-Ley, H. and Samaniego, del.F.: "Transient Pressure Analysis for Fractured Wells," JPT (Sept. 1981) 1749-1766.

49. Soliman, M.Y.: "Fracture Conductivity Distribution Studied," Oil & Gas J. (Feb. 10, 1986) 89-93.

50. Soliman, M.Y., Venditto, J.J., and Slusher, G.L. : "Evaluating Fractured Well Performance by Use of Type Curves," paper SPE 12598 presented at the 1984 SPE Permian Basin Oil & Gas Recovery Conference, Midland, March 8-9.

51. Anderson, S., Hansen, S., and Fieldgaard, K.: "Horizontal Drilling and Completion: Denmark," Paper SPE 18349 presented at the 1988 SPE European Petroleum Conference, London, Oct. 16-19.

52. Hudson, P.J. and Matson, R.P.: "Hydraulic Fracturing of Horizontal Wellbores," Paper SPE 23950 presented at the 1992 SPE Permian Basin Oil and Gas Recovery Conference, Midland, Texas, March 18-20, 1992.

53. Austin, C.E., Rose, R.E., and Schuh, F.J.: "Simultaneous Multiple Entry Hydraulic Fracture Treatments of Horizontally Drilled Wells," Paper SPE 18263 presented at the 63rd Annual SPE Technical Conference, Houston, 1988.

54. Overby, W.K., Yost, A.B. II, and Wilkens, D.A.: "Inducing Multiple Hydraulic Fractures from Horizontal Wellbore," Paper SPE 18249 presented at the 63rd Annual SPE Technical Conference, Houston, 1988.

55. Damgaard, A., Bangert, D.S., Murray, D.J., and Stout, G.W.: "A Unique Method for Perforating, Fracturing, and Completing Horizontal Wells ," Paper SPE 19282 presented at SPE Offshore Europe Conference, Aberdeen,1989.

56. Yost, A.B., and Overby, W.K.: "Production and Stimulation Analysis of Multiple Hydraulic Fracturing of a 2,000 ft Horizontal Well," Paper SPE 19090 presented at SPE Gas Technical Symposium, Dallas, 1989.

57. French Oil & Gas Industry Association Technical Committee: "Directional Drilling and Deviation Control Technology," Gulf Publishing Company, Houston (1990).

58. Crouse, P.C.: "Economic Analysis of Horizontal.Drilling Investment," Gulf Publishing Company, Houston (1991).

59. Aguilera, R.: "Volume 9: Horizontal Drilling, .Completion, and production," Gulf Publishing Company, Houston (March 1991).

60. "World Oil's Handbook of Horizontal Drilling and Completion Technology," Gulf Publishing Company, Houston (1991).

61. Aldrich, C.S. et al.: "Directional Drilling," SPE Reprint Series No. 30 (1991).

62. "Horizontal Drilling," SPE Reprint Series No. 33 (1991).

63. Kuich,N.: "Seismic and Horizontal Drilling Unlock Austin Chalk," World Oil, Sept. 1990, 211, No.3,47-54.

64. Pope, C.D., Handren, P.J.: "Completion Techniques for Horizontal Wells in the Pearsall Austin Chalk," Proc. 65th SPE Ann. Tech. Conf. and Exib., New Orleans, Sept. 23-26, 1990, Production Operations and Engineering Volume, 657-64; SPE 20682.

65. Styton, R.J.: "Underbalanced Horizontal Drilling Enhances Production of Austin Chalk," Paper SPE/IADC 19984 presented at the 1990 IADC/SPE Drilling Conference, Houston, Feb. 27-March 2.

66. Kirby, R.: "Horizontal MWD Tool Development and Application in the Austin Chalk," presented at 1991 World Oil 2nd Annual Horizontal Well Technology Regional Conference, San Antonio, Aug. 6-7.

67. Pritchwtt, J.L., and Waak, K.A.: " Completion of the KCC 378-H: A Case History," Paper SPE 23949 presented at the 1992 SPE Permian Basin Oil and Gas Recovery Conference, Midland, Texas, March 18-20, 1992.

68. Economides, M.J., Ben-Naceur, K. andKlem, R.C.: " Matrix Stimulation Method for Horizontal Wells," paper SPE 19719, 1989.

69. Ogden, S.: "Inflatable Packers Provide Options For Horizontal Wells," Pet. Eng. Int. (Nov. 1991) 37-47.

70. Holcomb, D.L. and Reed, D.A.: "Radioactive Tracers offer a Closer Lock at Horizontal Completions," World Oil (Nov. 1991) 86-92.

71. Joshi, S.D. :"Thermal Oil Recovery with Horizontal Well," JPT (Nov. 1991) 43, No. 11, 1302-04.

72. "Thermal Response rises at Horizontal/Steam Test," Oil & gas J. (May 8, 1989) 87, No. 19, 16-17.

73. Sahuquet, B.C., Spreux, A.M., Corre, B., and Guittard, M.P.: "Steam Injection in a Low-Permeability Reservoir Through A Horizontal Well in Lacq Superieur Field," Proc. 65th SPE Ann. Tech. Conf. and Exib., New Orleans (Sept. 23-26, 1990), EOR/General Petroleum Engineering Volume, 559-62; SPE 20526.

74. "Canadian Combine Steam Drive, Horizontal Well," Oil & gas J. (June 1, 1987) 85, No. 22, 22.

75. Dietrich, J.K.: "The Kern River Horizontal Well Steam Pilot," SPERE (Aug. 1988) 3, 935-44.

76. Butler, R.: "Development and Description of Steam Assisted Gravity Drainage Using Horizontal Wells," presented at the 3rd International Conference on Horizontal Well Technology, Houston, Nov. 12-14, 1991.

77. Ammer, J.R., Enick, R.M., and Klara, S.M.: "Modeling the Performance of Horizontal Injection Wells in Carbon Dioxide Miscible Displacement Processes," paper SPE 21220 presented at the 1991 SPE symposium on Reservoir Simulation, Anaheim, Feb. 17-20.

78. McAlpine, J.L., and Joshi, S.D.: "Horizontal-Well pilot Waterflood Tests Shallow, Abadoned Field," Oil & gas J. (Aug. 5, 1991) 89, No. 31, 46-47.

79. "Horizontal Waterflood Scheduled in Texas Carbonate Reservoir," Oil & gas J. (Sept. 2, 1991) 89, No. 35, 34.

80. Charles, D.D., Startzman, R.A., and Raghvan, R.: " Streametube Modeling of Horizontal Wells in Mixed-Pattern Waterfloods," paper SPE 23451 presented at the 1991 SPE Eastern Regional Meeting, Lexington, KY, Oct. 23-25.

81. Hansen, K.L.: "Application for Horizontal Well in a Wilcox Waterflood-A Case Study ," presented at the 3rd International Conference on Horizontal Well Technology, Houston, Nov. 12-14, 1991.

82. Pitts, J.P.: "Waterflood Offers Horizontal Hope," Midland, Reporter-Telegram (Aug. 25, 1991) 1E.

83. Taber, J.J., and Seright, R.S.: "Horizontal Injection and Production Wells for EOR or Waterflooding," Paper SPE 23949 presented at the 1992 SPE Permian Basin Oil and Gas Recovery Conference, Midland, Texas, March 18-20, 1992.

84. Muskat, M.: "Physical Principles of Oil Production," International Human Resources Development Corporation, 1981.

85. Supronowicz, R., and Butler, R.M.: "The Choice of Pattern Size and Shape for Regular Arrays of Horizontal Wells," Paper no. CIM/SPE 90-129, presented at the International Technical Meeting, The Petroleum Society of CIM and SPE, Calgary, June 10 to 13, 1990.

86. Aziz, K. and Settari, A.: "Petroleum Reservoir Simulation," Applied Science Publishers, London-NewYork, 1979.

87. Settari, A. and Aziz, K.: "Use of Irregular Grid in Reservoir Simulation," SPEJ, 12, No. 2, pp 103-114, 1972.

88. Craft, B.C., and Hawkins, M.F.: "Applied Petroleum Reservoir Engineering," Prentice-Hall, Inc., New Jersey, 1959.

89. Asafari, A., and Witheespoon, P.A. : "Numerical Simulation of Naturally Fractured Reservoirs," paper SPE 4290 presented at SPE 3rd Numerical Simulation of Reservoir Performance Symposium, Houston, Jan. 10-12, 1973.

90. Morse, R.A. and Von Gonten, D. : "Productivity of Stimulated Wells Prior to Stabilized Flow," paper SPE 3631 presented at SPE 46th Annual Fall Meeting, New Orleans, Oct. 3-6, 1971.

91. Morse, R.A. and Holditch, S.A. : "Large Fracture Treatments may Unlock Tight Reservoirs," Oil and Gas Journal, March 29, and April5, 1971.

92. Huskey, W.L., and Crawford, Paul B. : "Performance of Petroleum Reservoirs Containing Vertical Fractures in the Matrix," Soc. Pet. Eng. J (June 1967)221-228.

93. Parson, R.W. : "Permeability of Idealized Fractured Rock," Soc. Pet. Eng. J (June 1966)1926-1936.

94. Warren, T.E. and Root, P.J. : "The Behavior of Naturally Fractured Reservoirs," Soc. Pet. Eng. J (Sept. 1963)245-255.

95. Russel, D. and Truitt, N.E. : "Transient Pressure Behavior in Vertically Fractured Reservoirs," J. Pet. Tec. (Oct. 1964)1159-1170.

96. Tommo, W.J., Milam, R., and Crawford, W.R. : "How to Determine the Length of a Vertical Fracture from Transient Well Production Data," Oilweek (July 30, 1962)13,24,35.

97. Prats, M., Hazebrook,P., and Strickler, W.R. : "Effect of Vertical Fractures on Reservoir Behavior-Compressible Fluid Case," Soc. Pet. Eng. J (June 1962)87-94.

98. McGuire, W.J., and Sikora, V.J, : "The Effect of Vertical Fractures on Well Productivity," Soc. Pet. Eng. J (June 1962)87-94.

99. Baker, W.J. : "Flow in Fissured Formations," Proc. Fourth World Petroleum Congress, Section II/E, Paper 7, 1955.

100. Bear, J and Corapcioglu, M.Y. : "Advances in Transport Phenomena in Porous Media," NATO ASI Series, Series E: Applied Sciences - No. 128, Martinus Nijhoff Publishers, 1987.

101. Reiss, L.H. : "The Reservoir Engineering Aspects of Fractured Formations," Editions Technip, Paris, 1980.

102. Van Golf-Racht; T.D. : "Fundamentals of Fractured Reservoir Engineering," Elsevier Scientific Publishing Company, 1982.

103. Whillte, G.P.: " Waterflooding," SPE Textbook Series, Delolume 3, 1986.

104. Henley, D.H., Owens, W.W., and Craig, F.F., Jr.: "A Scale-Model Study of Bottom-Water Drive", JPT (January, 1961).

105. Perkins, F.M., Jr. and Collins, R.E.: "Scaling Laws for Laboratory Flow Models of Oil Reservoir", Trans., AIME (1960) 219, 383.

106. Cross, G.A., and Schwarz, N.: "Dimensionally Scaled Experiments and Theories on the Water-Drive Process", Trans., AIME (1955) 204 ,35.

107. Rapoport, L.A.: "Scaling Laws for Use in Design and Operation of Water-Oil Flows Models", Trans., AIME (1955) 204, 143.

108. Geertisma, J., Cross,G.A. and Schwarz, N.: "Theory of Dimensionally Scaled Models of Petroleum Reservoir", Trans., AIME (1956) 207, 119.

109. Leverett, M.C.: "Capillary Behavior in Porous Solids," Trans., AIME (1941) 142, 152-169.

110. Bird, R.B., Stewart, W. E., and Lightfoot, E.N.: " Transport Phenomena," John Wiley& Sons, New York, 1960.

111. Bear, J.: "Dynamics of Fluids in Porous Media," 1st ed., American Elsevier Environmental Science Series, New York,1972.

112. Aronofsky, J. S., Masse, L. and Natanson, S.G.: " A model for the Mechanism of Oil Recovery from the Porous Matrix Due to Water Invasion in Fractured Reservoirs," Trans., AIME, Vol. 213, 1958, pp. 17-19.

113. Graham, J.W. and Richardson, T.G.: "Theory and Application of Imbibition Phenomena in Recovery of Oil," Trans.,AIME, Vol. 216, 1959,pp. 377-385.

114. Bokserman, A.A., Zheltov, Y.P. and Kocheshlcov,A.A.: Motion of Immiscible Liquidsin a Cracked Porous Media," Soviet Physics Doklade, Vol. 9, No. 4, Oct. 1964, pp. 285- 287.

115. Kleppe, J. and Morse, R.A.: "Oil Production from Fractured Reservoirs by Water Displacement," presented at the Oct. 6-9, 1974, 49th Annual Fall Meeting of the Society of Petroleum Engineers, Houston, TX., (Preprint 5084).

116. Kazemi, H. and Merill, L.S.: "Numerical Simulation of Water Imbibition in Fractured Cores," SPEJ, Vol. 19, No. 3, June 1979, pp. 175-182.

117. Mannon, R.W. and Chilinger, G.V.: "Experiments on Effect of Water Injection Rate in Fractured Reservoirs," presented at the Oct. 8-11, 1972, 47th Annual Fall Meeting of the SPE, San Antonio, TX., (Preprint SPE 4101)

118. Mattax , C.C., and KYTE, J.R.: " Imbibition Oil Recovery from Fractured, Water Drive Reservoir," SPEJ, Vol. 2, No. 2, June 1962, pp. 177-184.

119. Collins, R.E.: " Flow of Fluids Through Porous Media" The Petroleum Publishing Company, Tulsa 1976.

120. Joshi, S.D.: " Production Forecasting Methods for Horizontal Wells" paper SPE 17580, presented at the SPE International Meeting, Tianjin, China, Nov. 1-4, 1988.

121. Williams, B.B., Gridley, J.L., Schechter, R.S.: " Acidizing Fundamentals, SPE Monograph No. 6, Dallas, Texas 1979.

122. Dake, L.P.: " Fundamentals of Reservoir Engineering" Elsevier science Publishing Company Inc., New York, 1978.

123. Dikken, B.J.: " Pressure Drop in Horizontal wells and its Effect on Production Performance", JPT (November 1990), pp. 1426-1433.

124. Butler, R.M.: " Gravity Drainage to Horizontal Wells," JCPT, (April 1992), pp. 31-37.

NOMENCLATURE

A	= area of the drainage pattern
a	= length of the drainage pattern
a_D	= effective well spacing
b	= width of the drainage pattern
B_o	= formation volume factor, RB/STB
b'	= penetration ratio
D	= distance between two lines of horizontal wells, ft,
N_p	= oil produced, cc
E_s	= sweep efficiency, dimensionless
F_{CD}	= dimensionless fracture conductivity
f_d	= microscopic displacement efficiency, dimensionless
FHW	= fractured horizontal well,
FVW	= fractured vertical well,
g	= acceleration by gravity
h	= oil zone thickness, ft
h_m	= oil thickness of the model, ft
h_p	= oil thickness of the prototype (reservoir), ft
h_{wf}	= water oil interface in the fracture
h_{wm}	= water oil interface in the matrix

h_p	= perforated interval, ft
HW/LF	= horizontal well with longitudinal fracture,
HW/MOF	= horizontal well with multiple-orthogonal fracture,
HW/SOF	= horizontal well with single-orthogonal fracture,
I_v	= distance between the gas/oil interface
I_h	= distance between the horizontal well and gas/oil interface
k_1	= matrix permeability, md
k_2	= fracture permeability, md
k_f	= fracture permeability, md
k_h	= permeability in the horizontal direction, md
k_m	= matrix permeability, md
k_m	= model permeability, md
k_o	= effective permeability to oil, md
k_p	= prototype permeability, md
k_{ro}	= relative permeability to oil
k_{rw}	= relative permeability to water
k_v	= permeability in the vertical direction, md
k_w	= effective permeability to water, md
k_x	= permeability in the x-direction, md
k_y	= permeability in the y-direction, md
k_z	= permeability in the z-direction, md
L	= horizontal well length, ft
L_D	= dimensionless well length

L_m	= model length, ft
L_p	= prototype length, ft
L_p	= perforated interval
L_{pD}	= dimensionless perforated interval
L_w	= horizontal well length, ft
m(p)	= real gas pseudopressure, sq.psi/cp
OWC	= oil water contact
P	= pressure, psi.
P_c	= capillary pressure, psi.
P_{cD}	= dimensionless capillary pressure.
Pinj	= pressure drop, psig.
P_D	= dimensionless pressure
P_o	= pressure in the oil phase, psi.
P_{oD}	= dimensionless pressure in the oil phase.
P_w	= pressure in the water phase, psi.
P_{wD}	= dimensionless pressure in the water phase.
$(PI)_H$	= productivity index of a horizontal well with a longitudinal fracture
$(PI)_V$	= productivity index of a fractured vertical well at steady state
q	= flow rate,
q_m	= model flow rate,
q_p	= prototype flow rate,

Q_c = critical flow rate, m^3/hr

q_c = critical flow rate, STB/d,

q_D = dimensionless rate.

q_f = flow rate through the fracture.

q_{HW} = flow rate between opposed parallel horizontal

wells, bbls/day

q_L = linear flow rate between parallel faces of

a reservoir block, bbls/day

q_{lc} = can be obtained from table (2.2)

q_{mf} = flow rate through the matrix.

q_o = flow rate, STB/day

$q_{o,v}$ = vertical well critical rate, STB/day

Rec = oil recovery, %OOIP

r_w = wellbore radius, ft.

r_{wD} = the dimensionless wellbore radius

r'_w = effective wellbore radius, ft

$(S_{ch})_c$ = choke skin effect

S_o = oil saturation, fraction

S_{o1} = oil saturation in the matrix, fraction

S_{o2} = oil saturation in the fracture, fraction

S_{oir} = residual oil saturation, fraction

S_w = water saturation, fraction

S_{w1} = water saturation in the matrix, fraction

S_{w2}	= water saturation in the fracture, fraction
S_{wc}	= connate water saturation, fraction
t	= time
t_{BT}	= breakthrough time
t_D	= dimensionless time
$(t_D)_m$	= dimensionless time of the model
$(t_D)_p$	= dimensionless time of the prototype
t_{DBT}	= dimensionless breakthrough time.
t_m	= time of the model.
t_p	= time of the prototype.
u_m	= fluid velocity in the model
u_p	= fluid velocity in the prototype
UHW	= unfractured horizontal well,
UVW	= unfractured vertical well,
W_D	= dimensionless position of the horizontal well
w_f	= fracture width, ft
WC	= produced water cut, %
W_m	= width of the model
WOC	= water oil contact
W_p	= cumulative water produced in cc
W_p	= width of the prototype
x	= distance in the x-direction
X_A	= Location of a constant pressure boundary, ft,

x_D	= dimensionless distance in the x-direction
X_e	= Location of an actual no flow boundary, ft,
X_e	= half well spacing, ft
x_f	= fracture half length, ft
x_w	= location of the horizontal well in the x-direction
x_{wD}	= dimensionless position in the x-direction
y	= distance in the y-direction
y_D	= dimensionless distance in the y-direction
Y_s	= distance of the summit of the water crest to the top of the reservoir ft.
y_w	= location of the horizontal well in the y-direction
y_{wD}	= dimensionless position in the y-direction
z	= distance in the z-direction
z_D	= dimensionless distance in the z-direction
z_r	= reference elevation in the z-direction
z_w	= location of the horizontal well in the z-direction
z_{wD}	= dimensionless position in the z-direction
Z_w	= vertical distance of horizontal well from oil water contact at time = 0, ft
Z_{wD}	= dimensionless vertical distance

Greek Symbols

β	$= A/L^2$
β	= anisotropic parameter

$$\nabla = i\frac{\partial}{\partial x} + j\frac{\partial}{\partial y} + k\frac{\partial}{\partial z}$$

330

Appendix A
DIMENSIONAL ANALYSIS

A.1 SCALED MODEL CONCEPTS

Physically-scaled laboratory models have been used to simulate the flow of fluids through tubular goods and porous media. In reservoir engineering, this concept is used to simulate the reservoir performance when the laboratory experiment is well designed and carried out in a prescribed manner [103].

The purpose of this Appendix is to derive the scaling requirements for an immiscible displacement process of oil by water in a porous media, highly conductive fracture and perforated interval using 3-dimensional laboratory model with horizontal well.

A.1.1 Scaling Theory, Principles and Procedure

The performance of oil reservoirs is governed by the values of a number of variables which can be combined into dimensionless groups. To represent a reservoir by a scaled laboratory model, these dimensionless groups must be the same in both the reservoir and the laboratory model [18,19,21,104-108,111]. The objective is to be able to predict the behavior of the prototype from the experiments performed on a model which represents

- 229 -

the prototype. In the theory of fluid flow through porous media, sand box models are the equivalent of the hydraulic models in which we recognize the concepts of geometric, kinematic and dynamic similarities.

A.1.1.1 Geometric Similarity

Geometric similarity implies that the ratios between all corresponding lengths in the two considered systems must be the same. For the case under study, these ratios are written as:

$$\frac{L_m}{W_m} = \frac{L_p}{W_p} \tag{A.1}$$

$$\frac{L_m}{h_m} = \frac{L_p}{h_p} \tag{A.2}$$

$$\frac{L_m}{L_p} = \frac{h_m}{h_p} = \frac{W_m}{W_p} \tag{A.3}$$

where L, W and h represent the length, width and thickness (height) of the model or the prototype. The subscripts m and p are assigned for the model and the prototype, respectively.

A.1.1.2 Kinematic Similarity

Kinematic similarity means similarity of the flow nets composed of streamlines and equipotential lines, i.e; the two sets of flow lines are geometrically similar. The kinematic similarity implies that the direction of the veloc-

ity remains unchanged and the ratio between velocities (and accelerations) at all homologous points in the two systems is the same throughout the domain, or:

$$\frac{u_p}{u_m} = constant$$

Where u is the velocity.

A.1.1.3 Dynamic Similarity

Dynamic similarity means that forces at homologous points and homologous times acting on homologous elements of fluid mass must be in the same ratio throughout the two systems. Forces here are those of gravity, pressure, friction (or viscosity) and capillary.

A.2 FLOW OF FLUIDS THROUGH POROUS MEDIA

A.2.1 Equations of Flow

Oil phase:

$$\nabla \left(\frac{\rho_o^2 k_o}{\mu_o} \nabla \Phi_o \right) = \frac{\partial}{\partial t} (\rho_o S_o \varphi) \tag{A.4}$$

Water phase:

$$\nabla \left(\frac{\rho_w^2 k_w}{\mu_w} V \Phi_w \right) = \frac{\partial}{\partial t}(\rho_w S_w \varphi) \tag{A.5}$$

Where for oil:

$$\Phi_o = \int_{P_{or}}^{P_o} \frac{\partial P_o}{P_o} + g(Z - Z_r) \tag{A.6}$$

And for water:

$$\Phi_w = \int_{P_{wr}}^{P_w} \frac{\partial P_w}{P_w} + g(Z - Z_r) \tag{A.7}$$

Where:

Φ_o = oil phase potential,

Φ_w = water phase potential,

k_o = oil phase effective permeability,

k_w = water phase effective permeability,

μ_o = oil viscosity,

μ_w = water viscosity,

S_o = oil saturation,

S_w = water saturation,

ρ_o = oil density,

ρ_w = water density,

P_o = pressure in the oil phase,

P_w = pressure in the water phase,

φ = porosity,

Z = elevation in the z-direction,

Z_r = reference elevation in the z-direction, and:

$$\nabla = i\frac{\partial}{\partial x} + j\frac{\partial}{\partial y} + k\frac{\partial}{\partial z} \tag{A.8}$$

Oil and water phase pressures are assumed to be related through the capillary-pressure/saturation curves:

$$P_c = P_o - P_w = P_c(S_w) \tag{A.9}$$

It is assumed that the process is isothermal, therefore, the energy equation is dropped.

A.2.2 Expressing the Flow Equations in Non-Dimensional Units

In order to recognize the scaling parameters, equations (A.4), (A.5) and (A.9) are written in dimensionless forms.

Dimensionless independent variables are:

$$x_D = x/L \tag{A.10}$$

$$y_D = y/L \tag{A.11}$$

$$z_D = z/h \tag{A.12}$$

$$t_D = \frac{qt}{WhL\varphi} = \frac{ut}{h\varphi} \tag{A.13}$$

Dimensionless dependent variables:

$$P_D = \frac{P}{q\mu_o/k_z h} \tag{A.14}$$

Where

L = length in the x − direction.

W = length in the y − direction.

h = thickness in the z − direction.

q = volumetric injection rate.

t = time.

The subscript D denotes dimensionless variables.

Saturations and relative permeabilities are dimensionless.

Details of Conversion of partial differential equations (A.4), (A.5), and (A.9) into dimensionless forms by using equations (A.10) through (A.14) is illustrated as follows:

Substitution of P for the potential (Φ) in eqns. (A.4) and (A.5) and using chain rule, we may write, in general, for x-component;

$$\frac{\partial}{\partial x}\left(\frac{\rho k_x}{\mu}\frac{\partial P}{\partial x}\right) = \frac{\partial}{\partial x_D}\left(\frac{\rho k_x}{\mu}\frac{\partial P_D}{\partial x_D}\frac{\partial P}{\partial P_D}\frac{\partial x_D}{\partial x}\right)\frac{\partial x_D}{\partial x} \qquad (A.15)$$

Where, from eqns. (A.10) and (A.14), we may write:

$$\frac{\partial x_D}{\partial x} = \frac{1}{L}, and; \qquad (A.16)$$

$$\frac{\partial P}{\partial P_D} = \frac{q\mu}{k_z h} \qquad (A.18)$$

$$k_{r_i} = \frac{k_i}{k} \qquad (A.19)$$

Where the subscript i is assigned for either oil or water.

Substitution of equations (A.16) through (A.19) into equation (A.15) gives:

$$\frac{\partial}{\partial x}\left(\frac{\rho k_x}{\mu}\frac{\partial P}{\partial x}\right) = \frac{\rho q}{L^2 h}\left(\frac{k_x}{k_z}\right)\frac{\partial}{\partial x_D}\left(k_{ri}\frac{\partial P_D}{\partial x_D}\right) \qquad (A.20)$$

The y-component is;

$$\frac{\partial}{\partial y}\left(\frac{\rho k_y}{\mu}\frac{\partial P}{\partial y}\right) = \frac{\rho q}{W^2 h}\left(\frac{k_y}{k_z}\right)\frac{\partial}{\partial y_D}\left(k_{ri}\frac{\partial P_D}{\partial y_D}\right) \qquad (A.21)$$

The z-component is;

$$\frac{\partial}{\partial z}\left(\frac{\rho k_z}{\mu}\left(\frac{\partial P}{\partial z} + \rho g\right)\right) = \frac{\rho q}{h^3}\frac{\partial}{\partial z_D}(k_{ri}\frac{\partial p_D}{\partial z_D}) + \frac{\rho^2 g k_z}{\mu h}\frac{\partial k_{ri}}{\partial z_D}$$

(A.22)

And finally the t-component may be written as;

$$\frac{\partial}{\partial t}(\rho\varphi S) = \frac{\rho q}{WhL}\frac{\partial S}{\partial t_D}$$

(A.23)

Substitution of equations (A.20) through (A.23) into equation (A.4) and (A.5) and using the subscripts o and w for oil and water, respectively, we obtain the following equations:

For oil phase:

$$\frac{P_o q}{L^2 h}\left(\frac{k_x}{k_z}\right)\frac{\partial}{\partial x_D}(k_{ro}\frac{\partial p_{oD}}{\partial x_D}) + \frac{P_o q}{W^2 h}\left(\frac{k_y}{k_z}\right)\frac{\partial}{\partial y_D}(k_{ro}\frac{\partial p_{oD}}{\partial y_D})$$

$$+ \frac{P_o q}{h^3}\frac{\partial}{\partial z_D}(k_{ro}\frac{\partial p_{oD}}{\partial z_D}) + \frac{P_o^2 g k_z}{\mu_o h}\left(\frac{\partial k_{ro}}{\partial z_D}\right)$$

$$= \frac{q P_o}{WhL}\frac{\partial S_o}{\partial t_D}$$

(A.24)

330

237

Division of both sides of equation (A.24) by $\dfrac{\rho_o q}{h^3}$ gives:

$$(\frac{h}{L})^2(\frac{k_x}{k_z}) \frac{\partial}{\partial x_D}(k_{ro}\frac{\partial p_{oD}}{\partial x_D}) + (\frac{h}{W})^2(\frac{k_y}{k_z}) \frac{\partial}{\partial y_D}(k_{ro}\frac{\partial p_{oD}}{\partial y_D})$$

$$+ \frac{\partial}{\partial z_D}(k_{ro}\frac{\partial p_{oD}}{\partial z_D}) + \frac{\rho_o g k_z h^2}{q\mu_o} \frac{\partial k_{ro}}{\partial z_D}$$

$$= \frac{h^2}{WL}\frac{\partial S_o}{\partial t_D} \tag{A.25}$$

For water phase:

$$(\frac{h}{L})^2(\frac{k_x}{k_z}) \frac{\partial}{\partial x_D}(k_{rw}\frac{\partial p_{wD}}{\partial x_D}) + (\frac{h}{W})^2(\frac{k_y}{k_z}) \frac{\partial}{\partial y_D}(k_{rw}\frac{\partial p_{wD}}{\partial y_D})$$

$$+ \frac{\partial}{\partial z_D}(k_{rw}\frac{\partial p_{wD}}{\partial z_D}) + \frac{\rho_w g k_z h^2}{q\mu_o} \frac{\partial k_{rw}}{\partial z_D}$$

$$= \frac{\mu_w}{\mu_o}\frac{h^2}{WL}\frac{\partial S_w}{\partial t_D} \tag{A.26}$$

A.2.3 Dimensionless Capillary Pressure

Leverrtt [109] derived the equations representing the capillary pressure between two immiscible fluids. The function $J(S_w)$ is frequently used in the literature to remove discrepancies in the P_c versus S_w curves and to reduce them to a common curve [119]

$$J(S_w) = \frac{P_c \sqrt{k/\varphi}}{\sigma \cos\theta}$$

(A.27)

Dimensionless form of capillary pressure is:

$$P_{cD} = P_{oD} - P_{wD} = \frac{\sigma h \cos\theta \sqrt{k_z \varphi}}{q\mu_o}$$

(A.28)

A.2.4 Dimensionless Saturation

Oil and water saturations in eqn.(A.29) are dimensionless.

$$S_o + S_w = 1$$

(A.29)

If capillary forces are neglected, then $P_c = 0$, and:

$$P_{oD} = P_{wD} = P_D$$

(A.30)

A.2.5 Scaling Parameters

In order to scale a reservoir to a model, the dimensionless parameters $x_D, y_D, z_D, t_D, P_{oD}$, and P_{wD}, should be equal in both model and prototype. Mathematically the dimensionless variables in equations (A.25), (A.26), and (A.28) must be equal in the model and prototype ,or:

$$\left[(\frac{h}{L})^2 (\frac{k_x}{k_z}) \right]_m = \left[(\frac{h}{L})^2 (\frac{k_x}{k_z}) \right]_p \qquad (A.31)$$

$$\left[(\frac{h}{W})^2 (\frac{k_y}{k_z}) \right]_m = \left[(\frac{h}{W})^2 (\frac{k_y}{k_z}) \right]_p \qquad (A.32)$$

$$\left[\frac{h^2}{WL} \right]_m = \left[\frac{h^2}{WL} \right]_p \qquad (A.33)$$

$$\left[\frac{\rho_o g k_z h^2}{q \mu_o} \right]_m = \left[\frac{\rho_o g k_z h^2}{q \mu_o} \right]_p \qquad (A.34)$$

$$\left[(\frac{\rho_w g k_z h^2}{q \mu_o} \right]_m = \left[(\frac{\rho_w g k_z h^2}{q \mu_o} \right]_p \qquad (A.35)$$

$$(\frac{\mu_w}{\mu_o})_m = (\frac{\mu_w}{\mu_o})_p ; \qquad (A.36)$$

Also;

$$(\frac{h^2}{WL} \frac{\mu_w}{\mu_o})_m = (\frac{h^2}{WL} \frac{\mu_w}{\mu_o})_p ; \qquad (A.37)$$

$$\left[\frac{\sigma h cos\theta \sqrt{k_z \varphi}}{q \mu_o} \right]_m = \left[\frac{\sigma h cos\theta \sqrt{k_z \varphi}}{q \mu_o} \right]_p \qquad (A.38)$$

$$(k_{rw}(S_w))_m = (k_{rw}(S_w))_p \quad ; and; \qquad (A.39)$$

$$(k_{ro}(S_w))_m = (k_{ro}(S_w))_p \tag{A.40}$$

Equations (A.34) and (A.35) may be combined to give:

$$\left[\frac{\Delta \rho g k_z h^2}{q \mu_o} \right]_m = \left[\frac{\Delta \rho g k_z h^2}{q \mu_o} \right]_p \tag{A.41}$$

If, in addition, the initial and boundary conditions are written in dimensionless forms and are equal in both the model and prototype, then the two systems are mathematically identical, that is:

$$(P_{oD}(x_D,y_D,z_D,t_D))_m = (P_{oD}(x_D,y_D,z_D,t_D))_p \tag{A.42}$$

$$(P_{wD}(x_D,y_D,z_D,t_D))_m = (P_{wD}(x_D,y_D,z_D,t_D))_p , \text{ and;} \tag{A.43}$$

$$(P_D(x_D,y_D,z_D,t_D))_m = (P_D(x_D,y_D,z_D,t_D))_p \tag{A.44}$$

Such systems are said to be "dynamically similar" [110].

Scaling of the Present Case

In order to solve equations (A.31), (A.32), (A.36), (A.38), (A.39), (A.40) and (A.41), we have to make some reasonable assumptions. Assume the porous medium is homogeneous and isotropic. Moreover, the rock type and pore

structure are considered identical so that wettability, relative permeability, and capillary pressure curves coincide for model and prototype, mathematically;

$$\varphi = constant. \tag{A.45}$$

$$k_x = k_y = k_z = k \tag{A.46}$$

$$(\sigma\cos\theta)_m = (\sigma\cos\theta)_p \tag{A.47}$$

We will be left with the following equations:

$$\left((\frac{h}{L})^2 \right)_m = \left((\frac{h}{L})^2 \right)_p ; \tag{A.48}$$

$$\left((\frac{h}{W})^2 \right)_m = \left((\frac{h}{W})^2 \right)_p ; \tag{A.49}$$

$$(\frac{\mu_w}{\mu_o})_m = (\frac{\mu_w}{\mu_o})_p ; \tag{A.50}$$

$$\left[\frac{h\sqrt{k\varphi}}{q\mu_o} \right]_m = \left[\frac{h\sqrt{k\varphi}}{q\mu_o} \right]_p \tag{A.51}$$

And finally;

$$\left[\frac{\Delta\rho g k h^2}{q\mu_o} \right]_m = \left[\frac{\Delta\rho g k h^2}{q\mu_o} \right]_p \tag{A.52}$$

Equations (A.48) and (A.49) represent the geometric scaling parameters and eqn. (A.50) represent the viscosity ratios. Equations (A.51) and (A.52) represent rock and fluid properties in terms of capillary to viscous forces and gravity to viscous forces, respectively. In order to keep the model and reservoir in dynamic similarity, these equations are solved for the unknowns parameters.

Equations (A.51) and (A.52) may be combined to give;

$$\frac{k_p}{k_m} = (\frac{h_m}{h_p})^2 (\frac{\varphi_p}{\varphi_m}) (\frac{\Delta p_m}{\Delta p_p})^2 \qquad . \qquad \text{(A.53)}$$

Equations (A.51), (A.53) may be combined to give the relation between the prototype nad the model rates as:

$$\frac{q_p}{q_m} = (\frac{(\mu_o)_m}{(\mu_o)_p})(\frac{\Delta p_m}{\Delta p_p})(\frac{\varphi_p}{\varphi_m}) \qquad \text{(A.54)}$$

From equations (A.13), (A.14) and the following two relations;

$$(t_D)_m = (t_D)_p \, and; \qquad \text{(A.55)}$$

$$(P_D)_m = (P_D)_p \qquad \text{(A.56)}$$

and using eqns (A.54) and (A.55) we may write the relations between the real time of the prototype to that of the model as follows:

$$\frac{t_p}{t_m} = (\frac{(\mu_o)_p}{(\mu_o)_m})(\frac{\Delta p_p}{\Delta p_m})(\frac{(WLh)_p}{(WLh)_m})$$

(A.57)

Where;

$(WLh)_p$ = reservoir bulk volume

(A.58)

Similar equation may be written for the pressure drops after using equations (A.14), (A.53), (A.54) and (A.56) as:

$$\frac{\Delta P_p}{\Delta P_m} = (\frac{g_p}{g_m})(\frac{\Delta p_p}{\Delta p_m})(\frac{h_m L_p^2}{h_p L_m^2})$$

(A.59)

If equations (A.53) through (A.59) are satisfied, the two systems would be dynamically similar.

Scaling Procedures:

1. A ratio R may be defined as: $R = \dfrac{L_p}{L_m} = \dfrac{W_p}{W_m} = \dfrac{h_p}{h_m}$.

2. This ratio R is taken as 75 in this study.

3. Equations. (A.53) through (A.59) may be used to calculate the prototype to the model parameters. Either the prototype or model parameters should be known. In this study, a laboratory physical model is

scaled to the prototype (field). it is assumed that the model and pro-

totype have the same fluid properties. Scaled parameters can be

found in table A.1.

TABLE A.1: Model and Prototype Scaling Parameters

Parameter	reservoir	model
Area, sq. ft	8,437.50	1.500
Length, ft	112.50	1.500
Width, ft	75.00	1.000
Thickness, ft	37.50	0.500
Porosity, %	10.00	36.200
Permeability, md	19.64	400,000
Oil viscosity, cp	2.03	2.030
Oil density, lb/cu.ft	50.86	50.860
Water viscosity, cp	1.08	1.080
Water density, lb/cu.ft	63.40	63.400
Maximum pressure drop, psi:		
Horizontal well	30.00	0.400
Vertical well	41.50	0.550

A.3   SCALING CRITERIA OF THE FRACTURE(s)

In order to keep dynamic similarity of the fluid flow through the fracture(s) in both the model and prototype, the dimensionless fracture conductivity (F_{CD}) should be similar, or from the definition of (F_{CD}) in equation (2.20);

$$(F_{CD})_m = (F_{CD})_p , \text{ or;} \tag{A.60}$$

$$(\frac{k_f w_f}{k z_f})_m = (\frac{k_f w_f}{k z_f})_p \tag{A.61}$$

Where

F_{CD} = dimensionless fracture conductivity

k_f = fracture permeability

w_f = fracture width

k = porous medium permeability, and;

z_f = fracture half length .

Close examination of eqn. (2.20) shows that (F_{CD}) is a function of the fracture permeability, width, and depth as well as the formation permeability, or;

$$F_{CD} = f(k_f, k, w_f, x_f) \tag{A.62}$$

As mentioned earlier, the fracture conductivity is considered to be infinite. F_{CD} may be taken as 400 or more [3,48]. It is kept 400 in this study.

Reference [35] presented the following equation for the conductivity of a rectangular fracture;

$$k_f = 54^*10^6 \, w_f^2 \qquad\qquad\qquad (A.63)$$

Where;

k_f = fracture permeability, darcies, and

w_f = the fracture width, inches.

Combining eqns. (A.60), (A.61) and (A.63) gives;

$$w_f^3 = \frac{F_{CD} \, k \, z_f}{54^*10^6} \qquad\qquad (A.64)$$

Eqn. (A.64) may be applied for both the model and prototype. Knowing k and F_{CD}, we may estimate w_f assuming values of the fracture depth, z_f. See table A.2 for scaled parameters of the fracture(s).

TABLE A.2: Model and Prototype Fracture Scaled Parameters

	Model				Prototype			
FCD	k darcy	Zf in.	W in.	kf 10^6 D	k md	Zf ft.	W in.	kf darcy
400	400	1.0	0.1417	1.085	19.64	6.25	0.0222	26568
400	400	2.0	0.1810	1.770	19.64	12.50	0.0280	42169
400	400	3.0	0.2100	2.320	19.64	18.75	0.0320	55257

A.4 SCALING OF THE PERFORATED INTERVAL

In order to keep the stream and potential lines similar, the dimensionless perforated interval length (L_{pD}) and position (x_{wD}, y_{wD}, z_{wD}) in both the model and prototype should be similar. In other words, the following equations should be preserved;

$$(L_{pD})_m = (L_{pD})_p. \tag{A.65}$$

$$\left[W_D(x_{wD}, y_{wD}, z_{wD}) \right]_m = \left[W_D(x_{wD}, y_{wD}, z_{wD}) \right]_p \tag{A.66}$$

Where;

$$L_{pD} = \frac{L_p}{L_w}$$

L_{pD} = the dimensionless perforated interval.

L_p = the perforated length, and;

L_w = the horizontal wellbore length.

W_D = dimensionless wellbore position

$$x_{wD} = \frac{x_w}{W}$$

$$y_{wD} = \frac{y_w \pm L_w/2}{L}$$

$$x_{wD} = \frac{z_w}{h}$$

L = length of the reservoir or model in the y-direction

W = width of the reservoir or model in the x-direction

h = thickness of the reservoir or model in the z-direction

(x_w, y_w, z_w) = location of the horizontal well.

Appendix B
PHYSICAL PROPERTIES OF FLUIDS
AND POROUS MEDIA

B.1 FLUIDS

The properties of oil and water, such as viscosity and density were measured using a viscometer and a hydrometer. The viscosities are 2.03 and 1.08 cp for oil and water, respectively. The densities are 0.815 and 1.016 g/cc for oil and water, respectively.

B.2 POROUS MEDIA

Porosity and permeability are selected based on scaling studies.

The porosity measurements of the pack was based on volumetric method which involves the measurements of both bulk and pore volume. The former was determined by measuring the volume of liquid. the model can hold without porous media. The pore volume can be determined by measuring the liquid volume the model can hold when it is packed.

The measurements of permeability was based on Darcy's law. The absolute permeability was measured at 100% water saturation.

Relative permeability of oil at connate water (effective permeability to oil) and relative permeability of water at residual oil saturation (effective permeability to water) were measured.

Porosity, absolute permeability and relative permeabilities at initial water saturation and residual oil saturation were measured using a linear cylindrical cell. This cell is 15.75 inches (40 cm) long and 1.54 inches (3.9 cm) inner diameter. Water manometer was used to achieve good accuracy in measuring the differential pressure through the pack. In all measurements the cell was kept in the vertical position.

B.3   MEASUREMENTS OF THE PHYSICAL PROPERTIES

B.3.1   Procedures

1. Air is evacuated from the pack for several hours until the vacuum pump pressure reads 2 mm Hg or 0.039 psig.

2. Water is injected from the bottom to saturate the pack. Injection is continued until steady state condition is reached. Fluid properties, flow rate and measured pressure drop are substituted in Darcy's Law. Absolute permeability is then calculated.

3. Kerosene is then injected at the top of the cell. Water and kerosene are produced at the bottom. Injection is continued until no more water is produced. Initial (connate) water saturation of 16.5% is calculated by balancing the volume of water injected to the volume of water produced.

Material balance is also applied on the oil phase to estimate the initial oil saturation. The sum of the initial oil and water saturations should be one, or:

$$S_{wi} + S_{oi} = 1.0 \qquad \text{(B.1)}$$

Where:

S_{wi} = initial water phase saturation, and;

S_{oi} = initial oil phase saturation.

4. Water is reinjected at the bottom until no oil is produced with water at the top. Residual oil saturation (S_{or}), effective and relative water permeabilities are calculated at S_{or}.

Following is a list of the measured properties using the linear model:

porosity	= 36.2 %
Initial water saturation	= 16.5 %
Residual oil saturation	= 9.83 %
Absolute permeability	= 400 darcies
Effective oil permeability at S_{wi}	= 135 darcies
Effective water permeability at S_{or}	= 284 darcies

Appendix C
EXPERIMENTAL DATA

In this appendix, the experimental data and results are presented. In this appendix the following abbreviations are used:

ΔN_p = incremental oil produced, cc

N_p = cumulative oil produced, cc

ΔW_p = incremental water produced, cc

W_p = cumulative water produced, cc

Rec. = oil recovery, %OOIP

PV_i = pore volume of water injected, cc

W.C. = produced water cut, %

P_{inj} = pressure drop, psig

TABLE C-1:   RUN # HW-04

Porosity	=	36.11	%	OOIP	=	5181.99	cc
Swi	=	30.78	%	Soi	=	69.22	%
Sor	=	23.24	%				

Observed and Calculated Results

Time (min)	ΔNp (cc)	Np (cc)	ΔNp+ΔWp (cc)	Np+Wp (cc)	PVi (PV)	Rec. (%OOIP)	W.C. (%)	Pinj (psig)
(1)	(2)	(3)	(4)	(5)	(6)	(7)	(8)	(9)
2.4	100.0	100.0	100.0	100.0	0.01	1.93	0.00	0.2650
4.9	100.0	200.0	100.0	200.0	0.03	3.86	0.00	0.2580
7.3	100.0	300.0	100.0	300.0	0.04	5.79	0.00	0.2560
9.8	100.0	400.0	100.0	400.0	0.05	7.72	0.00	0.2560
12.3	100.0	500.0	100.0	500.0	0.07	9.65	0.00	0.2570
14.8	100.0	600.0	100.0	600.0	0.08	11.58	0.00	0.2590
17.3	100.0	700.0	100.0	700.0	0.09	13.51	0.00	0.2600
19.8	100.0	800.0	100.0	800.0	0.11	15.44	0.00	0.2615
22.3	100.0	900.0	100.0	900.0	0.12	17.37	0.00	0.2625
24.8	100.0	1000.0	100.0	1000.0	0.13	19.30	0.00	0.2630
27.3	100.0	1100.0	100.0	1100.0	0.15	21.23	0.00	0.2660
29.7	100.0	1200.0	100.0	1200.0	0.16	23.16	0.00	0.2680
32.2	100.0	1300.0	100.0	1300.0	0.17	25.09	0.00	0.2720
34.7	100.0	1400.0	100.0	1400.0	0.19	27.02	0.00	0.2745
37.1	100.0	1500.0	100.0	1500.0	0.20	28.95	0.00	0.2770
39.6	100.0	1600.0	100.0	1600.0	0.21	30.88	0.00	0.2800
42.0	100.0	1700.0	100.0	1700.0	0.23	32.81	0.00	0.2823
44.5	100.0	1800.0	100.0	1800.0	0.24	34.74	0.00	0.2845
47.0	100.0	1900.0	100.0	1900.0	0.25	36.67	0.00	0.2872
49.4	100.0	2000.0	100.0	2000.0	0.27	38.60	0.00	0.2900
51.8	100.0	2100.0	100.0	2100.0	0.28	40.52	0.00	0.2920
54.3	100.0	2200.0	100.0	2200.0	0.29	42.45	0.00	0.2935
56.9	100.0	2300.0	100.0	2300.0	0.31	44.38	0.00	0.2940
59.4	100.0	2400.0	100.0	2400.0	0.32	46.31	0.00	0.2950
61.9	100.0	2500.0	100.0	2500.0	0.33	48.24	0.00	0.2960
64.4	100.0	2600.0	100.0	2600.0	0.35	50.17	0.00	0.2960
66.9	100.0	2700.0	100.0	2700.0	0.36	52.10	0.00	0.2970
69.4	100.0	2800.0	100.0	2800.0	0.37	54.03	0.00	0.2985
71.9	100.0	2900.0	100.0	2900.0	0.39	55.96	0.00	0.3030
74.4	99.8	2999.8	100.0	3000.0	0.40	57.89	0.20	0.3075
76.9	82.0	3081.8	100.0	3100.0	0.41	59.47	18.00	0.3450
79.4	56.0	3137.8	100.0	3200.0	0.43	60.55	44.00	0.3650
82.0	39.5	3177.3	102.5	3302.5	0.44	61.31	61.46	0.3780
84.5	31.0	3208.3	101.0	3403.5	0.45	61.91	69.31	0.3900
87.1	26.0	3234.3	100.0	3503.5	0.47	62.41	74.00	0.3920
89.6	20.0	3254.3	100.0	3603.5	0.48	62.80	80.00	0.3950

TABLE C-1: (Continued)

Observed and Calculated Results

Time (min)	ΔNp (cc)	Np (cc)	ΔNp+ΔWp (cc)	Np+Wp (cc)	PVi (PV)	Rec. (%OOIP)	W.C. (%)	Pinj (psig)
(1)	(2)	(3)	(4)	(5)	(6)	(7)	(8)	(9)
92.1	15.0	3269.3	100.0	3703.5	0.49	63.09	85.00	0.3880
94.6	13.0	3282.3	101.0	3804.5	0.51	63.34	87.13	0.3730
100.8	22.0	3304.3	250.0	4054.5	0.54	63.76	91.20	0.3200
107.1	16.0	3320.3	250.0	4304.5	0.57	64.07	93.60	0.3175
113.4	16.0	3336.3	252.0	4556.5	0.61	64.38	93.65	0.3175
119.7	12.5	3348.8	254.0	4810.5	0.64	64.62	95.08	0.3160
125.9	11.0	3359.8	248.0	5058.5	0.68	64.84	95.56	0.3160
132.1	8.5	3368.3	250.0	5308.5	0.71	65.00	96.60	0.3150
138.4	10.0	3378.3	250.0	5558.5	0.74	65.19	96.00	0.3100
144.6	6.0	3384.3	250.0	5808.5	0.78	65.31	97.60	0.3060
151.5	8.0	3392.3	273.5	6082.0	0.81	65.46	97.07	0.3100
157.8	8.0	3400.3	253.0	6335.0	0.85	65.62	96.84	0.3090
164.1	6.0	3406.3	250.0	6585.0	0.88	65.73	97.60	0.3020
170.3	4.0	3410.3	250.0	6835.0	0.91	65.81	98.40	0.3000
176.6	4.0	3414.3	250.0	7085.0	0.95	65.89	98.40	0.3020
183.0	4.0	3418.3	251.0	7336.0	0.98	65.96	98.41	0.3050
189.3	4.5	3422.8	253.0	7589.0	1.01	66.05	98.22	0.3055
196.6	3.0	3425.8	293.0	7882.0	1.05	66.11	98.98	0.3060
202.9	3.5	3429.3	252.0	8134.0	1.09	66.18	98.61	0.3050
209.2	3.0	3432.3	253.0	8387.0	1.12	66.24	98.81	0.3070
234.4	10.0	3442.3	1000.0	9387.0	1.25	66.43	99.00	0.3060

TABLE C-2:   RUN # HW-05

Porosity	=	36.03	%	OOIP	=	4929.60	cc
Swi	=	34.00	%	Soi	=	65.99	%
Sor	=	23.92	%				

Observed and Calculated Results

Time (min)	ΔNp (cc)	Np (cc)	ΔNp+ΔWp (cc)	Np+Wp (cc)	PVi (PV)	Rec. (%OOIP)	W.C. (%)	Pinj (psig)
(1)	(2)	(3)	(4)	(5)	(6)	(7)	(8)	(9)
2.8	100.0	100.0	100.0	100.0	0.01	2.03	0.00	0.2800
5.3	100.0	200.0	100.0	200.0	0.03	4.06	0.00	0.2850
7.8	100.0	300.0	100.0	300.0	0.04	6.09	0.00	0.2850
10.4	100.0	400.0	100.0	400.0	0.05	8.11	0.00	0.2860
12.9	100.0	500.0	100.0	500.0	0.07	10.14	0.00	0.2870
15.5	100.0	600.0	100.0	600.0	0.08	12.17	0.00	0.2900
18.0	100.0	700.0	100.0	700.0	0.09	14.20	0.00	0.2920
20.5	100.0	800.0	100.0	800.0	0.11	16.23	0.00	0.2935
23.0	100.0	900.0	100.0	900.0	0.12	18.26	0.00	0.2960
25.5	100.0	1000.0	100.0	1000.0	0.13	20.29	0.00	0.3000
28.0	100.0	1100.0	100.0	1100.0	0.15	22.31	0.00	0.3025
30.5	100.0	1200.0	100.0	1200.0	0.16	24.34	0.00	0.3045
32.9	100.0	1300.0	100.0	1300.0	0.17	26.37	0.00	0.3170
35.5	100.0	1400.0	100.0	1400.0	0.19	28.40	0.00	0.3250
38.0	100.0	1500.0	100.0	1500.0	0.20	30.43	0.00	0.3320
40.5	100.0	1600.0	100.0	1600.0	0.21	32.46	0.00	0.3370
43.0	100.0	1700.0	100.0	1700.0	0.23	34.49	0.00	0.3420
45.6	100.0	1800.0	100.0	1800.0	0.24	36.51	0.00	0.3460
48.1	100.0	1900.0	100.0	1900.0	0.25	38.54	0.00	0.3490
49.0	35.0	1935.0	35.0	1935.0	0.26	39.25	0.00	0.3530
51.1	95.0	2030.0	100.0	2035.0	0.27	41.18	5.00	0.3630
53.6	92.0	2122.0	100.0	2135.0	0.29	43.05	8.00	0.3680
56.1	90.0	2212.0	101.0	2236.0	0.30	44.87	10.89	0.3720
58.6	89.0	2301.0	101.0	2337.0	0.31	46.68	11.88	0.3750
61.1	87.0	2388.0	101.0	2438.0	0.33	48.44	13.86	0.3765
63.6	84.0	2472.0	100.0	2538.0	0.34	50.15	16.00	0.3769
66.0	81.0	2553.0	101.0	2639.0	0.35	51.79	19.80	0.3830
68.5	75.0	2628.0	100.0	2739.0	0.37	53.31	25.00	0.3865
71.0	70.0	2698.0	100.0	2839.0	0.38	54.73	30.00	0.3920
73.4	62.0	2760.0	101.0	2940.0	0.39	55.99	38.61	0.3970
75.9	55.0	2815.0	103.0	3043.0	0.41	57.10	46.60	0.4000
78.5	51.0	2866.0	104.0	3147.0	0.42	58.14	50.96	0.4020
80.9	46.0	2912.0	101.0	3248.0	0.43	59.07	54.46	0.4060
87.1	86.0	2998.0	250.0	3498.0	0.47	60.82	65.60	0.4050
93.3	31.0	3029.0	250.0	3748.0	0.50	61.45	87.60	0.3550

258

TABLE C-2: (Continued)

Observed and Calculated Results

Time (min)	ΔNp (cc)	Np (cc)	ΔNp+ΔWp (cc)	Np+Wp (cc)	PVi (PV)	Rec. (%OOIP)	W.C. (%)	Pinj (psig)
(1)	(2)	(3)	(4)	(5)	(6)	(7)	(8)	(9)
99.5	6.0	3035.0	250.0	3998.0	0.54	61.57	97.60	0.3530
124.3	56.0	3091.0	1000.0	4998.0	0.67	62.70	94.40	0.3550
149.0	26.0	3117.0	1000.0	5998.0	0.80	63.23	97.40	0.3750
174.1	18.0	3135.0	1000.0	6998.0	0.94	63.60	98.20	0.3570
195.0	8.0	3143.0	835.0	7833.0	1.05	63.76	99.04	0.3750

TABLE C-3:   RUN # HW-06

Porosity =	36.19 %	OOIP	=	4748.00 cc
Swi =	36.72 %	Soi	=	63.28 %
Sor =	20.03 %			

Observed and Calculated Results

Time (min)	ΔNp (cc)	Np (cc)	$\Delta Np+\Delta Wp$ (cc)	Np+Wp (cc)	PVi (PV)	Rec. (%OOIP)	W.C. (%)	Pinj (psig)
(1)	(2)	(3)	(4)	(5)	(6)	(7)	(8)	(9)
2.8	100.0	100.0	100.0	100.0	0.01	2.11	0.00	0.4320
5.4	100.0	200.0	100.0	200.0	0.03	4.21	0.00	0.4320
7.9	100.0	300.0	100.0	300.0	0.04	6.32	0.00	0.4330
10.5	100.0	400.0	100.0	400.0	0.05	8.42	0.00	0.4335
13.0	100.0	500.0	100.0	500.0	0.07	10.53	0.00	0.4336
15.4	100.0	600.0	100.0	600.0	0.08	12.64	0.00	0.4338
18.1	100.0	700.0	100.0	700.0	0.09	14.74	0.00	0.4335
20.6	100.0	800.0	100.0	800.0	0.11	16.85	0.00	0.4335
23.2	100.0	900.0	100.0	900.0	0.12	18.96	0.00	0.4334
25.7	100.0	1000.0	100.0	1000.0	0.13	21.06	0.00	0.4349
28.0	91.8	1091.8	92.0	1092.0	0.15	22.99	0.22	0.4800
30.6	98.0	1189.8	99.0	1191.0	0.16	25.06	1.01	0.4900
33.1	99.0	1288.8	104.0	1295.0	0.17	27.14	4.81	0.5020
35.8	90.5	1379.3	100.0	1395.0	0.19	29.05	9.50	0.5030
38.1	86.0	1465.3	96.0	1491.0	0.20	30.86	10.42	0.5150
40.8	95.5	1560.8	107.0	1598.0	0.21	32.87	10.75	0.5190
43.5	85.0	1645.8	100.0	1698.0	0.23	34.66	15.00	0.5200
46.1	80.5	1726.3	99.0	1797.0	0.24	36.36	18.69	0.5280
48.6	75.5	1801.8	100.0	1897.0	0.25	37.95	24.50	0.5310
51.1	71.0	1872.8	99.0	1996.0	0.27	39.44	28.28	0.5330
53.8	68.0	1940.8	100.0	2096.0	0.28	40.88	32.00	0.5380
56.4	61.0	2001.8	103.0	2199.0	0.29	42.16	40.78	0.5340
59.0	57.0	2058.8	100.0	2299.0	0.31	43.36	43.00	0.5340
61.5	55.0	2113.8	99.0	2398.0	0.32	44.52	44.44	0.5360
64.1	57.5	2171.3	103.0	2501.0	0.33	45.73	44.17	0.5400
66.7	54.0	2225.3	100.0	2601.0	0.35	46.87	46.00	0.5400
69.3	52.5	2277.8	100.0	2701.0	0.36	47.97	47.50	0.5400
71.9	51.0	2328.8	100.0	2801.0	0.37	49.05	49.00	0.5330
78.4	122.0	2450.8	249.0	3050.0	0.41	51.62	51.00	0.5380
85.1	106.0	2556.8	253.0	3303.0	0.44	53.85	58.10	0.5330
91.7	81.0	2637.8	251.0	3554.0	0.47	55.56	67.73	0.5310
98.4	70.0	2707.8	251.0	3805.0	0.51	57.03	72.11	0.4210
105.3	61.5	2769.3	265.0	4070.0	0.54	58.33	76.79	0.4210
111.8	51.0	2820.3	250.0	4320.0	0.58	59.40	79.60	0.4260
118.3	42.0	2862.3	250.0	4570.0	0.61	60.28	83.20	0.4270

TABLE C-3: (Continued)

Observed and Calculated Results

Time (min)	ΔNp (cc)	Np (cc)	$\Delta Np+\Delta Wp$ (cc)	Np+Wp (cc)	PVi (PV)	Rec. (%OOIP)	W.C. (%)	Pinj (psig)
(1)	(2)	(3)	(4)	(5)	(6)	(7)	(8)	(9)
124.8	42.0	2904.3	252.0	4822.0	0.64	61.17	83.33	0.4300
131.3	37.0	2941.3	250.0	5072.0	0.68	61.95	85.20	0.4250
137.8	36.0	2977.3	251.0	5323.0	0.71	62.71	85.66	0.4300
144.3	32.0	3009.3	253.0	5576.0	0.74	63.38	87.35	0.4250
150.9	28.0	3037.3	252.0	5828.0	0.78	63.97	88.89	0.4240
157.3	21.0	3058.3	251.0	6079.0	0.81	64.41	91.63	0.4240
163.1	21.0	3079.3	251.0	6330.0	0.84	64.85	91.63	0.4270
170.1	20.0	3099.3	250.0	6580.0	0.88	65.28	92.00	0.4320
176.8	18.0	3117.3	259.0	6839.0	0.91	65.66	93.05	0.4300
183.2	17.0	3134.3	250.0	7089.0	0.94	66.01	93.20	0.4310
189.6	17.0	3151.3	252.0	7341.0	0.98	66.37	93.25	0.4250
196.0	16.5	3167.8	250.0	7591.0	1.01	66.72	93.40	0.4300
202.3	14.5	3182.3	250.0	7841.0	1.05	67.02	94.20	0.4300
208.9	12.5	3194.8	250.5	8091.5	1.08	67.29	95.01	0.4320
215.2	12.0	3206.8	250.0	8341.5	1.11	67.54	95.20	0.4320
221.6	9.0	3215.8	250.0	8591.5	1.15	67.73	96.40	0.4350
228.1	9.0	3224.8	251.0	8842.5	1.18	67.92	96.41	0.4350
234.6	4.0	3228.8	250.0	9092.5	1.21	68.00	98.40	0.4360
240.9	8.0	3236.8	248.0	9340.5	1.24	68.17	96.77	0.4370
247.7	8.0	3244.8	263.0	9603.5	1.28	68.34	96.96	0.4380

TABLE C-4:   RUN # HW-07

Porosity	=	36.08	%	OOIP	=	5080.00	cc
Swi	=	32.09	%	Soi	=	67.91	%
Sor	=	8.45	%				

Observed and Calculated Results

Time (min)	ΔNp (cc)	Np (cc)	ΔNp+ΔWp (cc)	Np+Wp (cc)	PVi (PV)	Rec. (%OOIP)	W.C. (%)	Pinj (psig)
(1)	(2)	(3)	(4)	(5)	(6)	(7)	(8)	(9)
2.5	100.0	100.0	100.0	100.0	0.01	1.97	0.00	0.2500
5.0	100.0	200.0	100.0	200.0	0.03	3.94	0.00	0.2500
7.6	100.0	300.0	100.0	300.0	0.04	5.91	0.00	0.2500
10.1	100.0	400.0	100.0	400.0	0.05	7.87	0.00	0.2520
12.6	100.0	500.0	100.0	500.0	0.07	9.84	0.00	0.2525
15.1	100.0	600.0	100.0	600.0	0.08	11.81	0.00	0.2530
17.5	100.0	700.0	100.0	700.0	0.09	13.78	0.00	0.2540
20.0	100.0	800.0	100.0	800.0	0.11	15.75	0.00	0.2545
22.5	100.0	900.0	100.0	900.0	0.12	17.72	0.00	0.2560
24.9	100.0	1000.0	100.0	1000.0	0.13	19.69	0.00	0.2565
27.4	100.0	1100.0	100.0	1100.0	0.15	21.65	0.00	0.2570
29.9	100.0	1200.0	100.0	1200.0	0.16	23.62	0.00	0.2580
32.4	100.0	1300.0	100.0	1300.0	0.17	25.59	0.00	0.2590
34.9	100.0	1400.0	100.0	1400.0	0.19	27.56	0.00	0.2600
37.5	100.0	1500.0	100.0	1500.0	0.20	29.53	0.00	0.2605
40.0	100.0	1600.0	100.0	1600.0	0.21	31.50	0.00	0.2615
42.5	100.0	1700.0	100.0	1700.0	0.23	33.46	0.00	0.2625
45.1	100.0	1800.0	100.0	1800.0	0.24	35.43	0.00	0.2640
47.6	100.0	1900.0	100.0	1900.0	0.25	37.40	0.00	0.2600
50.1	100.0	2000.0	100.0	2000.0	0.27	39.37	0.00	0.2670
52.7	100.0	2100.0	100.0	2100.0	0.28	41.34	0.00	0.2695
55.1	100.0	2200.0	100.0	2200.0	0.29	43.31	0.00	0.2710
57.6	100.0	2300.0	100.0	2300.0	0.31	45.28	0.00	0.2725
60.0	100.0	2400.0	100.0	2400.0	0.32	47.24	0.00	0.2735
62.6	100.0	2500.0	100.0	2500.0	0.33	49.21	0.00	0.2750
65.2	100.0	2600.0	100.0	2600.0	0.35	51.18	0.00	0.2785
67.7	100.0	2700.0	100.0	2700.0	0.36	53.15	0.00	0.2800
70.2	100.0	2800.0	100.0	2800.0	0.37	55.12	0.00	0.2820
72.8	100.0	2900.0	100.0	2900.0	0.39	57.09	0.00	0.2835
75.2	100.0	3000.0	100.0	3000.0	0.40	59.06	0.00	0.2850
80.1	200.0	3200.0	200.0	3200.0	0.43	62.99	0.00	0.2855
82.7	100.0	3300.0	100.0	3300.0	0.44	64.96	0.00	0.2860
85.3	100.0	3400.0	100.0	3400.0	0.45	66.93	0.00	0.2870
87.8	100.0	3500.0	100.0	3500.0	0.47	68.90	0.00	0.2890
90.3	100.0	3600.0	100.0	3600.0	0.48	70.87	0.00	0.2900

TABLE C-4: (Continued)

Observed and Calculated Results

Time (min)	ΔNp (cc)	Np (cc)	ΔNp+ΔWp (cc)	Np+Wp (cc)	PVi (PV)	Rec. (%OOIP)	W.C. (%)	Pinj (psig)
(1)	(2)	(3)	(4)	(5)	(6)	(7)	(8)	(9)
92.8	100.0	3700.0	100.0	3700.0	0.49	72.83	0.00	0.2905
95.3	100.0	3800.0	100.0	3800.0	0.51	74.80	0.00	0.2910
97.8	100.0	3900.0	100.0	3900.0	0.52	76.77	0.00	0.2950
100.4	100.0	4000.0	100.0	4000.0	0.53	78.74	0.00	0.2985
102.4	100.0	4100.0	100.0	4100.0	0.55	80.71	0.00	0.3030
105.3	97.5	4197.5	100.0	4200.0	0.56	82.63	2.50	0.3350
108.0	50.0	4247.5	104.0	4304.0	0.58	83.61	51.92	0.3870
110.5	32.0	4279.5	101.0	4405.0	0.59	84.24	68.32	0.3800
113.1	25.0	4304.5	102.0	4507.0	0.60	84.73	75.49	0.3580
115.6	16.0	4320.5	100.0	4607.0	0.62	85.05	84.00	0.3300
118.1	13.5	4334.0	100.0	4707.0	0.63	85.32	86.50	0.3250
120.6	12.0	4346.0	100.0	4807.0	0.64	85.55	88.00	0.3260
123.3	10.0	4356.0	101.0	4908.0	0.66	85.75	90.10	0.3270
125.7	9.0	4365.0	101.0	5009.0	0.67	85.93	91.09	0.3270
128.4	9.0	4374.0	109.0	5118.0	0.68	86.10	91.74	0.3275
130.9	7.0	4381.0	101.0	5219.0	0.70	86.24	93.07	0.3280
133.4	6.5	4387.5	102.0	5321.0	0.71	86.37	93.63	0.3285
139.7	12.5	4400.0	251.0	5572.0	0.74	86.61	95.02	0.3280
146.1	9.0	4409.0	250.0	5822.0	0.78	86.79	96.40	0.3273
152.3	8.0	4417.0	250.0	6072.0	0.81	86.95	96.80	0.3270
158.5	7.0	4424.0	250.0	6322.0	0.85	87.09	97.20	0.3270
164.7	5.5	4429.5	250.0	6572.0	0.88	87.19	97.80	0.3260
170.5	4.0	4433.5	250.0	6822.0	0.91	87.27	98.40	0.3260
177.0	3.0	4436.5	250.0	7072.0	0.95	87.33	98.80	0.3250
183.2	2.5	4439.0	250.0	7322.0	0.98	87.38	99.00	0.3250
189.6	2.0	4441.0	250.0	7572.0	1.01	87.42	99.20	0.3250
195.0	2.0	4443.0	250.0	7822.0	1.05	87.46	99.20	0.3250
208.0	5.0	4448.0	512.0	8334.0	1.11	87.56	99.02	0.3250

TABLE C-5:   RUN # HW-08

Porosity	=	36.19	%	OOIP	=	5658.00	cc
Swi	=	24.59	%	Soi	=	75.41	%
Sor	=	12.83	%				

Observed and Calculated Results

Time (min)	ΔNp (cc)	Np (cc)	ΔNp+ΔWp (cc)	Np+Wp (cc)	PVi (PV)	Rec. (%OOIP)	W.C. (%)	Pinj (psig)
(1)	(2)	(3)	(4)	(5)	(6)	(7)	(8)	(9)
2.5	100.0	100.0	100.0	100.0	0.01	1.77	0.00	0.2610
5.1	100.0	200.0	100.0	200.0	0.03	3.53	0.00	0.2615
7.5	100.0	300.0	100.0	300.0	0.04	5.30	0.00	0.2620
10.1	100.0	400.0	100.0	400.0	0.05	7.07	0.00	0.2623
12.5	100.0	500.0	100.0	500.0	0.07	8.84	0.00	0.2625
15.1	100.0	600.0	100.0	600.0	0.08	10.60	0.00	0.2626
17.6	100.0	700.0	100.0	700.0	0.09	12.37	0.00	0.2628
20.1	100.0	800.0	100.0	800.0	0.11	14.14	0.00	0.2628
22.6	100.0	900.0	100.0	900.0	0.12	15.91	0.00	0.2630
25.1	100.0	1000.0	100.0	1000.0	0.13	17.67	0.00	0.2635
27.6	100.0	1100.0	100.0	1100.0	0.15	19.44	0.00	0.2640
30.2	100.0	1200.0	100.0	1200.0	0.16	21.21	0.00	0.2650
32.7	100.0	1300.0	100.0	1300.0	0.17	22.98	0.00	0.2655
35.2	100.0	1400.0	100.0	1400.0	0.19	24.74	0.00	0.2660
37.8	100.0	1500.0	100.0	1500.0	0.20	26.51	0.00	0.2665
40.4	100.0	1600.0	100.0	1600.0	0.21	28.28	0.00	0.2670
42.9	100.0	1700.0	100.0	1700.0	0.23	30.05	0.00	0.2675
45.5	100.0	1800.0	100.0	1800.0	0.24	31.81	0.00	0.2678
47.9	100.0	1900.0	100.0	1900.0	0.25	33.58	0.00	0.2680
50.5	100.0	2000.0	100.0	2000.0	0.27	35.35	0.00	0.2685
53.0	100.0	2100.0	100.0	2100.0	0.28	37.12	0.00	0.2690
55.5	100.0	2200.0	100.0	2200.0	0.29	38.88	0.00	0.2692
58.1	100.0	2300.0	100.0	2300.0	0.31	40.65	0.00	0.2698
60.6	100.0	2400.0	100.0	2400.0	0.32	42.42	0.00	0.2715
63.2	100.0	2500.0	100.0	2500.0	0.33	44.19	0.00	0.2750
65.8	100.0	2600.0	100.0	2600.0	0.35	45.95	0.00	0.2765
68.3	100.0	2700.0	100.0	2700.0	0.36	47.72	0.00	0.2767
70.9	100.0	2800.0	100.0	2800.0	0.37	49.49	0.00	0.2770
73.3	100.0	2900.0	100.0	2900.0	0.39	51.25	0.00	0.2780
75.9	100.0	3000.0	100.0	3000.0	0.40	53.02	0.00	0.2790
78.5	100.0	3100.0	100.0	3100.0	0.41	54.79	0.00	0.2795
81.0	100.0	3200.0	100.0	3200.0	0.43	56.56	0.00	0.2798
83.6	100.0	3300.0	100.0	3300.0	0.44	58.32	0.00	0.2800
86.1	100.0	3400.0	100.0	3400.0	0.45	60.09	0.00	0.2810
88.7	100.0	3500.0	100.0	3500.0	0.47	61.86	0.00	0.2820

TABLE C-5: (Continued)

Observed and Calculated Results

Time (min)	ΔNp (cc)	Np (cc)	ΔNp+ΔWp (cc)	Np+Wp (cc)	PVi (PV)	Rec. (%OOIP)	W.C. (%)	Pinj (psig)
(1)	(2)	(3)	(4)	(5)	(6)	(7)	(8)	(9)
91.3	100.0	3600.0	100.0	3600.0	0.48	63.63	0.00	0.2824
93.9	100.0	3700.0	100.0	3700.0	0.49	65.39	0.00	0.2830
96.4	100.0	3800.0	100.0	3800.0	0.51	67.16	0.00	0.2835
98.8	100.0	3900.0	100.0	3900.0	0.52	68.93	0.00	0.2840
101.4	100.0	4000.0	100.0	4000.0	0.53	70.70	0.00	0.2845
103.9	100.0	4100.0	100.0	4100.0	0.55	72.46	0.00	0.2850
106.5	100.0	4200.0	100.0	4200.0	0.56	74.23	0.00	0.2860
109.1	100.0	4300.0	100.0	4300.0	0.57	76.00	0.00	0.2890
111.7	100.0	4400.0	100.0	4400.0	0.59	77.77	0.00	0.2900
114.1	77.0	4477.0	100.0	4500.0	0.60	79.13	23.00	0.3450
116.8	38.0	4515.0	100.0	4600.0	0.61	79.80	62.00	0.3650
119.3	27.0	4542.0	100.0	4700.0	0.63	80.28	73.00	0.3750
121.9	22.0	4564.0	101.0	4801.0	0.64	80.66	78.22	0.3870
124.5	16.0	4580.0	101.0	4902.0	0.65	80.95	84.16	0.3890
127.1	11.0	4591.0	100.0	5002.0	0.67	81.14	89.00	0.3830
129.7	8.0	4599.0	102.0	5104.0	0.68	81.28	92.16	0.3670
132.3	10.0	4609.0	99.0	5203.0	0.69	81.46	89.90	0.3500
134.9	8.0	4617.0	100.0	5303.0	0.71	81.60	92.00	0.32C0
137.5	5.0	4622.0	101.0	5404.0	0.72	81.69	95.05	0.2980
140.1	4.0	4626.0	100.0	5504.0	0.73	81.76	96.00	0.2970
142.6	5.0	4631.0	100.0	5604.0	0.75	81.85	95.00	0.2960
149.3	11.0	4642.0	254.0	5858.0	0.78	82.04	95.67	0.2950
155.8	10.0	4652.0	250.0	6108.0	0.81	82.22	96.00	0.2930
162.5	7.0	4659.0	250.0	6358.0	0.85	82.34	97.20	0.2880
169.1	7.0	4666.0	252.0	6610.0	0.88	82.47	97.22	0.2875
175.8	5.5	4671.5	250.0	6860.0	0.91	82.56	97.80	0.2875
182.4	5.5	4677.0	252.0	7112.0	0.95	82.66	97.82	0.2880
190.0	4.0	4681.0	280.0	7392.0	0.99	82.73	98.57	0.2880
203.6	8.0	4689.0	503.0	7895.0	1.05	82.87	98.41	0.2882
217.1	6.0	4695.0	488.0	8383.0	1.12	82.98	98.77	0.2885

TABLE C-6:   RUN # HW-09

Porosity	=	36.83	%	OOIP	=	5400.00	cc
Swi	=	29.27	%	Soi	=	70.73	%
Sor	=	8.93	%				

Observed and Calculated Results

Time (min)	ΔNp (cc)	Np (cc)	ΔNp+ΔWp (cc)	Np+Wp (cc)	PVi (PV)	Rec. (%OOIP)	W.C. (%)	Pinj (psig)
(1)	(2)	(3)	(4)	(5)	(6)	(7)	(8)	(9)
2.1	100.0	100.0	100.0	100.0	0.01	1.85	0.00	0.2450
4.3	100.0	200.0	100.0	200.0	0.03	3.70	0.00	0.2455
6.7	100.0	300.0	100.0	300.0	0.04	5.56	0.00	0.2460
8.9	100.0	400.0	100.0	400.0	0.05	7.41	0.00	0.2470
11.2	100.0	500.0	100.0	500.0	0.07	9.26	0.00	0.2480
13.4	100.0	600.0	100.0	600.0	0.08	11.11	0.00	0.2490
15.6	100.0	700.0	100.0	700.0	0.09	12.96	0.00	0.2500
18.0	100.0	800.0	100.0	800.0	0.10	14.81	0.00	0.2510
20.2	100.0	900.0	100.0	900.0	0.12	16.67	0.00	0.2520
22.6	100.0	1000.0	100.0	1000.0	0.13	18.52	0.00	0.2525
24.8	100.0	1100.0	100.0	1100.0	0.14	20.37	0.00	0.2535
27.2	100.0	1200.0	100.0	1200.0	0.16	22.22	0.00	0.2545
29.6	100.0	1300.0	100.0	1300.0	0.17	24.07	0.00	0.2555
32.2	100.0	1400.0	100.0	1400.0	0.18	25.93	0.00	0.2565
34.7	100.0	1500.0	100.0	1500.0	0.20	27.78	0.00	0.2575
37.3	100.0	1600.0	100.0	1600.0	0.21	29.63	0.00	0.2585
39.7	100.0	1700.0	100.0	1700.0	0.22	31.48	0.00	0.2595
42.3	100.0	1800.0	100.0	1800.0	0.24	33.33	0.00	0.2603
44.7	100.0	1900.0	100.0	1900.0	0.25	35.19	0.00	0.2615
47.3	100.0	2000.0	100.0	2000.0	0.26	37.04	0.00	0.2630
49.7	100.0	2100.0	100.0	2100.0	0.28	38.89	0.00	0.2640
52.2	100.0	2200.0	100.0	2200.0	0.29	40.74	0.00	0.2648
54.7	100.0	2300.0	100.0	2300.0	0.30	42.59	0.00	0.2660
57.3	100.0	2400.0	100.0	2400.0	0.31	44.44	0.00	0.2670
59.8	100.0	2500.0	100.0	2500.0	0.33	46.30	0.00	0.2680
62.3	100.0	2600.0	100.0	2600.0	0.34	48.15	0.00	0.2695
64.9	100.0	2700.0	100.0	2700.0	0.35	50.00	0.00	0.2705
67.4	100.0	2800.0	100.0	2800.0	0.37	51.85	0.00	0.2720
70.0	100.0	2900.0	100.0	2900.0	0.38	53.70	0.00	0.2730
72.5	100.0	3000.0	100.0	3000.0	0.39	55.56	0.00	0.2750
75.1	100.0	3100.0	100.0	3100.0	0.41	57.41	0.00	0.2765
77.6	100.0	3200.0	100.0	3200.0	0.42	59.26	0.00	0.2775
82.8	200.0	3400.0	200.0	3400.0	0.45	62.96	0.00	0.2800
85.3	100.0	3500.0	100.0	3500.0	0.46	64.81	0.00	0.2820
87.9	100.0	3600.0	100.0	3600.0	0.47	66.67	0.00	0.2835

TABLE C-6: (Continued)

Observed and Calculated Results

Time (min)	ΔNp (cc)	Np (cc)	ΔNp+ΔWp (cc)	Np+Wp (cc)	PVi (PV)	Rec. (%OOIP)	W.C. (%)	Pinj (psig)
(1)	(2)	(3)	(4)	(5)	(6)	(7)	(8)	(9)
90.4	100.0	3700.0	100.0	3700.0	0.48	68.52	0.00	0.2840
93.0	100.0	3800.0	100.0	3800.0	0.50	70.37	0.00	0.2850
95.6	100.0	3900.0	100.0	3900.0	0.51	72.22	0.00	0.2880
97.0	100.0	4000.0	100.0	4000.0	0.52	74.07	0.00	0.2890
98.1	100.0	4100.0	100.0	4100.0	0.54	75.93	0.00	0.2892
100.6	100.0	4200.0	100.0	4200.0	0.55	77.78	0.00	0.2900
103.1	100.0	4300.0	100.0	4300.0	0.56	79.63	0.00	0.2915
105.7	100.0	4400.0	100.0	4400.0	0.58	81.48	0.00	0.2930
108.3	100.0	4500.0	100.0	4500.0	0.59	83.33	0.00	0.3050
110.8	62.0	4562.0	100.0	4600.0	0.60	84.48	38.00	0.3530
113.4	38.0	4600.0	100.0	4700.0	0.62	85.19	62.00	0.3480
116.1	22.0	4622.0	100.0	4800.0	0.63	85.59	78.00	0.2950
118.6	13.0	4635.0	100.0	4900.0	0.64	85.83	87.00	0.2920
121.3	11.0	4646.0	101.0	5001.0	0.66	86.04	89.11	0.2922
123.8	8.0	4654.0	100.0	5101.0	0.67	86.19	92.00	0.2915
126.4	7.0	4661.0	100.0	5201.0	0.68	86.31	93.00	0.2912
129.0	6.0	4667.0	101.0	5302.0	0.69	86.43	94.06	0.2910
131.6	5.0	4672.0	100.0	5402.0	0.71	86.52	95.00	0.2910
134.2	4.5	4676.5	100.0	5502.0	0.72	86.60	95.50	0.2910
136.8	4.0	4680.5	101.0	5603.0	0.73	86.68	96.04	0.2905
139.4	2.5	4683.0	100.0	5703.0	0.75	86.72	97.50	0.2901
145.9	7.0	4690.0	250.0	5953.0	0.78	86.85	97.20	0.2900
152.4	6.0	4696.0	250.0	6203.0	0.81	86.96	97.60	0.2890
158.9	5.0	4701.0	250.0	6453.0	0.85	87.06	98.00	0.2880
165.4	4.0	4705.0	250.0	6703.0	0.88	87.13	98.40	0.2878
171.9	3.0	4708.0	250.0	6953.0	0.91	87.19	98.80	0.2875
178.5	2.0	4710.0	250.0	7203.0	0.94	87.22	99.20	0.2875
185.1	1.5	4711.5	250.0	7453.0	0.98	87.25	99.40	0.2875
191.6	2.0	4713.5	250.0	7703.0	1.01	87.29	99.20	0.2875
204.9	3.0	4716.5	500.0	8203.0	1.07	87.34	99.40	0.2875
211.4	1.5	4718.0	253.0	8456.0	1.11	87.37	99.41	0.2875

3C

267

TABLE C-7:   RUN # HW-10

Porosity	=	36.16	%	OOIP	=	5508.00	cc
Swi	=	28.04	%	Soi	=	71.96	%
Sor	=	11.33	%				

Observed and Calculated Results

Time (min)	ΔNp (cc)	Np (cc)	ΔNp+ΔWp (cc)	Np+Wp (cc)	PVi (PV)	Rec. (%OOIP)	W.C. (%)	Pinj (psig)
(1)	(2)	(3)	(4)	(5)	(6)	(7)	(8)	(9)
2.6	100.0	100.0	100.0	100.0	0.01	1.82	0.00	0.2815
5.2	100.0	200.0	100.0	200.0	0.03	3.63	0.00	0.2820
7.8	100.0	300.0	100.0	300.0	0.04	5.45	0.00	0.2824
10.5	100.0	400.0	100.0	400.0	0.05	7.26	0.00	0.2827
13.2	100.0	500.0	100.0	500.0	0.07	9.08	0.00	0.2829
15.9	100.0	600.0	100.0	600.0	0.08	10.89	0.00	0.2830
18.1	100.0	700.0	100.0	700.0	0.09	12.71	0.00	0.2834
20.3	100.0	800.0	100.0	800.0	0.10	14.52	0.00	0.2838
22.7	100.0	900.0	100.0	900.0	0.12	16.34	0.00	0.2840
24.9	100.0	1000.0	100.0	1000.0	0.13	18.16	0.00	0.2845
27.3	100.0	1100.0	100.0	1100.0	0.14	19.97	0.00	0.2850
29.7	100.0	1200.0	100.0	1200.0	0.16	21.79	0.00	0.2852
32.1	100.0	1300.0	100.0	1300.0	0.17	23.60	0.00	0.2855
34.6	100.0	1400.0	100.0	1400.0	0.18	25.42	0.00	0.2860
37.0	100.0	1500.0	100.0	1500.0	0.20	27.23	0.00	0.2870
39.5	100.0	1600.0	100.0	1600.0	0.21	29.05	0.00	0.2875
42.0	100.0	1700.0	100.0	1700.0	0.22	30.86	0.00	0.2879
44.6	100.0	1800.0	100.0	1800.0	0.24	32.68	0.00	0.2880
47.1	100.0	1900.0	100.0	1900.0	0.25	34.50	0.00	0.2882
49.6	100.0	2000.0	100.0	2000.0	0.26	36.31	0.00	0.2888
52.1	100.0	2100.0	100.0	2100.0	0.27	38.13	0.00	0.2891
54.5	100.0	2200.0	100.0	2200.0	0.29	39.94	0.00	0.2893
57.0	100.0	2300.0	100.0	2300.0	0.30	41.76	0.00	0.2894
59.6	100.0	2400.0	100.0	2400.0	0.31	43.57	0.00	0.2896
62.0	100.0	2500.0	100.0	2500.0	0.33	45.39	0.00	0.2897
64.5	100.0	2600.0	100.0	2600.0	0.34	47.20	0.00	0.2898
67.0	100.0	2700.0	100.0	2700.0	0.35	49.02	0.00	0.3000
69.6	100.0	2800.0	100.0	2800.0	0.37	50.84	0.00	0.3015
72.1	100.0	2900.0	100.0	2900.0	0.38	52.65	0.00	0.3025
74.5	100.0	3000.0	100.0	3000.0	0.39	54.47	0.00	0.3035
77.0	100.0	3100.0	100.0	3100.0	0.41	56.28	0.00	0.3050
79.5	100.0	3200.0	100.0	3200.0	0.42	58.10	0.00	0.3070
82.0	100.0	3300.0	100.0	3300.0	0.43	59.91	0.00	0.3080
84.5	100.0	3400.0	100.0	3400.0	0.44	61.73	0.00	0.3090
87.0	100.0	3500.0	100.0	3500.0	0.46	63.54	0.00	0.3110
89.5	100.0	3600.0	100.0	3600.0	0.47	65.36	0.00	0.3120

TABLE C-7: (Continued)

Observed and Calculated Results

Time (min)	ΔNp (cc)	Np (cc)	ΔNp+ΔWp (cc)	Np+Wp (cc)	PVi (PV)	Rec. (%OOIP)	W.C. (%)	Pinj (psig)
(1)	(2)	(3)	(4)	(5)	(6)	(7)	(8)	(9)
92.1	100.0	3700.0	100.0	3700.0	0.48	67.18	0.00	0.3130
94.6	100.0	3800.0	100.0	3800.0	0.50	68.99	0.00	0.3140
97.1	100.0	3900.0	100.0	3900.0	0.51	70.81	0.00	0.3160
99.6	100.0	4000.0	100.0	4000.0	0.52	72.62	0.00	0.3170
102.0	100.0	4100.0	100.0	4100.0	0.54	74.44	0.00	0.3180
104.5	100.0	4200.0	100.0	4200.0	0.55	76.25	0.00	0.3200
107.0	97.0	4297.0	100.0	4300.0	0.56	78.01	3.00	0.3400
109.5	70.0	4367.0	100.0	4400.0	0.57	79.28	30.00	0.3550
112.1	50.0	4417.0	102.0	4502.0	0.59	80.19	50.98	0.3640
115.5	40.5	4457.5	100.0	4602.0	0.60	80.93	59.50	0.3740
117.1	33.0	4490.5	101.0	4703.0	0.61	81.53	67.33	0.3800
119.6	23.0	4513.5	100.0	4803.0	0.63	81.94	77.00	0.3850
122.1	18.5	4532.0	100.0	4903.0	0.64	82.28	81.50	0.3750
124.6	14.5	4546.5	100.0	5003.0	0.65	82.54	85.50	0.3600
127.1	13.0	4559.5	100.0	5103.0	0.67	82.78	87.00	0.3500
129.6	11.0	4570.5	100.0	5203.0	0.68	82.98	89.00	0.3450
132.1	8.0	4578.5	101.0	5304.0	0.69	83.12	92.08	0.3415
134.5	7.0	4585.5	100.0	5404.0	0.71	83.25	93.00	0.3410
140.8	12.0	4597.5	250.0	5654.0	0.74	83.47	95.20	0.3410
147.0	9.0	4606.5	250.0	5904.0	0.77	83.63	96.40	0.3415
153.2	8.0	4614.5	250.0	6154.0	0.80	83.78	96.80	0.3420
159.4	6.0	4620.5	250.0	6404.0	0.84	83.89	97.60	0.3415
165.9	6.0	4626.5	266.0	6670.0	0.87	84.00	97.74	0.3415
171.3	3.0	4629.5	250.0	6920.0	0.90	84.05	98.80	0.3420
178.0	3.0	4632.5	250.0	7170.0	0.94	84.10	98.80	0.3420
184.1	2.5	4635.0	250.0	7420.0	0.97	84.15	99.00	0.3410
190.1	2.0	4637.0	250.0	7670.0	1.00	84.19	99.20	0.3400
196.1	1.5	4638.5	250.0	7920.0	1.03	84.21	99.40	0.3385
202.1	1.0	4639.5	250.0	8170.0	1.07	84.23	99.60	0.3370
212.3	1.5	4641.0	427.0	8597.0	1.12	84.26	99.65	0.3360

TABLE C-8:   RUN # HW-11

Porosity	=	36.30	%	OOIP	=	5792.00	cc
Swi	=	26.40	%	Soi	=	73.59	%
Sor	=	11.30	%				

Observed and Calculated Results

Time (min)	ΔNp (cc)	Np (cc)	ΔNp+ΔWp (cc)	Np+Wp (cc)	PVi (PV)	Rec. (%OOIP)	W.C. (%)	Pinj (psig)
(1)	(2)	(3)	(4)	(5)	(6)	(7)	(8)	(9)
2.5	100.0	100.0	100.0	100.0	0.01	1.73	0.00	0.2820
5.0	100.0	200.0	100.0	200.0	0.03	3.45	0.00	0.2840
7.5	100.0	300.0	100.0	300.0	0.04	5.18	0.00	0.2850
10.0	100.0	400.0	100.0	400.0	0.05	6.91	0.00	0.2870
12.4	100.0	500.0	100.0	500.0	0.06	8.63	0.00	0.2880
14.9	100.0	600.0	100.0	600.0	0.08	10.36	0.00	0.2890
17.5	100.0	700.0	100.0	700.0	0.09	12.09	0.00	0.2900
20.0	100.0	800.0	100.0	800.0	0.10	13.81	0.00	0.2910
22.4	100.0	900.0	100.0	900.0	0.11	15.54	0.00	0.2920
24.9	100.0	1000.0	100.0	1000.0	0.13	17.27	0.00	0.2930
27.3	100.0	1100.0	100.0	1100.0	0.14	18.99	0.00	0.2940
29.9	100.0	1200.0	100.0	1200.0	0.15	20.72	0.00	0.2950
32.4	100.0	1300.0	100.0	1300.0	0.17	22.44	0.00	0.2960
34.9	100.0	1400.0	100.0	1400.0	0.18	24.17	0.00	0.2970
37.4	100.0	1500.0	100.0	1500.0	0.19	25.90	0.00	0.2980
40.0	100.0	1600.0	100.0	1600.0	0.20	27.62	0.00	0.2990
42.5	100.0	1700.0	100.0	1700.0	0.22	29.35	0.00	0.3000
45.1	100.0	1800.0	100.0	1800.0	0.23	31.08	0.00	0.3010
47.7	100.0	1900.0	100.0	1900.0	0.24	32.80	0.00	0.3020
50.0	100.0	2000.0	100.0	2000.0	0.25	34.53	0.00	0.3030
52.8	100.0	2100.0	100.0	2100.0	0.27	36.26	0.00	0.3040
55.3	100.0	2200.0	100.0	2200.0	0.28	37.98	0.00	0.3050
57.8	100.0	2300.0	100.0	2300.0	0.29	39.71	0.00	0.3060
60.2	100.0	2400.0	100.0	2400.0	0.30	41.44	0.00	0.3070
63.1	100.0	2500.0	100.0	2500.0	0.32	43.16	0.00	0.3080
65.2	100.0	2600.0	100.0	2600.0	0.33	44.89	0.00	0.3090
68.2	100.0	2700.0	100.0	2700.0	0.34	46.62	0.00	0.3105
70.9	100.0	2800.0	100.0	2800.0	0.36	48.34	0.00	0.3120
73.4	100.0	2900.0	100.0	2900.0	0.37	50.07	0.00	0.3130
76.1	100.0	3000.0	100.0	3000.0	0.38	51.80	0.00	0.3140
78.7	100.0	3100.0	100.0	3100.0	0.39	53.52	0.00	0.3150
81.4	100.0	3200.0	100.0	3200.0	0.41	55.25	0.00	0.3160
84.1	100.0	3300.0	100.0	3300.0	0.42	56.98	0.00	0.3170
86.9	100.0	3400.0	100.0	3400.0	0.43	58.70	0.00	0.3180
89.6	100.0	3500.0	100.0	3500.0	0.44	60.43	0.00	0.3190

TABLE C-8: (Continued)

Observed and Calculated Results

Time (min)	ΔNp (cc)	Np (cc)	ΔNp+ΔWp (cc)	Np+Wp (cc)	PVi (PV)	Rec. (%OOIP)	W.C. (%)	Pinj (psig)
(1)	(2)	(3)	(4)	(5)	(6)	(7)	(8)	(9)
92.5	100.0	3600.0	100.0	3600.0	0.46	62.15	0.00	0.3200
95.2	100.0	3700.0	100.0	3700.0	0.47	63.88	0.00	0.3210
97.9	100.0	3800.0	100.0	3800.0	0.48	65.61	0.00	0.3220
100.6	100.0	3900.0	100.0	3900.0	0.50	67.33	0.00	0.3230
103.3	100.0	4000.0	100.0	4000.0	0.51	69.06	0.00	0.3240
105.9	100.0	4100.0	100.0	4100.0	0.52	70.79	0.00	0.3270
108.7	100.0	4200.0	100.0	4200.0	0.53	72.51	0.00	0.3290
111.4	98.0	4298.0	100.0	4300.0	0.55	74.21	2.00	0.3500
114.3	83.0	4381.0	100.0	4400.0	0.56	75.64	17.00	0.3800
117.0	72.0	4453.0	100.0	4500.0	0.57	76.88	28.00	0.3950
119.8	62.0	4515.0	100.0	4600.0	0.58	77.95	38.00	0.4050
122.5	54.0	4569.0	100.0	4700.0	0.60	78.88	46.00	0.4070
125.4	48.0	4617.0	100.0	4800.0	0.61	79.71	52.00	0.4110
128.2	40.0	4657.0	100.0	4900.0	0.62	80.40	60.00	0.4130
131.1	34.0	4691.0	100.0	5000.0	0.64	80.99	66.00	0.4170
133.9	29.0	4720.0	101.0	5101.0	0.65	81.49	71.29	0.4170
136.7	24.0	4744.0	100.0	5201.0	0.66	81.91	76.00	0.4160
139.4	19.0	4763.0	100.0	5301.0	0.67	82.23	81.00	0.4110
142.2	15.5	4778.5	100.0	5401.0	0.69	82.50	84.50	0.4090
145.1	14.0	4792.5	100.0	5501.0	0.70	82.74	86.00	0.3990
152.1	26.5	4819.0	250.0	5751.0	0.73	83.20	89.40	0.3920
159.3	18.0	4837.0	250.0	6001.0	0.76	83.51	92.80	0.3850
166.4	12.0	4849.0	251.0	6252.0	0.79	83.72	95.22	0.3800
233.4	10.0	4859.0	250.0	6502.0	0.83	83.89	96.00	0.3810
180.7	8.0	4867.0	258.0	6760.0	0.86	84.03	96.90	0.3820
187.9	7.0	4874.0	250.0	7010.0	0.89	84.15	97.20	0.3825
195.1	6.0	4880.0	250.0	7260.0	0.92	84.25	97.60	0.3830
202.2	6.0	4886.0	250.0	7510.0	0.95	84.36	97.60	0.3835
209.1	5.0	4891.0	250.0	7760.0	0.99	84.44	98.00	0.3840
216.1	4.0	4895.0	250.0	8010.0	1.02	84.51	98.40	0.3850
222.8	3.5	4898.5	250.0	8260.0	1.05	84.57	98.60	0.3860
234.5	4.0	4902.5	435.0	8695.0	1.10	84.64	99.08	0.3870

TABLE C-9:   RUN # HW-12

Porosity	=	36.24	%	OOIP	=	5021.00	cc
Swi	=	35.72	%	Soi	=	64.28	%
Sor	=	9.44	%				

Observed and Calculated Results

Time (min)	ΔNp (cc)	Np (cc)	ΔNp+ΔWp (cc)	Np+Wp (cc)	PVi (PV)	Rec. (%OOIP)	W.C. (%)	Pinj (psig)
(1)	(2)	(3)	(4)	(5)	(6)	(7)	(8)	(9)
1.3	50.0	50.0	50.0	50.0	0.01	1.00	0.00	0.2810
3.9	100.0	150.0	100.0	150.0	0.02	2.99	0.00	0.2815
6.4	100.0	250.0	100.0	250.0	0.03	4.98	0.00	0.2820
8.9	100.0	350.0	100.0	350.0	0.04	6.97	0.00	0.2825
11.4	100.0	450.0	100.0	450.0	0.06	8.96	0.00	0.2830
14.0	100.0	550.0	100.0	550.0	0.07	10.95	0.00	0.2840
16.5	100.0	650.0	100.0	650.0	0.08	12.95	0.00	0.2850
18.9	100.0	750.0	100.0	750.0	0.10	14.94	0.00	0.2860
21.4	100.0	850.0	100.0	850.0	0.11	16.93	0.00	0.2870
23.8	100.0	950.0	100.0	950.0	0.12	18.92	0.00	0.2880
26.2	100.0	1050.0	100.0	1050.0	0.13	20.91	0.00	0.2890
28.6	100.0	1150.0	100.0	1150.0	0.15	22.90	0.00	0.2900
31.0	100.0	1250.0	100.0	1250.0	0.16	24.90	0.00	0.2910
33.4	100.0	1350.0	100.0	1350.0	0.17	26.89	0.00	0.2920
35.8	100.0	1450.0	100.0	1450.0	0.19	28.88	0.00	0.2930
38.2	100.0	1550.0	100.0	1550.0	0.20	30.87	0.00	0.2940
40.7	100.0	1650.0	100.0	1650.0	0.21	32.86	0.00	0.2950
43.1	100.0	1750.0	100.0	1750.0	0.22	34.85	0.00	0.2960
45.6	100.0	1850.0	100.0	1850.0	0.24	36.85	0.00	0.2970
48.0	100.0	1950.0	100.0	1950.0	0.25	38.84	0.00	0.2980
50.4	100.0	2050.0	100.0	2050.0	0.26	40.83	0.00	0.2990
52.8	100.0	2150.0	100.0	2150.0	0.28	42.82	0.00	0.3010
55.2	100.0	2250.0	100.0	2250.0	0.29	44.81	0.00	0.3020
57.7	100.0	2350.0	100.0	2350.0	0.30	46.80	0.00	0.3030
60.2	100.0	2450.0	100.0	2450.0	0.31	48.80	0.00	0.3040
62.6	100.0	2550.0	100.0	2550.0	0.33	50.79	0.00	0.3050
65.1	100.0	2650.0	100.0	2650.0	0.34	52.78	0.00	0.3060
67.6	100.0	2750.0	100.0	2750.0	0.35	54.77	0.00	0.3070
70.0	100.0	2850.0	100.0	2850.0	0.36	56.76	0.00	0.3080
72.5	100.0	2950.0	100.0	2950.0	0.38	58.75	0.00	0.3090
74.9	100.0	3050.0	100.0	3050.0	0.39	60.74	0.00	0.3100
77.3	100.0	3150.0	100.0	3150.0	0.40	62.74	0.00	0.3110
79.8	100.0	3250.0	100.0	3250.0	0.42	64.73	0.00	0.3120
82.3	100.0	3350.0	100.0	3350.0	0.43	66.72	0.00	0.3130
84.7	100.0	3450.0	100.0	3450.0	0.44	68.71	0.00	0.3140
87.2	100.0	3550.0	100.0	3550.0	0.45	70.70	0.00	0.3160

TABLE C-9: (Continued)

Observed and Calculated Results

Time (min)	ΔNp (cc)	Np (cc)	ΔNp+ΔWp (cc)	Np+Wp (cc)	PVi (PV)	Rec. (%OOIP)	W.C. (%)	Pinj (psig)
(1)	(2)	(3)	(4)	(5)	(6)	(7)	(8)	(9)
89.7	100.0	3650.0	100.0	3650.0	0.47	72.69	0.00	0.3180
92.2	100.0	3750.0	100.0	3750.0	0.48	74.69	0.00	0.3225
94.6	97.5	3847.5	100.0	3850.0	0.49	76.63	2.50	0.3425
97.1	84.5	3932.0	101.0	3951.0	0.51	78.31	16.34	0.3655
99.6	71.5	4003.5	101.0	4052.0	0.52	79.74	29.21	0.3700
102.1	49.0	4052.5	100.0	4152.0	0.53	80.71	51.00	0.3725
104.5	36.0	4088.5	100.0	4252.0	0.54	81.43	64.00	0.3775
107.0	30.0	4118.5	100.0	4352.0	0.56	82.03	70.00	0.3785
109.5	24.0	4142.5	100.0	4452.0	0.57	82.50	76.00	0.3775
112.0	16.5	4159.0	100.0	4552.0	0.58	82.83	83.50	0.3735
114.4	14.0	4173.0	100.0	4652.0	0.60	83.11	86.00	0.3525
116.9	10.5	4183.5	100.0	4752.0	0.61	83.32	89.50	0.3435
119.4	10.0	4193.5	100.0	4852.0	0.62	83.52	90.00	0.3435
121.9	9.3	4202.8	100.5	4952.5	0.63	83.70	90.75	0.3435
124.3	7.0	4209.8	100.0	5052.5	0.65	83.84	93.00	0.3436
130.6	14.0	4223.8	250.0	5302.5	0.68	84.12	94.40	0.3437
136.8	11.0	4234.8	250.0	5552.5	0.71	84.34	95.60	0.3435
143.0	5.0	4239.8	250.0	5802.5	0.74	84.44	98.00	0.3430
149.3	5.0	4244.8	250.0	6052.5	0.77	84.54	98.00	0.3430
155.6	5.0	4249.8	250.0	6302.5	0.81	84.64	98.00	0.3430
161.9	5.0	4254.8	250.0	6552.5	0.84	84.74	98.00	0.3435
168.2	4.0	4258.8	250.0	6802.5	0.87	84.82	98.40	0.3445
174.6	4.0	4262.8	250.0	7052.5	0.90	84.90	98.40	0.3450
180.9	4.0	4266.8	250.0	7302.5	0.93	84.98	98.40	0.3455
187.3	3.5	4270.3	250.0	7552.5	0.97	85.05	98.60	0.3460
200.1	7.0	4277.3	500.0	8052.5	1.03	85.19	98.60	0.3465
212.7	6.0	4283.3	492.0	8544.5	1.09	85.31	98.78	0.3470

TABLE C-10:   RUN # HW-13

Porosity	=	36.09	%	OOIP	=	5500.00	cc
Swi	=	28.01	%	Soi	=	71.99	%
Sor	=	12.24	%				

Observed and Calculated Results

Time (min)	ΔNp (cc)	Np (cc)	ΔNp+ΔWp (cc)	Np+Wp (cc)	PVi (PV)	Rec. (%OOIP)	W.C. (%)	Pinj (psig)
(1)	(2)	(3)	(4)	(5)	(6)	(7)	(8)	(9)
1.2	50.0	50.0	50.0	50.0	0.01	0.91	0.00	0.3100
4.9	100.0	150.0	100.0	150.0	0.02	2.73	0.00	0.3100
7.4	100.0	250.0	100.0	250.0	0.03	4.55	0.00	0.3100
9.9	100.0	350.0	100.0	350.0	0.05	6.36	0.00	0.3100
12.4	100.0	450.0	100.0	450.0	0.06	8.18	0.00	0.3110
14.9	100.0	550.0	100.0	550.0	0.07	10.00	0.00	0.3120
17.5	100.0	650.0	100.0	650.0	0.09	11.82	0.00	0.3125
20.0	100.0	750.0	100.0	750.0	0.10	13.64	0.00	0.3125
22.5	100.0	850.0	100.0	850.0	0.11	15.45	0.00	0.3128
25.1	100.0	950.0	100.0	950.0	0.12	17.27	0.00	0.3132
27.5	100.0	1050.0	100.0	1050.0	0.14	19.09	0.00	0.3135
30.0	100.0	1150.0	100.0	1150.0	0.15	20.91	0.00	0.3140
32.6	100.0	1250.0	100.0	1250.0	0.16	22.73	0.00	0.3145
35.1	100.0	1350.0	100.0	1350.0	0.18	24.55	0.00	0.3150
37.7	100.0	1450.0	100.0	1450.0	0.19	26.36	0.00	0.3155
40.3	100.0	1550.0	100.0	1550.0	0.20	28.18	0.00	0.3160
42.8	100.0	1650.0	100.0	1650.0	0.22	30.00	0.00	0.3165
45.3	100.0	1750.0	100.0	1750.0	0.23	31.82	0.00	0.3170
47.8	100.0	1850.0	100.0	1850.0	0.24	33.64	0.00	0.3175
50.3	100.0	1950.0	100.0	1950.0	0.26	35.45	0.00	0.3180
52.7	100.0	2050.0	100.0	2050.0	0.27	37.27	0.00	0.3185
55.2	100.0	2150.0	100.0	2150.0	0.28	39.09	0.00	0.3190
57.7	100.0	2250.0	100.0	2250.0	0.29	40.91	0.00	0.3196
60.2	100.0	2350.0	100.0	2350.0	0.31	42.73	0.00	0.3230
62.7	100.0	2450.0	100.0	2450.0	0.32	44.55	0.00	0.3240
65.2	100.0	2550.0	100.0	2550.0	0.33	46.36	0.00	0.3255
67.8	100.0	2650.0	100.0	2650.0	0.35	48.18	0.00	0.3270
70.3	100.0	2750.0	100.0	2750.0	0.36	50.00	0.00	0.3280
72.8	100.0	2850.0	100.0	2850.0	0.37	51.82	0.00	0.3290
75.3	100.0	2950.0	100.0	2950.0	0.39	53.64	0.00	0.3300
77.8	100.0	3050.0	100.0	3050.0	0.40	55.45	0.00	0.3315
80.3	100.0	3150.0	100.0	3150.0	0.41	57.27	0.00	0.3330
82.9	100.0	3250.0	100.0	3250.0	0.43	59.09	0.00	0.3340
85.4	100.0	3350.0	100.0	3350.0	0.44	60.91	0.00	0.3355
87.9	100.0	3450.0	100.0	3450.0	0.45	62.73	0.00	0.3370

TABLE C-10: (Continued)

Observed and Calculated Results

Time (min)	ΔNp (cc)	Np (cc)	ΔNp+ΔWp (cc)	Np+Wp (cc)	PVi (PV)	Rec. (%OOIP)	W.C. (%)	Pinj (psig)
(1)	(2)	(3)	(4)	(5)	(6)	(7)	(8)	(9)
90.4	100.0	3550.0	100.0	3550.0	0.46	64.55	0.00	0.3380
93.0	100.0	3650.0	100.0	3650.0	0.48	66.36	0.00	0.3400
95.5	100.0	3750.0	100.0	3750.0	0.49	68.18	0.00	0.3410
98.1	100.0	3850.0	100.0	3850.0	0.50	70.00	0.00	0.3420
100.6	100.0	3950.0	100.0	3950.0	0.52	71.82	0.00	0.3440
102.6	100.0	4050.0	100.0	4050.0	0.53	73.64	0.00	0.3500
105.7	102.0	4152.0	107.0	4157.0	0.54	75.49	4.67	0.3850
108.2	64.5	4216.5	99.0	4256.0	0.56	76.66	34.85	0.4050
110.7	49.0	4265.5	100.0	4356.0	0.57	77.55	51.00	0.4200
113.2	42.5	4308.0	100.0	4456.0	0.58	78.33	57.50	0.4320
115.8	35.0	4343.0	100.0	4556.0	0.60	78.96	65.00	0.4400
118.3	28.0	4371.0	100.0	4656.0	0.61	79.47	72.00	0.4450
120.8	23.0	4394.0	100.0	4756.0	0.62	79.89	77.00	0.4420
123.3	20.5	4414.5	100.0	4856.0	0.64	80.26	79.50	0.4350
125.8	17.5	4432.0	100.0	4956.0	0.65	80.58	82.50	0.4250
128.3	15.0	4447.0	101.0	5057.0	0.66	80.85	85.15	0.4100
130.9	11.0	4458.0	100.0	5157.0	0.68	81.05	89.00	0.3850
133.4	10.0	4468.0	100.0	5257.0	0.69	81.24	90.00	0.3800
135.9	9.0	4477.0	100.0	5357.0	0.70	81.40	91.00	0.3750
142.2	19.0	4496.0	250.0	5607.0	0.73	81.75	92.40	0.3750
148.5	16.0	4512.0	250.0	5857.0	0.77	82.04	93.60	0.3760
154.9	12.0	4524.0	250.0	6107.0	0.80	82.25	95.20	0.3770
161.3	8.5	4532.5	250.0	6357.0	0.83	82.41	96.60	0.3780
167.6	7.5	4540.0	250.0	6607.0	0.86	82.55	97.00	0.3800
173.9	6.0	4546.0	250.0	6857.0	0.90	82.65	97.60	0.3820
180.1	5.0	4551.0	250.0	7107.0	0.93	82.75	98.00	0.3840
186.7	5.0	4556.0	251.0	7358.0	0.96	82.84	98.01	0.3860
193.1	2.5	4558.5	250.0	7608.0	1.00	82.88	99.00	0.3880
199.5	2.5	4561.0	250.0	7858.0	1.03	82.93	99.00	0.3900
212.7	4.0	4565.0	500.0	8358.0	1.09	83.00	99.20	0.3920

TABLE C-11:   RUN # HW-14

Porosity	=	36.27	%	OOIP	=	5353.00	cc
Swi	=	31.51	%	Soi	=	68.49	%
Sor	=	9.03	%				

Observed and Calculated Results

Time (min)	ΔNp (cc)	Np (cc)	ΔNp+ΔWp (cc)	Np+Wp (cc)	PVi (PV)	Rec. (%OOIP)	W.C. (%)	Pinj (psig)
(1)	(2)	(3)	(4)	(5)	(6)	(7)	(8)	(9)
1.3	50.0	50.0	50.0	50.0	0.01	0.93	0.00	0.0000
3.7	100.0	150.0	100.0	150.0	0.02	2.80	0.00	0.0000
6.3	100.0	250.0	100.0	250.0	0.03	4.67	0.00	0.0000
8.7	100.0	350.0	100.0	350.0	0.04	6.54	0.00	0.0000
11.2	100.0	450.0	100.0	450.0	0.06	8.41	0.00	0.0000
13.7	100.0	550.0	100.0	550.0	0.07	10.27	0.00	0.0000
16.2	100.0	650.0	100.0	650.0	0.08	12.14	0.00	0.0000
18.7	100.0	750.0	100.0	750.0	0.10	14.01	0.00	0.0000
21.2	100.0	850.0	100.0	850.0	0.11	15.88	0.00	0.0000
23.7	100.0	950.0	100.0	950.0	0.12	17.75	0.00	0.0000
26.2	100.0	1050.0	100.0	1050.0	0.13	19.62	0.00	0.0000
28.7	100.0	1150.0	100.0	1150.0	0.15	21.48	0.00	0.0000
31.1	100.0	1250.0	100.0	1250.0	0.16	23.35	0.00	0.0000
33.6	100.0	1350.0	100.0	1350.0	0.17	25.22	0.00	0.0000
36.2	100.0	1450.0	100.0	1450.0	0.19	27.09	0.00	0.0000
38.7	100.0	1550.0	100.0	1550.0	0.20	28.96	0.00	0.0000
41.2	100.0	1650.0	100.0	1650.0	0.21	30.82	0.00	0.0000
43.7	100.0	1750.0	100.0	1750.0	0.22	32.69	0.00	0.0000
46.2	100.0	1850.0	100.0	1850.0	0.24	34.56	0.00	0.0000
48.7	100.0	1950.0	100.0	1950.0	0.25	36.43	0.00	0.0000
51.2	100.0	2050.0	100.0	2050.0	0.26	38.30	0.00	0.0000
53.8	100.0	2150.0	100.0	2150.0	0.28	40.16	0.00	0.0000
56.3	100.0	2250.0	100.0	2250.0	0.29	42.03	0.00	0.0000
58.8	100.0	2350.0	100.0	2350.0	0.30	43.90	0.00	0.0000
61.3	100.0	2450.0	100.0	2450.0	0.31	45.77	0.00	0.0000
63.8	100.0	2550.0	100.0	2550.0	0.33	47.64	0.00	0.0000
66.4	100.0	2650.0	100.0	2650.0	0.34	49.50	0.00	0.0000
68.9	100.0	2750.0	100.0	2750.0	0.35	51.37	0.00	0.0000
71.5	100.0	2850.0	100.0	2850.0	0.36	53.24	0.00	0.0000
74.0	100.0	2950.0	100.0	2950.0	0.38	55.11	0.00	0.0000
76.4	100.0	3050.0	100.0	3050.0	0.39	56.98	0.00	0.0000
78.9	100.0	3150.0	100.0	3150.0	0.40	58.85	0.00	0.0000
81.4	100.0	3250.0	100.0	3250.0	0.42	60.71	0.00	0.0000
83.9	100.0	3350.0	100.0	3350.0	0.43	62.58	0.00	0.0000
86.4	100.0	3450.0	100.0	3450.0	0.44	64.45	0.00	0.0000

TABLE C-11: (Continued)

Observed and Calculated Results

Time (min) (1)	ΔNp (cc) (2)	Np (cc) (3)	ΔNp+ΔWp (cc) (4)	Np+Wp (cc) (5)	PVi (PV) (6)	Rec. (%OOIP) (7)	W.C. (%) (8)	Pinj (psig) (9)
88.9	100.0	3550.0	100.0	3550.0	0.45	66.32	0.00	0.0000
91.4	100.0	3650.0	100.0	3650.0	0.47	68.19	0.00	0.0000
93.9	100.0	3750.0	100.0	3750.0	0.48	70.05	0.00	0.0000
96.4	100.0	3850.0	100.0	3850.0	0.49	71.92	0.00	0.0000
98.9	100.0	3950.0	100.0	3950.0	0.51	73.79	0.00	0.0000
101.3	100.0	4050.0	100.0	4050.0	0.52	75.66	0.00	0.0000
103.8	100.0	4150.0	100.0	4150.0	0.53	77.53	0.00	0.0000
106.2	99.0	4249.0	100.0	4250.0	0.54	79.38	1.00	0.0000
108.8	95.0	4344.0	101.0	4351.0	0.56	81.15	5.94	0.0000
111.3	65.0	4409.0	100.0	4451.0	0.57	82.37	35.00	0.0000
113.9	50.0	4459.0	100.0	4551.0	0.58	83.30	50.00	0.0000
116.5	28.0	4487.0	110.0	4661.0	0.60	83.82	74.55	0.0000
119.2	12.0	4499.0	100.0	4761.0	0.61	84.05	88.00	0.0000
121.8	12.0	4511.0	100.0	4861.0	0.62	84.27	88.00	0.0000
124.2	12.0	4523.0	100.0	4961.0	0.63	84.49	88.00	0.0000
126.8	11.5	4534.5	99.0	5060.0	0.65	84.71	88.38	0.0000
129.3	12.0	4546.5	100.0	5160.0	0.66	84.93	88.00	0.0000
131.8	13.0	4559.5	101.0	5261.0	0.67	85.18	87.13	0.0000
134.4	13.0	4572.5	101.0	5362.0	0.69	85.42	87.13	0.0000
136.9	4.0	4576.5	101.0	5463.0	0.70	85.49	96.04	0.0000
143.4	9.5	4586.0	251.0	5714.0	0.73	85.67	96.22	0.0000
149.7	9.0	4595.0	250.0	5964.0	0.76	85.84	96.40	0.0000
155.1	8.5	4603.5	250.0	6214.0	0.80	86.00	96.60	0.0000
161.4	8.5	4612.0	250.0	6464.0	0.83	86.16	96.60	0.0000
167.1	8.0	4620.0	250.0	6714.0	0.86	86.31	96.80	0.0000
173.5	7.5	4627.5	251.0	6965.0	0.89	86.45	97.01	0.0000
179.0	6.0	4633.5	250.0	7215.0	0.92	86.56	97.60	0.0000
185.4	6.0	4639.5	253.0	7468.0	0.96	86.67	97.63	0.0000
191.9	2.0	4641.5	250.0	7718.0	0.99	86.71	99.20	0.0000
199.5	2.0	4643.5	280.0	7998.0	1.02	86.75	99.29	0.0000
214.8	4.0	4647.5	590.0	8588.0	1.10	86.82	99.32	0.0000

TABLE C-12:   RUN # HW-15

Porosity	=	36.62	%	OOIP	=	6050.00	cc
Swi	=	23.80	%	Soi	=	76.20	%
Sor	=	11.20	%				

Observed and Calculated Results

Time (min)	ΔNp (cc)	Np (cc)	ΔNp+ΔWp (cc)	Np+Wp (cc)	PVi (PV)	Rec. (%OOIP)	W.C. (%)	Pinj (psig)
(1)	(2)	(3)	(4)	(5)	(6)	(7)	(8)	(9)
1.3	50.0	50.0	50.0	50.0	0.01	0.83	0.00	0.2920
4.9	100.0	150.0	100.0	150.0	0.02	2.48	0.00	0.2921
7.4	100.0	250.0	100.0	250.0	0.03	4.13	0.00	0.2922
9.7	100.0	350.0	100.0	350.0	0.04	5.79	0.00	0.2923
12.2	100.0	450.0	100.0	450.0	0.06	7.44	0.00	0.2924
14.8	100.0	550.0	100.0	550.0	0.07	9.09	0.00	0.2925
17.3	100.0	650.0	100.0	650.0	0.08	10.74	0.00	0.2930
19.8	100.0	750.0	100.0	750.0	0.09	12.40	0.00	0.2935
22.3	100.0	850.0	100.0	850.0	0.11	14.05	0.00	0.2940
24.8	100.0	950.0	100.0	950.0	0.12	15.70	0.00	0.2945
27.3	100.0	1050.0	100.0	1050.0	0.13	17.36	0.00	0.2950
29.8	100.0	1150.0	100.0	1150.0	0.14	19.01	0.00	0.2955
32.3	100.0	1250.0	100.0	1250.0	0.16	20.66	0.00	0.2960
34.8	100.0	1350.0	100.0	1350.0	0.17	22.31	0.00	0.2965
37.3	100.0	1450.0	100.0	1450.0	0.18	23.97	0.00	0.2970
39.8	100.0	1550.0	100.0	1550.0	0.20	25.62	0.00	0.2980
42.3	100.0	1650.0	100.0	1650.0	0.21	27.27	0.00	0.2990
44.7	100.0	1750.0	100.0	1750.0	0.22	28.93	0.00	0.3000
47.2	100.0	1850.0	100.0	1850.0	0.23	30.58	0.00	0.3010
49.7	100.0	1950.0	100.0	1950.0	0.25	32.23	0.00	0.3020
52.2	100.0	2050.0	100.0	2050.0	0.26	33.88	0.00	0.3030
54.6	100.0	2150.0	100.0	2150.0	0.27	35.54	0.00	0.3040
57.1	100.0	2250.0	100.0	2250.0	0.28	37.19	0.00	0.3050
59.6	100.0	2350.0	100.0	2350.0	0.30	38.84	0.00	0.3060
62.1	100.0	2450.0	100.0	2450.0	0.31	40.50	0.00	0.3070
64.6	100.0	2550.0	100.0	2550.0	0.32	42.15	0.00	0.3080
67.1	100.0	2650.0	100.0	2650.0	0.33	43.80	0.00	0.3090
69.6	100.0	2750.0	100.0	2750.0	0.35	45.45	0.00	0.3100
72.1	100.0	2850.0	100.0	2850.0	0.36	47.11	0.00	0.3110
74.6	100.0	2950.0	100.0	2950.0	0.37	48.76	0.00	0.3120
77.1	100.0	3050.0	100.0	3050.0	0.38	50.41	0.00	0.3130
79.6	100.0	3150.0	100.0	3150.0	0.40	52.07	0.00	0.3140
82.1	100.0	3250.0	100.0	3250.0	0.41	53.72	0.00	0.3150
84.6	100.0	3350.0	100.0	3350.0	0.42	55.37	0.00	0.3160
87.1	100.0	3450.0	100.0	3450.0	0.43	57.02	0.00	0.3170

TABLE C-13:   RUN # HW-16

Porosity	=	36.65	%	OOIP	=	5753.00	cc
Swi	=	27.58	%	Soi	=	72.41	%
Sor	=	9.89	%				

Observed and Calculated Results

Time (min)	ΔNp (cc)	Np (cc)	ΔNp+ΔWp (cc)	Np+Wp (cc)	PVi (PV)	Rec. (%OOIP)	W.C. (%)	Pinj (psig)
(1)	(2)	(3)	(4)	(5)	(6)	(7)	(8)	(9)
2.6	100.0	100.0	100.0	100.0	0.01	1.74	0.00	0.2765
5.1	100.0	200.0	100.0	200.0	0.03	3.48	0.00	0.2777
7.6	100.0	300.0	100.0	300.0	0.04	5.21	0.00	0.2776
10.1	100.0	400.0	100.0	400.0	0.05	6.95	0.00	0.2784
12.5	100.0	500.0	100.0	500.0	0.06	8.69	0.00	0.2792
15.0	100.0	600.0	100.0	600.0	0.08	10.43	0.00	0.2800
17.5	100.0	700.0	100.0	700.0	0.09	12.17	0.00	0.2808
19.9	100.0	800.0	100.0	800.0	0.10	13.91	0.00	0.2816
22.4	100.0	900.0	100.0	900.0	0.11	15.64	0.00	0.2824
24.9	100.0	1000.0	100.0	1000.0	0.13	17.38	0.00	0.2832
27.4	100.0	1100.0	100.0	1100.0	0.14	19.12	0.00	0.2840
30.0	100.0	1200.0	100.0	1200.0	0.15	20.86	0.00	0.2850
32.5	100.0	1300.0	100.0	1300.0	0.16	22.60	0.00	0.2856
35.0	100.0	1400.0	100.0	1400.0	0.18	24.34	0.00	0.2864
37.6	100.0	1500.0	100.0	1500.0	0.19	26.07	0.00	0.2872
40.2	100.0	1600.0	100.0	1600.0	0.20	27.81	0.00	0.2881
42.7	100.0	1700.0	100.0	1700.0	0.21	29.55	0.00	0.2890
45.3	100.0	1800.0	100.0	1800.0	0.23	31.29	0.00	0.2897
47.7	100.0	1900.0	100.0	1900.0	0.24	33.03	0.00	0.2905
50.1	100.0	2000.0	100.0	2000.0	0.25	34.76	0.00	0.2913
53.6	100.0	2100.0	100.0	2100.0	0.26	36.50	0.00	0.2921
55.0	100.0	2200.0	100.0	2200.0	0.28	38.24	0.00	0.2929
57.6	100.0	2300.0	100.0	2300.0	0.29	39.98	0.00	0.2940
60.0	100.0	2400.0	100.0	2400.0	0.30	41.72	0.00	0.2945
62.6	100.0	2500.0	100.0	2500.0	0.31	43.46	0.00	0.2953
65.0	100.0	2600.0	100.0	2600.0	0.33	45.19	0.00	0.2961
67.4	100.0	2700.0	100.0	2700.0	0.34	46.93	0.00	·0.2970
69.9	100.0	2800.0	100.0	2800.0	0.35	48.67	0.00	0.2980
72.4	100.0	2900.0	100.0	2900.0	0.37	50.41	0.00	0.2985
74.8	100.0	3000.0	100.0	3000.0	0.38	52.15	0.00	0.2993
77.3	100.0	3100.0	100.0	3100.0	0.39	53.88	0.00	0.3001
79.8	100.0	3200.0	100.0	3200.0	0.40	55.62	0.00	0.3009
82.2	100.0	3300.0	100.0	3300.0	0.42	57.36	0.00	0.3020
84.7	100.0	3400.0	100.0	3400.0	0.43	59.10	0.00	0.3025
87.2	100.0	3500.0	100.0	3500.0	0.44	60.84	0.00	0.3033

TABLE C-13: (Continued)

Observed and Calculated Results

Time (min)	ΔNp (cc)	Np (cc)	ΔNp+ΔWp (cc)	Np+Wp (cc)	PVi (PV)	Rec. (%OOIP)	W.C. (%)	Pinj (psig)
(1)	(2)	(3)	(4)	(5)	(6)	(7)	(8)	(9)
89.7	100.0	3600.0	100.0	3600.0	0.45	62.58	0.00	0.3042
92.2	100.0	3700.0	100.0	3700.0	0.47	64.31	0.00	0.3050
94.7	100.0	3800.0	100.0	3800.0	0.48	66.05	0.00	0.3058
97.2	100.0	3900.0	100.0	3900.0	0.49	67.79	0.00	0.3066
99.7	100.0	4000.0	100.0	4000.0	0.50	69.53	0.00	0.3074
102.2	100.0	4100.0	100.0	4100.0	0.52	71.27	0.00	0.3082
104.6	100.0	4200.0	100.0	4200.0	0.53	73.01	0.00	0.3095
107.2	100.0	4300.0	100.0	4300.0	0.54	74.74	0.00	0.3098
109.6	100.0	4400.0	100.0	4400.0	0.55	76.48	0.00	0.3106
112.1	100.0	4500.0	100.0	4500.0	0.57	78.22	0.00	0.3114
114.6	100.0	4600.0	100.0	4600.0	0.58	79.96	0.00	0.3122
117.1	100.0	4700.0	100.0	4700.0	0.59	81.70	0.00	0.3130
119.5	94.0	4794.0	100.0	4800.0	0.60	83.33	6.00	0.3300
122.1	50.0	4844.0	101.0	4901.0	0.62	84.20	50.50	0.3750
124.5	26.0	4870.0	100.0	5001.0	0.63	84.65	74.00	0.3800
127.1	13.5	4883.5	100.0	5101.0	0.64	84.89	86.50	0.3700
129.6	9.5	4893.0	100.0	5201.0	0.65	85.05	90.50	0.3600
132.1	6.0	4899.0	100.0	5301.0	0.67	85.16	94.00	0.3500
134.6	5.5	4904.5	100.0	5401.0	0.68	85.25	94.50	0.3420
137.1	5.5	4910.0	101.0	5502.0	0.69	85.35	94.55	0.3370
139.6	4.0	4914.0	102.0	5604.0	0.71	85.42	96.08	0.3340
142.1	3.8	4917.8	100.0	5704.0	0.72	85.48	96.20	0.3330
144.6	3.5	4921.3	100.0	5804.0	0.73	85.54	96.50	0.3310
147.1	3.0	4924.3	100.0	5904.0	0.74	85.60	97.00	0.3320
149.6	2.5	4926.8	100.0	6004.0	0.76	85.64	97.50	0.3320
155.9	6.0	4932.8	250.0	6254.0	0.79	85.74	97.60	0.3330
162.2	5.0	4937.8	250.0	6504.0	0.82	85.83	98.00	0.3340
168.6	4.8	4942.6	250.0	6754.0	0.85	85.91	98.08	0.3350
174.9	4.3	4946.9	250.0	7004.0	0.88	85.99	98.28	0.3365
181.2	4.5	4951.4	253.0	7257.0	0.91	86.07	98.22	0.3375
187.6	3.0	4954.4	250.0	7507.0	0.94	86.12	98.80	0.3385
193.9	2.5	4956.9	250.0	7757.0	0.98	86.16	99.00	0.3400
206.3	5.0	4961.9	500.0	8257.0	1.04	86.25	99.00	0.3425
220.0	5.0	4966.9	515.0	8772.0	1.10	86.34	99.03	0.3450

TABLE C-14:   RUN # HW-17

Porosity	=	36.78	%	OOIP	=	5840.00	cc
Swi	=	26.76	%	Soi	=	73.24	%
Sor	=	9.90	%				

Observed and Calculated Results

Time (min)	ΔNp (cc)	Np (cc)	ΔNp+ΔWp (cc)	Np+Wp (cc)	PVi (PV)	Rec. (%OOIP)	W.C. (%)	Pinj (psig)
(1)	(2)	(3)	(4)	(5)	(6)	(7)	(8)	(9)
2.6	100.0	100.0	100.0	100.0	0.01	1.71	0.00	0.0000
5.2	100.0	200.0	100.0	200.0	0.03	3.42	0.00	0.0000
7.6	100.0	300.0	100.0	300.0	0.04	5.14	0.00	0.0000
10.2	100.0	400.0	100.0	400.0	0.05	6.85	0.00	0.0000
12.7	100.0	500.0	100.0	500.0	0.06	8.56	0.00	0.0000
15.2	100.0	600.0	100.0	600.0	0.08	10.27	0.00	0.0000
17.7	100.0	700.0	100.0	700.0	0.09	11.99	0.00	0.0000
20.1	100.0	800.0	100.0	800.0	0.10	13.70	0.00	0.0000
22.6	100.0	900.0	100.0	900.0	0.11	15.41	0.00	0.0000
25.1	100.0	1000.0	100.0	1000.0	0.13	17.12	0.00	0.0000
27.4	100.0	1100.0	100.0	1100.0	0.14	18.84	0.00	0.0000
29.9	100.0	1200.0	100.0	1200.0	0.15	20.55	0.00	0.0000
32.4	100.0	1300.0	100.0	1300.0	0.16	22.26	0.00	0.0000
34.9	100.0	1400.0	100.0	1400.0	0.18	23.97	0.00	0.0000
37.4	100.0	1500.0	100.0	1500.0	0.19	25.68	0.00	0.0000
39.9	100.0	1600.0	100.0	1600.0	0.20	27.40	0.00	0.0000
42.3	100.0	1700.0	100.0	1700.0	0.21	29.11	0.00	0.0000
44.8	100.0	1800.0	100.0	1800.0	0.23	30.82	0.00	0.0000
47.2	100.0	1900.0	100.0	1900.0	0.24	32.53	0.00	0.0000
49.6	100.0	2000.0	100.0	2000.0	0.25	34.25	0.00	0.0000
52.1	100.0	2100.0	100.0	2100.0	0.26	35.96	0.00	0.0000
54.5	100.0	2200.0	100.0	2200.0	0.28	37.67	0.00	0.0000
57.0	100.0	2300.0	100.0	2300.0	0.29	39.38	0.00	0.0000
59.4	100.0	2400.0	100.0	2400.0	0.30	41.10	0.00	0.0000
62.0	100.0	2500.0	100.0	2500.0	0.31	42.81	0.00	0.0000
64.5	100.0	2600.0	100.0	2600.0	0.33	44.52	0.00	0.0000
67.1	100.0	2700.0	100.0	2700.0	0.34	46.23	0.00	0.0000
69.6	100.0	2800.0	100.0	2800.0	0.35	47.95	0.00	0.0000
72.2	100.0	2900.0	100.0	2900.0	0.36	49.66	0.00	0.0000
74.7	100.0	3000.0	100.0	3000.0	0.38	51.37	0.00	0.0000
77.2	100.0	3100.0	100.0	3100.0	0.39	53.08	0.00	0.0000
79.7	100.0	3200.0	100.0	3200.0	0.40	54.79	0.00	0.0000
82.3	100.0	3300.0	100.0	3300.0	0.41	56.51	0.00	0.0000
84.8	100.0	3400.0	100.0	3400.0	0.43	58.22	0.00	0.0000
87.4	100.0	3500.0	100.0	3500.0	0.44	59.93	0.00	0.0000

TABLE C-14: (Continued)

Observed and Calculated Results

Time (min) (1)	ΔNp (cc) (2)	Np (cc) (3)	$\Delta Np + \Delta Wp$ (cc) (4)	Np+Wp (cc) (5)	PVi (PV) (6)	Rec. (%OOIP) (7)	W.C. (%) (8)	Pinj (psig) (9)
89.9	100.0	3600.0	100.0	3600.0	0.45	61.64	0.00	0.0000
92.5	100.0	3700.0	100.0	3700.0	0.46	63.36	0.00	0.0000
95.1	100.0	3800.0	100.0	3800.0	0.48	65.07	0.00	0.0000
97.6	100.0	3900.0	100.0	3900.0	0.49	66.78	0.00	0.0000
100.2	100.0	4000.0	100.0	4000.0	0.50	68.49	0.00	0.0000
102.7	100.0	4100.0	100.0	4100.0	0.51	70.21	0.00	0.0000
105.2	100.0	4200.0	100.0	4200.0	0.53	71.92	0.00	0.0000
107.8	100.0	4300.0	100.0	4300.0	0.54	73.63	0.00	0.0000
110.3	100.0	4400.0	100.0	4400.0	0.55	75.34	0.00	0.0000
112.8	100.0	4500.0	100.0	4500.0	0.56	77.05	0.00	0.0000
115.3	100.0	4600.0	100.0	4600.0	0.58	78.77	0.00	0.0000
117.9	100.0	4700.0	100.0	4700.0	0.59	80.48	0.00	0.0000
120.3	100.0	4800.0	100.0	4800.0	0.60	82.19	0.00	0.0000
122.8	88.0	4888.0	100.0	4900.0	0.61	83.70	12.00	0.0000
125.3	55.0	4943.0	100.0	5000.0	0.63	84.64	45.00	0.0000
127.8	29.0	4972.0	100.0	5100.0	0.64	85.14	71.00	0.0000
130.3	17.0	4989.0	100.0	5200.0	0.65	85.43	83.00	0.0000
132.8	12.0	5001.0	100.0	5300.0	0.66	85.63	88.00	0.0000
135.3	8.5	5009.5	100.0	5400.0	0.68	85.78	91.50	0.0000
137.8	5.0	5014.5	100.0	5500.0	0.69	85.86	95.00	0.0000
140.3	4.5	5019.0	100.0	5600.0	0.70	85.94	95.50	0.0000
142.8	3.5	5022.5	100.0	5700.0	0.71	86.00	96.50	0.0000
145.3	3.0	5025.5	100.0	5800.0	0.73	86.05	97.00	0.0000
147.7	2.0	5027.5	100.0	5900.0	0.74	86.09	98.00	0.0000
150.2	2.0	5029.5	101.0	6001.0	0.75	86.12	98.02	0.0000
156.4	4.0	5033.5	250.0	6251.0	0.78	86.19	98.40	0.0000
162.6	2.0	5035.5	250.0	6501.0	0.82	86.22	99.20	0.0000
168.8	2.0	5037.5	251.0	6752.0	0.85	86.26	99.20	0.0000
175.0	2.0	5039.5	252.0	7004.0	0.88	86.29	99.21	0.0000
181.5	1.0	5040.5	265.0	7269.0	0.91	86.31	99.62	0.0000
188.0	2.0	5042.5	267.0	7536.0	0.95	86.34	99.25	0.0000
194.2	1.0	5043.5	251.0	7787.0	0.98	86.36	99.60	0.0000
206.5	4.0	5047.5	502.0	8289.0	1.04	86.43	99.20	0.0000
220.0	3.0	5050.5	555.0	8844.0	1.11	86.48	99.46	0.0000

TABLE C-15:   RUN # HW-18

Porosity	=	36.80	%	OOIP	=	5500.00	cc
Swi	=	31.08	%	Soi	=	68.92	%
Sor	=	15.46	%				

Observed and Calculated Results

Time (min)	ΔNp (cc)	Np (cc)	ΔNp+ΔWp (cc)	Np+Wp (cc)	PVi (PV)	Rec. (%OOIP)	W.C. (%)	Pinj (psig)
(1)	(2)	(3)	(4)	(5)	(6)	(7)	(8)	(9)
1.2	50.0	50.0	50.0	50.0	0.01	0.91	0.00	0.3050
3.5	100.0	150.0	100.0	150.0	0.02	2.73	0.00	0.3055
5.9	100.0	250.0	100.0	250.0	0.03	4.55	0.00	0.3060
8.3	100.0	350.0	100.0	350.0	0.04	6.36	0.00	0.3065
10.8	100.0	450.0	100.0	450.0	0.06	8.18	0.00	0.3070
13.2	100.0	550.0	100.0	550.0	0.07	10.00	0.00	0.3075
15.7	100.0	650.0	100.0	650.0	0.08	11.82	0.00	0.3080
18.1	100.0	750.0	100.0	750.0	0.09	13.64	0.00	0.3085
20.6	100.0	850.0	100.0	850.0	0.11	15.45	0.00	0.3086
23.0	100.0	950.0	100.0	950.0	0.12	17.27	0.00	0.3088
25.4	100.0	1050.0	100.0	1050.0	0.13	19.09	0.00	0.3090
27.9	100.0	1150.0	100.0	1150.0	0.14	20.91	0.00	0.3095
30.3	100.0	1250.0	100.0	1250.0	0.16	22.73	0.00	0.3098
32.7	100.0	1350.0	100.0	1350.0	0.17	24.55	0.00	0.3105
35.2	100.0	1450.0	100.0	1450.0	0.18	26.36	0.00	0.3110
37.6	100.0	1550.0	100.0	1550.0	0.19	28.18	0.00	0.3120
40.1	100.0	1650.0	100.0	1650.0	0.21	30.00	0.00	0.3130
42.5	100.0	1750.0	100.0	1750.0	0.22	31.82	0.00	0.3140
45.0	100.0	1850.0	100.0	1850.0	0.23	33.64	0.00	0.3143
47.5	100.0	1950.0	100.0	1950.0	0.24	35.45	0.00	0.3148
49.9	100.0	2050.0	100.0	2050.0	0.26	37.27	0.00	0.3150
52.3	100.0	2150.0	100.0	2150.0	0.27	39.09	0.00	0.3160
54.7	100.0	2250.0	100.0	2250.0	0.28	40.91	0.00	0.3170
57.2	100.0	2350.0	100.0	2350.0	0.29	42.73	0.00	0.3175
59.6	100.0	2450.0	100.0	2450.0	0.31	44.55	0.00	0.3180
62.1	100.0	2550.0	100.0	2550.0	0.32	46.36	0.00	0.3185
64.5	100.0	2650.0	100.0	2650.0	0.33	48.18	0.00	0.3195
67.0	100.0	2750.0	100.0	2750.0	0.34	50.00	0.00	0.3205
69.4	100.0	2850.0	100.0	2850.0	0.36	51.82	0.00	0.3210
71.8	100.0	2950.0	100.0	2950.0	0.37	53.64	0.00	0.3215
74.3	100.0	3050.0	100.0	3050.0	0.38	55.45	0.00	0.3220
76.7	100.0	3150.0	100.0	3150.0	0.39	57.27	0.00	0.3225
79.1	100.0	3250.0	100.0	3250.0	0.41	59.09	0.00	0.3230
81.5	100.0	3350.0	100.0	3350.0	0.42	60.91	0.00	0.3235
84.0	100.0	3450.0	100.0	3450.0	0.43	62.73	0.00	0.3250

TABLE C-15: (Continued)

Observed and Calculated Results

Time (min)	ΔNp (cc)	Np (cc)	ΔNp+ΔWp (cc)	Np+Wp (cc)	PVi (PV)	Rec. (%OOIP)	W.C. (%)	Pinj (psig)
(1)	(2)	(3)	(4)	(5)	(6)	(7)	(8)	(9)
86.4	100.0	3550.0	100.0	3550.0	0.44	64.55	0.00	0.3270
88.9	100.0	3650.0	100.0	3650.0	0.46	66.36	0.00	0.3300
91.3	100.0	3750.0	100.0	3750.0	0.47	68.18	0.00	0.3320
93.7	75.0	3825.0	100.0	3850.0	0.48	69.55	25.00	0.3850
96.2	46.0	3871.0	100.0	3950.0	0.49	70.38	54.00	0.3960
98.7	32.5	3903.5	100.0	4050.0	0.51	70.97	67.50	0.4050
101.2	28.0	3931.5	100.0	4150.0	0.52	71.48	72.00	0.4050
103.7	23.0	3954.5	101.0	4251.0	0.53	71.90	77.23	0.4020
106.1	20.5	3975.0	100.0	4351.0	0.55	72.27	79.50	0.4000
108.6	18.0	3993.0	100.0	4451.0	0.56	72.60	82.00	0.3970
111.0	17.5	4010.5	101.0	4552.0	0.57	72.92	82.67	0.3930
113.5	16.0	4026.5	100.0	4652.0	0.58	73.21	84.00	0.3880
115.9	15.0	4041.5	100.0	4752.0	0.60	73.48	85.00	0.3850
118.4	14.0	4055.5	100.0	4852.0	0.61	73.74	86.00	0.3820
120.8	13.5	4069.0	100.0	4952.0	0.62	73.98	86.50	0.3800
127.0	27.0	4096.0	250.0	5202.0	0.65	74.47	89.20	0.3750
133.0	25.0	4121.0	250.0	5452.0	0.68	74.93	90.00	0.3640
139.1	21.0	4142.0	250.0	5702.0	0.71	75.31	91.60	0.3600
145.4	20.0	4162.0	262.0	5964.0	0.75	75.67	92.37	0.3690
151.5	16.5	4178.5	250.0	6214.0	0.78	75.97	93.40	0.3580
157.5	15.5	4194.0	250.0	6464.0	0.81	76.25	93.80	0.3580
163.7	12.0	4206.0	250.0	6714.0	0.84	76.47	95.20	0.3580
169.8	10.0	4216.0	250.0	6964.0	0.87	76.65	96.00	0.3578
175.9	9.0	4225.0	250.0	7214.0	0.90	76.82	96.40	0.3575
181.9	9.0	4234.0	251.0	7465.0	0.94	76.98	96.41	0.3573
188.0	8.0	4242.0	250.0	7715.0	0.97	77.13	96.80	0.3570
194.1	7.5	4249.5	250.0	7965.0	1.00	77.26	97.00	0.3568
200.3	7.0	4256.5	250.0	8215.0	1.03	77.39	97.20	0.3565
206.8	5.0	4261.5	271.0	8486.0	1.06	77.48	98.15	0.3560
213.8	5.0	4266.5	295.0	8781.0	1.10	.77.57	98.31	0.3550

TABLE C-16:   RUN # HW-19

Porosity =	36.62 %	OOIP	=	6072.00 cc
Swi =	23.52 %	Soi	=	76.49 %
Sor =	13.58 %			

Observed and Calculated Results

Time (min)	ΔNp (cc)	Np (cc)	ΔNp+ΔWp (cc)	Np+Wp (cc)	PVi (PV)	Rec. (%OOIP)	W.C. (%)	Pinj (psig)
(1)	(2)	(3)	(4)	(5)	(6)	(7)	(8)	(9)
2.3	100.0	100.0	100.0	100.0	0.01	1.65	0.00	0.3050
4.7	100.0	200.0	100.0	200.0	0.03	3.29	0.00	0.3050
7.0	100.0	300.0	100.0	300.0	0.04	4.94	0.00	0.3050
9.4	100.0	400.0	100.0	400.0	0.05	6.59	0.00	0.3050
11.9	100.0	500.0	100.0	500.0	0.06	8.23	0.00	0.3050
14.3	100.0	600.0	100.0	600.0	0.08	9.88	0.00	0.3050
16.7	100.0	700.0	100.0	700.0	0.09	11.53	0.00	0.3050
19.1	100.0	800.0	100.0	800.0	0.10	13.18	0.00	0.3051
21.6	100.0	900.0	100.0	900.0	0.11	14.82	0.00	0.3052
24.1	100.0	1000.0	100.0	1000.0	0.13	16.47	0.00	0.3053
26.5	100.0	1100.0	100.0	1100.0	0.14	18.12	0.00	0.3054
28.9	100.0	1200.0	100.0	1200.0	0.15	19.76	0.00	0.3055
31.4	100.0	1300.0	100.0	1300.0	0.16	21.41	0.00	0.3060
33.8	100.0	1400.0	100.0	1400.0	0.18	23.06	0.00	0.3065
36.3	100.0	1500.0	100.0	1500.0	0.19	24.70	0.00	0.3070
38.6	100.0	1600.0	100.0	1600.0	0.20	26.35	0.00	0.3080
41.1	100.0	1700.0	100.0	1700.0	0.21	28.00	0.00	0.3090
43.6	100.0	1800.0	100.0	1800.0	0.23	29.64	0.00	0.3120
46.0	100.0	1900.0	100.0	1900.0	0.24	31.29	0.00	0.3130
48.4	100.0	2000.0	100.0	2000.0	0.25	32.94	0.00	0.3140
50.9	100.0	2100.0	100.0	2100.0	0.26	34.58	0.00	0.3150
53.4	100.0	2200.0	100.0	2200.0	0.28	36.23	0.00	0.3160
55.8	100.0	2300.0	100.0	2300.0	0.29	37.88	0.00	0.3175
58.3	100.0	2400.0	100.0	2400.0	0.30	39.53	0.00	0.3185
60.8	100.0	2500.0	100.0	2500.0	0.31	41.17	0.00	0.3200
63.3	100.0	2600.0	100.0	2600.0	0.33	42.82	0.00	0.3220
65.8	100.0	2700.0	100.0	2700.0	0.34	44.47	0.00	0.3230
68.2	100.0	2800.0	100.0	2800.0	0.35	46.11	0.00	0.3245
70.6	100.0	2900.0	100.0	2900.0	0.37	47.76	0.00	0.3260
73.1	100.0	3000.0	100.0	3000.0	0.38	49.41	0.00	0.3270
75.5	100.0	3100.0	100.0	3100.0	0.39	51.05	0.00	0.3280
77.9	100.0	3200.0	100.0	3200.0	0.40	52.70	0.00	0.3295
80.4	100.0	3300.0	100.0	3300.0	0.42	54.35	0.00	0.3331
82.9	100.0	3400.0	100.0	3400.0	0.43	55.99	0.00	0.3325
85.4	100.0	3500.0	100.0	3500.0	0.44	57.64	0.00	0.3340

TABLE C-16: (Continued)

Observed and Calculated Results

Time (min)	ΔNp (cc)	Np (cc)	ΔNp+ΔWp (cc)	Np+Wp (cc)	PVi (PV)	Rec. (%OOIP)	W.C. (%)	Pinj (psig)
(1)	(2)	(3)	(4)	(5)	(6)	(7)	(8)	(9)
87.8	100.0	3600.0	100.0	3600.0	0.45	59.29	0.00	0.3350
90.3	100.0	3700.0	100.0	3700.0	0.47	60.94	0.00	0.3365
92.7	100.0	3800.0	100.0	3800.0	0.48	62.58	0.00	0.3380
95.2	100.0	3900.0	100.0	3900.0	0.49	64.23	0.00	0.3390
98.6	100.0	4000.0	100.0	4000.0	0.50	65.88	0.00	0.3400
100.0	100.0	4100.0	100.0	4100.0	0.52	67.52	0.00	0.3420
102.4	100.0	4200.0	100.0	4200.0	0.53	69.17	0.00	0.3430
104.9	100.0	4300.0	100.0	4300.0	0.54	70.82	0.00	0.3440
107.4	100.0	4400.0	100.0	4400.0	0.55	72.46	0.00	0.3500
109.9	69.0	4469.0	100.0	4500.0	0.57	73.60	31.00	0.3720
112.4	61.0	4530.0	100.0	4600.0	0.58	74.60	39.00	0.3750
114.9	55.0	4585.0	100.0	4700.0	0.59	75.51	45.00	0.3755
117.4	45.0	4630.0	100.0	4800.0	0.60	76.25	55.00	0.3760
119.9	38.0	4668.0	100.0	4900.0	0.62	76.88	62.00	0.3770
122.4	31.0	4699.0	100.0	5000.0	0.63	77.39	69.00	0.3760
124.9	27.0	4726.0	100.0	5100.0	0.64	77.83	73.00	0.3740
127.3	25.0	4751.0	100.0	5200.0	0.65	78.24	75.00	0.3735
129.7	21.0	4772.0	100.0	5300.0	0.67	78.59	79.00	0.3772
132.1	19.0	4791.0	100.0	5400.0	0.68	78.90	81.00	0.3700
134.6	17.0	4808.0	100.0	5500.0	0.69	79.18	83.00	0.3675
137.0	15.0	4823.0	100.0	5600.0	0.71	79.43	85.00	0.3650
142.6	32.0	4855.0	250.0	5850.0	0.74	79.96	87.20	0.3500
149.6	28.0	4883.0	250.0	6100.0	0.77	80.42	88.80	0.3510
154.6	19.0	4902.0	250.0	6350.0	0.80	80.73	92.40	0.3520
161.6	16.0	4918.0	250.0	6600.0	0.83	80.99	93.60	0.3530
167.6	15.0	4933.0	250.0	6850.0	0.86	81.24	94.00	0.3540
173.6	13.0	4946.0	250.0	7100.0	0.89	81.46	94.80	0.3550
179.6	11.0	4957.0	250.0	7350.0	0.93	81.64	95.60	0.3560
185.6	10.0	4967.0	250.0	7600.0	0.96	81.80	96.00	0.3570
191.6	8.0	4975.0	250.0	7850.0	0.99	81.93	96.80	0.3580
198.6	7.0	4982.0	250.0	8100.0	1.02	82.05	97.20	0.3590
212.6	11.5	4993.5	568.0	8668.0	1.09	82.24	97.98	0.3600

TABLE C-17:   RUN # HW-20

Porosity	=	36.58	%	OOIP	=	5600.00	cc
Swi	=	29.38	%	Soi	=	70.62	%
Sor	=	18.47	%				

Observed and Calculated Results

Time (min)	ΔNp (cc)	Np (cc)	ΔNp+ΔWp (cc)	Np+Wp (cc)	PVi (PV)	Rec. (%OOIP)	W.C. (%)	Pinj (psig)
(1)	(2)	(3)	(4)	(5)	(6)	(7)	(8)	(9)
2.3	100.0	100.0	100.0	100.0	0.01	1.79	0.00	0.3150
4.5	100.0	200.0	100.0	200.0	0.03	3.57	0.00	0.3151
6.9	100.0	300.0	100.0	300.0	0.04	5.36	0.00	0.3153
9.2	100.0	400.0	100.0	400.0	0.05	7.14	0.00	0.3156
11.6	100.0	500.0	100.0	500.0	0.06	8.93	0.00	0.3160
13.9	100.0	600.0	100.0	600.0	0.08	10.71	0.00	0.3165
16.3	100.0	700.0	100.0	700.0	0.09	12.50	0.00	0.3170
18.7	100.0	800.0	100.0	800.0	0.10	14.29	0.00	0.3175
21.1	100.0	900.0	100.0	900.0	0.11	16.07	0.00	0.3179
23.7	100.0	1000.0	100.0	1000.0	0.13	17.86	0.00	0.3183
26.1	100.0	1100.0	100.0	1100.0	0.14	19.64	0.00	0.3186
28.6	100.0	1200.0	100.0	1200.0	0.15	21.43	0.00	0.3190
31.0	100.0	1300.0	100.0	1300.0	0.16	23.21	0.00	0.3195
33.5	100.0	1400.0	100.0	1400.0	0.18	25.00	0.00	0.3200
36.0	100.0	1500.0	100.0	1500.0	0.19	26.79	0.00	0.3205
38.4	100.0	1600.0	100.0	1600.0	0.20	28.57	0.00	0.3210
40.9	100.0	1700.0	100.0	1700.0	0.21	30.36	0.00	0.3220
43.5	100.0	1800.0	100.0	1800.0	0.23	32.14	0.00	0.3230
46.0	100.0	1900.0	100.0	1900.0	0.24	33.93	0.00	0.3250
48.5	100.0	2000.0	100.0	2000.0	0.25	35.71	0.00	0.3270
51.0	100.0	2100.0	100.0	2100.0	0.26	37.50	0.00	0.3290
53.5	100.0	2200.0	100.0	2200.0	0.28	39.29	0.00	0.3320
56.1	100.0	2300.0	100.0	2300.0	0.29	41.07	0.00	0.3330
58.6	100.0	2400.0	100.0	2400.0	0.30	42.86	0.00	0.3340
61.2	100.0	2500.0	100.0	2500.0	0.32	44.64	0.00	0.3350
63.8	100.0	2600.0	100.0	2600.0	0.33	46.43	0.00	0.3360
66.3	100.0	2700.0	100.0	2700.0	0.34	48.21	0.00	0.3180
68.9	100.0	2800.0	100.0	2800.0	0.35	50.00	0.00	0.3400
71.4	100.0	2900.0	100.0	2900.0	0.37	51.79	0.00	0.3410
74.0	100.0	3000.0	100.0	3000.0	0.38	53.57	0.00	0.3430
76.5	100.0	3100.0	100.0	3100.0	0.39	55.36	0.00	0.3440
79.1	100.0	3200.0	100.0	3200.0	0.40	57.14	0.00	0.3460
81.6	100.0	3300.0	100.0	3300.0	0.42	58.93	0.00	0.3475
84.1	100.0	3400.0	100.0	3400.0	0.43	60.71	0.00	0.3480
86.6	100.0	3500.0	100.0	3500.0	0.44	62.50	0.00	0.3530

TABLE C-17: (Continued)

Observed and Calculated Results

Time (min)	ΔNp (cc)	Np (cc)	ΔNp+ΔWp (cc)	Np+Wp (cc)	PVi (PV)	Rec. (%OOIP)	W.C. (%)	Pinj (psig)
(1)	(2)	(3)	(4)	(5)	(6)	(7)	(8)	(9)
89.2	92.0	3592.0	100.0	3600.0	0.45	64.14	8.00	0.3870
91.7	69.0	3661.0	100.0	3700.0	0.47	65.38	31.00	0.4000
94.3	59.0	3720.0	101.0	3801.0	0.48	66.43	41.58	0.4060
96.8	43.0	3763.0	101.0	3902.0	0.49	67.20	57.43	0.4100
99.4	38.0	3801.0	100.0	4002.0	0.50	67.88	62.00	0.4100
102.0	33.0	3834.0	100.0	4102.0	0.52	68.46	67.00	0.4100
104.5	27.0	3861.0	100.0	4202.0	0.53	68.95	73.00	0.4100
107.1	22.0	3883.0	100.0	4302.0	0.54	69.34	78.00	0.4090
109.7	21.0	3904.0	100.0	4402.0	0.56	69.71	79.00	0.4085
112.3	19.5	3923.5	101.0	4503.0	0.57	70.06	80.69	0.3875
114.7	16.0	3939.5	100.0	4603.0	0.58	70.35	84.00	0.3870
117.2	14.5	3954.0	100.0	4703.0	0.59	70.61	85.50	0.3850
123.5	31.0	3985.0	250.0	4953.0	0.62	71.16	87.60	0.3850
129.8	25.0	4010.0	251.0	5204.0	0.66	71.61	90.04	0.3800
136.1	19.0	4029.0	251.0	5455.0	0.69	71.95	92.43	0.3770
142.4	15.0	4044.0	250.0	5705.0	0.72	72.21	94.00	0.3680
148.6	12.5	4056.5	250.0	5955.0	0.75	72.44	95.00	0.3680
154.9	11.5	4068.0	250.0	6205.0	0.78	72.64	95.40	0.3690
161.0	10.5	4078.5	250.0	6455.0	0.81	72.83	95.80	0.3700
167.2	9.5	4088.0	250.0	6705.0	0.85	73.00	96.20	0.3700
173.3	9.0	4097.0	250.0	6955.0	0.88	73.16	96.40	0.3690
179.5	8.0	4105.0	250.0	7205.0	0.91	73.30	96.80	0.3680
185.5	7.0	4112.0	250.0	7455.0	0.94	73.43	97.20	0.3680
191.6	6.0	4118.0	250.0	7705.0	0.97	73.54	97.60	0.3670
197.6	5.0	4123.0	250.0	7955.0	1.00	73.63	98.00	0.3670
202.8	4.5	4127.5	250.0	8205.0	1.03	73.71	98.20	0.3660
208.8	4.0	4131.5	250.0	8455.0	1.07	73.78	98.40	0.3660
217.8	4.0	4135.5	335.0	8790.0	1.11	73.85	98.81	0.3650

TABLE C-18:   RUN # HW-03

Porosity =	36.20	%	OOIP	=	137.93	cc
Swi	=	16.50	%	Soi	=	83.50	%
Sor	=	6.35	%				

Observed and Calculated Results

Time	ΔNp	ΔNp+ΔWp	pvi	Rec.	W.C.
(min)	(cc)	(cc)	(cc)	(%OOIP)	(%)
1.00	9.40	9.40	0.06	6.82	0.00
2.00	12.90	12.90	0.14	16.17	0.00
3.00	4.10	4.10	0.16	19.14	0.00
4.00	1.55	1.55	0.17	20.26	0.00
5.00	5.20	5.20	0.20	24.03	0.00
6.00	5.70	5.70	0.24	28.17	0.00
7.00	6.40	6.40	0.27	32.81	0.00
8.00	7.20	7.20	0.32	38.03	0.00
9.00	9.80	9.80	0.38	45.13	0.00
10.00	8.40	8.40	0.43	51.22	0.00
11.00	7.90	7.90	0.48	56.95	0.00
12.00	6.50	6.50	0.51	61.66	0.00
13.00	5.80	5.80	0.55	65.87	0.00
14.00	5.00	5.00	0.58	69.49	0.00
15.00	4.50	4.50	0.61	72.76	0.00
16.00	4.20	4.20	0.63	75.80	0.00
17.00	4.15	4.15	0.66	78.81	0.00
18.00	3.80	3.80	0.68	81.57	0.00
19.00	2.10	2.10	0.69	83.09	0.00
20.00	0.50	0.50	0.70	83.45	0.00
21.00	0.50	3.60	0.72	83.81	86.11
22.00	2.00	4.30	0.74	85.26	53.49
23.00	0.55	1.95	0.76	85.66	71.79
24.00	0.40	1.60	0.77	85.95	75.00
25.00	0.20	1.30	0.77	86.10	84.62
26.00	0.15	1.50	0.78	86.21	90.00
27.00	0.12	1.62	0.79	86.29	92.59
28.00	0.00	2.10	0.81	86.29	100.00
29.00	0.10	2.20	0.82	86.37	95.45
30.00	0.20	1.80	0.83	86.51	88.89
31.00	0.02	2.32	0.84	86.52	99.14
32.00	0.00	2.40	0.86	86.52	100.00
33.00	0.00	0.95	0.86	86.52	100.00
34.25	1.00	25.50	1.02	87.25	96.08

TABLE C-18: (Continued)

Observed and Calculated Results

Time (min)	ΔNp (cc)	ΔNp+ΔWp (cc)	pvi (cc)	Rec. (%OOIP)	W.C. (%)
37.50	0.50	25.50	1.17	87.61	98.04
39.73	1.00	25.00	1.32	88.34	96.00
44.93	1.50	25.00	1.48	89.42	94.00
47.77	2.00	25.00	1.63	90.87	92.00
50.45	0.60	25.00	1.78	91.31	97.60
53.00	0.50	24.50	1.93	91.67	97.96
55.78	0.00	25.00	2.08	91.67	100.00
58.60	0.50	26.00	2.24	92.03	98.08
61.65	0.50	29.50	2.41	92.40	98.31
64.33	0.00	25.00	2.57	92.40	100.00
67.48	0.00	29.00	2.74	92.40	100.00
70.17	0.00	25.40	2.89	92.40	100.00
80.88	0.00	100.00	3.50	92.40	100.00
91.62	0.00	100.00	4.11	92.40	100.00
93.15	0.00	100.00	4.71	92.40	100.00

Appendix D
INJECTION RATES AND PRESSURE DROPS

TABLE D.1: Injection Rate vs Pressure Drop

Rate	Pressure Drop, psi		Time to inject
cc/min	Oil	water	1.0 pv, minutes
* 0.00	0.1764	0.2200	
10.00	0.1766	0.2200	768.8
20.00	0.1768	0.2201	384.4
30.00	0.1769	0.2202	256.3
40.00	0.1771	0.2203	192.2
50.00	0.1772	0.2204	153.8
60.00	0.1774	0.2204	128.1
70.00	0.1776	0.2205	109.8
80.00	0.1777	0.2206	96.1
90.00	0.1779	0.2207	85.4
100.00	0.1780	0.2208	76.9
110.00	0.1782	0.2208	69.9
120.00	0.1783	0.2209	64.1
130.00	0.1785	0.2210	59.1
140.00	0.1787	0.2211	54.9
150.00	0.1788	0.2211	51.3
160.00	0.1790	0.2212	48.1
170.00	0.1791	0.2213	45.2
180.00	0.1793	0.2214	42.7
190.00	0.1794	0.2215	40.5
200.00	0.1796	0.2215	38.4

Pressure drops are calculated from Darcy's for single phase oil or water using equations (4.1) and (4.2).

* Pressure due to gravity with no flow.